

23 March 2007 | \$10

# Science

## The Large Hadron Collider

Europe Takes the Lead  
in Particle Physics

AAAS



# PCR Arrays

Profile your pathway using qRT-PCR.

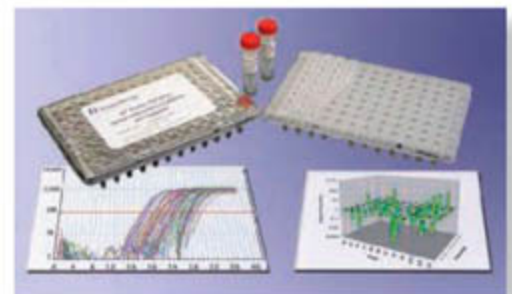


Disease  
Neuroscience  
Inflammation  
Apoptosis

Cancer  
Toxicology  
Stem Cell Biology  
Cell Signaling  
Cytokines

## RT<sup>2</sup> Profiler™ PCR Arrays

RT<sup>2</sup> Profiler™ PCR Arrays are powerful new tools for monitoring the expression of focused gene panels. With PCR Arrays, you can accurately profile gene expression for a biological pathway or disease using the real-time quantitative PCR instrument in your lab.



Focus on your Pathway

[www.superarray.com](http://www.superarray.com)

 **SuperArray**  
Bioscience Corporation





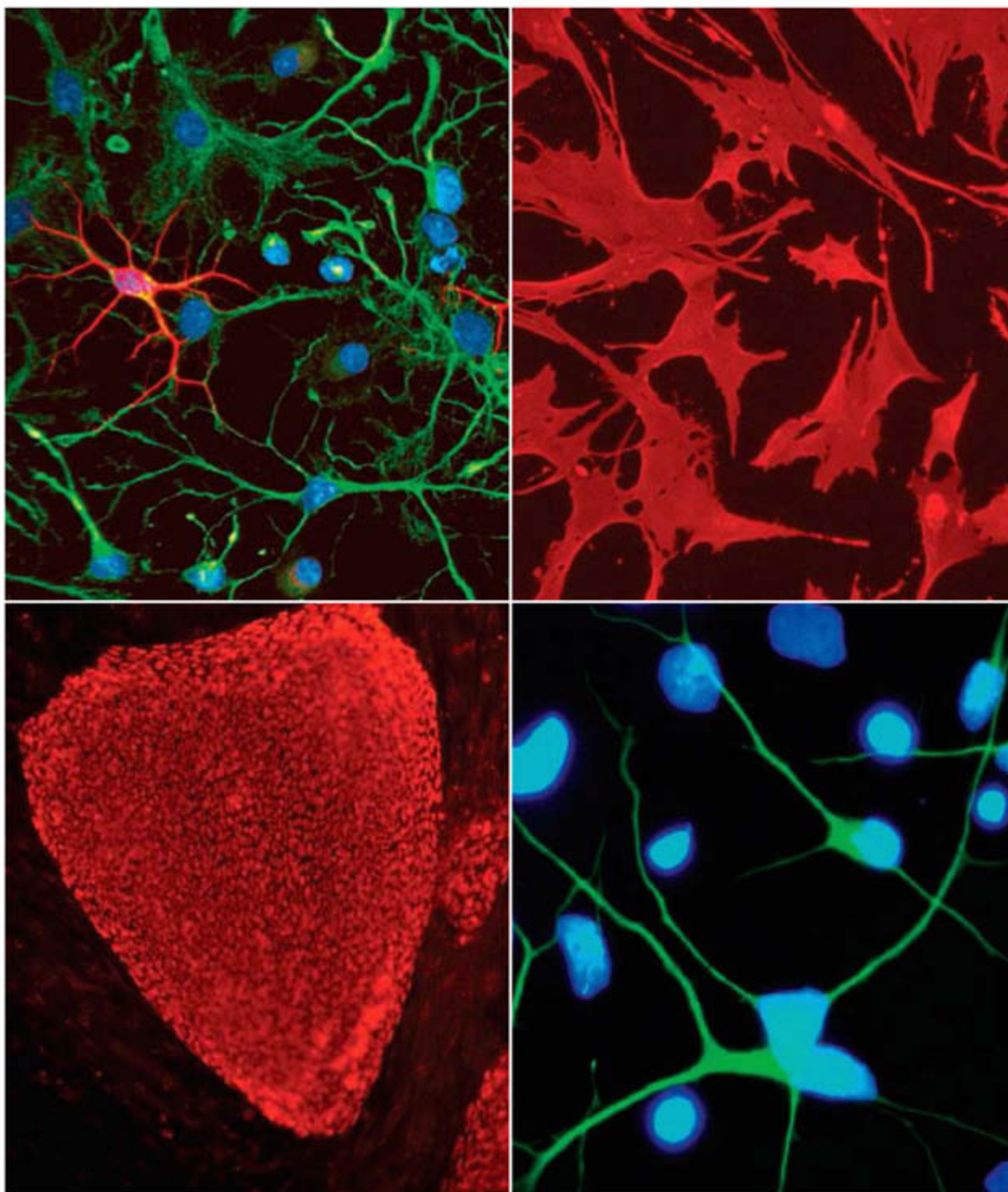
# R&D Systems

Discoveries happen every day.

**Over 6,000  
Antibodies for:**

- Immuno-histochemistry
- Flow Cytometry
- ELISA
- Western Blot
- Neutralization
- Immuno-precipitation

Check out our  
**NEW**  
NorthernLights™  
Secondary  
Antibodies



U.S. & Canada  
**R&D Systems, Inc.**  
Tel: (800) 343-7475  
info@RnDSystems.com

Europe  
**R&D Systems Europe Ltd.**  
Tel: +44 (0)1235 529449  
info@RnDSystems.co.uk

Germany  
**R&D Systems GmbH**  
Tel: 0800 909 4455  
info@RnDSystems.co.uk

France  
**R&D Systems Europe**  
Tel: 0800 90 72 49  
info@RnDSystems.co.uk

R&D Systems is a registered  
trademark of TECHNE Corporation.

For research use only. Not for use in humans or diagnostic procedures except where noted.

Selection expanding weekly—visit [www.RnDSystems.com](http://www.RnDSystems.com)

**R&D**  
SYSTEMS®



# Bringing protein analysis to life with Ettan DIGE and Amersham ECL

When it comes to life sciences, GE Healthcare is setting the standard. Tens of thousands of scientists worldwide rely on our products and proven expertise in protein analysis and detection every day. But we're never content to stand still. We're constantly striving for innovations that boost accuracy and deliver quantitative data.

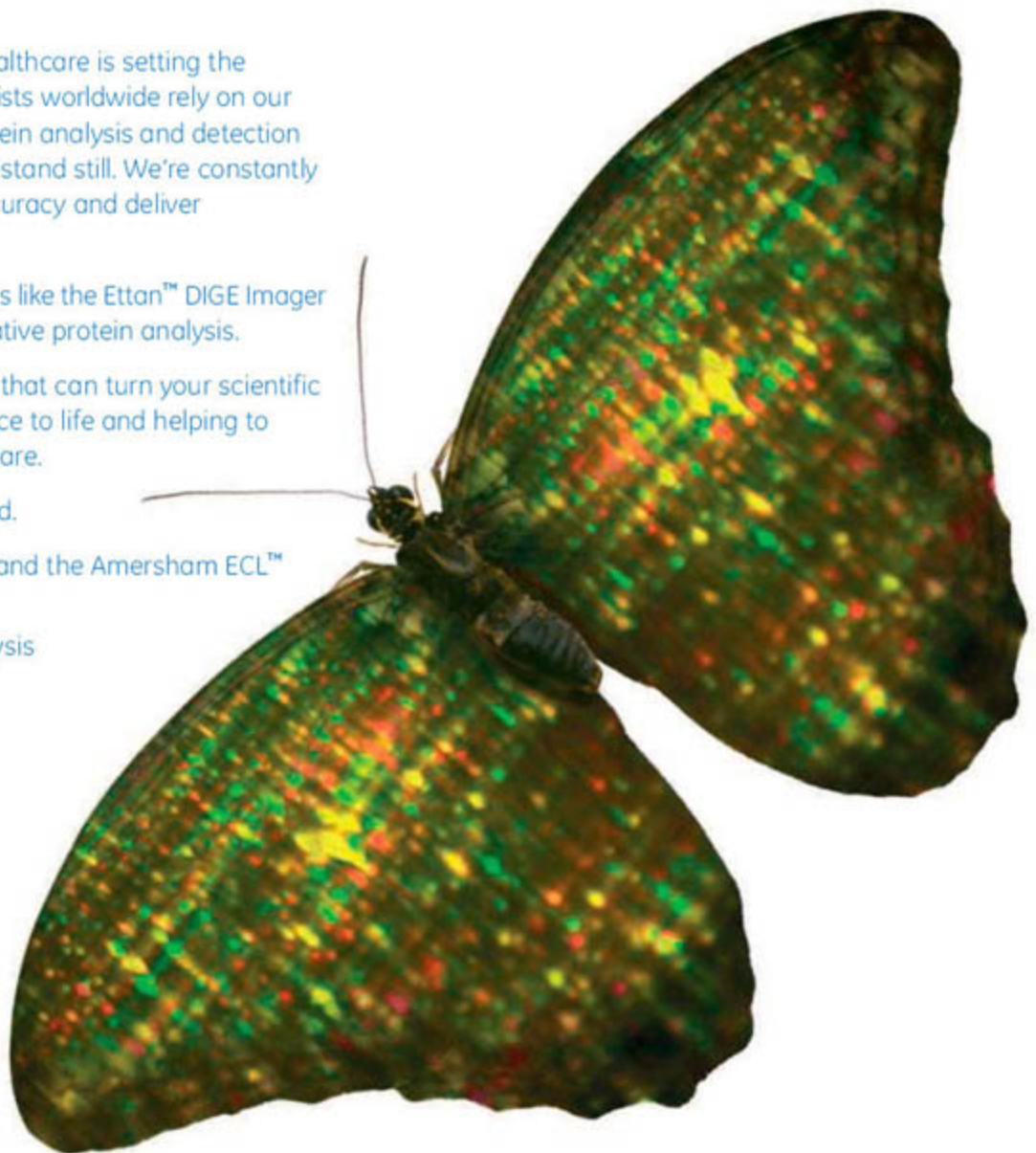
The result is new fluorescence platforms like the Ettan™ DIGE Imager and Amersham ECL Plex™ for quantitative protein analysis.

By continually developing technology that can turn your scientific ideas into reality, we're bringing science to life and helping to transform drug discovery and healthcare.

We call it Protein Analysis Re-imagined.

Discover the full power of Ettan DIGE and the Amersham ECL™ family of Western blotting systems.

[www.gehealthcare.com/protein\\_analysis](http://www.gehealthcare.com/protein_analysis)



imagination at work





## COVER

Part of the cylindrical Compact Muon Solenoid particle detector descends to a hall 100 meters underground at the European particle physics laboratory CERN. The detector will capture the hail of particles produced when CERN's Large Hadron Collider smashes protons at unprecedented energies. A special News report beginning on page 1652 profiles the new collider.

Photo: Maximilien Brice, CERN

## DEPARTMENTS

- 1631 Science Online
- 1633 This Week in Science
- 1638 Editors' Choice
- 1640 Contact Science
- 1643 Random Samples
- 1645 Newsmakers
- 1733 New Products
- 1734 Science Careers

## EDITORIAL

- 1637 A United European Astronomy  
by Catherine Cesarsky

## NEWS OF THE WEEK

- Senators Offer Sympathetic Ear to Complaints on NIH's Fiscal Slide 1646
- Mapping the 248-Fold Way 1647
- House OKs Whistleblower Bill 1649
- SCIENCE SCOPE** 1649
- New Bacterial Defense Against Phage Invaders Identified >> Report p. 1709 1650
- A Trace of the Earliest Plate Tectonics Turns Up in Greenland >> Report p. 1704 1650

## NEWS FOCUS

### Large Hadron Collider

- Having a Blast, Wish You Were Here 1652
- Stability, International Character Honed CERN's Competitive Edge 1654
- Physicists' Nightmare Scenario: The Higgs and Nothing Else 1657
- A Sluggish Response to Humanity's Biggest Mass Poisoning 1659
- A Young Scientist Shaped by Adversity



1659

## LETTERS

- The Loss of a Valuable Dolphin *M. D. Kass* 1663
- The Ethics of Transcranial Magnetic Stimulation  
*L. S. Jones* Response *D. Knoch, A. Pascual-Leone, E. Fehr*
- Comparing Neanderthal and Human Genomes  
*T. C. Erren, P. Cullen, M. Erren*  
Response *E. M. Rubin and J. P. Noonan*
- What the Scientific Community Can Do *H. S. Bienen*

## BOOKS ET AL.

- The Measure of Merit Talents, Intelligence, and Inequality in the French and American Republics, 1750–1940 *J. Carson*, reviewed by *A. S. Henderson* 1668
- The Great Lead Water Pipe Disaster 1669  
*W. Troesken*, reviewed by *R. Renner*

## POLICY FORUM

- Carbon Trading Over Taxes 1670  
*W. Chameides and M. Oppenheimer*

## PERSPECTIVES

- Balancing Cellular Energy 1671  
*D. G. Hardie*  
>> Report p. 1726
- How Does the Proton Spin? 1672  
*S. D. Bass*
- Asymmetry and Immune Memory 1673  
*D. R. Littman and H. Singh*  
>> Research Article p. 1687
- The Next Great Earthquake 1675  
*R. McCaffrey*
- A Plant Receptor with a Big Family 1676  
*E. Grill and A. Christmann*  
>> Report p. 1712
- Retrospective: Alan G. MacDiarmid (1927–2007) 1678  
*R. H. Baughman*



1668

CONTENTS continued >>



# RNAi solutions by QIAGEN

Knock down reliably

- Predesigned and validated siRNA
- Flexible, user-defined siRNA plates and sets
- Custom siRNA design and synthesis
- Matching siRNA and RT-PCR assays
- miRNA purification kits

Contact QIAGEN today or visit [www.qiagen.com/goto/RNAi](http://www.qiagen.com/goto/RNAi).



Sample & Assay Technologies





## SCIENCE EXPRESS

[www.scienceexpress.org](http://www.scienceexpress.org)

### MOLECULAR BIOLOGY

Control of Stress-Dependent Cardiac Growth and Gene Expression by a MicroRNA

*E. van Rooij et al.*

An miRNA coded within an intron of a myosin gene increases the maladaptive expression of embryonic myosin after stress.

10.1126/science.1139089

### GENETICS

Multiple High-Throughput Analyses Monitor the Response of *E. coli* to Perturbations

*N. Ishii et al.*

In maintaining metabolic homeostasis, bacteria respond to genetic disruptions with large changes in metabolites but to environmental disturbance with changes in enzyme levels.

10.1126/science.1132067

### PHYSICS

Negative Refraction at Visible Frequencies

*H. J. Lezec, J. A. Dionne, H. A. Atwater*

A thin waveguide composed of thin layers of gold, silicon nitride, and silver produces a negative index of refraction in the blue and green parts of the spectrum.

10.1126/science.1139266

### PLANETARY SCIENCE

The Variable Rotation Period of the Inner Region of Saturn's Plasma Disk

*D. A. Gurnett et al.*

Saturn's distinct radio emission, thought to reflect the trace of the actual rotation of the planet, instead is produced by convection in its plasma disk independent of its rotation.

10.1126/science.1138562

## TECHNICAL COMMENT ABSTRACTS

### ECOLOGY

Comment on "Why Are There So Many Species of Herbivorous Insects in Tropical Rainforests?" 1666

*D. A. Norton and R. K. Didham*

full text at [www.sciencemag.org/cgi/content/full/315/5819/1666b](http://www.sciencemag.org/cgi/content/full/315/5819/1666b)

Response to Comment on "Why Are There So Many Species of Herbivorous Insects in Tropical Rainforests?"

*V. Novotny et al.*

full text at [www.sciencemag.org/cgi/content/full/315/5819/1666c](http://www.sciencemag.org/cgi/content/full/315/5819/1666c)

## REVIEW

### ATMOSPHERIC SCIENCE

Restoration of the Mississippi Delta: Lessons from Hurricanes Katrina and Rita 1679

*J. W. Day Jr. et al.*



CREDIT (BOTTOM): EARTH SCAN LABORATORY, LOUISIANA STATE UNIVERSITY

## BREVIA

### EVOLUTION

Gene Co-Inheritance and Gene Transfer 1685

*Y. Brandvain, M. S. Barker, M. J. Wade*

Unexpectedly, in plant taxa that reproduce by self-pollination or cloning, more mitochondrial genes have shifted to the nucleus than in taxa that reproduce sexually.

### APPLIED PHYSICS

Far-Field Optical Hyperlens Magnifying Sub-Diffraction-Limited Objects 1686

*Z. Liu, H. Lee, Y. Xiong, C. Sun, X. Zhang*

A lens with a negative refractive index can magnify an object that is smaller than the diffraction limit of light and project it so it can be seen with a conventional microscope.

## RESEARCH ARTICLE

### IMMUNOLOGY

Asymmetric T Lymphocyte Division in the Initiation of Adaptive Immune Responses 1687

*J. T. Chang et al.*

Upon antigen binding, immune cells generate pathogen-fighting cells from daughters arising close to the antigen and memory cells from daughters away from it.

>> Perspective p. 1673

## REPORTS

### CHEMISTRY

Enhanced Bonding of Gold Nanoparticles on Oxidized TiO<sub>2</sub> (110) 1692

*D. Matthey et al.*

Interactions between gold and oxygen atoms cause gold clusters to adhere strongly to titanium oxide, perhaps helping to explain why gold nanoclusters are such good catalysts.

CONTENTS continued >>





# ACS AuthorChoice Free Access

## A NEW CHOICE FOR AUTHORS

For authors who wish or need to sponsor open access to their published research articles, you are encouraged to take advantage of the *ACS AuthorChoice* option. First launched in October 2006, *ACS AuthorChoice* provides a fee-based mechanism for individual authors or their research funding agencies to sponsor the open availability of their articles on the Web at the time of online publication.

Under this policy, the ACS as copyright holder enables unrestricted Web access to a contributing author's publication from the Society's website, in exchange for a fixed payment from the sponsoring author. Significant discounts are applied for contributing authors who are ACS members and subscribers. *ACS AuthorChoice* also enables such authors to post electronic copies of published articles on their own personal websites and institutional repositories for non-commercial scholarly purposes.

JOIN THE ACS <sup>Author</sup> CYCLE OF EXCELLENCE

*contribute* | *publish* | *review*

View more information about *ACS AuthorChoice* and a list of published *ACS AuthorChoice* articles at <http://pubs.acs.org/4authors/authorchoice>



ACS PUBLICATIONS  
HIGH QUALITY. HIGH IMPACT.



## REPORTS CONTINUED...

### PHYSICS

**An Atomic Seesaw Switch Formed by Tilted Asymmetric Sn-Ge Dimers on a Ge (001) Surface** 1696  
*K. Tomatsu et al.*

Changing the position of tin atoms incorporated into a germanium surface switches the electrical conductivity on or off along folds in the surface.

### APPLIED PHYSICS

**Magnifying Superlens in the Visible Frequency Range** 1699  
*I. I. Smolyaninov, Y.-J. Hung, C. C. Davis*

A lens formed from concentric circles of a polymer with positive and negative indices of diffraction on a gold film can resolve objects as small as 70 nanometers.

### CLIMATE CHANGE

**Coupled Thermal and Hydrological Evolution of Tropical Africa over the Last Deglaciation** 1701

*J. W. H. Weijers, E. Schefuß, S. Schouten, J. S. S. Damsté*  
During deglaciation, warming of tropical Africa relative to the Atlantic Ocean increased the land-sea thermal gradient and thus central African rainfall.

### GEOLOGY

**A Vestige of Earth's Oldest Ophiolite** 1704  
*H. Furnes et al.*

Remnants of oceanic crust formed at a spreading center 3.8 billion years ago are preserved in Greenland, implying that some form of plate tectonics was operating then. >> *News story p. 1650*

### ATMOSPHERIC SCIENCE

**Bottom-Up Determination of Air-Sea Momentum Exchange Under a Major Tropical Cyclone** 1707

*E. Jarosz, D. A. Mitchell, D. W. Wang, W. J. Teague*  
Direct observations reveal that the transfer of momentum by winds to ocean currents and waves is greatest just before a storm reaches hurricane strength.

### MICROBIOLOGY

**CRISPR Provides Acquired Resistance Against Viruses in Prokaryotes** 1709  
*R. Barrangou et al.*

Clustered, variable repeat sequences can be acquired by bacterial genomes from bacteriophage or plasmids and act like RNA interference to block infection by viruses. >> *News story p. 1650*

### PLANT SCIENCE

**A G Protein-Coupled Receptor Is a Plasma Membrane Receptor for the Plant Hormone Abscisic Acid** 1712

*X. Liu, Y. Yue, B. Li, Y. Nie, W. Li, W.-H. Wu, L. Ma*  
The cell surface receptor for an important growth regulator in plants binds to its ligand with high affinity and activates downstream targets. >> *Perspective p. 1676*

### CELL BIOLOGY

**Tunability and Noise Dependence in Differentiation Dynamics** 1716

*G. M. Süel et al.*  
A genetic circuit for bacterial cell differentiation exhibits a surprisingly varied repertoire of dynamic responses that depend on the amount of noise in the component biochemical reactions.

### NEUROSCIENCE

**Temporal Frequency of Subthreshold Oscillations Scales with Entorhinal Grid Cell Field Spacing** 1719

*L. M. Giocomo, E. A. Zilli, E. Fransén, M. E. Hasselmo*  
As rats move about, the oscillation frequencies of cortical neurons arrayed in a grid represent how neural activity maps the rat's position in space.

### NEUROSCIENCE

**Emergence of Novel Color Vision in Mice Engineered to Express a Human Cone Photopigment** 1723

*G. H. Jacobs, G. A. Williams, H. Cahill, J. Nathans*  
Mice engineered to express the human long-wavelength opsin in addition to its own two color vision pigments acquire a new ability to distinguish colors.

### STRUCTURAL BIOLOGY

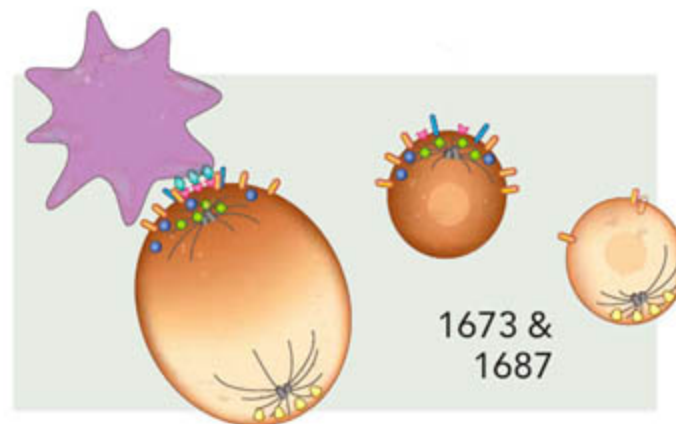
**Crystal Structures of the Adenylate Sensor from Fission Yeast AMP-Activated Protein Kinase** 1726

*R. Townley and L. Shapiro*  
The crystal structure of a key metabolic regulator reveals how it senses the ratio of ATP to AMP, initiating feedback processes to optimize ATP levels in the cell. >> *Perspective p. 1671*

### STRUCTURAL BIOLOGY

**Structure of Nup58/45 Suggests Flexible Nuclear Pore Diameter by Intermolecular Sliding** 1729

*I. Melčák, A. Hoelz, G. Blobel*  
Pores in the nuclear envelope consist of tetramers with a variable lateral offset that may allow the opening to be adjusted according to the size of molecules passing through.



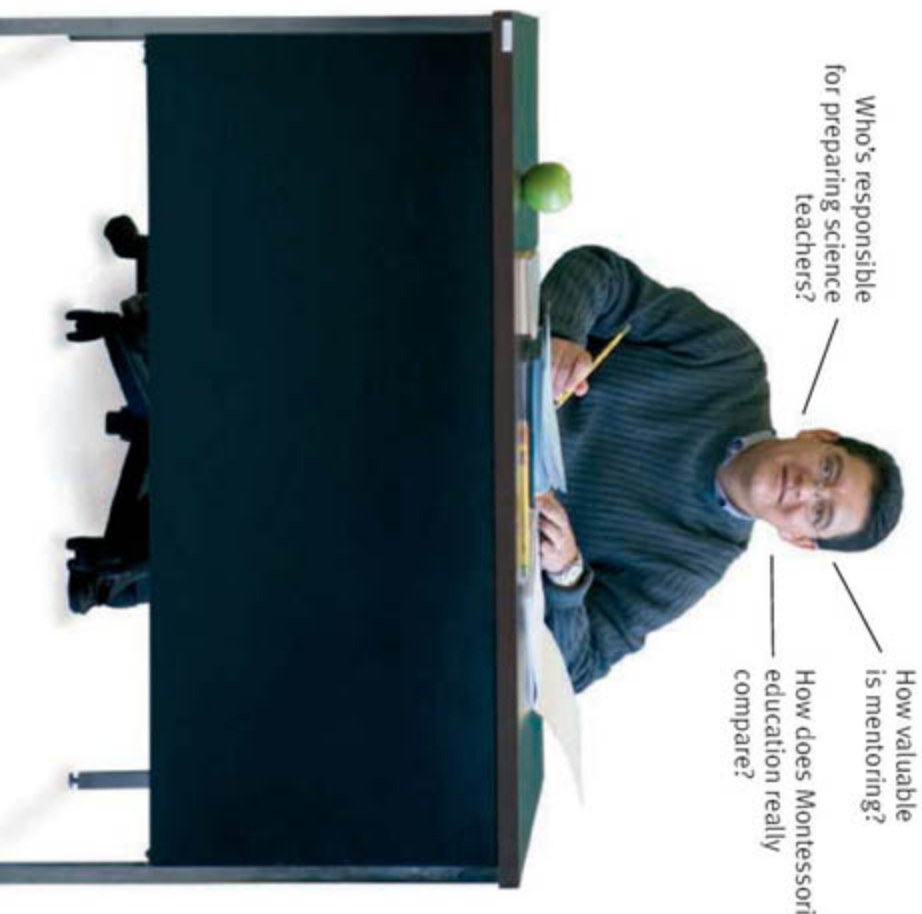
SCIENCE (ISSN 0036-8075) is published weekly on Friday, except the last week in December, by the American Association for the Advancement of Science, 1200 New York Avenue, NW, Washington, DC 20005. Periodicals Mail postage (publication No. 484460) paid at Washington, DC, and additional mailing offices. Copyright © 2007 by the American Association for the Advancement of Science. The title SCIENCE is a registered trademark of the AAAS. Domestic individual membership and subscription (\$1 issues): \$142 (\$74 allocated to subscription). Domestic institutional subscription (\$1 issues): \$710; Foreign postage extra: Mexico, Caribbean (surface mail) \$55; other countries (air assist delivery) \$85. First class, airmail, student, and emeritus rates on request. Canadian rates with GST available upon request, GST #1254 88122. Publications Mail Agreement Number 1069624. Printed in the U.S.A.

Change of address: Allow 4 weeks, giving old and new addresses and 8-digit account number. Postmaster: Send change of address to AAAS, P.O. Box 96178, Washington, DC 20090-6178. Single-copy sales: \$10.00 current issue, \$15.00 back issue prepaid includes surface postage; bulk rates on request. Authorization to photocopy material for internal or personal use under circumstances not falling within the fair use provisions of the Copyright Act is granted by AAAS to libraries and other users registered with the Copyright Clearance Center (CCC) Transactional Reporting Service, provided that \$18.00 per article is paid directly to CCC, 222 Rosewood Drive, Danvers, MA 01923. The identification code for Science is 0036-8075. Science is indexed in the Reader's Guide to Periodical Literature and in several specialized indexes.

CONTENTS continued >>



# Fresh angles on the science of education



## A wealth of knowledge

The *Science Education Forum* is a dynamic source of information and new ideas on every aspect of science education, as well as the science and policy of education. The forum is published in the last issue of every month and online, in collaboration with the Howard Hughes Medical Institute.

Keep up-to-date with the latest developments at [www.sciencemag.org/education](http://www.sciencemag.org/education)

### What's your perspective?

Do you have ideas or research you'd like to share in the *Science Education Forum*? We're now looking for thoughtful, concise submissions (around 2,000 words) for 2007. To submit your paper, go to [www.submit2science.org](http://www.submit2science.org)







Nuthatches (right) eavesdrop on chickadees (left).

## SCIENCE NOW

[www.sciencenow.org](http://www.sciencenow.org) DAILY NEWS COVERAGE

### Danger in the Air

Nuthatches profile approaching predators by decoding another bird's alarm call.

### Mosquitoes Made Better in the Lab

Malaria-resistant insects may help keep the disease from humans.

### Rabbits Shed Light on Virus's Origins

'Fossil' lentivirus could provide clues to evolution of HIV and other related retroviruses.



Maximizing your conference experience.

## SCIENCE CAREERS

[www.sciencecareers.org](http://www.sciencecareers.org) CAREER RESOURCES FOR SCIENTISTS

### GLOBAL: Mastering Your Ph.D.—Your First Conference Experience

*B. Noordam and P. Gosling*

Find out how to make the most of your first scientific sojourn.

### US: A 'Comprehensive' Career

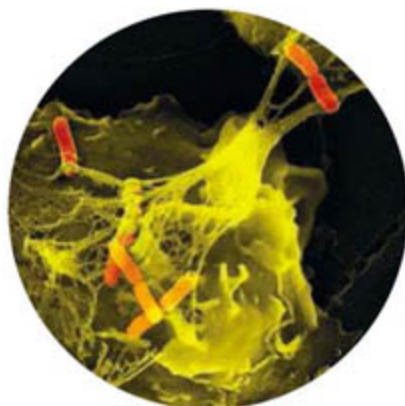
*S. Webb*

Faculty members at smaller public colleges find ways to pursue scholarship with heavy teaching loads.

### US: A Question of Balance

*A. Sasso*

Joan Brenner Coltrain built a rewarding career in anthropology—and on her own terms.



Trapping bacteria in NETs.

## SCIENCE'S STKE

[www.stke.org](http://www.stke.org) SIGNAL TRANSDUCTION KNOWLEDGE ENVIRONMENT

### PERSPECTIVE: Unconventional Roles of the NADPH Oxidase—Signaling, Ion Homeostasis, and Cell Death

*B. E. Steinberg and S. Grinstein*

Phagocytic NADPH oxidase contributes to various neutrophil processes including the formation of neutrophil extracellular traps (NETs).

### EVENTS

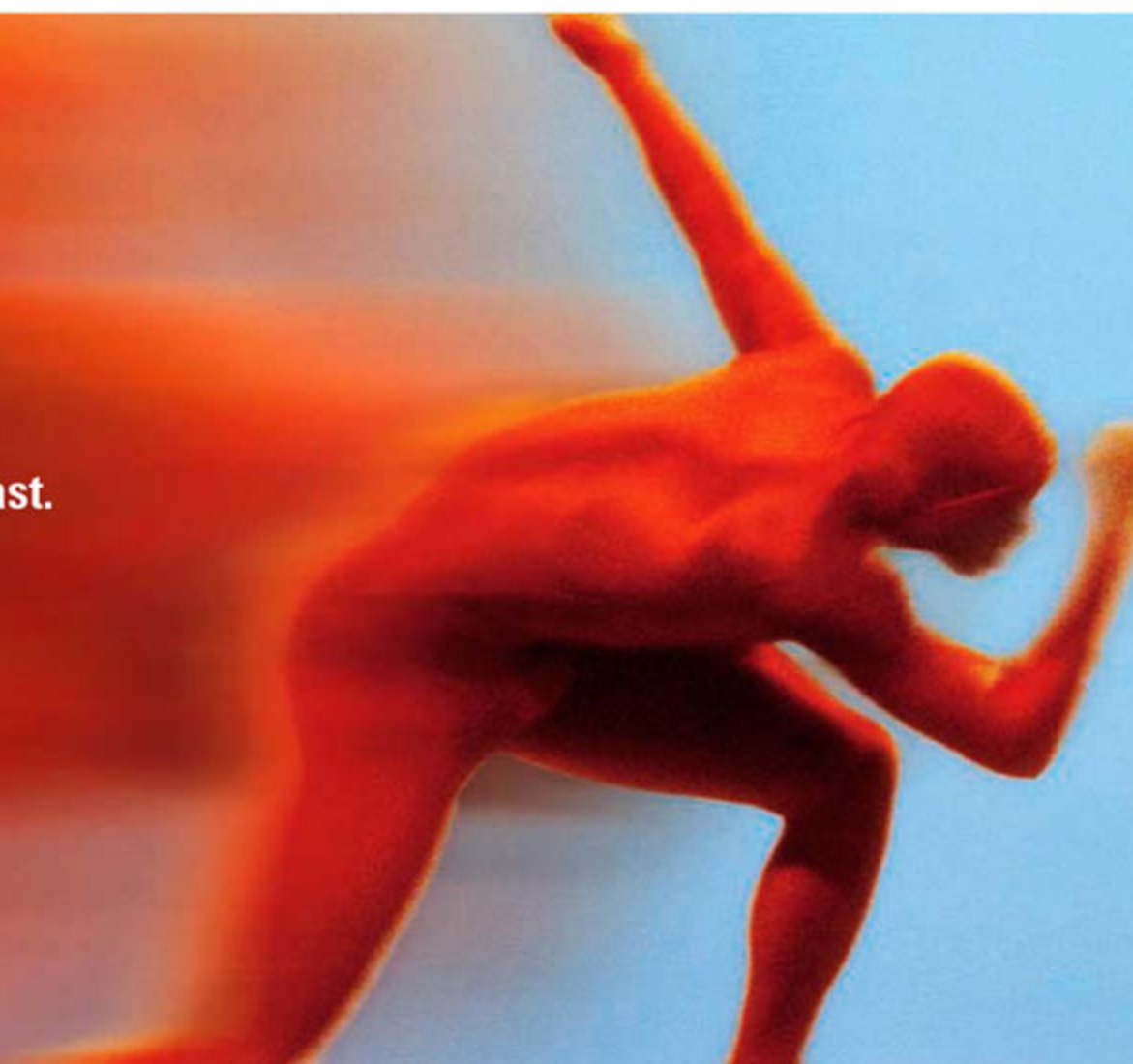
Plan to attend one of the more than 30 upcoming meetings related to cell signaling.

Separate individual or institutional subscriptions to these products may be required for full-text access.





in a word, fast.







## Phusion™ High-Fidelity DNA Polymerase from New England Biolabs

EXTREME PRECISION WITH UNPARALLELED SPEED AND ROBUSTNESS

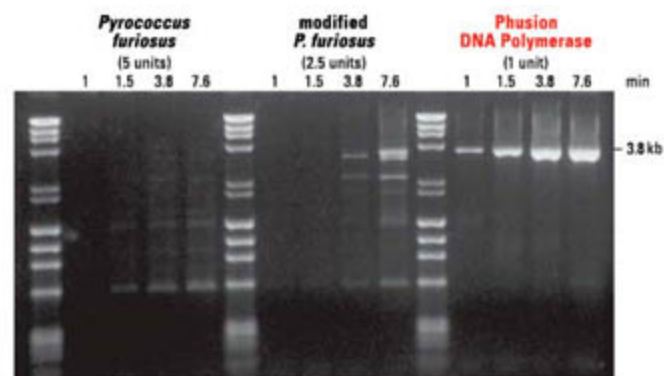
With Phusion High-Fidelity DNA Polymerase, there is no need to compromise any aspect of your PCR performance. A superior choice for cloning, this recombinant polymerase has an error rate 50-fold lower than *Taq* DNA Polymerase, making it the most accurate thermostable polymerase available. Phusion DNA Polymerase is supplied in a variety of formats, or with a **hot start modification** for increased specificity.

### Advantages:

- Extreme Fidelity – Highest of any thermostable polymerase
- High Speed – Extension times are dramatically reduced
- Robustness – Reduce reaction failures with minimal optimization
- High Yield – Increase product yields with minimal enzyme amounts
- Specificity – Hot start modification reduces non-specific amplification

- **Phusion High-Fidelity DNA Polymerase**  **F-530S/L**
- **Phusion Hot Start High-Fidelity DNA Polymerase**  **F-540S/L**
- **Phusion High-Fidelity PCR Master Mix with HF Buffer with GC Buffer**  **F-531S/L**  
**F-532S/L**
- **Phusion High-Fidelity PCR Kit**  **F-553S/L**

 = Recombinant



Experience extreme speed and yield with Phusion High-Fidelity DNA Polymerase. A 3.8 kb fragment from human beta globin gene was amplified according to suppliers' recommendations using varying extension times. Phusion DNA Polymerase was able to amplify the fragment with a combined annealing and extension step of only 1 minute. Also, a single unit of Phusion DNA Polymerase produced higher yields than 2.5 or 5 units of *Pyrococcus furiosus* DNA Polymerases.

Phusion™ is a trademark of Finnzymes Oy

For more information please visit [www.neb.com](http://www.neb.com)

- **New England Biolabs Inc.** 1-800-NEB-LABS Tel. (978) 927-5054 Fax (978) 921-1350 [info@neb.com](mailto:info@neb.com)
- **Canada** Tel. (800) 387-1095 [info@ca.neb.com](mailto:info@ca.neb.com)
- **Germany** Tel. 0800/246 5227 [info@de.neb.com](mailto:info@de.neb.com)
- **UK** Tel. (0800) 318486 [info@uk.neb.com](mailto:info@uk.neb.com)
- **China** Tel. 010-82378266 [beijing@neb-china.com](mailto:beijing@neb-china.com)

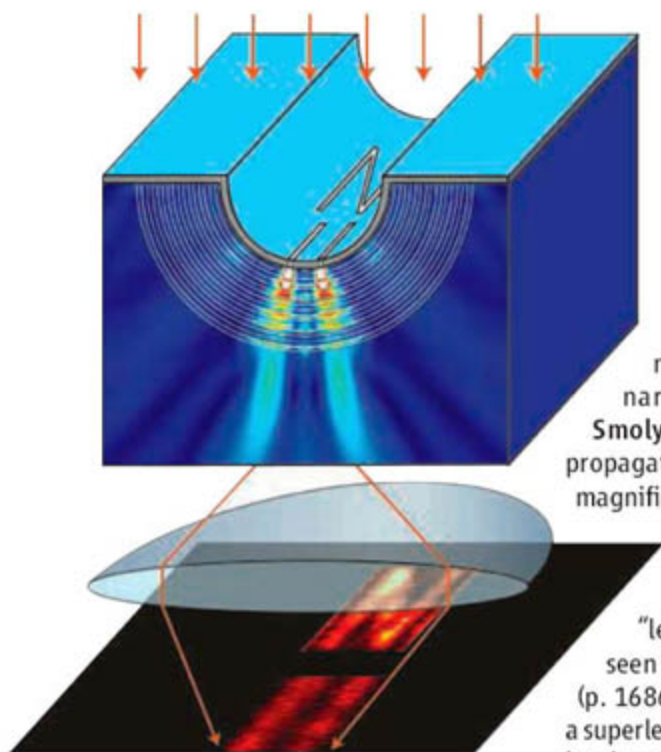
Produced by



Distributed by







## << Magnifying Superlenses

Although the spatial resolution of a conventional optical microscope is limited by diffraction to a value of the order of 200 nanometers, a “superlens” based on specially structured metamaterials designed to exhibit a negative refractive index could overcome this limitation. However, the planar superlenses demonstrated to date cannot provide magnification. Smolyaninov *et al.* (p. 1699) describe a magnifying superlens based on the propagation of surface-plasmon polaritons (SPP). The object to be imaged and magnified is placed inside the center region of their lens, a structure of concentric circles of a polymer deposited on a gold substrate. The light scatters off the object and creates SPPs in the gold film. With the structured lens designed properly, the SPPs propagate radially outward through the “lens” of concentric circles. The magnified image of the object can then be seen at the outermost circle with a conventional microscope. In Brevia, Liu *et al.* (p. 1686) have used curved nanoscale multilayers of silver and alumina to create a superlens that projects the image of an object onto a far-field surface, where it can be viewed with a conventional microscope.

## A Tin Toggle Switch

Although changes in bonding should affect the conductivity of atomic and molecular scale wires, direct evidence for switching between conducting and insulating configuration of atoms has been rare. Tomatsu *et al.* (p. 1696), using scanning tunneling microscopy (STM), show that when tin (Sn) atoms are deposited on the (001) of germanium (Ge) surface, they incorporate into the topmost rows of buckled Ge dimers that form one-dimensional conductors. The STM tip can be used to switch the Sn atom from being the “up” or “down” atom of these asymmetric dimers. When the Sn atom is up, the row remains conducting, but when it is switched down, it reflects electrons in the  $\pi^*$  state and terminates the wire.

## Tropical African Rain Records

A wealth of marine sedimentary records have been used to document changes in sea surface temperatures (SSTs) between the Last Glacial Maximum 25,000 years ago and the present warm period, the Holocene. The construction of continental records of land surface temperature for the same interval has been more challenging, particularly for tropical Africa. Weijers *et al.* (p. 1701) have now analyzed terrestrial and marine biomarkers in a marine sedimentary record from near the mouth of the Congo River and developed parallel records of terrestrial and nearby oceanic conditions that facilitated the comparison of conditions in the two regimes. Tropical African land temperatures rose by about

4°C during the last deglaciation, approximately twice the amount that nearby SSTs rose. This changing land-sea temperature difference exerted an important control on precipitation patterns in central Africa.

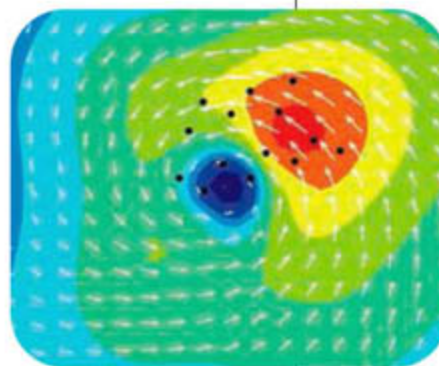
## Damaging Winds and Waves

In 2005, a pair of strong hurricanes (Katrina and Rita) struck near the mouth of the Mississippi River a few weeks apart. Day *et al.* (p. 1679) show that their slightly different tracks provide comparative information for assessing the reasons for the damage and flooding of New Orleans and other regions, and also evaluate what needs to be done to rebuild the region for greater resiliency in the future. Hurricanes create damaging storm surges and high waves by transferring wind energy to the sea surface. The magnitude of this transfer normally is estimated from observations of the surface wind fields in a storm, but that approach suffers from artifacts caused by the presence of waves and ocean spray, and is highly uncertain for the high-wind regimes of major tropical cyclones. Jarosz *et al.* (p. 1707) used full water-column ocean-current velocity data collected during the passage of

Hurricane Ivan in 2004 to determine this air-sea momentum transfer directly from the water side. The efficiency of energy transfer has a maximum at a wind speed of around 72 miles per hour (just under hurricane category 1 levels), which decreases to around half of that value once the hurricane reaches the transition from category 2 to category 3 strength at wind speeds of 111 miles per hour. These findings should help improve forecasts of storm track and intensity, as well as those of the associated ocean waves, surges, and tides.

## Dating Crust Creation

The Earth’s crust is continually being formed at mid-ocean spreading ridges, where plates roll apart, and above subduction zones, where plate edges can grow by accretion. Was the creation of crustal plates ongoing early in the Earth’s history, or was it restricted to the latter half of the Earth’s 4.5 billion year existence? Furnes *et al.* (p. 1704; see the news story by Kerr) show that crustal formation caused by seafloor spreading was under way as long ago as 3.8 billion years. They have identified and dated an ophiolite sequence of rocks in Greenland that is the oldest known example of oceanic crust. The sequence of rocks includes gabbro, pillow lavas, and sheeted dikes, indicating it was formed on the sea floor by processes similar to those seen today.



*Continued on page 1635*



## METABOLIC DISEASE MODELS



**Insulin  
resistance**

**Obesity**

**Nephropathy**

**Type 2  
diabetes**

Charles River offers a series of rat disease models useful in Metabolic Disease research. Please contact us for additional information, including baseline data and availability. Control data is also on our web site.

US: 1.877.CRIVER.1  
Europe: info@eu.crl.com  
WWW.CRIVER.COM

  
**CHARLES RIVER**  
LABORATORIES  
*Research Models and Services*

Get the experts behind you.

[www.ScienceCareers.org](http://www.ScienceCareers.org)



- Search Jobs
- Next Wave now part of ScienceCareers.org
- Job Alerts
- Resume/CV Database
- Career Forum
- Career Advice
- Meetings and Announcements
- Graduate Programs

All these features are **FREE** to job seekers.

**ScienceCareers.org**  
We know science 

*IBC's 2nd Annual International Conference and Exhibition*

# Drug Discovery and Development Partnering, Licensing and R&D Innovation Summit

*Building Your Drug Candidate Pipeline through Global Alliances,  
Compound Acquisitions and Innovative R&D*

**April 25-27, 2007 • Tower Hall Funabori • Tokyo, Japan**

*The ONLY international conference in Japan providing multiple speaker case studies of successful international alliances and R&D strategies PLUS themed networking events to help you find partners and meet new companies from Japan, USA, Europe and Asia.*

*250+ attended  
our 2006 event!*

- Benefit from Case Studies on How to Successfully Bring Your Products to Market in Japan and Globally
- Examine Japan's Industry Evolution and Marketing/Partnering Opportunities to Enhance Your Global Strategies
- Meet New Companies at the Drug Candidate/Technology Showcase and Alliance Strategy Session
- Learn How to "Globalize" Your R&D Efforts in Asia and Around the World
- Find Partners in Themed Sessions on Antibodies/Biologics, RNAi and PGx

*In Association with:*



*Produced by the Organizers of:*



[www.IBCLifeSciences.com/Japan](http://www.IBCLifeSciences.com/Japan)

Tel: (+65) 6835-5136 • Fax: (+65) 6733-5087 • E-mail: [enquiry@ibcasia.com.sg](mailto:enquiry@ibcasia.com.sg)

**J  
A  
P  
A  
N**



Continued from page 1633

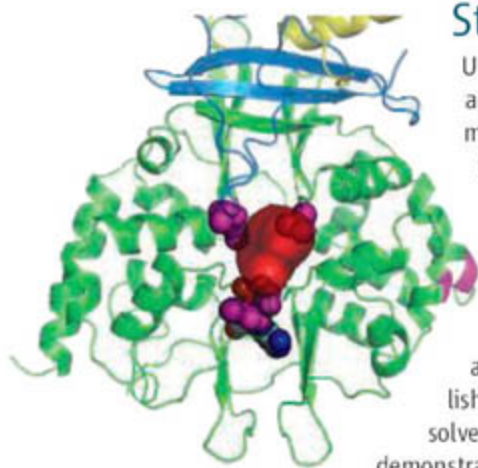
## Division Decisions

During an immune reaction, T cells divide rapidly and differentiate producing a variety of T cell types that respond appropriately to the particular threat. Memory T cells also emerge from the same population and remain in the body until such time as a new infection calls once again for their attention.

**Chang et al.** (p. 1687, published online 1 March; see the Perspective by **Littman and Singh**) now show that single T cells undergo an initial asymmetric cell division in response to a pathogen, producing two daughter cells with alternate fates. After forming an immune synapse with an antigen-presenting cell (APC), various proteins, including some responsible for signaling and asymmetric cell division, were reoriented within the T cells. After division, daughters that were proximal to the APC–T cell synapse became effector cells, while their distal sisters became more memory-like and able to confer better protection when transferred to mice.

## The Final Crunch

Regular clusters of repeats separated by spacers of similar length (CRISPR) are widely distributed in the genomes of Bacteria and Archaea, and are distinctively hypervariable. The spacers share sequence homology with bacteriophage and plasmid sequences, and may provide immunity against foreign genetic elements via RNA interference. During the natural generation of phage-resistant *Streptococcus thermophilus* using lytic phage obtained from yogurt, **Barrangou et al.** (p. 1709; see the news story by **Marx**) found that the integration of viral sequences as new spacers into CRISPR loci indeed confers immunity against virulent phages in a specific, acquired, and heritable manner. Addition and deletion of spacers alters sensitivity to viruses, and CRISPR-associated genes may be directly involved in the resistance mechanism.



## Staying in Charge

Under normal conditions, the intracellular concentration of adenosine triphosphate (ATP) is on the order of 1 millimolar. Numerous enzymes and regulatory proteins rely on this universal currency of energy for anabolic, catabolic, and general housekeeping processes. One of the primary enzymes that regulates ATP levels is the AMP-activated protein kinase (AMPK), which senses the relative ratio of ATP to AMP. When this ratio falls, AMPK phosphorylates metabolic enzymes, which then consume less ATP and make more of it. **Townley and Shapiro** (p. 1726, published online 8 February; see the Perspective by **Hardie**) have solved the structure of the fission yeast AMPK homolog and demonstrate the competitive binding of ATP and AMP at a single

nucleotide site, where the absence of counterions appears to amplify the discrimination between the mono- and triphosphate ligands.

## Plant Hormone Signaling Receptor

The hormone abscisic acid (ABA) regulates a variety of developmental and physiological processes in higher plants. **Liu et al.** (p. 1712, published online 8 March; see the Perspective by **Grill and Christmann**) have now identified a membrane-bound protein that functions as an ABA receptor. The protein, GCR2, has features of a G protein-coupled receptor, which have thousands of variants in animal cells, but very few known variants in plant cells.

## Diameter Modulators of the Nuclear Pore

The nuclear pore complex (NPC) controls the exchange of molecules between the cytoplasm and the nucleus. This supramolecular assembly is composed of a set of proteins termed nucleoporins (nups). **Melčák et al.** (p. 1729) describe the structure of a complex of nup58 and nup45, which are essential components of the central channel of the NPC. The two nucleoporins form stable dimers that further associate into tetramers. Two crystal forms contained four conformers of the tetramer, which differed in the lateral offset between dimers. Thus, these nucleoporins may have dynamic interaction interfaces, and slide relative to each other in order to adjust the diameter of the transport channel to the size of the cargo.

CREDIT: TOWNLEY AND SHAPIRO

## Who inspires brainwaves while I study water waves?



“ I study the mathematical equations that describe the motion of water waves. Different equations represent different waves – waves coming onto a beach, waves in a puddle, or waves in your bathtub. Then when I’ve surfed the math, I like nothing better than to spend the rest of the day surfing the waves.

This field is very important. The better we can model water waves, the better we can predict the patterns of beach erosion and natural disasters.

Being a member of AAAS means I get to learn about areas of interest I might not otherwise encounter. It gives me valuable opportunities to exchange ideas with colleagues in other fields. And this helps me find new approaches to my own work. ”

Dr. Katherine Socha is an assistant professor of mathematics at St. Mary's College, Maryland. She's also a member of AAAS.

See video clips of this story and others at [www.aaas.org/stories](http://www.aaas.org/stories)





# Looking for solid ground in the ever-changing landscape of science & technology policy and budget issues?

Join the nation's top S&T experts at the 32nd Annual AAAS Forum on Science & Technology Policy  
3-4 May 2007 • Washington DC  
International Trade Center in the  
Ronald Reagan Building



The AAAS Forum on Science and Technology Policy provides a setting for discussion and debate about the federal budget and other policy issues facing the science, engineering, and higher education communities. Initiated in 1976 as the AAAS R&D Colloquium with about 100 participants, the Forum has emerged as the major public meeting in the U.S. devoted to science and technology policy issues. It annually draws upwards of 500 of the nation's top S&T policy experts.

- Get a full analysis of the President's federal R&D funding proposals.
  - Have an opportunity to meet directly with key S&T policymakers.
  - Learn how the changes in Congress are affecting S&T policy issues.
  - Network with colleagues, including top decisionmakers in science and technology policy from all sectors.
  - Learn about broader national and international developments that will affect strategic planning in universities, industries, and government.
- Registrants will receive, at the Forum, *AAAS Report XXXII: Research and Development, FY 2008*, a comprehensive analysis of the proposals for the FY 2008 budget, prepared by AAAS and a group of its affiliated scientific, engineering, and higher education associations.

For more complete details on the program, hotel registration and on-line registration, please visit the website: [www.aaas.org/forum](http://www.aaas.org/forum).



[www.aaas.org/forum](http://www.aaas.org/forum)





Catherine Cesarsky is director general of the European Southern Observatory and president of the International Astronomical Union.

## A United European Astronomy

AT A TIME WHEN THE POLITICAL VISION OF EUROPE IS STRUGGLING TO REGAIN FOCUS AND momentum, European astronomers are working together more than ever on new projects. Despite the fact that modern astronomy emerged from the European Renaissance, the continent's lead crumbled in the 20th century. At that time, visionary minds in the United States exploited large economic fortunes to construct great observatories that opened a new window onto the distant universe. Europe, recovering from the world wars, was unable to compete when the United States launched its overwhelmingly comprehensive space program in the 1950s and 1960s. But today, the American and European situations in astronomy are more balanced, and European astronomers look toward the future with renewed optimism, even though they are well aware that, given the cost of projects and the available funds, hard choices will have to be made.

One important reason for the European resurgence is that farsighted scientific and political leaders created the European Southern Observatory (ESO) in 1962 to develop observatories in the Southern Hemisphere. Somewhat later, the European Space Agency (ESA) embarked on a well-planned program of space missions. An important advantage of these intergovernmental organizations is that they can rely on a stable budget, year after year. Despite a budget less than one-fifth that of the U.S. National Aeronautics and Space Administration (NASA), ESA has launched successful missions with well-chosen goals, such as the Hipparcos satellite and the Infrared Space Observatory. On the ground, ESO's flagship, the Very Large Telescope in Chile, has achieved recognition as the world's most powerful optical telescope, providing a wealth of data on objects ranging from the solar system to the farthest reaches of the universe. As a result, ESO has attracted new member states, with consequential increases in the budget and in collaborating institutions. Considerable human exchange and networking, often fostered by the European Union (EU), have resulted in several bilateral or multilateral undertakings within and beyond Europe. The result has been an equalizing of competition that has enhanced, rather than hindered, ties across the Atlantic. ESA has long worked in partnership with NASA (although the relationship was not always easy). On the ground, Europe, North America, and East Asia are now involved in constructing ALMA, a world-class array of telescopes to explore the cold universe. ESO is leading the European efforts, putting its expertise in managing large-infrastructure projects at the disposal of submillimeter radio astronomy.

European astronomy is now considering its future. ESA's community has established an ambitious inventory of scientific opportunities in space astronomy and planetology in the 2015–2025 time frame, called "Cosmic Vision." ESA has just issued a call for proposals for the program's first space exploratory missions. ESO and its community are conducting studies on the European Extremely Large Telescope, a novel design for the world's largest optical/infrared telescope, which will revolutionize ground-based astronomy. Its target for construction is 2010. European radio astronomers, boosted by Europe's Low Frequency Array project, are heavily involved in forging a future worldwide project, the Square Kilometer Array (to be sited in Australia or South Africa). The high cost of such new projects, and the universality of science, have encouraged astronomers from both sides of the Atlantic to form partnerships with astronomers from other continents of the world, an effort that is further supported by the International Astronomical Union.

To achieve even greater unity, the funding agencies of various European countries have come together with ESO and ESA in an EU-sponsored network, ASTRONET, to establish a road map for the next 20 years that will encompass ESO and ESA programs and foster collaborations among European countries in other endeavors. Major organizations such as ESA and ESO are able to pool and retain critical mass, with respect to both human and financial resources, over long periods of time. Of equal importance is that, as public bodies, they must serve the community. This provides a powerful impetus for excellence in the ways in which they operate. It also ensures constant upgrading of facilities to remain competitive. If Europe's global agenda includes keeping astronomy at the forefront, maintaining the unity of European organizations and their missions will be vital.

— Catherine Cesarsky

10.1126/science.1141963





**GEOLOGY**

## Diamond Diversity

The chemistry of diamonds brought up from Earth's mantle—notably their widely ranging nitrogen contents and nitrogen and carbon isotope values—has complicated understanding of their origins. It is commonly thought that many diamonds form from the movement of carbon-rich fluids into deep mantle rocks of a contrasting composition, thereby inducing diamond precipitation. To better constrain these fluids and sources, Thomassot *et al.* studied in detail nearly 60 diamonds contained within one small (<30 cm<sup>3</sup>) mantle sample carried to the surface in a kimberlite volcano in South Africa. Surprisingly, the nitrogen contents and isotopic values of these diamonds in this one sample spanned a large part of the ranges observed from all diamonds worldwide. The covariations of the data imply that these diamonds formed from a methane-rich fluid, not a more oxidized fluid as commonly assumed. The wide variation can be produced by the fractionation of nitrogen and carbon during growth of the diamonds over time. Such fluids may also account for the variable oxidation state of the mantle beneath Earth's most ancient crust. — BH



*Earth Planet. Sci. Lett.* 10.1016/j.epsl.2007.02.020 (2007).

**BIOCHEMISTRY**

## Activating En Passant

Autotransporters are a family of bacterial virulence proteins that are first translocated across the inner membrane and then inserted into the outer membrane. The smaller C-terminal domain adopts a  $\beta$  barrel structure that spans the outer membrane and serves as a transitway for the larger N-terminal "passenger" domain, which is transported through the barrel; some passenger domains are released into the extracellular space by proteolysis.

In an extensive series of genetic and biochemical experiments, Dautin *et al.* show that the passenger domain of *Escherichia coli* autotransporter EspP is cleaved in an unusual fashion: not by a periplasmic or outer membrane protease, but by itself. Enzymatic hydrolysis of a peptide bond is customarily initiated by an activated nucleophile. Like the classical serine protease catalytic triad, where the carboxylate of an aspartate residue pulls on the hydroxyl proton of the active-site serine (via an intermediary histidine), EspP also uses an aspartate, which happens to reside on the inner surface of the  $\beta$  barrel and is located roughly halfway across the thickness of the outer membrane. This carboxylate pulls on the amide proton of an asparagine residue in the transiting passenger domain; this activates the amide nitrogen for attack on and cleavage of the peptide backbone, yielding a succinimide that could be resolved as a mixture of asparagine and iso-asparagine. This asparagine-aspartate self-cleav-

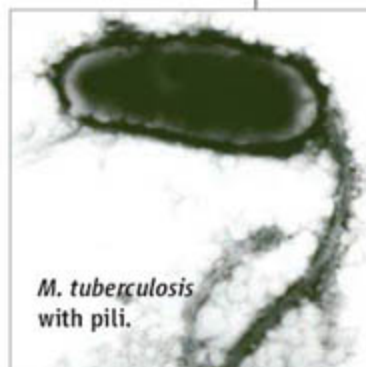
ing mechanism appears to be utilized by other autotransporters as well as by eukaryotic viruses during capsid maturation. — GJC

*EMBO J.* 26, 10.1038/sj.emboj.7601638 (2007).

**MICROBIOLOGY**

## At the Point of Attack

Tuberculosis kills approximately 3 million people each year. The pathogenic agent *Mycobacterium tuberculosis* invades and replicates within macrophages, constructing for itself an intracellular vacuole that shelters it from immune surveillance and attack. Alteri *et al.* have investigated how *M. tuberculosis* binds to and invades potential host cells. On the surface of the microbe, they discovered fine fibers, referred to as pili, that are 2 to 3 nm wide and are likely to be important in enabling the microbe to adhere to target cells. They isolated the pili and have characterized their composition using mass spectrometry and immunochemistry. The pili are assembled from low-molecular-weight protein subunits; these bind to the protein laminin, which is an abundant component of the extracellular matrix within human tissues. Furthermore,



*M. tuberculosis* with pili.

the sera of tuberculosis patients contained antibodies that recognized the pilin subunit. The unanticipated identification of what may represent a key protein in the early stages of host colonization by *M. tuberculosis* may lead to the development of new therapies and vaccines. — SMH

*Proc. Natl. Acad. Sci. U.S.A.* 104, 5145 (2007).

**CHEMISTRY**

## Sorting Storage Options

In the search for a practical mode of hydrogen storage for vehicle applications, light metal hydride compounds such as LiBH<sub>4</sub> are appealing because of their high weight percentage of hydrogen. However, many such compounds are thermodynamically quite stable, and so require excessive heating to liberate H<sub>2</sub>. One means of addressing this problem is to mix together two or more hydride compounds which, on releasing hydrogen, can form a stable co-product that drives the reaction—MgH<sub>2</sub>, for example, reacts with LiBH<sub>4</sub> to yield MgB<sub>2</sub>. Alapati *et al.* have used plane wave density functional theory in an effort to narrow the dauntingly large range of potential compound combinations worth exploring in this vein. Specifically, they performed a rough energy calculation of 152 known light metal solids and used the results to screen more than

CREDITS (TOP TO BOTTOM): DAVE G. HOUSER/CORBIS; ALTERI ET AL., PROC. NATL. ACAD. SCI. U.S.A., 104, 5145 (2007)



300 unreported possible reactions among them. Thirteen reactions that fell within a promising range of enthalpies (including a lower as well as upper bound, so as to ensure feasible rehydrogenation of the material) were then subjected to more computationally intensive phonon density-of-states calculations. The authors note that their approach is limited by the assumption of reaction to a known morphology and also leaves open the question of favorable kinetics. Nonetheless, computed enthalpies of known reactions proved sufficiently accurate (within 10 kJ/mol of experiment) to offer a promising preliminary sifting mechanism for guiding future experiments. — JSY

*Phys. Chem. Chem. Phys.* **9**, 10.1039/b617927d (2007).

## BIOMEDICINE

## Natural Sunblock

Before the health hazards of ultraviolet (UV) light exposure were fully appreciated, sun worshippers applied lotions hoping to tan rather than burn. Skin tanning results from the production of the pigment melanin, which absorbs UV radiation and can partially protect cells from the UV-induced DNA damage that can ultimately cause skin cancer. Without melanin, cells are highly susceptible to sunlight; sunburn is the body's response to this damage.

Cui *et al.* show that the tumor suppressor p53, which functions as a transcription factor and is one of the most intensely studied proteins in biology, plays a crucial role in UV-induced melanin production. Studying p53-deficient mice as well as normal human skin samples, they find that UV light activates p53 in skin keratinocytes (the outermost cells) and that p53 activates the gene encoding pro-opiomelanocortin (POMC). The POMC protein is then cut in several places to generate peptides, including  $\alpha$ -melanocyte-stimulating hormone, which stimulates melanocytes (cells located at the base of the epidermis) to produce melanin. Interestingly, POMC proteolysis also generates the opioid peptide  $\beta$ -endorphin, which the authors speculate might contribute to sun-seeking behavior in humans. — PAK

*Cell* **128**, 853 (2007).

## PSYCHOLOGY

## An Empathy Block

Everyday experience confirms the general belief that humans are social animals; the neural pathways subserving prosocial behaviors are a subject of current research, and the evolutionary origins of these behaviors are hotly debated. Although there is evidence that social exclusion can elicit redoubled efforts to develop social

connections, the consequences of exclusion are predominantly negative—feeling hurt, acting belligerently, or adopting a lone-wolf lifestyle—and Twenge *et al.* have begun to examine what might mediate these apparently atypical responses.

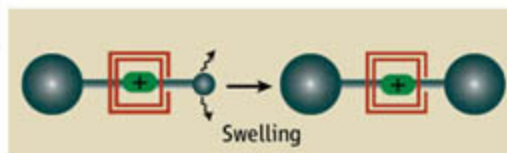
Using a variety of experimental contexts (such as the canonical spilled-pencils incident) and measures (such as donations of money or cooperation in a prisoner's dilemma game), they find that being characterized as having a high likelihood of a prosocial lifestyle with many strong relationships, such as marriage, resulted in participants helping to pick up pencils (on average, 8 out of 20 spilled) versus the performance of those labeled as being apt to lead solitary lives (less than 1 pencil picked up). As to what factors mediate the extent (or absence) of prosocial behavior, some of the likely candidates (trusting the other or having a sense of belonging) did not register, whereas empathic concern did. Combining this finding with an earlier one, which showed that social exclusion activates the neural circuits encoding pain, produces the speculation that an after-effect of rejection is an emotional numbness or an inability to mirror the affective states of others. — GJC

*J. Pers. Soc. Psych.* **92**, 56 (2007).

## CHEMISTRY

## A Swell Stopper

In rotaxane molecules, macrocycles are held onto rodlike cores by bulky end groups that effectively act as stoppers. Rotaxane synthesis usually requires first threading an open-ended rod through the cycle, followed by the addition

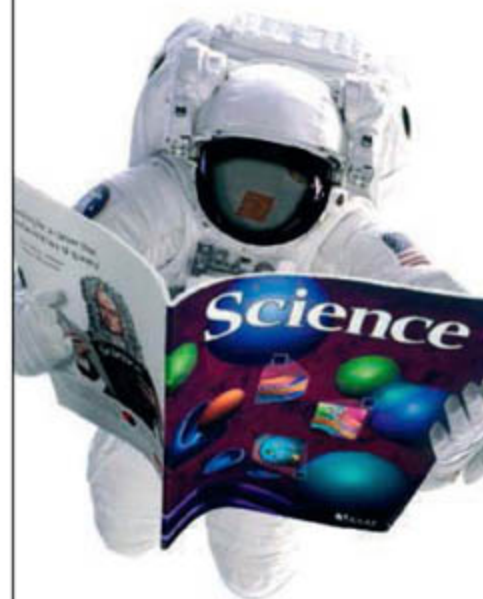


of a third molecule to the free end of the rod in order to form the second stopper. Chiu *et al.* present a two-component system in which an enyl-2-vinylcyclopropane end group of the rodlike molecule "swells" after the macrocycle has been threaded. A Cope rearrangement that is slow at room temperature occurs after 2 days of heating at 50°C, creating a bulky cycloheptadiene capping group. Hydrogenation of the racemic product mixture yields a single saturated isomer for the rodlike molecule. The authors demonstrate the technique with two different macrocycles, confirming by nuclear magnetic resonance spectroscopy that the rods and rings successfully interlock. — PDS

*J. Am. Chem. Soc.* **129**, 10.1021/ja069362i (2007).

## From life on Mars to life sciences

For careers in science, turn to *Science*



If you want your career to skyrocket, visit ScienceCareers.org. We are committed to helping you find the right job, and delivering useful advice. Our knowledge is firmly founded on the expertise of *Science*, and the long experience of AAAS in advancing science around the world. ScienceCareers.org is the natural selection.

[www.sciencecareers.org](http://www.sciencecareers.org)

Features include:

- Thousands of job postings
- Career tools from Next Wave
- Grant information
- Resume/CV Database
- Career Forum

**ScienceCareers.org**

We know science

AAAS



1200 New York Avenue, NW  
Washington, DC 20005

Editorial: 202-326-6550, FAX 202-289-7562  
News: 202-326-6500, FAX 202-371-9227

Bateman House, 82-88 Hills Road  
Cambridge, UK CB2 1LQ

+44 (0) 1223 326500, FAX +44 (0) 1223 326501

**SUBSCRIPTION SERVICES** For change of address, missing issues, new orders and renewals, and payment questions: 866-434-AAAS (2227) or 202-326-6417, FAX 202-842-1065. Mailing addresses: AAAS, P.O. Box 96178, Washington, DC 20090-6178 or AAAS Member Services, 1200 New York Avenue, NW, Washington, DC 20005

**INSTITUTIONAL SITE LICENSES** please call 202-326-6755 for any questions or information

**REPRINTS:** Author Inquiries 800-635-7181  
Commercial Inquiries 803-359-4578  
Corrections 202-326-6501

**PERMISSIONS** 202-326-7074, FAX 202-682-0816

**MEMBER BENEFITS** Bookstore: AAAS/BarnesandNoble.com bookstore www.aaas.org/bn; Car purchase discount: Subaru VIP Program 202-326-6417; Credit Card: MBNA 800-847-7378; Car Rentals: Hertz 800-654-2200 CDP#343457, Dollar 800-800-4000 #AA1115; AAAS Travels: Bethcart Expeditions 800-252-4910; Life Insurance: Seabury & Smith 800-424-9883; Other Benefits: AAAS Member Services 202-326-6417 or www.aaasmember.org.

science\_editors@aaas.org (for general editorial queries)  
science\_letters@aaas.org (for queries about letters)  
science\_reviews@aaas.org (for returning manuscript reviews)  
science\_bookrevs@aaas.org (for book review queries)

Published by the American Association for the Advancement of Science (AAAS), *Science* serves its readers as a forum for the presentation and discussion of important issues related to the advancement of science, including the presentation of minority or conflicting points of view, rather than by publishing only material on which a consensus has been reached. Accordingly, all articles published in *Science*—including editorials, news and comment, and book reviews—are signed and reflect the individual views of the authors and not official points of view adopted by the AAAS or the institutions with which the authors are affiliated.

AAAS was founded in 1848 and incorporated in 1874. Its mission is to advance science and innovation throughout the world for the benefit of all people. The goals of the association are to: foster communication among scientists, engineers and the public; enhance international cooperation in science and its applications; promote the responsible conduct and use of science and technology; foster education in science and technology for everyone; enhance the science and technology workforce and infrastructure; increase public understanding and appreciation of science and technology; and strengthen support for the science and technology enterprise.

## INFORMATION FOR AUTHORS

See pages 120 and 121 of the 5 January 2007 issue or access www.sciencemag.org/feature/contribinfo/home.shtml

EDITOR-IN-CHIEF **Donald Kennedy**

EXECUTIVE EDITOR **Monica M. Bradford**

DEPUTY EDITORS

**R. Brooks Hanson, Barbara R. Jasny,  
Katrina L. Kelen**

NEWS EDITOR

**Colin Norman**

**EDITORIAL SUPERVISORY SENIOR EDITOR** Phillip D. Szuroni; **SENIOR EDITOR/PERSPECTIVES** Lisa D. Chong; **SENIOR EDITORS** Gilbert J. Chin, Pamela J. Hines, Paula A. Kiberstis (Boston), Marc S. Lavine (Toronto), Beverly A. Purnell, L. Bryan Ray, Guy Riddihough, H. Jesse Smith, Valda Vinson, David Voss; **ASSOCIATE EDITORS** Jake S. Yeston, Laura M. Zahn; **ONLINE EDITOR** Stewart Wills; **ASSOCIATE ONLINE EDITOR** Tara S. Marathe; **BOOK REVIEW EDITOR** Sherman J. Suter; **ASSOCIATE LETTERS EDITOR** Etta Kavanagh; **EDITORIAL MANAGER** Cara Tate; **SENIOR COPY EDITORS** Jeffrey E. Cook, Cynthia Howe, Harry Jach, Barbara P. Ordway, Jennifer Sills, Trista Waggoner; **COPY EDITORS** Lauren Kmec, Peter Mooreside; **EDITORIAL COORDINATORS** Carolyn Kyle, Beverly Shields; **PUBLICATIONS ASSISTANTS** Ramatoulaye Diop, Chris Filiatreau, Joi S. Granger, Jeffrey Hearn, Lisa Johnson, Scott Miller, Jerry Richardson, Brian White, Anita Wynn; **EDITORIAL ASSISTANTS** Maris M. Bish, Emily Guise, Patricia M. Moore, Jennifer A. Seibert; **EXECUTIVE ASSISTANT** Sylvia S. Kihara; **ADMINISTRATIVE SUPPORT** Maryrose Polke

**NEWS SENIOR CORRESPONDENT** Jean Marx; **DEPUTY NEWS EDITORS** Robert Coontz, Eliot Marshall, Jeffrey Mervis, Leslie Roberts; **CONTRIBUTING EDITORS** Elizabeth Colotta, Polly Shulman; **NEWS WRITERS** Yudhijit Bhattacharjee, Adrian Cho, Jennifer Couzin, David Grimm, Constance Holden, Jocelyn Kaiser, Richard A. Kerr, Eli Kintisch, Andrew Lawler (New England), Greg Miller, Elizabeth Pennisi, Robert F. Service (Pacific NW), Erik Stokstad, John Simpson (Intern); **CONTRIBUTING CORRESPONDENTS** Barry A. Cipra, Jon Cohen (San Diego, CA), Daniel Ferber, Ann Gibbons, Robert Irion, Mitch Leslie, Charles C. Mann, Evelyn Strauss, Gary Taubes, Ingrid Wickelgren; **COPY EDITORS** Linda B. Felaco, Rachel Curran, Sean Richardson; **ADMINISTRATIVE SUPPORT** Scherraine Mack, Fannie Groom; **BUREAU** Berkeley, CA: 510-652-0302, FAX 510-652-1867, New England: 207-549-7755, San Diego, CA: 760-942-3252, FAX 760-942-4979, Pacific Northwest: 503-963-1940

**PRODUCTION DIRECTOR** James Landry; **SENIOR MANAGER** Wendy K. Shank; **ASSISTANT MANAGER** Rebecca Doshi; **SENIOR SPECIALISTS** Jay Covert, Chris Redwood; **SPECIALIST** Steve Forrester; **PREFLIGHT DIRECTOR** David M. Tompkins; **MANAGER** Marcus Spiegler; **SPECIALIST** Jessie Mudjtaba

**ART DIRECTOR** Kelly Buckheit Krause; **ASSOCIATE ART DIRECTOR** Aaron Morales; **ILLUSTRATORS** Chris Bickel, Katharine Sutfitt; **SENIOR ART ASSOCIATES** Holly Bishop, Laura Creveling, Preston Huey; **ASSOCIATES** Nayomi Kevitiyagala, Jessica Newfield; **PHOTO EDITOR** Leslie Blizard

## SCIENCE INTERNATIONAL

**EUROPE** science@science-int.co.uk **EDITORIAL: INTERNATIONAL MANAGING EDITOR** Andrew M. Sugden; **SENIOR EDITOR/PERSPECTIVES** Julia Falkenkamp-Uppenbrink; **SENIOR EDITORS** Caroline Ash (Geneva: +41 (0) 222 346 3106), Stella M. Hurlter, Ian S. Osborne, Stephen J. Simpson, Peter Stern; **ASSOCIATE EDITOR** Joanne Baker **EDITORIAL SUPPORT** Alice Whaley; **DEBORAH DENNISON ADMINISTRATIVE SUPPORT** Janet Clements, Jill White; **NEWS: EUROPE NEWS EDITOR** John Travis; **DEPUTY NEWS EDITOR** Daniel Cleary; **CORRESPONDENT** Gretchen Vogel (Berlin: +49 (0) 30 2809 3902, FAX +49 (0) 30 2809 8365); **CONTRIBUTING CORRESPONDENTS** Michael Balter (Paris), Martin Enserink (Amsterdam and Paris), John Bohannon (Vienna); **INTERN** Krista Zala

**ASIA** Japan Office: Asca Corporation, Eiko Ishioka, Fusako Tamura, 1-8-13, Hirano-cho, Chuo-ku, Osaka-shi, Osaka, 541-0046 Japan; +81 (0) 6 6202 6272, FAX +81 (0) 6 6202 6271; asca@os.gulf.or.jp; **ASIA NEWS EDITOR** Richard Stone +66 2 662 5818 (rstone@aaas.org); **JAPAN NEWS BUREAU** Dennis Normile (contributing correspondent, +81 (0) 3 3391 0630, FAX 81 (0) 3 5936 3531; dnormile@gol.com); **CHINA REPRESENTATIVE** Hao Xin, +86 (0) 10 6307 4439 or 6307 3676, FAX +86 (0) 10 6307 4358; cindyhao@gmail.com; **SOUTH ASIA** Pallava Bagla (contributing correspondent +91 (0) 11 2271 2896; pbagla@vsnl.com)

**AFRICA** Robert Koenig (contributing correspondent, rob.koenig@gmail.com)

EXECUTIVE PUBLISHER **Alan I. Leshner**

PUBLISHER **Beth Rosner**

**FULFILLMENT & MEMBERSHIP SERVICES** (membership@aaas.org) **DIRECTOR** Marlene Zendell; **MANAGER** Waylon Butler; **SYSTEMS SPECIALIST** Andrew Vargo; **CUSTOMER SERVICE SUPERVISOR** Pat Butler; **SPECIALISTS** Laurie Baker, Tamara Alfson, Karena Smith, Vicki Linton, Latoya Casteel; **CIRCULATION ASSOCIATE** Christopher Refice; **DATA ENTRY SUPERVISOR** Cynthia Johnson; **SPECIALISTS** Tomeka Diggs, Tarrica Hill, Erin Layne

**BUSINESS OPERATIONS AND ADMINISTRATION DIRECTOR** Deborah Rivera-Wienhold; **BUSINESS MANAGER** Randy Yi; **SENIOR BUSINESS ANALYST** Lisa Donovan; **BUSINESS ANALYST** Jessica Tierney; **FINANCIAL ANALYSTS** Michael LoBue, Farida Yeasmin; **RIGHTS AND PERMISSIONS: ADMINISTRATOR** Emilie David; **ASSOCIATE** Elizabeth Sandler; **MARKETING: DIRECTOR** John Meyers; **MARKETING MANAGERS** Darryl Walter, Allison Pritchard; **MARKETING ASSOCIATES** Julianne Wielga, Mary Ellen Crowley, Catherine Featherston, Alison Chandler, Lauren Lamoureux; **INTERNATIONAL MARKETING MANAGER** Wendy Sturley; **MARKETING EXECUTIVE** Jennifer Reeves; **MARKETING/MEMBER SERVICES EXECUTIVE** Linda Rusz; **JAPAN SALES** Jason Hannaford; **SITE LICENSE SALES: DIRECTOR** Tom Ryan; **SALES AND CUSTOMER SERVICE** Mehan Dossani, Kiki Forsythe, Catherine Holland, Wendy Wise; **ELECTRONIC MEDIA: MANAGER** Elizabeth Harman; **PROJECT MANAGER** Trista Snyder; **ASSISTANT MANAGER** Lisa Stanford **PRODUCTION ASSOCIATES** Nichele Johnston, Kimberly Oster

**ADVERTISING DIRECTOR WORLDWIDE AD SALES** Bill Moran

**PRODUCT** (science\_advertising@aaas.org); **MIDWEST** Rick Bongiovanni: 330-405-7080, FAX 330-405-7081 • **WEST COAST/ CANADA** Teola Young: 650-964-2266 EAST COAST/ CANADA Christopher Breslin: 443-512-0330, FAX 443-512-0331 • **EUROPE/ASIA** Julie Skeet: +44 (0) 1223-326-524, FAX +44 (0) 1223-325-532 **JAPAN** Masuyoshi Yoshikawa: +81 (0) 33235 5961, FAX +81 (0) 33235 5852 **TRAFFIC MANAGER** Carol Maddox; **SALES COORDINATOR** Delandra Simms

**COMMERCIAL EDITOR** Sean Sanders: 202-326-6430

**CLASSIFIED** (advertise@sciencecareers.org); **U.S.: RECRUITMENT SALES MANAGER** Ian King: 202-326-6528, FAX 202-289-6742; **U.S./INDUSTRY:** Darrell Bryant: 202-326-6533; **MIDWEST/CANADA:** Daryl Anderson: 202-326-6543; **NORTHEAST:** Allison Millar: 202-326-6572; **SOUTHEAST:** Fernando Junco: 202-326-6740; **WEST:** Katie Putney: 202-326-6577; **SALES COORDINATORS** Erika Bryant, Rohan Edmonson, Shirley Young; **INTERNATIONAL SALES MANAGER** Tracy Holmes: +44 (0) 1223 326525, FAX +44 (0) 1223 326532; **SALES** Christina Harrison, Svetlana Barnes; **SALES ASSISTANT** Louise Moore; **JAPAN:** Jason Hannaford: +81 (0) 52 757 5360, FAX +81 (0) 52 757 5361; **ADVERTISING PRODUCTION OPERATIONS MANAGER** Deborah Tompkins; **ASSOCIATES** Christine Hall, Amy Hardcastle; **PUBLICATIONS ASSISTANTS** Robert Buck, Mary Lagnaoui

**AAAS BOARD OF DIRECTORS** **RETIRED PRESIDENT, CHAIR** John P. Holdren; **PRESIDENT** David Baltimore; **PRESIDENT-ELECT** James J. McCarthy; **TREASURER** David E. Shaw; **CHIEF EXECUTIVE OFFICER** Alan I. Leshner; **BOARD** John E. Dowling, Lynn W. Enquist, Susan M. Fitzpatrick, Alice Gast, Linda P. B. Katehi, Cheryle A. Murray, Thomas D. Pollard, Kathryn D. Sullivan



ADVANCING SCIENCE. SERVING SOCIETY

## SENIOR EDITORIAL BOARD

**John I. Brauman**, Chair, Stanford Univ.  
**Richard Losick**, Harvard Univ.  
**Robert May**, Univ. of Oxford  
**Marcia McNutt**, Monterey Bay Aquarium Research Inst.  
**Linda Partridge**, Univ. College London  
**Vera C. Rubin**, Carnegie Institution of Washington  
**Christopher R. Somerville**, Carnegie Institution  
**George M. Whitesides**, Harvard University

## BOARD OF REVIEWING EDITORS

**Joanna Aizenberg**, Bell Labs/Lucent  
**R. McNeill Alexander**, Leeds Univ.  
**David Altschuler**, Broad Institute  
**Arturo Alvarez-Buylla**, Univ. of California, San Francisco  
**Richard Amasino**, Univ. of Wisconsin, Madison  
**Meinrat O. Andreae**, Max Planck Inst., Mainz  
**Kristi S. Anseth**, Univ. of Colorado  
**John A. Bargh**, Yale Univ.  
**Cornelia I. Bargmann**, Rockefeller Univ.  
**Brenda Bass**, Univ. of Utah  
**Marisa Bartolomei**, Univ. of Penn. School of Med.  
**Ray H. Baughman**, Univ. of Texas, Dallas  
**Stephen J. Benkovic**, Pennsylvania St. Univ.  
**Michael J. Bevan**, Univ. of Washington  
**Ton Bisseling**, Wageningen Univ.  
**Mina Bissell**, Lawrence Berkeley National Lab  
**Peer Bork**, EMBL  
**Dianna Bowles**, Univ. of York  
**Robert W. Boyd**, Univ. of Rochester  
**Dennis Bray**, Univ. of Cambridge  
**Stephen Buratowski**, Harvard Medical School  
**William M. Burkiak**, Univ. of Alberta  
**Joseph A. Burns**, Cornell Univ.  
**William P. Butz**, Population Reference Bureau  
**Peter Carmeliet**, Univ. of Leuven, VIB  
**Gerbrand Ceder**, MIT  
**Mildred Cho**, Stanford Univ.  
**David Clapham**, Children's Hospital, Boston  
**David Clary**, Oxford University

**J. M. Claverie**, CNRS, Marseille  
**Jonathan D. Cohen**, Princeton Univ.  
**Stephen M. Cohen**, EMBL  
**Robert H. Crabtree**, Yale Univ.  
**F. Fleming Crim**, Univ. of Wisconsin  
**William Cumberland**, UCLA  
**George O. Daley**, Children's Hospital, Boston  
**Edward DeLong**, MIT  
**Emmanouil T. Dermizakis**, Wellcome Trust Sanger Inst.  
**Robert Desimone**, MIT  
**Dennis Discher**, Univ. of Pennsylvania  
**W. Ford Doolittle**, Dalhousie Univ.  
**Jennifer A. Doudna**, Univ. of California, Berkeley  
**Julian Downward**, Cancer Research UK  
**Denis Duboule**, Univ. of Geneva  
**Christopher Dye**, WHO  
**Richard Ellis**, Cal Tech  
**Gerhard Ertl**, Fritz-Haber-Institut, Berlin  
**Douglas H. Erwin**, Smithsonian Institution  
**Barry Everitt**, Univ. of Cambridge  
**Paul G. Falkowski**, Rutgers Univ.  
**Ernst Fehr**, Univ. of Zurich  
**Tom Fenchel**, Univ. of Copenhagen  
**Alain Fischer**, INSERM  
**Jeffrey S. Flier**, Harvard Medical School  
**Chris D. Frith**, Univ. College London  
**John Gearhart**, Johns Hopkins Univ.  
**Wulfram Gerstner**, Swiss Fed. Inst. of Technology  
**Charles Godfray**, Univ. of Oxford  
**Jennifer M. Graves**, Australian National Univ.  
**Christian Haass**, Ludwig Maximilians Univ.  
**Dennis L. Hartmann**, Univ. of Washington  
**Chris Hawkesworth**, Univ. of Bristol  
**Christin Heimann**, Max Planck Inst., Jena  
**James A. Hendler**, Univ. of Maryland  
**Ray Hilborn**, Univ. of Washington  
**Ove Hoegh-Guldberg**, Univ. of Queensland  
**Ary A. Hoffmann**, La Trobe Univ.  
**Ronald R. Hoy**, Cornell Univ.  
**Evelyn L. Hu**, Univ. of California, SB  
**Olli Ikkala**, Helsinki Univ. of Technology  
**Meyer B. Jackson**, Univ. of Wisconsin Med. School  
**Stephen Jackson**, Univ. of Cambridge

**Seven Jacobsen**, Univ. of California, Los Angeles  
**Peter Jonas**, Universität Freiburg  
**Daniel Kahne**, Harvard Univ.  
**Bernhard Keimer**, Max Planck Inst., Stuttgart  
**Elizabeth A. Kellog**, Univ. of Missouri, St. Louis  
**Alan B. Krueger**, Princeton Univ.  
**Lee Kump**, Penn State  
**Mitchell A. Lazar**, Univ. of Pennsylvania  
**Virginia Lee**, Univ. of Pennsylvania  
**Anthony J. Leggett**, Univ. of Illinois, Urbana-Champaign  
**Michael J. Lenardo**, NIAID, NIH  
**Norman L. Letvin**, Beth Israel Deaconess Medical Center  
**Olle Lindvall**, Univ. Hospital, Lund  
**Richard Losick**, Harvard Univ.  
**Ke Lu**, Chinese Acad. of Sciences  
**Andrew P. MacKenzie**, Univ. of St. Andrews  
**Raul Madariga**, Ecole Normale Supérieure, Paris  
**Anne Magurran**, Univ. of St. Andrews  
**Michael Malim**, King's College, London  
**Virginia Miller**, Washington Univ.  
**Yasushi Miyashita**, Univ. of Tokyo  
**Richard Morris**, Univ. of Edinburgh  
**Edward Moser**, Norwegian Univ. of Science and Technology  
**Andrew Murray**, Harvard Univ.  
**Naoto Nagaosa**, Univ. of Tokyo  
**James Nelson**, Stanford Univ. School of Med.  
**Roland Nolte**, Univ. of Nijmegen  
**Helga Nowotny**, European Research Advisory Board  
**Eric N. Olson**, Univ. of Texas, SW  
**Erin O'Shea**, Harvard Univ.  
**Elinor Ostrom**, Indiana Univ.  
**Jonathan T. Overpeck**, Univ. of Arizona  
**John Pendry**, Imperial College  
**Philippe Poulin**, CNRS  
**Mary Power**, Univ. of California, Berkeley  
**Molly Przeworski**, Univ. of Chicago  
**David J. Read**, Univ. of Sheffield  
**Les Real**, Emory Univ.  
**Colin Renfrew**, Univ. of Cambridge  
**Trevor Robbins**, Univ. of Cambridge  
**Barbara A. Romanowicz**, Univ. of California, Berkeley  
**Nancy Ross**, Virginia Tech  
**Edward M. Rubin**, Lawrence Berkeley National Lab

**J. Roy Sambles**, Univ. of Essex  
**Jürgen Sandkühler**, Medical Univ. of Vienna  
**David S. Schimel**, National Center for Atmospheric Research  
**Georg Schulz**, Albert-Ludwigs-Universität  
**Paul Schulze-Lefer**, Max Planck Inst., Cologne  
**Terrence J. Sejnowski**, The Salk Institute  
**David Sibley**, Washington Univ.  
**Montgomery Slatkin**, Univ. of California, Berkeley  
**George Somero**, Stanford Univ.  
**Joan Steitz**, Yale Univ.  
**Elisbeth Stern**, ETH Zürich  
**Thomas Stocker**, Univ. of Bern  
**Jerome Strauss**, Virginia Commonwealth Univ.  
**Marc Tatar**, Brown Univ.  
**Glenn Telling**, Univ. of Kentucky  
**Marc Tessier-Lavigne**, Genentech  
**Michiel van der Klis**, Astronomical Inst. of Amsterdam  
**Derek van der Kooy**, Univ. of Toronto  
**Bert Vogelstein**, Johns Hopkins  
**Christopher A. Walsh**, Harvard Medical School  
**Graham Warren**, Yale Univ. School of Med.  
**Colin Watts**, Univ. of Dundee  
**Julia R. Weertman**, Northwestern Univ.  
**Jonathan Weissman**, Univ. of California, San Francisco  
**Ellen D. Williams**, Univ. of Maryland  
**R. Sanders Williams**, Duke University  
**Ian A. Wilson**, The Scripps Res. Inst.  
**Jerry Workman**, Stowers Inst. for Medical Research  
**John R. Yates III**, The Scripps Res. Inst.  
**Martin Zatz**, NIMH, NIH  
**Huda Zoghbi**, Baylor College of Medicine  
**Maria Zuber**, MIT

## BOOK REVIEW BOARD

**John Aldrich**, Duke Univ.  
**David Bloom**, Harvard Univ.  
**Angela Creager**, Princeton Univ.  
**Richard Shweder**, Univ. of Chicago  
**Ed Wasserman**, DuPont  
**Lewis Wolpert**, Univ. College, London



# RETHINK.

Finnyzymes offers new gear for high performance PCR



Top View – Shown To Scale

Free 5-Year  
Warranty\*

## Slide-sized PCR plates

Slidetiter™ describes a novel PCR plate which is the footprint of a microscope slide. Not only is the size condensed, but the wall thickness is reduced to half that of conventional thin-wall plates for ultra-quick PCR protocols. Four Slidetiter plates can insert into a single frame producing the equivalent of a standard microplate. This advance allows the use of existing lab equipment to prepare and analyze PCR samples.



Slidetiter frame (blue) with three 96-well Slidetiter plates assembled and one plate removed.

## Super compact PCR machine

The Piko™ thermal cycler relies upon our Slidetiter plate to achieve a tiny footprint – less than half the size of any cycler. Our unique design delivers unparalleled thermal performance completing a PCR protocol in less than 10 minutes. And with an automated lid, CD drive-like loading mechanism, and multiple block formats (24-, 96- or 384-well) the Piko is a natural fit for any lab.



• Half the price • Twice the speed • Licensed for PCR •

Finnyzymes • Tel. 1-800-993-1283 • Fax 1-617-245-1962 • info@finnyzymes.com • www.finnyzymesinstruments.com

\* Offer valid for units shipped by December 31st, 2007. See website for more details. Purchase of this instrument conveys a limited non-transferable immunity from suit for the purchaser's own internal research and development and applied fields other than human in vitro diagnostics under non-real-time thermal cycler patents of Applied Biosystems Corporation.

**FINNZYMES**  
TOOLS FOR MOLECULAR BIOLOGY



# You could be next

## Yes, it can happen to you:

If you're a young scientist making inroads in neurobiology research, the next Eppendorf and *Science* Prize for Neurobiology could be yours!

This annual research prize recognizes accomplishments in neurobiology research based on methods of molecular and cell biology. The winner and finalists are selected by a committee of independent scientists, chaired by the Editor-in-Chief of *Science*. Past winners include post-doctoral scholars and assistant professors.

To be eligible, you must be 35 years of age or younger. If you're selected as this year's winner, you will receive \$25,000, have your work published in the prestigious journal *Science* and be invited to visit Eppendorf in Hamburg, Germany.

## Get recognized!

Deadline for entries:

**June 15, 2007**

[www.eppendorf.com/prize](http://www.eppendorf.com/prize)

[www.eppendorfsceinceprize.org](http://www.eppendorfsceinceprize.org)

**\$25,000  
Prize**

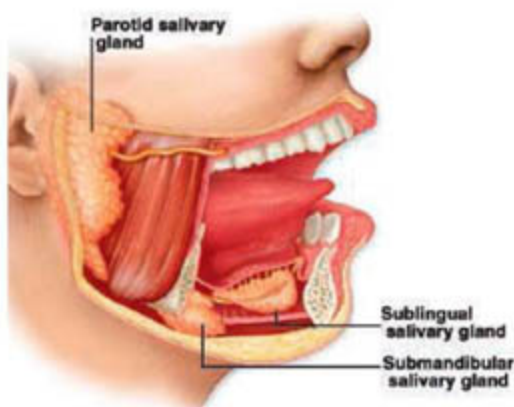
*"I feel incredibly  
honored to receive this  
prestigious prize."*

2006 Winner  
Doris Tsao, Ph.D.  
Institute for Brain Research  
University of Bremen  
Germany



**eppendorf  
& Science**  
**PRIZE FOR  
NEUROBIOLOGY**





## A Proteome to Drool Over

Saliva is a world of its own, teeming with bacteria, mucus, enzymes, skin cells, blood cells, and hundreds of different proteins—the product of multiple glands, serum leakage, drainage from nasal cavities, and whatever you put in your mouth. Saliva is routinely used to test for hormone levels and illegal drugs. But so far the only disease it is used to detect is AIDS.

That may soon change, thanks to the Saliva Proteome Project. For 3 years, several institutions have been cataloging every protein that appears in healthy people's spit. With 1500 proteins in the data bank, scientists now want to collect samples from patients with diseases that might reveal their presence via saliva, dental researcher David Wong of the University of California, Los Angeles, told the International Association for Dental Research this week in New Orleans, Louisiana.

Although the AIDS saliva test merely checks for HIV antibodies, scientists look toward more complex tests—monitoring ratios of various substances in the saliva—in the future. Wong expects that tests for oral cancer and Sjögren's syndrome, an autoimmune disease that affects saliva production, will be available in the next couple of years. Further down the road, he predicts scientists will be able to detect protein markers for lung, breast, and pancreatic cancers, as well as diabetes and even Alzheimer's disease.

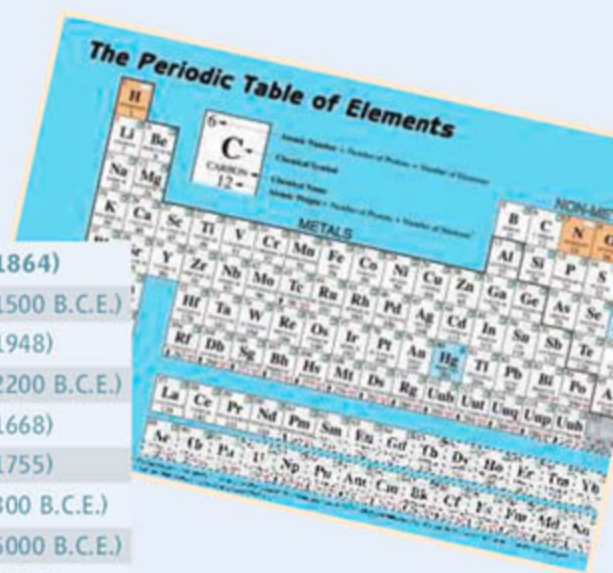
Wong says a "Salivary Diagnostic Roadmap"—combining both the proteome and data from another project cataloging pieces of RNA that relate to the proteins—will be available in about 4 months.

Susan Fisher, who works on the Saliva Proteome Project at the University of California, San Francisco, says that as biochemistry is unraveled, "there are always very interesting surprises"—as scientists have discovered, for example, from the blood test for prostate cancer. So she says it's possible saliva will yield information that can't be obtained from blood tests.

## Great Materials Moments

Who says materials science isn't sexy? At the international meeting of the Minerals, Metals, and Materials Society last month in Orlando, Florida, 4200 members voted on a list of the Greatest Materials Moments in History. Here's their top 10.

- 1 **The Periodic Table of Elements** (1864)
- 2 **Iron smelting** (1500 B.C.E.)
- 3 **Transistor** (1948)
- 4 **Glass** (2200 B.C.E.)
- 5 **Optical microscopy** (1668)
- 6 **Concrete** (1755)
- 7 **Crucible steelmaking** (300 B.C.E.)
- 8 **Copper extraction and casting** (5000 B.C.E.)
- 9 **X-ray diffraction** (1912)
- 10 **Bessemer process** (1856)



## Rehabilitating Pluto

The latest strike in the Pluto wars has come from the New Mexico State House of Representatives. Lawmakers there last week defied the decision by the International Astronomical Union (IAU) to reclassify Pluto as a "dwarf planet." In a statement approved 70–0, the House declared Pluto "a planet" and 13 March—the day of the vote—as "Pluto Planet Day" in New Mexico. It was on 13 March 1930 that 24-year-old Clyde Tombaugh of Las Cruces, an amateur astronomer, announced his discovery of Pluto, inspiring local pride that apparently endures. Tombaugh died in 1997, but his widow Patsy was present for the vote.

"There are people who take [the IAU's action] as an affront to American astronomy," says planetary scientist S. Alan Stern of the Southwest Research Institute in San Antonio, Texas. "The discovery of Pluto was epochal. It was heralding the Kuiper belt—one of the hottest topics in planetary science." The New Mexico Senate must vote on the measure to make it official.



## Taxonomy, the Early Years

By the late 1700s, scientists had categorized more than 4000 species of animals. Often tucked away in out-of-print publications, these early descriptions can be difficult for modern researchers to hunt down. AnimalBase from the University of Göttingen in Germany opens up the classic taxonomic literature.

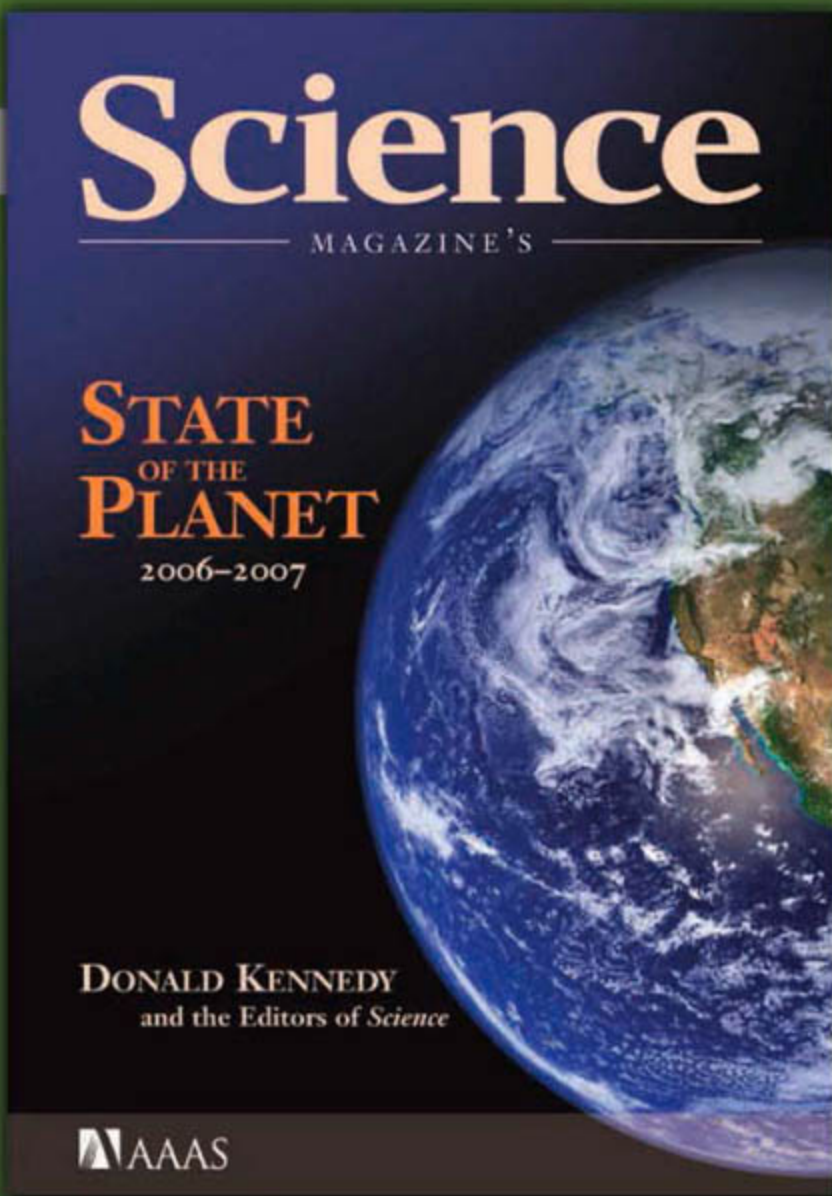
**Goatskin-covered books from late 17th and early 18th centuries.**

Nicolaus Laurenti that describes the true toads (*Bufo*). To help visitors track down the first use of a particular scientific name, curators have begun combing the texts for mentions of species and other taxonomic groups. >>

[www.animalbase.org](http://www.animalbase.org)

The library stores or links to digitized versions of more than 700 books and papers, some from as far back as the 1550s. Along with a stack of works by Carolus Linnaeus, the Swedish botanist who reformed taxonomy in the 1700s, the holdings include lesser-known contributions such as the 1768 treatise by the Austrian naturalist Josephus





Science Magazine's  
**State of  
the Planet  
2006-2007**

Donald Kennedy, Editor-in-Chief,  
and the Editors of *Science*

The American Association for  
the Advancement of Science

The most authoritative voice in science, *Science* magazine, brings you current knowledge on the most pressing environmental challenges, from population growth to biodiversity loss.

COMPREHENSIVE • CLEAR • ACCESSIBLE



**ISLAND**PRESS

**Science**



*islandpress.org*





## Pioneers

**IDLING.** Vijay Pande doesn't want to stop children from playing video games. In fact, the Stanford University chemist thinks they can help him understand what triggers Alzheimer's disease.

Last week, Pande and Sony Computer Entertainment America announced that by the end of this month, Sony PlayStation 3 (PS3) computer entertainment systems will be able to connect to Pande's Folding@Home (F@H) program. The program is a distributed computing project on protein folding and misfolding, which can lead to Alzheimer's disease, among others. If PS3 users activate the connection, their machines—when idle—will

automatically synch up with Pande's network and crunch numbers in protein-folding simulations. The faster processor chips in the PS3 will extend the work done on F@H by nearly 2 million desktop computers since October 2000.

Pande is hoping the project might even steer some students toward careers in science by giving them the chance to watch the protein-folding simulation in real time and manipulate proteins on screen. "It's a unique way to educate people about science on a molecular scale," he says.

## AWARDS

**FOR CHILDREN.** Two women have won the March of Dimes Prize in Development Biology, which honors scientific research aimed at improving the health of babies. Janet Rossant, a stem cell researcher at the University of Toronto in Canada, receives the award for work that helped identify the genes responsible for the growth and specialization of embryonic stem cells. And Anne McLaren, a research associate at the University of Cambridge, U.K., wins the honor for her contributions to the field of reproductive technology, including the first successful attempt at growing a mouse embryo in a test tube and then implanting it for natural birth. The two winners share \$250,000.

## MOVERS

**GOING HOME.** Irish biologist Frank Gannon, 59, has been appointed director general of the Science Foundation of Ireland (SFI), a funding agency with a €175 million annual budget. He had announced his retirement as director of the European Molecular Biology Organization (EMBO) in Heidelberg, Germany, in December (*Science*, 15 December 2006, p. 1665).

Gannon, who also headed a group studying gene control by the estrogen receptor at

the European Molecular Biology Laboratory, succeeds William Harris, who left SFI last year to become head of the Science Foundation Arizona. EMBO is still looking for a successor.



## BACK TO PHYSICS.

Stanford Linear Accelerator Center (SLAC) Director Jonathan Dorfan will step down this fall after 8 years as head of the facility, which is funded by the U.S. Department of Energy (DOE) and

managed by Stanford University. The contract to run the \$300 million lab is expected to be put up for bid soon. Stanford plans to compete, but Dorfan wants the university to find a new leader. "I'm thinking of SLAC's future," he says.

Dorfan has been at Stanford for 30 years and says he's looking forward to returning to the bench to explore the "very significant mysteries" in dark matter and cosmology. Dorfan also plans to help with efforts to bring the International Linear Collider to the United States, which he says would sustain U.S. high-energy physics for a generation.



## Three Q's >>

Antidoping researcher **Donald Catlin** is stepping down as director of the Olympic Analytical Laboratory, which he founded 25 years ago at the University of California, Los Angeles. Catlin, 68, is credited with uncovering many sports doping schemes. He will devote his time to research at the Anti-Doping Research Institute, a nonprofit he set up last year.

### Q: Looking back, are there any discoveries or drug busts you're especially proud of?

You know, it's hard to be proud of a bust. I think norbolethone is one of the most important ones we ever did. That was a forerunner of designer steroids. When I figured that one out, I knew that there were people scheming and developing designer steroids that we couldn't see or find.

### Q: Has your work changed how you feel about sports?

Yeah, in a way. I really love the Olympic model, where 200 countries can all get out their best athletes and compete, and the best men and women win. It's beautiful and exciting, and it should be very pure. But nowadays sometimes your hopes are dashed when you read that so-and-so is dirty.

### Q: Do you think we'll ever be able to put an end to this?

If your objective is to get all drugs out of all sports forever, you're going to die very unhappy. But you should be able to get control enough so that the really high-end sports, where the big names are competing, are clean.

Got a tip for this page? E-mail [people@aaas.org](mailto:people@aaas.org)





Among friends, NIH Director Elias Zerhouni offered senators a strong endorsement of stem cell research.

## 2008 BUDGET

## Senators Offer Sympathetic Ear to Complaints on NIH's Fiscal Slide

Two powerful champions of biomedical research blasted the White House's proposal to cut funding for the National Institutes of Health (NIH) in 2008 and invited research leaders to vent their own frustrations at a Senate hearing this week. Senators Tom Harkin (D-IA) and Arlen Specter (R-PA), who head the subcommittee that handles NIH funding, grilled NIH Director Elias Zerhouni on 19 March about the impact of what would be the fifth consecutive year of subinflationary budgets for NIH. They heard senior scientists describe a bleak research climate in which the percentage of funded NIH grant applications has dropped from 30% to 20%. And the senators promised to press for more money for biomedical research in 2008.

None of this was unexpected; Harkin and Specter helped win NIH a 2% increase in 2007 that the White House didn't request (*Science*, 23 February, p. 1062). More surprising was an impassioned speech by Zerhouni about the need for federally funded human embryonic stem cell research. In response to a question, he diverged from Administration policy, asserting that statements that adult stem cells can perform the same tasks as the embryonic variety "do not hold scientific water." He added that any attempt "to sideline NIH on an issue of such importance is shortsighted."

President George W. Bush has ruled that

only stem cell lines created before 9 August 2001 may be used in federally funded research. However, Zerhouni said, "it's very clear ... that these cell lines will not be sufficient to do all the research that we need to do." The Administration has declined to fund new human embryonic stem cell lines and said little about the extent to which federal dollars should back this research.

Zerhouni's call for boosting funding for human embryonic stem cell research comes as NIH is still struggling to apportion its \$28.9 billion 2007 budget, enacted 5 weeks ago. Other agencies are struggling, too; the president's 2008 budget proposes "pretty much flat-funding everything other than defense," says Jon Retzlaff, director of legislative relations for the Federation of American Societies for Experimental Biology in Bethesda, Maryland. Some agencies that fund research in the physical sciences, including the National Science Foundation, would, however, receive real increases under the Administration's budget proposals (*Science*, 9 February, p. 750).

Ironically, even though Congress gave NIH a small increase in 2007, the agency is under a particular strain because it is coming off flush times in 1998 to 2003, when it saw its budget double. That prompted many universities to expand, construct new facilities, and recruit new investigators, says Retzlaff.

Between 1998 and 2007, the number of standard investigator-initiated (R01) grants roughly doubled to about 50,000. Such expansion requires long-term commitments, researchers said, because the agency provides most researchers with at least a portion of their salary and covers overhead costs.

"We bought in" to the doubling, "and now we're getting cut," says Joan Brugge, chair of the cell biology department at Harvard Medical School, in an interview before she testified at the hearing. Brugge, who began to study cancer in college after her sister was diagnosed with a fatal brain tumor, says that the slowdown is especially frustrating given recent advances in understanding the basic biology of cancer. "This not only forestalls progress but creates an atmosphere of uncertainty and anxiety," she told the senators.

Scientists also spoke of undergraduates and graduate students turning away from biomedical research and senior investigators leaving the field after being unable to secure NIH funding. Robert Siliciano, who studies HIV at Johns Hopkins University in Baltimore, Maryland, said he used to spend 30% of his time applying for grants. Now, he told the senators, it's jumped to 60%.

Universities are already mobilizing to lobby for more funding. Immediately after the Senate hearing, a coalition of nine institutions and 20 scientists, including the four who testified, released a glossy, 21-page report that describes recent strides in cancer, spinal cord injury, and other diseases, arguing that NIH grants are well spent and lamenting the effects of flat funding.

But beyond the anecdotes, the researchers and university administrators offered up few hard figures on the harm flat budgets are causing. "I know this will not work out to be a mathematical formula," said Specter, but he professed frustration at a lack of data that he might offer his more skeptical Senate colleagues. "What's going to happen to NIH if the budget is cut by \$500 million?" he wanted to know. "It would be very helpful to know how many research projects you are undertaking and how many you're turning away."

The hearing was the Senate's opening move in its consideration of NIH's 2008 budget, a process that is expected to take at least until the fall.

—JENNIFER COUZIN

CREDIT: TOM WILLIAMS





## MATHEMATICS

## Mapping the 248-Fold Way

For more than a century, mathematicians have struggled to comprehend a vast, 248-dimensional entity, known to them only as  $E_8$ . They have described it as “magic” and “miraculous,” but until now, they could not really understand how it is put together.

This week, an international team of 18 mathematicians and computer scientists called the Atlas Project, headed by Jeffrey Adams of the University of Maryland, College Park, announced that a supercomputer called Sage has successfully “mapped”  $E_8$ . In the words of Gregg Zuckerman, a mathematician at Yale University, “never before has the marriage of pure mathematics and supercomputing produced such a prized offspring.”

Launched in 2002, the Atlas Project has roots deep in mathematical history. The ancient Greeks were fascinated by crystals and polyhedra because of their rich symmetry. In a crystal, however, symmetry comes in discrete chunks and limited numbers. In the late 19th century, the Norwegian mathematician Sophus Lie (pronounced “lee”) started studying objects with smooth rotational symmetries. Such objects are rare in three-dimensional space: spheres, cylinders, doughnuts, and cones. But in higher dimen-

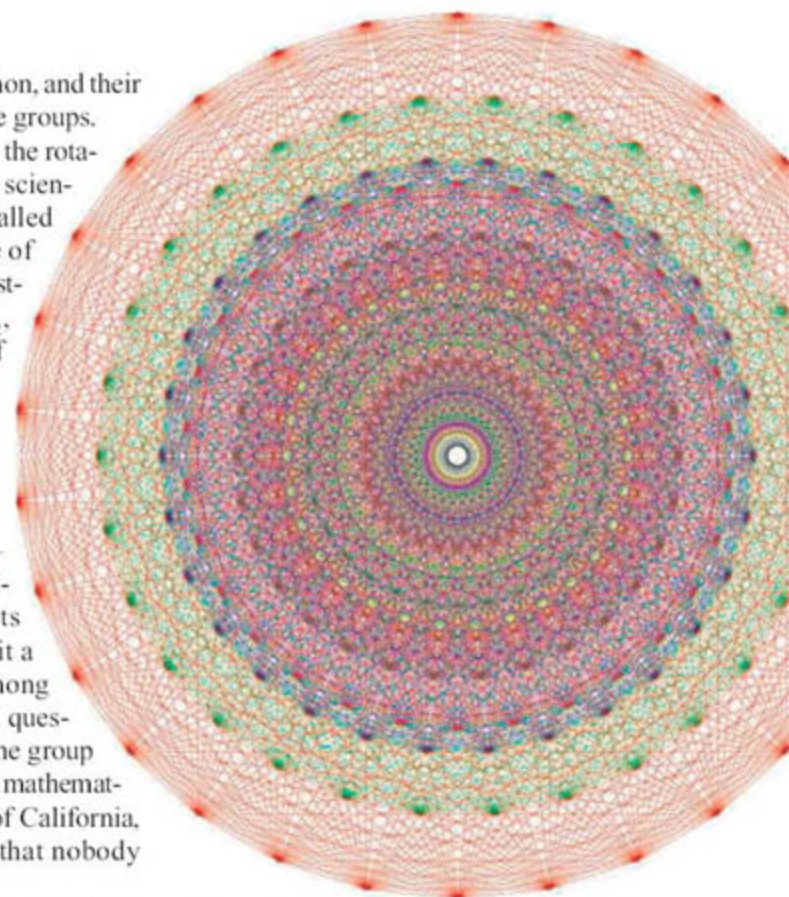
sions, they are much more common, and their symmetries are expressed by Lie groups.

Even the simplest Lie group, the rotations of a sphere, has profound scientific importance. This group, called  $SO(3)$  or  $A_1$ , controls the shape of electron orbitals. The next interesting Lie group,  $SU(3)$  or  $A_2$ , describes the symmetries of quarks. Murray Gell-Mann nicknamed it the “Eightfold Way,” because it is an eight-dimensional group. Physicists’ quest for grand unified theories has led to ever-larger groups—and  $E_8$  is the biggest, most exotically symmetric of them all. Its mathematical richness makes it a magnet for string theorists, among others. “There’s a philosophical question of why nature would pick one group over another,” says John Baez, a mathematical physicist at the University of California, Riverside. “ $E_8$  is so awesome that nobody could quarrel with this choice.”

The German mathematician Wilhelm Killing posited the existence of  $E_8$  in 1887, in a paper that broke all possible Lie groups down into four infinite families (labeled A through D) plus five “exceptional groups” ( $G_2$ ,  $F_4$ ,  $E_6$ ,  $E_7$ , and  $E_8$ ). His French colleague Elie Cartan described  $E_8$  in 1894. In essence, Killing and Cartan together supplied the taxonomy of Lie groups. The Atlas Project aimed to compute their genomes.

In mathematical terms, the team set out to map each group’s “irreducible representations”: the set of different  $n$ -dimensional spaces on which the group’s rotations can act. Earlier mathematicians, including Zuckerman (who was Adams’s thesis adviser), had proved that the representations can be divided into families, each generated by its own formula. In theory, it should be possible to use the formulas to crank out irreducible representations of every group—including  $E_8$ —in a finite time. But no one knew how long the computation might take, or even if it was feasible.

One person made it feasible. Fokko du Cloux was a Belgian mathematician and computer scientist with a gift for turning the



**Visions of symmetry.** The eight-dimensional root lattice of  $E_8$  (here projected into a plane) is like a cell’s nucleus—a place where information about its representations is stored in compressed form.

abstract, and sometimes flawed, theorems of group theorists into working algorithms. “Mathematicians often take shortcuts because they know what has to be true, but the computer doesn’t,” says David Vogan of the Massachusetts Institute of Technology, one of the participants in the project. “Fokko went back and found all the details that weren’t quite right and made it all perfect.”

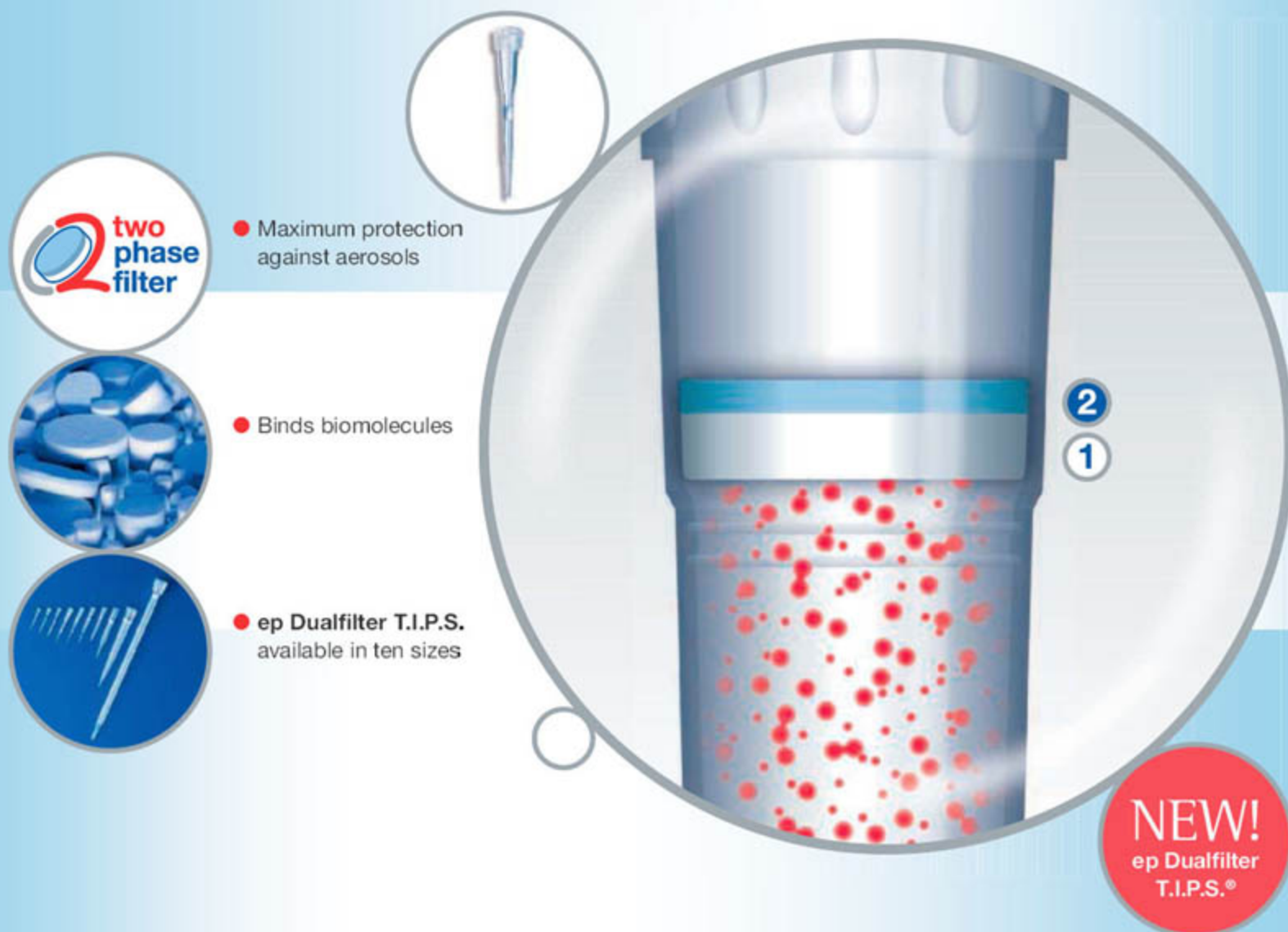
Du Cloux calculated that  $E_8$  has 453,060 families. (Vogan had expected about a billion.) That meant the “genome” of  $E_8$  would be a table with 453,060 rows and 453,060 columns, or more than 200 billion entries. Du Cloux conquered all the groups through  $E_7$ , but he didn’t have a big enough computer to touch  $E_8$ .

Then disaster struck. In November 2005, du Cloux was diagnosed with amyotrophic lateral sclerosis. By May, he was bedridden and could breathe only with a respirator. “But he was completely engaged,” says Adams. ▶

**Final effort.** Mathematician-programmer Fokko du Cloux spent his last months trying to finish the  $E_8$  project.







● Maximum protection against aerosols



● Binds biomolecules



● ep Dualfilter T.I.P.S. available in ten sizes



# Stop aerosols!

Unique two-phase filter protection with ep Dualfilter T.I.P.S.®

The new Eppendorf ep Dualfilter T.I.P.S., with their unique two-phase filter, provide the perfect shield against contamination.

The filter consists of two visible phases, each with a different pore size. This two-phase filter protection ensures ultimate absorption of aerosols ❶ and biomolecules ❷, outmatching all conventional filters. Rely on it.

For more information go to [www.eppendorf.com/dualfilter](http://www.eppendorf.com/dualfilter)

## Features of the ep Dualfilter T.I.P.S.

Double protection provided by the two phase filter

- Provides maximum protection for both pipette and sample
- Ultimate absorption of aerosols and biomolecules
- Free from PCR inhibitor additives
- Patent pending two phase filter technology
- Supplied sterile, Eppendorf PCR clean and pyrogen-free
- IvD conformity
- Batch-related certificates available





**Symmetry unwrapped.** A functional view of the 240 vertices of  $E_8$ 's root lattice, with eight colors indicating relationships between the roots.

"He would lie on his back in Lyons, with a video projector pointing at the ceiling. I would type here in Baltimore, and he would see on the ceiling what I was typing. We would use Skype to talk. All he wanted to talk about was mathematics—he never complained about this terrible thing that happened to him."

Du Cloux finally streamlined the software enough that a super-computer might be able to do the calculation. But he did not live to see its completion. He died on 10 November 2006.

On 8 January, Sage, a super-computer at the University of Washington, computed the last entry in the table for  $E_8$ . But the Atlas Project is not finished. Like the Human Genome Project, it has produced far too much data for mathematicians to assimilate overnight. Also, it

includes a lot of representations that aren't "unitary," which are the equivalent of junk DNA in the human genome. Nevertheless, Adams expects the work to have a practical impact very soon, especially for number theorists. "The typical thing is that I get a call from a number theorist who says 'I have such and such a representation. Can you tell me if it is unitary?'" says Adams. "Until now, that's been a very painful procedure to figure out." With the atlas, it could become a simple lookup. "If there were such an atlas, I'd buy it immediately," says Peter Sarnak, a number theorist at Princeton University.

Mathematicians and physicists look likely to mine the database for years to come. Hermann Nicolai, a theoretical physicist at the University of Potsdam in Germany, says the fingerprints of  $E_8$  can be found all over heterotic string theory, the most popular version of quantum gravity. "If you ask me if this will be helpful tomorrow, I cannot say yet," says Nicolai. "In the end, I think the symmetry of quantum gravity might be realized in a more subtle way than we understand yet. In that event, it will be very useful to have a guide or atlas." —DANA MACKENZIE

Dana Mackenzie is a writer in Santa Cruz, California.

## OPEN GOVERNMENT

# House OKs Whistleblower Bill

The U.S. House of Representatives has broadened protection for government scientists who claim that their bosses have undermined the scientific process or suppressed information. Last week, legislators passed The Whistleblower Protection Enhancement Act by a margin wide enough—331 to 94—to withstand a promised veto from President George W. Bush. But the measure faces an uphill road in the Senate.

The bill, H.R. 985, covers incidents involving the "dissemination of false or misleading" scientific information or actions that compromise "the validity" of federal research. It defines those actions as an "abuse of authority." The legislation, which would also apply to instances in which government scientists are prevented from publishing data, includes provisions that open-government advocates say will give whistleblowers a better chance to prevail in federal court and to avoid retribution.

"It's very important," says David Ross, a former Food and Drug Administration (FDA) staffer whose accusations that the agency ignored data on liver damage in patients before approving the antibiotic Ketek in 2004

have spawned a congressional investigation. Ross says the bill is needed because current protections are "worse than useless" at regulatory agencies such as the FDA and do not cover scientific disputes.

But others feel the bill would force the courts to address scientific questions outside their expertise. "If an agency or the Administration disagrees with the findings of a particular scientist, we should not be opening up our judicial system for those disagreements to be litigated as federal employee personnel issues," said Representative Bill Sali (R-ID) during an unsuccessful effort on the floor to scrap the science provisions. Science policy expert Roger Pielke of the University of Colorado, Boulder, wonders how the provisions would be enforced, positing a situation in which an incorrect weather forecast could be labeled an abuse of authority because it contained false information.

A lobbyist for the Union of Concerned Scientists, which supports the legislation, says that such arguments could hold sway in the Senate, which presents a "much more challenging" environment. —ELI KINTISCH

## Itching for a Space Fight

The battle between the White House and congressional Democrats over NASA's budget dominated two hearings last week. Senator Barbara Mikulski (D-MD), who chairs NASA's funding panel, told NASA Administrator Michael Griffin that "there is simply too much pressure on NASA's budget." Her proposed solution—adding \$1 billion to the agency's \$17.3 billion 2008 request—would reprise a bipartisan effort that failed last year.

Earlier the same day, House Science and Technology Committee Chair Representative Bart Gordon (D-TN) warned Griffin that "NASA is headed for a train wreck." Both lawmakers fear that science will be robbed to pay for rising space station, shuttle, and exploration costs. The White House is likely to oppose a bigger budget. —ANDREW LAWLER

## Bignami Back in Orbit

**TURIN, ITALY**—Giovanni Bignami has returned to the Italian space agency, this time as its director. The space scientist was scientific director from 1997 to 2002, resigning after Italy decided to save \$20 million by backing off its commitment to build a radar instrument for a NASA spacecraft going to Mars.

Bignami says he accepted the job, offered last week, because he "strongly believes" Italy is committed to relaunching its space research program. Bignami currently chairs the space science advisory committee for the European Space Agency. "His high international profile will help Italian space science," says Marcello Onofri of the University of Rome, La Sapienza.

—FRANCESCO DE PRETIS

## Reflowing the Oceans

The ocean science community is reuniting two of its organizations in hopes that one voice will speak louder to Congress and the White House. The Consortium for Ocean Research and Education (CORE)—a 13-year-old advocate for ocean research, education, and policy—and the 31-member Joint Oceanographic Institutions (JOI)—manager of large-scale research programs such as ocean drilling—had separated in 2000 at a time of expanding support for ocean research. But now, many of those projects are being squeezed by soaring oil prices.

The merged organization will provide "a united voice for the community," says JOI board chair Marcia McNutt of the Monterey Bay Aquarium Research Institute in Moss Landing, California. Steven Bohlen now runs JOI, and retired Admiral Richard West heads up CORE.

—RICHARD A. KERR



## MICROBIOLOGY

## New Bacterial Defense Against Phage Invaders Identified

Humans are not alone in having to fend off pathogens; even the simplest organisms are under a constant threat of invasion. Bacteria, for example, are awash in a sea of viruses known as bacteriophages. "Every 2 days, half the bacteria on Earth are killed [by bacteriophages]," says phage expert Vincent Fischetti of Rockefeller University in New York City. "It's a constant battle." Researchers have now identified a new defense mechanism that helps bacteria hold their own in this battle.

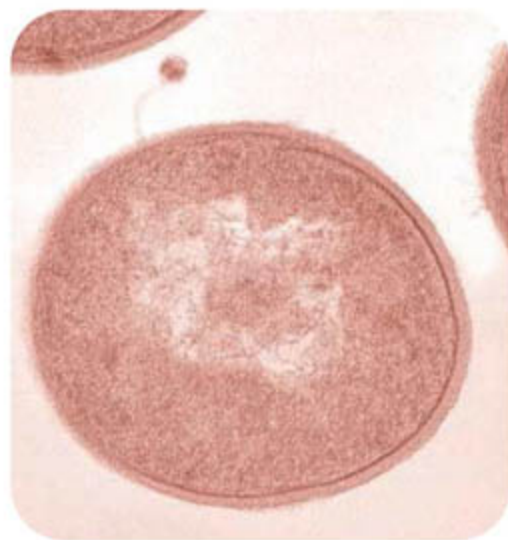
On page 1709, a team led by Philippe Horvath and Rodolphe Barrangou of Danisco, a Danish company that produces bacterial cultures and other materials for the food-processing industry, reports that bacteria use a system, apparently akin to the RNA interference (RNAi) system of higher organisms, to block phage reproduction, thus making them resistant to infection.

The work could help the food and biotechnology industries, which use bacterial cultures to make products such as cheese and yogurt as well as proteins for human medicine. These industries, Fischetti says, "have a

terrible problem with phage" ruining their cultures and could benefit from better phage-resistant bacterial strains.

The Danisco team's work also provides the first biological evidence for a function of so-called CRISPR sequences, which were identified in 2002 by Leo Schouls of the National Institute of Public Health in Bilthoven, the Netherlands, and his colleagues. These sequences, formally known by the descriptive name of "clustered regularly interspaced short palindromic repeats" because of the way they are arranged in the genome, are widely distributed in the genomes of both Bacteria and Archaea.

Accompanying the CRISPR sequences are a suite of perhaps four to 10 *cas* (CRISPR-associated) genes. Researchers have made a number of proposals about what these genes might do. For example, Eugene Koonin and Kira Makarova of the U.S. National Center for Biotechnology Information in Bethesda, Maryland, and their colleagues analyzed the *cas* sequences and, based on those structures, suggested in 2002 that they



**Invasion.** Bacteria such as this one may acquire key defensive sequences from infectious bacteriophage, attached at top.

might encode a new DNA repair system. But more recently, Koonin says, another idea emerged as several groups found that the spacer sequences within CRISPR regions resemble those of sequences in phage and also in plasmids, small extrachromosomal pieces of DNA that can be transmitted between bacterial species.

In a second analysis, published by *Biology Direct* on 16 March of last year, Makarova, Koonin, and colleagues ▶

## GEOLOGY

## A Trace of the Earliest Plate Tectonics Turns Up in Greenland

Geologists have discovered the earliest known remnants—by billions of years—of plate tectonics, the large-scale movement of Earth's crust. The rocks are preserved in plain sight among the intensely studied ancient rocks of southwest Greenland, a group of geologists reports on page 1704. These days, hot new sea floor forms from magma at mid-ocean ridges, spreads away as it cools, and eventually dives back into the deep interior. In its early days, Earth was still so hot throughout that researchers have wondered whether the planet might have been ridding itself of heat by some entirely different means. But the new discovery "indicates there was a modern-day plate tectonics operating shortly after formation of Earth," says geologist Yildirim Dilek of Miami University in Oxford, Ohio.

Innumerable geologists have walked and flown over southwest Greenland's 12-kilometer-long stretch of baked, twisted, and tortured rock known as the Isua supracrustal belt.

Dating from Earth's early adolescence 3.8 billion years ago, the Isua rocks hold clues to how the young planet worked, back when life might have gotten started. In fact, it was the search for microscopic signs of early life that brought geologist Harald Furnes of the University of Bergen, Norway, and colleagues to Isua in 2006. Furnes had long studied much younger scraps of ocean crust that had become stranded on land, called ophiolites, but that day he was looking for sea-floor lavas that might hold traces of ancient microbial borings.

Then Furnes and his colleagues came upon the sheeted dikes. These banded rocks are the hallmark of ophiolites and thus of sea-floor spreading. Built like a stack of cards, they are composed entirely of the thin sheets of once-molten rock injected into the crests of mid-ocean ridges as the newly formed plates spread away from the ridge. The Isua sheeted dikes are near previously identified components of ophiolites: distinctive "pillow" lavas extruded on

the sea floor from underlying dikes, rock that solidified in magma chambers that fed the dikes, and never-melted mantle rock below that. "The major components [of an ophiolite] appear to be all there," says geologist Kent Condie of the New Mexico Institute of Mining and Technology in Socorro. "I'm convinced."

So Earth had sea-floor spreading almost 2 billion years earlier than previously known. What about the other end of the tectonic process? Today, old sea floor dives steeply into the deep interior on top of a relatively cold, rigid slab of tectonic plate, a process called subduction. But some geophysicists had suspected that old ocean plates might once have recycled themselves differently—say, by sinking straight into a hot magma mush as if it were quicksand.

Furnes thinks, but can't prove, that something like modern-day subduction was going on 3.8 billion years ago. Rocks adjacent to the Isua ophiolite geochemically resemble ▶

CREDIT: SYLVAIN MOINEAU



proposed that the Cas proteins and CRISPR spacer sequences, which were presumably picked up by the bacteria during prior phage infections, together constitute a bacterial immune system that works by a mechanism similar to that of RNAi in higher organisms. The idea is that the spacers make short RNA sequences that can bind to complementary sequences in messenger RNAs made by invading phages. This would block their translation into proteins and mark them for degradation by Cas proteins, some of which resemble those known to be involved in RNAi.

The Danisco group has now provided direct evidence for that hypothesis. Working with the bacterium *Streptococcus thermophilus*, which is widely used to make yogurt and cheese, the researchers found that infection of the bacteria with phage leads to incorporation of phage-related spacer sequences within a CRISPR region. Such bacteria became resistant to further infection by the phage strains that contributed those sequences. But “if you take the spacers out, the resistance is lost,” says Horvath, who works at Danisco’s lab in Dangé-Saint-Romain, France. The team also showed that at least one *cas* gene, which encodes a possible RNA-dicing nuclease, is necessary for the phage resistance. This shows, Fischetti says, that bacteria have “a very neat mechanism by which they are able

to keep bacteriophage under control.”

Dennis Romero, a member of the Danisco team at the company’s lab in Madison, Wisconsin, says that the CRISPR system may have a wider function as well. “In addition to matching phage, the spacers also match chromosomal and plasmid sequences,” he notes, and thus they might help control normal bacterial gene activity.

Whether or not that is the case, the findings open the door to using the CRISPR system to block specific gene activity in bacteria, just as RNAi is used in higher organisms. And then there is the possibility of producing more phage-resistant bacterial strains for industrial use. This could be accomplished by genetically engineering bacteria with appropriate CRISPR spacer sequences; Horvath says, however, that “Danisco has no plans to do that in light of consumer concerns about the use of GMO [genetically modified organisms], particularly in Europe.”

The researchers plan instead to simply expose bacteria to various phage strains and then select for those that are resistant. They can, however, use their knowledge of the CRISPR spacers to help screen for bacteria that carry the right spacers to confer the resistance they want. “Although we can genetically engineer,” Romero says, “we found that nature can do the work for us.”

—JEAN MARX



**Signature rock.** Vertically layered rock discovered in Greenland confirms plate tectonics on early Earth.

rocks called boninites. These rocks are cooked up only beneath island chains perched over subduction zones like those in today’s western Pacific. If Isua has bona fide boninites, a magma mush would not work.

All the Isua rocks come from “a pretty well established subduction zone similar to what we have today,” concludes Dilek.

“They’re hard to explain in any other way.” Condie can’t quite agree. “I don’t think it’s 100% definitive,” he says. “There’s just enough ambiguity that it may or may not” have been entirely modern subduction. Enough ambiguity that Isua geologists will be heading back to the field with new eyes this summer.

—RICHARD A. KERR

## New Strategy to Fight AIDS

**PRETORIA, SOUTH AFRICA**—A new government plan aims to cut South Africa’s HIV infection rate in half and to quadruple the number of infected persons receiving anti-retroviral (ARV) therapy by 2011. The 5-year strategy, presented at a conference last week, sets targets to meet the commitments made by South Africa’s vice president in December (*Science*, 1 December 2006, p. 1378). The government will ask Parliament for nearly \$2 billion, about 40% of which would pay for ARV medications, and wants business donors to match that sum. Francois Venter, head of the Southern African HIV Clinicians Society, estimates that “more than a million” South Africans would be on ARVs in 5 years if the plan is fully implemented.

About 5.5 million South Africans are infected by HIV, and roughly 230,000 now receive ARV therapy. Robin Wood, co-director of the Desmond Tutu HIV Centre in Cape Town, calls the plan “a great advance.” Although the goal may be difficult to reach, he says, “it’s better to set targets too high than to have no targets.”

—ROBERT KOENIG

## Purdue Welcomes Mann Institute

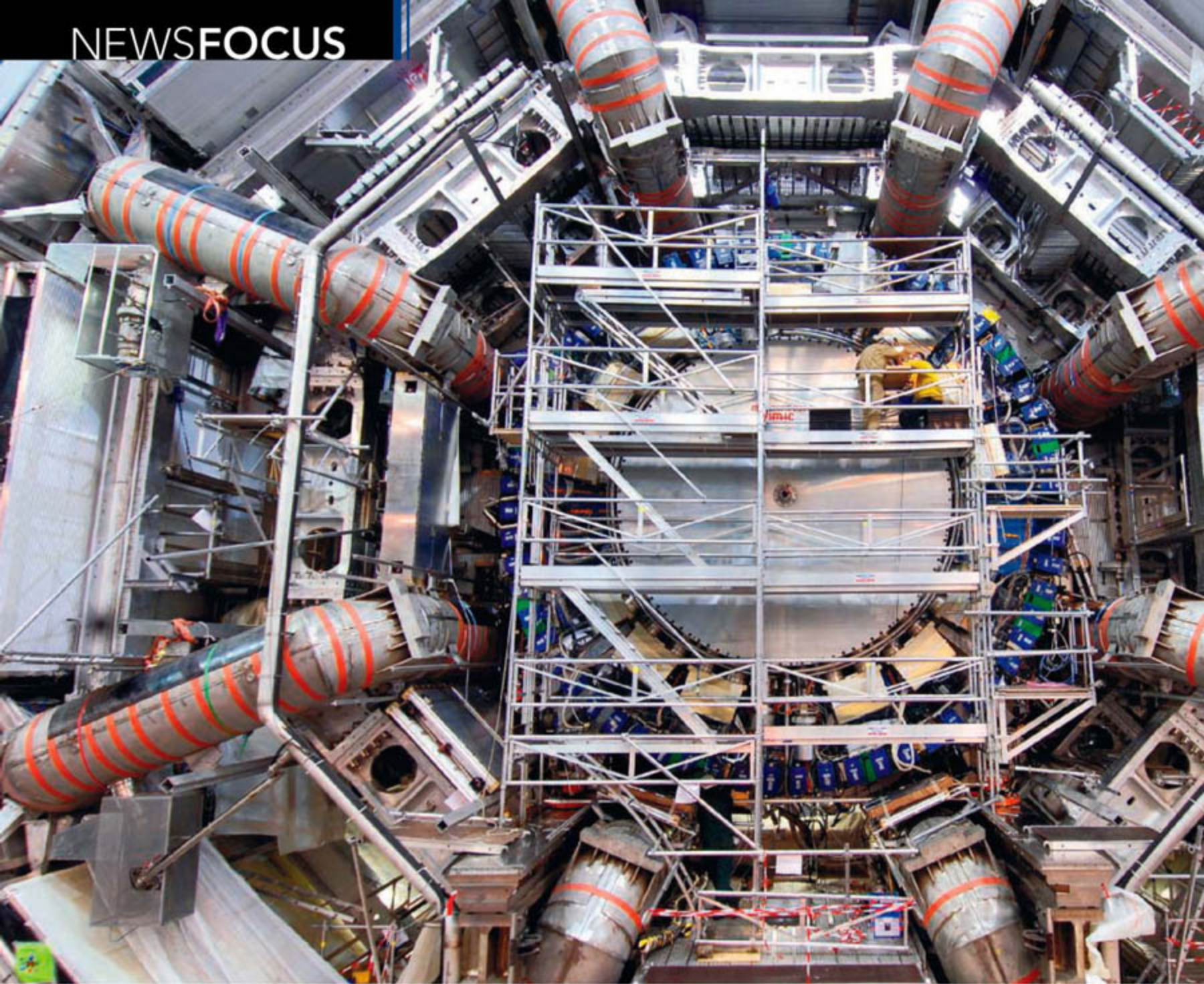
Purdue University in West Lafayette, Indiana, has clinched a deal to join what the Alfred Mann Foundation hopes will be a billion-dollar-plus network to shepherd university biomedical inventions to the market.

Alfred Mann institutes are designed to be governed by a board equally split between the university and the California-based Mann Foundation. Some universities have balked at the proposed arrangement, fearing a loss of control over their intellectual property. Last year, two North Carolina universities turned thumbs down on a Mann endowment (*Science*, 26 May 2006, p. 1127), although Mark Crowell, technology transfer official at the University of North Carolina, Chapel Hill, says the door is still open to negotiations.

One provision gives priority to Indiana companies in licensing or purchasing technologies developed at the institute. Purdue President Martin Jischke won’t discuss other details of the agreement, announced 16 March, but says everyone’s very happy with it. Mann intends to finance at least 10 more institutes. A prototype was set up in 1998 at the University of Southern California in Los Angeles, and a second was created last October at Technion University in Israel.

—CONSTANCE HOLDEN





# Having a Blast, Wish You Were Here

**The Large Hadron Collider at CERN will smash particles at unprecedented energy and may open new realms of discovery. It will secure Europe's ascendancy in particle physics for years to come**

NEAR GENEVA, SWITZERLAND—Measuring 15 meters across and weighing 13,010 metric tons, the enormous disk of machinery dangles from bundles of cables like a gigantic yo-yo. Sectioned like an orange and festooned with electrical cables, the contraption could be mistaken for a flying saucer hoisted on edge. In fact, it's part of a huge barrel-shaped particle detector, the Compact Muon Solenoid (CMS), that will soon snare bits of matter from the new

highest-energy particle smasher, the Large Hadron Collider (LHC) here at the European particle physics laboratory, CERN.

The colossus hovers a few centimeters above the concrete floor of a cavernous subterranean hall. All day, workers have lowered it down a shaft barely wide enough to take it. The 100-meter journey strains the nerves, says Hubert Gerwig, an engineer at CERN.

Now that it's almost over, Gerwig can relax a little. "Want to see it move?" he asks

Archana Sharma, a physicist at CERN. Gerwig pushes the wall of metal. "If you get a feel for the resonant frequency, you can excite it" to oscillate, he says. Sure enough, the giant stirs. "Okay, okay, it's moving!" shouts Sharma, as millions of dollars' worth of delicate equipment sways ever so slightly across the grain of the concrete.

Gerwig isn't the only one here who is a little giddy with nervous excitement. In a few months, CERN researchers will have completed the 27-kilometer-long LHC, and in November, they hope to put the largest and most complex experimental device ever built through its warm-up laps. Smashing particles at energies seven times higher than

CREDIT: MAXIMILIEN BRICE/CERN





◀ **Broad shoulders.** Protons will collide in the centers of titanic ATLAS and three other detectors.

Sweden. "And the U.S. recognizes that because it's investing a lot of money in the experiments here."

No one knows what the LHC will find. But this much is clear: The LHC has already created a revolution in particle physics.

#### LHC or -EST

It is difficult to describe the LHC without resorting to superlatives. Not only will the LHC smash particles at the highest energies, but it will also feed the largest and most complex particle detectors ever built for a collider. They will pump out the greatest torrent of data; in a year, each could fill a stack of DVDs 25 kilometers high. The LHC will consume a record 120 megawatts of power, enough to sustain every household in the canton of Geneva. At a cost of 4.7 billion Swiss francs (\$3.8 billion), it's the most expensive collider ever built. The United States is chipping in \$531 million, mostly for detectors.

Numbers alone cannot convey the immensity of the project, however. Step into the hall housing the ATLAS detector, and you find yourself face to face with a machine eight stories tall and half as long as a soccer field. The thing could fill the nave of a cathedral, but instead of the Holy Spirit, it's packed with particle trackers, light-emitting crystals, and enough other gizmos to fill 100 million data channels. And it's as precise as it is big, says CERN's Peter Jenni, spokesperson for the 1800-member ATLAS collaboration. It can measure the curving path of a particle called a muon to within 40 micrometers, half the width of a human hair.

Circling below the French countryside between Lake Geneva to the east and the Jura Mountains to the west, the accelerator itself looks a bit like a glorified sewer pipe. Visitors to the LHC's otherworldly tunnel must carry oxygen packs in case the machine's cryogenic system leaks suffocating helium; workers on bikes sneak up on the inattentive. The LHC lies along one side of the gently curving tunnel, an endless line of big blue cylinders connected end to end like sausages. These are the revolutionary magnets that steer the beams around the ring. Twice as strong as those at Fermilab's Tevatron, they in fact house two accelerators carrying protons in opposite directions.

The brawny collider aims foremost to discover one thing: a long-sought particle called the Higgs boson. The Higgs would complete the so-called standard model of the known particles, says Jonathan Ellis, a

theorist at CERN. "You could consider the Higgs boson the period on the end of the standard-model sentence," he says. But physicists hope the standard model is not the final word and that LHC will blast out other particles and surprises (see p. 1657). "We had Stephen Hawking here, and he told us that he wasn't so sure we'd find the Higgs boson and that he was more interested in mini-black holes," Jenni says. "People have different ideas."

Mighty ATLAS and CMS will race for those breakthroughs at the energy frontier. "It's going to come down to who is better prepared and whose detector is more complete" when the LHC starts running, says Tejinder Virdee of Imperial College London, spokesperson for the 2359-member CMS collaboration. "They can confirm [our discoveries], that's allowed." The LHC could discover the particles predicted by a concept called supersymmetry after running for just a year, Virdee says. But the

**"Society is willing to pay a certain amount and no more, and to make the LHC possible, we had to be innovative."**

—Lyndon Evans, CERN



LHC will also feed two specialized detectors to stake claims to leadership in other areas as well.

A detector called LHCb will study the asymmetries between particles containing elementary bits of matter called bottom quarks and their antimatter foils. Physicists at specialized colliders in the United States and Japan have studied the subtle differences as the bottoms decay to other "flavors" of quark, in hopes of finding hints of new particles (*Science*, 13 October 2006, p. 248). Even if ATLAS and CMS see those particles directly, "you want to study how things

the previous record, the LHC should blast out the one bit of matter missing from physicists' theory of the known particles. It could also spit out a slew of other particles and open a new era of discovery. The LHC will make CERN the world's center for particle physics.

Considering its size and technological complexity, the LHC "is the modern equivalent of the pyramids," says Peter Limon of Fermi National Accelerator Laboratory (Fermilab) in Batavia, Illinois, who is working on the machine. But the LHC is more than a technological marvel. It embodies a broader movement in particle physics. For decades, the United States paced the field. Now, as the LHC eclipses Fermilab's Tevatron collider, Europe takes the lead. "It is certainly true that the center of gravity of physics has moved to CERN," says Hans-Ake Gustafsson, an experimenter from Lund University in



couple to these new particles,” says CERN’s Tatsuya Nakada. “And that’s what you can do with flavor physics.”

Seven kilometers away, a detector named ALICE will study a soup of particles called a quark-gluon plasma. The ultrahot plasma filled the infant universe, and physicists at Brookhaven National Laboratory in Upton, New York, have recreated it by smashing gold nuclei with their Relativistic Heavy Ion Collider (RHIC). For a few weeks a year, the LHC will smash lead nuclei at energies 28 times higher, letting ALICE peer deeper into the fleeting plasma, says CERN’s Jürgen Schukraft. “The things you can look at here you can’t look at with RHIC even if you run it for 50 years,” he says.

### Two decades in the making

But first, researchers must complete the collider. After a decade of construction, they are on schedule to finish this year, says CERN’s Lyndon Evans, who leads the effort. (Researchers expect to lower the last magnet into the tunnel in mid-April.) A Welshman with a sonorous voice and silver hair, Evans has the phlegmatic demeanor of one who has dealt with crises large and small. On his computer he pulls up graph after graph of progress on the LHC’s myriad subsystems. On each a rising red “just in time” line stands out. “It has some magical properties,” Evans says. “Things tend to bounce off it” to stay on schedule.

In spite of the dash to the finish, the push

for the LHC has been a marathon. Physicists dreamt the collider up more than 20 years ago even as CERN built another machine, the Large Electron-Positron Collider (LEP), which ran from 1989 to 2000. In fact, they planned to reuse LEP’s tunnel and feed the LHC with existing accelerators. “Without that, it would have been impossible to build the machine on a constant [lab] budget,” says CERN Director General Robert Aymar. At the time, physicists in the United States were planning the 87-kilometer-long Superconducting Super Collider (SSC). The LHC couldn’t match the SSC’s energy, but it could smash more particles, says CERN chief scientist Jos Engelen. In 1993, the U.S. Congress killed the uncompleted SSC, leaving the field



## Stability, International Character Honed CERN’s Competitive Edge

The qualities that helped the lab make the LHC a reality could put it a step ahead in the race for the next great particle smasher

In the 1980s, physicists hammered out plans for a gargantuan particle smasher that would reveal the key bit of matter that would complete their theory of the known particles. The behemoth would also blast out scads of new particles and open new vistas of inner space. It would be the hub about which the world of particle physics would turn for decades.

Meanwhile, a few researchers at the European lab, CERN, near Geneva, Switzerland, mused of building a smaller machine on the cheap. They called it the

Large Hadron Collider (LHC).

Two decades later, the LHC is about to chase the discoveries never made by that other machine, the infamous Superconducting Super Collider (SSC). Designed to reach energies three times higher than those of the LHC, the SSC died uncompleted in 1993 when its budget ballooned from \$4.6 billion to more than \$8.3 billion and the U.S. Congress killed it.

Why did the SSC fail and the LHC succeed? Physicists can point to many stumbling

blocks that tripped up the SSC (*Science*, 3 October 2003, p. 38). Instead of building at an existing lab, officials chose a remote site in Waxahachie, Texas; researchers made a small but expensive design change; the United States tried to go it alone and sought international partners only belatedly. The LHC succeeded for reasons equally concrete—and those factors could give CERN the edge in the competition for the next gigantic collider, the proposed 31-kilometer-long straight-shot International Linear Collider (ILC).

All agree that CERN’s rock-steady budget was a key to its success in building the LHC. In keeping with the treaty that created the lab in 1954, each of CERN’s now 20 member nations supports the lab in proportion to its gross domestic product. “The treaty creates stability because the member countries recognize that this isn’t something

CREDIT: CERN



open for CERN, which gave the LHC the green light the following year.

Even recycling as much as they could, researchers had to push the limits of technology, Evans says: "Society is willing to pay a certain amount and no more, and to make the LHC possible, we had to be innovative." Researchers have designed the strongest magnets by far for an accelerator, crammed two accelerators into one set of magnets, used wires of high-temperature superconductor to distribute power, and pioneered a type of radiation-hard electronics for their detectors. They even chill the liquid helium that cools the magnets to an extra-frigid 1.9 kelvin to make it a free-flowing superfluid, which is also an out-

standing heat conductor.

To be sure, the LHC has hit some potholes along the way. In 2001, a review showed that the project was running behind schedule and 20% over budget, forcing the lab to scale back other projects and refinance the LHC (*Science*, 28 June 2002, p. 2317). In 2004, problems emerged with the cryogenic lines that transport the liquid helium to the magnets. Workers had to rip out, repair, and reinstall 3 kilometers of line, creating an enormous backup of the magnets they'd been installing as soon as they arrived. "I'd imagined storage for 50 magnets, and in the end I had to find room for 1000," says Evans, who scattered them all over the lab.

Now, about 2 years behind their original schedule, researchers see the light—or,

more correctly, the other end of the accelerator—at the end of the tunnel. Soon workers will put down their wrenches and welding torches, and researchers will begin to bring the machine to life. "We are very excited," Engelen says, "and a bit worried because now we have to deliver."

### See you in Switzerland

Already, physicists are flocking to CERN in anticipation. Some 7500 of 111 different nationalities have registered to work on the site, as the LHC lures talent away from other experiments, such as CDF and D0 at Fermilab. "When I was hired, I started to work on D0," says Adam Yurkewicz, a postdoc at Stony Brook University in New York. "But I

**Cosmopolitan.** CERN (*foreground*) hosts scientists of 111 different nationalities.

you vote up or down every year," says CERN Director General Robert Aymar. The arrangement sets the lab budget 5 years in advance and even allows officials to borrow against future income, as they did in 2002 when they found that the LHC was running 20% over budget. In contrast, the SSC was far more vulnerable. In the United States, Congress funds the national labs year by year, which means lab budgets fluctuate and projects such as the SSC face the ax repeatedly.

When building the LHC, CERN also benefited from moving continuously from one collider to the next. CERN researchers began designing the LHC even as they built another machine, the Large Electron-Positron Collider (LEP), which ran from 1989 to 2000. By using LEP's tunnel to house the LHC and existing accelerators to feed it, CERN officials saved billions of Swiss francs and built the LHC without an increase in the lab's budget.

Continuity has also helped the lab accrue talented personnel. "The most important thing to making a project like this work is the quality of the people working under you," says CERN's Lyndon Evans, who leads LHC construction. "One of our advantages [in maintaining staff] is that we came off another project, LEP, which wasn't so long ago."

Even before the LHC is up and running, physicists around the world are looking toward the next big accelerator and are trying to draw some lessons from the contrasting fates of the LHC and the SSC. They say they will need the ILC to study in detail the new particles the LHC should spot (*Science*, 21 February 2003, p. 1171). Researchers in the United States, Japan, and Europe all

want to build the machine close to home, and "the U.S. and Japan had better look up and humbly learn from CERN's history and experience," says Nobu Toge of the Japanese accelerator laboratory KEK in Tsukuba. Still, Toge adds, "everyone has a long way to go to learn how to make the ILC a successful global project before jumping over each other to see who is to host it."



**"Very probably, CERN has an advantage over any other place to host an even-more-international effort than" the LHC.**

—Robert Aymar, CERN

That hasn't stopped early jockeying, however. Europeans point to CERN's success with the LHC and its explicitly international character as big plusses. "Very probably, CERN has an advantage over any other place to host an even-more-international effort than already exists," says CERN's Aymar.

But Japanese and American physicists say they have advantages of their own. For exam-

ple, CERN's unwavering budget could actually be a liability in the competition for the ILC. Although CERN's funding doesn't dip unpredictably, it also doesn't climb quickly, as all 20 member nations must agree on any increase. In contrast, the U.S. government can rapidly ramp up funding for projects. "The U.S. system is more dynamic and can react to things more quickly," says Pier Oddone, director of Fermi National Accelerator Laboratory in Batavia, Illinois. That may be important for the ILC, which will probably cost between \$10 billion and \$15 billion, with the host picking up half the tab.

Physicists in North America and Asia also note that, although CERN is an international laboratory, it does not embrace all countries equally. CERN's 20 member nations enjoy a special status compared to "guest" nations such as Japan and the United States, and many question whether the treaty structure is flexible enough to accommodate a truly global project.

Timing may be key. CERN will be paying off the LHC until 2011, and after that, the lab plans to upgrade the machine to produce even more collisions. So CERN will have its hands full until the middle of the next decade. In contrast, the United States will have no colliders for particle physics in operation after 2009. Japan has a smaller collider that it may upgrade and will soon be finishing a large proton accelerator complex. "If we plan to build the ILC in the 2020s, CERN is a good candidate," says KEK's Mitsuaki Nozaki. "However, if we wish to start construction soon after the first physics results come out of the LHC around 2010, then the U.S. and Japan are the only realistic candidates."

Of course, whether the ILC gets built at all depends on whether the LHC discovers anything worthy of further study. —A.C.





**Bargain basement.** CERN saved billions by building the LHC in a tunnel drilled for an earlier accelerator.

told them I wanted to switch to ATLAS because it's the forefront; it's the place for discovery."

In fact, CERN feels a bit like a resort for the nerdy set. Motley buildings nestle along streets named for Einstein, Feynman, and other famous physicists. Here and there lies equipment awaiting assembly. In the evenings, friends meet in the cafeteria to chat over a beer, a Danish Carlsberg or Czech Budweiser. "There is a different atmosphere than in the U.S.," says David Silvermyr, a Swede from Oak Ridge National Laboratory in Tennessee. "If you go to lunch here, people are talking about, 'We're excited about this,' or 'We're going to build that.' In the U.S., people talk about budgets."

But if the LHC is changing the map of particle physics, it also marks a leap in the field's evolution toward ever-bigger projects. Since the 1960s, experimental collaborations have grown to include dozens, then hundreds, and now thousands of scientists. That explosive expansion has led some particle physicists to seek more intimate environs in other fields (*Science*, 5 January, p. 56). But it doesn't faze those who have chosen to work at the LHC. "I'd still have a sense of satisfaction no matter what was discovered and how big a role I had in it," Yurkewicz says. "I'd know that I contributed."

Nevertheless, researchers recognize the challenge of rising from such a crowd to a position of leadership. "It is a very competitive environment," says Rosy Nikolaidou of CEA Saclay, France, who works on ATLAS. "Each day, you have to prove that you are the best and that you deserve your chance." Nektarios Benekos, an ATLAS member from the Max Planck Institute for Physics in Munich, Germany, says young researchers must think strategically to avoid, for example, being pigeonholed. "For sure, you must not stick too much to a par-

ticular subsystem, because you lose touch with the entire detector," he says.

Those who cannot move to Europe face the challenge of keeping contact with experiments thousands of kilometers away. That's a big problem for American physicists, who make up 20% of the ATLAS team and 30% of the CMS team. To address it, physicists are relying in part on a high-capacity computing network called the Grid to transmit data to key labs in other countries. Those "analysis support centers" will serve as gathering places that bring the LHC a little closer to home, says Michael Tuts of Columbia University, who manages the U.S.'s ATLAS research program. "They're places where you can go and get the water-cooler conversation," he says.

In fact, even as CERN draws people, the Grid should help extend the reach of particle physics across the globe, says Harvey Newman of the California Institute of Technology in Pasadena, who chairs the board that oversees the U.S.'s CMS team. "There are countries that weren't in the field in a serious way, and now they are there," he says. For example, physicists in Pakistan, India, and Brazil will have access to the LHC data in their home countries.

### Waking the giant

The full torrent of terabytes may be a while in coming, however. Researchers plan to send protons around the ring in November and begin taking data next spring. Even then they will start at low energy—less than half the Tevatron's—and with low beam intensity, or "luminosity." "If we can get up to a tenth of design [luminosity at full energy] after the first year, I think that would be miraculous," says Michael Lamont, an accelerator physicist at CERN. "And I think the experimenters would be quite happy with that."

Researchers must go slow because the LHC is the first collider powerful enough to destroy itself. Each of the LHC's beams packs a staggering 362 megajoules of energy, the equivalent of 90 kilograms of TNT and enough to melt 500 kilograms of copper. Should the machine accidentally steer a beam into its own innards, the protons could drill a hole tens of meters long, potentially taking the LHC out of action for months.

To prevent such a calamity, accelerator physicists have gone to extremes to protect the LHC from itself. More than 4000 super-fast beam-loss monitors will sense protons spraying out of the beam. Independently, beam-current monitors will infer losses by measuring the amount of circulating charge. And beam-position monitors will sense when the beams stray from their proper course. These systems can trigger magnets that can safely kick the beams out of the machine in the few hundred microseconds it takes to make two or three revolutions, less time than it takes a wobbly beam to veer off course entirely. "For the LHC, we've tried from the start to cover all the different possible failure scenarios so that we don't have an accident," says CERN's Rüdiger Schmidt.

Even if nothing goes wrong, physicists must take extraordinary steps just to make the LHC run. The collider is designed to pack  $10^{14}$  protons into each beam, and if just one 10-millionth of them flew into a magnet, they would heat it enough to temporarily kill its superconductivity, triggering a beam dump. To avoid such "quenches," researchers have installed hundreds of adjustable constrictions called collimators that will catch the inevitable wayward particles. "Out of every 1000 particles [headed toward the collimators], not more than one should escape to reach the magnets downstream," says CERN's Ralph Assmann. "Without this system, the LHC cannot run."

Those are just the technical challenges. When the time finally arrives to power up the machine, the main challenge will be managing the people, Lamont says. "There's going to be a lot of people standing in the control room, maybe not twiddling the knobs but looking over your shoulder, and that's as it should be; this is as exciting as it gets," Lamont says. "But what you really want is four guys sitting behind closed doors quietly figuring out how to make it work." Those four will have to cope with the crowd. Who could blame anyone for wanting to be there when the LHC ushers in a new era in particle physics?

—ADRIAN CHO

CREDIT: CERN



# Physicists' Nightmare Scenario: The Higgs and Nothing Else

Many fear the LHC will cough up only the one particle they've sought for decades. Some would rather see nothing new at all

Suppose you are a particle physicist. A score of nations has given you several billion Swiss francs to build a machine that will probe the origins of mass, that ineffable something that keeps an object in steady motion unless shoved by a force. Your proposed explanation of mass requires a new particle, cryptically dubbed the Higgs boson, that your machine aims to spy. When, after 2 decades of preparation, you get ready to switch on your rig, you would fear nothing more than the possibility that you were wrong and the particle doesn't exist, right? Not exactly.

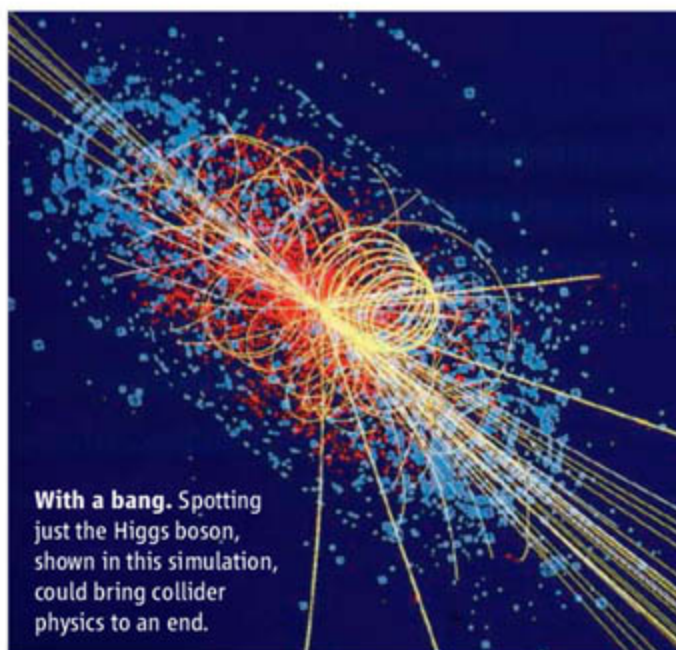
Many particle physicists say their greatest fear is that their grand new machine—the Large Hadron Collider (LHC) under construction at the European particle physics laboratory, CERN, near Geneva, Switzerland—will spot the Higgs boson and nothing else. If so, particle physics could grind to halt, they say. In fact, if the LHC doesn't reveal a plethora of new particles in addition to the Higgs, many say they would rather it see nothing new at all.

That may seem perverse, but put yourself again in the shoes of a particle physicist. In the 1960s and 1970s, researchers hammered out a theory called the standard model that, in spite of leaving out gravity and suffering from other shortcomings, has explained everything seen in collider experiments ever since and left physicists with few clues to a deeper theory. At the energies the LHC will reach, the standard model goes haywire, spitting out negative probabilities and other nonsense. So the collider has to cough up *something* new, researchers say. If it spits out only the Higgs, however, the new golden age of discovery could end as soon as it begins.

If the lone Higgs has just the right mass—about 190 times the mass of a proton—it would tie up the standard model's loose ends and leave physicists even more thoroughly stymied than before, says Jonathan Ellis, a theorist at CERN. "This would be the real five-star disaster," he says, "because that would mean there wouldn't need to be any new physics all the way up to the Planck

scale," the mind-bogglingly high energy at which gravity pulls as hard as the other forces of nature. The Higgs alone could essentially mark a dissatisfying end to the ages-long quest into the essence of matter.

If, on the other hand, the LHC sees no new particles at all, then the very rules of quantum mechanics and even Einstein's special theory of relativity must be wrong. "It would mean that everything we thought we knew about everything falls apart," says



With a bang. Spotting just the Higgs boson, shown in this simulation, could bring collider physics to an end.

Harvey Newman, an experimenter at the California Institute of Technology in Pasadena. That would thrill many but is so unlikely that it would be "essentially impossible" for the LHC to see nothing new, Newman says. Others agree.

Physicists have no similar guarantee that the LHC will reveal not only the Higgs but also exotic new particles that would point to new physics and open a new era of discovery. So the LHC is a gamble, and many are pulling for the more exciting long shots.

## Quack like a Higgs

Easily the most famous particle not yet discovered, the Higgs has even been crowned the "God particle" by one Nobel laureate. In reality, however, it is merely an ad hoc solution to an abstruse problem in the standard model: how to give particles mass.

The particular challenge is to give mass to particles called the W and Z bosons, which convey the weak nuclear force. According to the standard model, the weak force that causes a type of radioactive decay and the electromagnetic force that powers lightning and laptop computers are two facets of the same single thing. The two forces aren't precisely interchangeable: Electromagnetic forces can stretch between the stars, whereas the weak force doesn't even reach across the atomic nucleus. That range difference arises because photons, the quantum particles that make up an electromagnetic field, have no mass. In contrast, the particles that make up the weak force field, the W and Z bosons, are about 86 and 97 times as massive as the proton.

Unfortunately, the persnickety standard model falls apart if theorists simply assign masses to the W, Z, and other particles. So the masses must somehow arise from interactions of the otherwise massless particles themselves. In the 1960s, Peter Higgs, a theorist at Edinburgh University in the U.K., realized that empty space might be filled with a field, a bit like an electric field, that could drag on particles to give them inertia, the essence of mass. The field would consist of a new particle, the Higgs boson, lurking "virtually" in the vacuum.

Nature appears to follow this scheme. Using it, theorists predicted the masses of the W and Z. And at CERN in 1983, the two particles weighed in just as expected, in collisions energetic enough to pop them out of the vacuum.

Now, mounds of data point to the Higgs. For example, the lifetime and other properties of the Z depend on the cloud of virtual particles flitting around it like flies swarming a rotten ham sandwich. Precise studies of the Z suggest that a Higgs at most 200 times as hefty as the proton lurks in that cloud. Comparing the masses of the W and a particle called the top quark shows a similar thing, says Gordon Kane, a theorist at the University of Michigan, Ann Arbor. "These are two completely independent pieces of evidence that there is something that walks and talks and quacks like a Higgs," Kane says. "The existence of the Higgs in the LHC range is essentially certain."

Discovering the Higgs would complete the standard model. But finding *only* the Higgs would give physicists little to go on in



their quest to answer deeper questions, such as whether the four forces of nature are somehow different aspects of the same thing, says Aldo Deandrea, a theorist at the University of Lyon I in France. "If you have just a Higgs that is consistent with the standard model, then you probably don't know what to do next," he says. "What then?"

### Good taste and extra dimensions

Most researchers say they'll never face that question because the LHC will discover plenty of other things. Many expect it to blast out particles predicted by a concept called supersymmetry (SUSY), which posits a heavier "superpartner" for every known particle. That may seem unduly complicated, but SUSY solves problems within the standard model, points toward a deeper theory, and may even explain the mysterious dark matter whose gravity holds the galaxies together. "SUSY is unique in that it does all these things automatically," CERN's Ellis says.

Most concretely, SUSY solves a technical problem caused by the Higgs boson itself. The Higgs, too, must be shrouded in virtual particles, and they ought to send its mass skyrocketing. SUSY would explain why the Higgs is as light as it appears to be, because mathematically the effects of partner and superpartner on the Higgs mass tend to cancel each other. SUSY would also help explain the origin of the Higgs, which is just tacked onto the standard model but emerges naturally from the structure of SUSY.

SUSY could also help unify the four forces. The standard model accounts for three of them: the electromagnetic force, the weak force, and the strong nuclear force that binds particles called quarks into protons, neutrons, and other particles. The strengths of the three increase with the energy of collisions, and if the universe is supersymmetric, then all begin to tug equally hard at precisely the same energy somewhere below the Planck scale. That should make it easier to roll them and gravity together in one grand unified theory, says Frank Wilczek, a theorist at the Massachusetts Institute of Technology in Cambridge.

SUSY might even provide the dark matter that glues the galaxies together. Physicists believe that dark matter must consist of some stable particle that barely



If it has the right mass, the Higgs and nothing else "would be the real five-star disaster, because that would mean there wouldn't need to be any new physics."

—Jonathan Ellis, CERN

interacts with normal matter, and the least massive superpartner might just fit the bill. With all this evidence supporting it, SUSY is almost too beautiful to be wrong, some theorists say. "All these clues could be misleading," Wilczek says, "but that would be a really cruel joke by Mother Nature—and in really bad taste on her part."

The LHC might also reveal far wilder phenomena, such as inner parts to electrons and other supposedly indivisible bits of matter, tiny black holes, or even new dimensions of space that open only at very high energies. The spare room

could explain, for example, why gravity is so much weaker than the other forces. "Something like extra dimensions I give a very small probability," says Michael Tuts, a physicist at Columbia University. "But the potential is so big that it's very exciting."

### A sure bet

None of these more exotic possibilities is guaranteed. And particle physicists say that just discovering the Higgs would be a triumph. "If the Higgs is anything like theorists predict, we will find it," says Peter Jenni, an experimenter at CERN. "We shouldn't be disappointed if we do."

Physicists also admit that, regardless of the intellectual foment it would cause, finding nothing would create problems, at least with the governments that paid for the LHC. "Just imagine if we go to the CERN Council and say, 'Thank you very much, we've just spent billions of Swiss francs, and there's nothing there,'" Ellis says. "I think they might be a tad disappointed."

However, finding only the Higgs may make life nearly as difficult for physicists trying to persuade governments to build the next great particle smasher, the proposed International Linear Collider (ILC). Costing between \$10 billion and \$15 billion, the ILC would map out the conceptual terrain opened by the LHC (*Science*, 9 February, p. 746). By colliding indivisible electrons and positrons, the ILC would generate cleaner collisions that should reveal details of new particles that will be obscured by the messy proton-on-proton collision at LHC.

But if the ILC has only the Higgs to study, then it becomes "a very hard sell both scientifically and politically," says David Cinabro, a particle-physicist-turned-astronomer at Wayne State University in Detroit, Michigan. "I think you'll have a really hard time arguing that's what you want \$10 billion for," he says.

Others say such speculation is premature and pessimistic. "We are so used to discussing the new territory that we are going to enter that sometimes we think that we know what we are going to find," says Jos Engelen, chief scientist at CERN. "Well, we don't, and I think it will be much more exciting than we expect." That may be, but this much is certain already: Everyone hopes for more than just the Higgs.

—ADRIAN CHO

CREDIT: CERN

**LHC Stakes** 1.49 million furlongs per second.

**Purse:** Nobel Prize for long-sought particles, well-motivated theoretical concepts, and speculative guesses.

DISCOVERY	COMMENTS	ODDS*
Standard Model Higgs	As good as discovered, some say	2-1
Big surprises	Expect the unexpected	2-1
Supersymmetry	Too beautiful to be wrong?	5-1
Extra dimensions	More an inspired guess than a prediction	14-1
Composite electrons, etc.	Bigger fleas have littler fleas ...	14-1
Leptoquarks	Weird particles hinted at by another collider	49-1
Nothing	Be careful what you wish for	7-1

\* Based on survey of roughly 300 grad students, postdocs, and professors at Fermilab, as reported in the January/February issue of *Symmetry Magazine*. Respondents could choose more than one prediction.





◀ **Home wrecker.** Gouchan and Renubala Ari lost their son and daughter-in-law to skin cancer attributed to drinking arsenic-contaminated water.

## TOXICOLOGY

## A Sluggish Response to Humanity's Biggest Mass Poisoning

**Arsenic-laced water has sickened thousands in South Asia. After delays and false starts, India is addressing the problem with a \$500 million safe-water initiative**

**CHANDALATHI, INDIA**—Until the mid-1990s, the biggest foe of Gouchan and Renubala Ari and their extended family was poverty. Then a more insidious menace began to stalk the Ari home in Chandalathi, a cluster of mud huts on the edge of a yellow mustard field some 60 kilometers north of Kolkata. The first signs of trouble were brown spots on their hands and feet that, as the months passed, developed into thick calluses and lesions. It was several years later that doctors visiting the area recognized the hallmark symptoms of arsenic poisoning.

Tests confirmed that water from the well the Aris were using was laden with arsenic. Their oldest son and his wife were diagnosed with skin cancer, a disease linked with chronic low-level arsenic exposure. Gouchan sold his cow, goats, and ducks to pay for their treatment. The couple died anyway. Afraid of suffering the same fate, two younger sons moved to other parts of India. "Arsenic destroyed our home," says Gouchan, a frail 76-year-old who walks with a limp because of arsenic lesions. "I'm tired of showing my calluses to strangers," adds Renubala. "Who can understand our misery?"

Thousands of families in the state of West Bengal have been affected by this blight. More than 40 million people here live in areas with elevated levels of naturally occurring arsenic in the groundwater. Authorities estimate that 5 million in West Bengal drink water with arsenic concentrations above the government standard of 50 micrograms per liter. In neighboring Bangladesh, more than 82 million people live in contaminated areas. And the problem is widening: In recent years, researchers have found high levels of groundwater arsenic in several other Indian states, including Uttar Pradesh, Bihar, and Manipur.

Although there are no reliable statistics on arsenic victims in India and Bangladesh, one research group has counted at least 14,000 cases of arsenicosis in West Bengal alone. The

arsenic scourge, says Allan Smith, an epidemiologist at the University of California, Berkeley, is the "largest poisoning of a population in history."

It didn't have to turn out this way—certainly not in India, whose government frequently touts the country's burgeoning science and technology capacity. Here in West Bengal, officials have had a quarter-century to tackle the contamination. (Bangladesh learned of the threat a decade later.) Yet the government failed to investigate it adequately or provide alternative water resources to affected areas, critics charge. "For many years, government officials accused us of lying and exaggerating the problem," says dermatologist Kshitish Saha, who uncovered the first cases of arsenicosis while at the School of Tropical Medicine in Kolkata.

Since the early 1990s, when Indian authorities began to respond more vigorously to the crisis, state and national governments have pumped tens of millions of dollars into solutions aimed at providing safe water. The results have been lackluster. A \$7 million initiative to fit wells with arsenic filtration units failed because of improper maintenance. Another strategy—drilling deep wells that bypass arsenic-tainted aquifers—has produced mixed results.

The most deplorable aspect of the tragedy, critics say, is that Indian officials have resisted educating villagers about the threat, partly out of concern that this could lead to societal unrest. This is unconscionable, says Dipankar Chakraborti, an environmental scientist at Jadavpur University (JU) in Kolkata. "If people are made to realize the dangers of drinking arsenic-contaminated water, they will take care of their own safety," he says.

West Bengal officials acknowledge that the state erred. But they say that a half-billion-dollar initiative now under way to install eight surface-water treatment plants and 360 high-capacity, deep wells fitted with arsenic-removal facilities will provide a long-term remedy to what ranks as one of the biggest public health disasters of the modern world. "Yes, there have been



**Mark of a killer.** Renubala's palms bear the brown calluses that are a hallmark symptom of arsenicosis.



delays,” says D. N. Guha Majumdar, a gastroenterologist on West Bengal’s arsenic task force. “But the government is acting now.”

### Shallow reactions

Until the mid-1960s, much of West Bengal relied on untreated water from ponds, rivers, and open wells; as a result, cholera and other lethal waterborne diseases took a heavy toll. A savior arrived in the form of shallow tube wells, pipes bored into the ground with a hand pump at the top. When the technology for sinking this sort of well became affordable, the government and private citizens began installing them by the thousands. Deaths from infectious diseases fell sharply.

But the tube wells spawned a new epidemic. After Saha first linked brown calluses to groundwater arsenic in 1982, the local government appointed a panel to examine the problem and find countermeasures. Over the next 5 years, teams from the School of Tropical Medicine, the All India Institute of Hygiene and Public Health, and other institutions documented evidence of chronic toxicity among hundreds of villagers in six districts of West Bengal.

Although some experts early on blamed the illnesses on industrial pollution, it soon became clear that the culprit was arsenic in alluvial aquifers. Researchers studying the phenomenon—seen in many other countries, including China, Vietnam, Chile, and the United States—now believe that soil microbes liberate arsenic from harmless pyrites in the alluvium. Open wells, even in arsenic-rich areas, typically have low arsenic concentrations because when the water stands exposed to air for days, the metal binds to iron oxides and other compounds and precipitates out of the water column. This does not happen in an enclosed tube well.

The crisis persuaded Chakraborti to give up a career in the United States and return to his Kolkata roots in 1988 to found the School of Environmental Studies at JU. Over the next 6 years, he and his group tested hundreds of tube wells, as well as skin, hair, nail, and urine samples. They found that arsenic contamination was widespread. In some areas, the government dug deep wells. But officials disputed the magnitude of the problem and ignored calls from Chakraborti and others to harness West Bengal’s plentiful surface-water resources for a long-term solution.

Frustrated, Chakraborti took off his gloves. (It is easy to mistake the pugnacious scientist for an activist. He once scolded the state’s environment minister for smoking at a meeting; on another occasion, he advised a prominent arsenic researcher to take a course in water testing.) Chakraborti organized an international conference at JU in February 1995, at least in part, he says, to embarrass officials into action (*Science*, 11 October 1996, p. 174). He put victims front and center. “I had 19 arsenic patients sitting in the first row,” he says. Seventeen have since died.

The 1995 conference made Chakraborti persona non grata to the state government: He

been installed in areas with potable groundwater, while 73 were delivering water with arsenic concentrations above the permissible limit. And some 175 units allowed water through with unacceptable levels of iron. “Overall, the study showed that 82% of the [units] were not useful,” the researchers reported last year in the *Water Quality Research Journal of Canada*. They blamed it on a lack of maintenance, including a failure to periodically replace adsorption media.

West Bengal officials dispute Chakraborti’s analysis. Amiya Banerjee, chief engineer of the state’s Public Health Engineering Directorate, claims that 70% of the installed arsenic-

removal units are working fine. But he acknowledges that they are not being maintained well. Even before Chakraborti’s study came out, the West Bengal government in early 2006 announced that it would no longer equip hand pumps with arsenic-removal units. “We realized that the government cannot oversee the maintenance of these units,” Banerjee says.

Chakraborti’s group has also assailed the government’s strategy for boring deep tube wells indiscriminately. In the past 10 years, the researchers have found that at least 20 deep wells—100 to 150 meters deep—in West Bengal’s North 24 Parganas and Murshidabad districts have gone from having virtually no arsenic in the water at the outset to concentrations ranging from 50 to 150 micrograms per liter (exceeding the 50-microgram limit) within 7 years. Even now,

people seem blind to the risks: In interviews with *Science*, some villagers in North 24 Parganas district said they trusted that the water they drink from one of these wells is safe. Chakraborti argues that deep tube wells should be sunk only in areas where there is a thick clay barrier between the shallow, arsenic-contaminated aquifer and the deeper aquifer being tapped. “Subsurface geology should guide the strategy,” he says.

Others disagree. Alexander van Geen, a geologist at Columbia University, is a strong advocate of deep tube wells as a short-term solution in Bangladesh. He says that mechanical failure of the wells, not arsenic leaching into deeper aquifers, is to blame for the handful of tainted wells. “Because of flawed construction, you end up drawing the shallow water,” says van Geen, whose team has documented four such failures out of 51 deep tube wells monitored over 5 years in the Atraihar region in



says he has been shut out of government-sponsored meetings and accused of being a traitor. But the event had an impact. The next year, West Bengal officials requested \$200 million from the national government for countermeasures, receiving less than half of the request. Part of the money expanded an initiative to sink deep tube wells in an effort to tap untainted water below the alluvial aquifers. And in 1998, West Bengal began equipping 2400 hand-pumped shallow tube wells with arsenic-removal units: \$1500 adsorption towers packed with substances such as alumina or iron oxide granules. The state also began building a surface-water treatment plant in Malda, one of the worst-affected districts.

For Chakraborti, this was not enough. Between 1999 and 2005, he and his colleagues evaluated the performance of nearly 600 of the hand-pumped arsenic-removal units. They uncovered numerous problems. Fifty units had



Bangladesh. Although he agrees with Chakraborti's push for surface water as a long-term solution, van Geen says deep tube wells, regularly monitored, are "hard to beat" as a source of safe water over the next 10 years.

Technical fixes may be debated, but nobody disputes the need for better public awareness. Years ago, the West Bengal government decided to paint tube wells with potable water blue or green and leave unsafe tube wells unmarked—rather than paint them red, as suggested by the government's arsenic task force. "The administration thought that would create unnecessary panic," says Chandan Sengupta, a task force member who formerly managed a UNICEF project aimed at tackling the arsenic problem. When JU researchers in the mid-1990s took it upon themselves to paint unsafe wells red, Chakraborti says, "one legislator had the tube wells painted green and went around with a loudspeaker telling villagers that the water in them was fine."

### Overcoming inertia

The headquarters of West Bengal's Public Health Engineering Directorate is located on the sixth floor of a dull high-rise in the heart of Kolkata. Dim stairwells are splattered with red marks from people spitting *paan*, a popular snack consisting of fragrant condiments wrapped in a leaf. Hallways throng with vendors making tea on little kerosene stoves. In a large, open office room, desks are covered with mountains of paper, but many of the directorate's clerks and mid-ranking employees are nowhere to be seen. Across the hall, aides stand guard outside the private offices of senior officials, such as chief engineer Amiya Banerjee.

Banerjee says that the government's handling of the arsenic crisis is now robust. "We knew all along that surface water had to be the long-term solution, but we needed a quick fix in the interim," he says, referring to the deep tube wells and arsenic-removal units for hand-pumped wells. Banerjee also defends the decision not to paint unsafe

tube wells red, explaining that doing so would likely have deterred villagers from drawing water for safe uses such as washing.

In any case, Banerjee says, the government is now implementing long-term solutions.

## A Young Scientist Shaped by Adversity

**KOLKATA**—First his uncle succumbed. Then his father, then his aunt. In 2004, when Kartik Biswas saw his mother, Dulali, develop the same lesions that presaged the deaths of his other family members, he took a 5-hour ride by bus and train from his village in Nadia district to Kolkata to seek out Dipankar Chakraborti, a crusading arsenic researcher at Jadavpur University. The encounter changed Biswas's life.

Chakraborti helped get Dulali admitted to a government hospital. Tests confirmed arsenicosis, and she underwent a skin graft on her palm. After bringing his mother home, Biswas spread the word on arsenic—for instance, by advising villagers which tube wells had tested positive for arsenic in Chakraborti's lab—and collected water samples for further testing. In 2005, Dulali got sick again and was diagnosed with skin cancer. Doctors amputated her arm, but the cancer had already spread, and she died last October.

This fall, Biswas, who is completing a master's degree in geography at a local college, will join Chakraborti's lab as a Ph.D. student to study countermeasures to groundwater contamination. Says Biswas, whose palms and feet bear the marks of mild arsenicosis, "Nobody should have to see their mother suffer like I did."

—Y.B.



Groundwater will continue to be the mainstay. Under a \$500 million initiative funded jointly by the state and national governments, West Bengal is sinking 360 large-diameter deep tube wells equipped with arsenic-treatment facilities to pipe water to 70% of the affected population. Government engineers will supervise maintenance of the treatment plants, Banerjee says.

Chakraborti contends that fitting each well with an arsenic-treatment plant is a waste of money, considering that only a small percentage of wells is likely to become contaminated. Van Geen too labels the plan as flawed. "Instead of setting up the treatment plants right away, it makes more sense to design a pumping system that could be connected to an arsenic-treatment module in the future if the need arises," he says. If the government is determined to install large arsenic-treatment plants, he

argues, it would be wiser to purify water from shallow, contaminated aquifers and conserve the deeper, arsenic-free aquifers for future use.

Also under the West Bengal initiative, five surface-water treatment plants are being

built. Together with three plants already commissioned in North 24 Parganas, South 24 Parganas, and Malda, they will serve 30% of the affected population. To pay for operating costs, the government will charge families a connection fee and about \$1 a month. That's a risky strategy. Indian villagers typically don't pay for water, which officials acknowledge makes it difficult to get them to switch from a public tube well to a piped water connection. In the 3 years that the South 24 Parganas plant has been in operation, only 25,000 out of the 300,000 homes intended to be covered by the plant have taken a connection.

Other efforts under way include the distribution of cheap domestic filters and a drive to ensure that all 600,000 private tube wells are tested for arsenic. Majumdar of West Bengal's arsenic task force expects that everybody in West Bengal will have safe drinking water within 3 years.

Chakraborti is not as optimistic. And he wonders how many more people will suffer if awareness is not made an urgent priority. On a recent visit to Nadia district, he met a man with classic arsenicosis lesions who had never heard about arsenic before doctors diagnosed his disease last December. "This man drank contaminated water for years and then had to sell his land to find out what he was suffering from," Chakraborti says. "What is happening here is a grave injustice."

—YUDHIJIT BHATTACHARJEE



**Defunct.** Numerous arsenic-removal units installed by the West Bengal government no longer work due to lack of maintenance.



Q What can *Science* STKE give me?

A The definitive resource on  
cellular regulation



STKE – Signal Transduction  
Knowledge Environment offers:

- A weekly electronic journal
- Information management tools
- A lab manual to help you organize your research
- An interactive database of signaling pathways

STKE gives you essential tools to power your understanding of cell signaling. It is also a vibrant virtual community, where researchers from around the world come together to exchange information and ideas. For more information go to [www.stke.org](http://www.stke.org)

To sign up today, visit [promo.aaas.org/stkeas](http://promo.aaas.org/stkeas)

Sitewide access is available for institutions.

To find out more e-mail [stkelicense@aaas.org](mailto:stkelicense@aaas.org)





Dealing with differences

1668



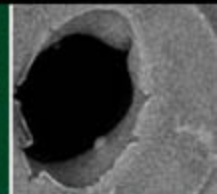
Meeting emission targets

1670



Plant hormone receptors

1676



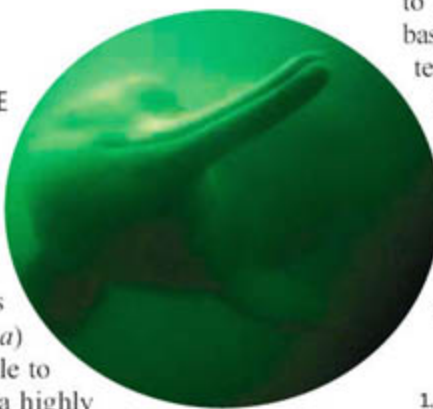
LETTERS | BOOKS | POLICY FORUM | EDUCATION FORUM | PERSPECTIVES

## LETTERS

edited by Etta Kavanagh

### The Loss of a Valuable Dolphin

JERRY GUO'S ARTICLE "RIVER DOLPHINS DOWN FOR THE count, and perhaps out" (News of the Week, 22 Dec. 2006, p. 1860) revealed no sightings of a baiji dolphin (*Lipotes vexillifer*) during a recent comprehensive survey. If, as expected, this species is truly extinct, then the loss to both the natural and physical sciences is more profound than most realize. This animal is one of only two species of river dolphins (the other being the Ganges river dolphin, *Platanista gangetica*) that, although bereft of vision and olfactory sense, are able to migrate, locate prey, and find mates while navigating in a highly dynamic riverine environment (1). The biology of both species is poorly known. However, insight into their biology could be expected to lead to advancements in acoustic-based sensors, geolocation, and navigation in extreme environments, as well as the development of technologies to assist vision-impaired persons.



The loss of this organism highlights the need for unbiased prioritization of conservation biology projects within the scientific community. Broader scientific potential contributions need to be considered in addition to general ecosystem health. Perhaps, other species at risk would receive more attention if the ramifications of their demise were better presented to the public.

MICHAEL D. KASS

Oak Ridge National Laboratory, Oak Ridge, TN 37831, USA.

#### Reference

1. See <http://nationalzoo.si.edu/Publications/ZooGoer/2003/5/RiverDolphins.cfm>.

### The Ethics of Transcranial Magnetic Stimulation

WHEN *SCIENCE* PUBLISHES RESEARCH USING healthy human subjects, one assumes there was minimal risk and/or vital clinical value. This does not appear to be the case for the work by D. Knoch and colleagues ("Diminishing reciprocal fairness by disrupting the right prefrontal cortex," Reports, 3 Nov. 2006, p. 829). Their results on the dorsolateral prefrontal cortex's role in judgments of fairness and self-interest are interesting, but they largely validated what was already suspected.

Experimental subjects received repetitive transcranial magnetic stimulation (rTMS) for 15 min to produce "suppression of activity in the stimulated brain region." The rTMS generated an electric maelstrom powerful enough to

disrupt all activity for 7 min. Animal rTMS research (with overexposure as in LD50 drug toxicity studies) shows that anything studied (e.g., receptor levels) is modified. For rTMS in humans, known risks range from headaches to, more rarely, seizures or psychosis (1). Long-term occult changes and self-reported symptoms in healthy subjects have not been studied, and rTMS continues to be used for studies both fascinating and frivolous (just check the literature).

The use of rTMS on healthy subjects does not meet the definition of "minimal risk" (45 CFR section 46.102: risks... "not greater ... than those ... encountered in daily life"). We know that healthy subjects don't risk seizures or psychosis in their "daily life." What we don't know is what the residual effects of this activity-swamping tsunami of electrical current are. The Report demon-

strates a naiveté about the possibility of rTMS having long-term or negative consequences. Oddly, some of these authors have used rTMS to treat neuropsychiatric disorders on the basis of its long-lasting effects (2). Roentgen's technology was also once thought harmless, and x-rays were used to check shoe sizes (3). We know better now.

LESLIE SARGENT JONES

Associate Professor, Pharmacology, Physiology and Neuroscience, School of Medicine, Member, Institutional Review Board, University of South Carolina, Columbia, SC 29208, USA. E-mail: [leslie.jones@schc.sc.edu](mailto:leslie.jones@schc.sc.edu)

#### References

1. K. Machii, D. Cohen, C. Ramos-Estebanez, A. Pascual-Leone, *Clin. Neurophysiol.* **117**, 455 (2006).
2. C. M. Miller, *Newsweek*, "Minds and magnets," 11 Dec. 2006 (<http://www.msnbc.msn.com/id/16008890/site/newsweek/>).
3. J. Duffin, C. R. R. Hayter, *Isis* **91**, 260 (2000).

#### Response

WE THANK JONES FOR HER LETTER, WHICH offers the opportunity to discuss the safety of transcranial magnetic stimulation (TMS) and the ethics of TMS research in humans and to address common prejudices about its application in healthy subjects. Research on human subjects should indeed be done with utmost attention to the protection of all participants. An international workshop on the safety of TMS held at the National Institutes of Health in June 1996 concluded that the risks of single-pulse, paired-pulse, and slow repetitive TMS ( $\leq 1$  Hz) are minimal for populations without certain predisposing conditions, provided that appropriate safety guidelines and precautions are followed (1). In our study, we applied slow, 1-Hz repetitive TMS (rTMS) in strict adherence to the recommended guidelines (1), which have been endorsed by the International Federation for Clinical Neurophysiology (2).

In predisposed patients, e.g., those on certain medications or with underlying neuropsychiatric conditions, there is a rare possibility for serious adverse effects, most notably a seizure or the induction of psychotic symptoms (3). However, these have never occurred with slow rTMS in healthy subjects. In addition, in all our studies, each subject partici-



pated voluntarily and on the basis of the provision of all relevant information. The experimental nature of the intended procedure was made clear at the outset, and all participants were fully informed of any reasonably foreseeable risks or discomforts and about the fact that they would not derive any direct benefit from their participation in the study. This included notification of the possibility of seizures.

Contrary to the opinion expressed by Jones, we firmly believe that the findings of our study provide novel insights into the role of the right dorsolateral prefrontal cortex (DLPFC) in the control of self-centered motives and in overriding economic temptations. Such findings may have profound applications for a variety of neuropsychiatric conditions. For example, increasing the level of activity in the right DLPFC might promote the inhibitory control of prepotent, impulsive responses and therefore diminish excessive risk-taking behavior in patients with impulse control disorders. If so, such an intervention might, for example, prove useful in clinical populations with drug or non-substance addictions (e.g., pathological gambling), in which impairments of decision-making seem to reflect a breakdown of these control processes (4). Preliminary findings in cocaine addicts reveal that high-frequency rTMS to the right DLPFC, which is thought to increase cortical excitability in the targeted brain region, reduces craving (5).

The ethical principles discussed in relation to TMS research in human subjects were initially articulated by Green *et al.* (6), and subsequent discussions and updates have appeared (7, 8). We believe that our study followed these articulated high standards and thus disagree with Jones's implications about the appropriateness of our experiment.

DARIA KNOCH,<sup>1</sup> ALVARO PASCUAL-LEONE,<sup>2</sup>  
ERNST FEHR<sup>3</sup>

<sup>1</sup>Institute for Empirical Research in Economics, University of Zurich, Blümlisalpstrasse 10, 8006 Zurich, Switzerland.

<sup>2</sup>Center for Noninvasive Brain Stimulation, Harvard Medical School and Beth Israel Deaconess Medical Center, Boston, MA 02115, USA.

#### References

1. E. M. Wassermann, *Electroencephalogr. Clin. Neurophysiol.* **108**, 1 (1998).
2. M. Hallett, E. M. Wassermann, A. Pascual-Leone, J. Valls-Sole, in *Recommendations for the Practice of Clinical Neurophysiology: Guidelines of the International Federation of Clinical Neurophysiology*, G. Deuschl, A. Eisen, Ed. (*Electroencephalogr. Clin. Neurophysiol. Suppl.* **52**, Elsevier, Amsterdam, 1999), pp. 105–113.
3. K. Machii, D. Cohen, C. Ramos-Estebanez, A. Pascual-Leone, *Clin. Neurophysiol.* **117**, 455 (2006).
4. S. E. Starkstein, R. G. Robinson, *J. Nerv. Ment. Dis.* **185**, 108 (1997).
5. J. A. Camprodon, J. Martinez-Raga, M. Alonso-Alonso, M. C. Shih, A. Pascual-Leone, *Drug Alcohol Depend.* **86**, 91 (2007).
6. R. M. Green, A. Pascual-Leone, E. M. Wasserman, *Irish J.* **19**, 1 (1997).

7. A. Pascual-Leone, N. Davey, E. M. Wassermann, J. Rothwell, B. K. Puri, *Handbook of Transcranial Magnetic Stimulation* (Arnold Press, London, 2001).
8. M. S. Steven, A. Pascual-Leone, in *Neuroethics: Defining the Issues in Research, Practice and Policy*, J. Illes, Ed. (Oxford Univ. Press, Oxford, UK, 2005), pp. 201–211.

## Comparing Neanderthal and Human Genomes

THE RECENT SEQUENCING OF SUBSTANTIAL parts of Neanderthal DNA ["Sequencing and analysis of Neanderthal genomic DNA," J. P. Noonan *et al.*, Research Article, 17 Nov. 2006, p. 1113; (1)] was preceded by releases of drafts of the chimpanzee and human genomes in 2005 and 2001, respectively. Green *et al.* (1) expect recovery of the complete Neanderthal genome within the next 2 years, which, it is hoped, will allow comparison of all three genomes to examine the genetic basis of functional differences between the species. With regard to many evolutionary questions, Lambert and Millar (2) suggested that analyzing differences between Neanderthal and human brains would be of great interest.

However, although such comparisons are of interest, it is not the static genome but rather the dynamic proteome that determines the phenotype of an organism. Salient examples include the caterpillar and the tadpole, which share genomes with the butterfly and frog, respectively, but which have very different proteomes making them into very different organisms. Thus, rather than performing untargeted comparisons of sizable genomes, we suggest that it might be more useful to address this question using a standard hypothesis-driven approach. One such avenue might be the "fat utilization" hypothesis, which holds that the key mutations that differentiate us from Neanderthals and great apes are in the genes coding for proteins regulating fat metabolism, in particular, those regulating the phospholipids in brain synapses (3, 4). A specific search for variations in genomic DNA or gene expression related to lipid biochemistry and metabolism could be carried out.

Charles Darwin was once asked if he thought that natural historians should collect data without the prejudice of a preformed hypothesis, or whether they should be observing nature with a particular theory in mind (5). In a stinging reply to his friend, the economist Henry Fawcett, Darwin wrote that they may as well "go into a gravel-pit and count the pebbles and describe the colours" (6). Plus ça change...

THOMAS C. ERREN,<sup>1</sup> PAUL CULLEN,<sup>2</sup>  
MICHAEL ERREN<sup>3</sup>

<sup>1</sup>Institute and Polyclinic for Occupational and Social Medicine, School of Medicine and Dentistry, University of Cologne, Joseph-Stelzmann-Str. 9, 50924 Köln, Lindenthal,

Germany. <sup>2</sup>Medizinisches Versorgungszentrum für Laboratoriumsmedizin Dr. Löer, Dr. Treder, Hafengeweg 11, 49155 Münster, Germany. <sup>3</sup>Institute of Clinical Chemistry and Laboratory Medicine, Westphalian Wilhelms-University of Münster, 48149 Münster, Germany.

#### References

1. R. E. Green *et al.*, *Nature* **444**, 330 (2006).
2. D. M. Lambert, C. D. Millar, *Nature* **444**, 275 (2006).
3. D. F. Horrobin, *The Madness of Adam and Eve: How Schizophrenia Shaped Humanity* (Bantam Press, London, 2001).
4. T. C. Erren, M. Erren, *Prostaglandins Leukot. Essent. Fatty Acids* **70**, 345 (2004).
5. L. Hurst, *New Sci.* **178**, 58 (2003).
6. F. Darwin, *More Letters of Charles Darwin* (Murray, London, 1903).

## Response

ERREN *ET AL.* APPEAR TO HAVE NO TECHNICAL objections to our study, but rather put forth a general philosophical objection to whole-genome analysis. They would prefer that we search for the molecular basis of human-specific traits by focusing on particular classes of genes speculated to contribute to some biological difference between humans and other species. We fail to see the advantage of this approach over unbiased whole-genome comparisons. The reason such candidate gene strategies were used in the past was due to the lack of genomic data sets. The sequencing of multiple genomes, including human and chimpanzee, has removed this obstacle. We do not know in advance which genes or other functional elements have changed in human evolution. It therefore seems shortsighted to guess that mutations in lipid genes, to cite the authors' example, are responsible for functional differences between human and Neanderthal brains. If changes in genes regulating fat metabolism do contribute to human-specific traits, a whole-genome approach will efficiently detect that signal, as well as all the other genes that the authors' "lipid-centric" approach would miss.

EDWARD M. RUBIN  
AND JAMES P. NOONAN

U.S. Department of Energy Joint Genome Institute, Walnut Creek, CA 94598, USA, and Genomics Division, Lawrence Berkeley National Laboratory, Berkeley, CA 94720, USA.

## Letters to the Editor

Letters (~300 words) discuss material published in *Science* in the previous 3 months or issues of general interest. They can be submitted through the Web ([www.submit2science.org](http://www.submit2science.org)) or by regular mail (1200 New York Ave., NW, Washington, DC 20005, USA). Letters are not acknowledged upon receipt, nor are authors generally consulted before publication. Whether published in full or in part, letters are subject to editing for clarity and space.



Receive a free TaqMan® Low Density Array Upgrade and 20 Free TaqMan® Array cards\*  
Visit 7900HT.com to learn more.

# Proven Performance in Labs Everywhere. Customized for Yours.



Applied Biosystems 7900HT Fast Real-Time PCR System Meets Your Changing Needs.



#### The gold standard in real-time PCR

Used by researchers all over the world and referenced in hundreds of journals, the Applied Biosystems 7900HT Fast Real-Time PCR System is the recognized gold standard in real-time PCR.



#### Interchangeable blocks

Configurable and highly flexible, the 7900HT Fast System offers user-interchangeable thermal cycling blocks, cycling times as low as 35 minutes and automated plate loading/unloading for higher throughput.



#### The world's largest collection of assays

Choose from over 2 million TaqMan® Gene Expression, Genotyping and miRNA Assays.



#### Easy, pre-loaded assays in a micro fluidic card format

For the ultimate in ease-of-use, order your assays pre-loaded in the 384-well TaqMan® Low Density Array.

To see how the 7900HT Fast System meets your changing research needs, visit [www.7900HT.com](http://www.7900HT.com)

**AB** Applied Biosystems

\* Receive a Low Density Array Upgrade and 20 Free TaqMan® Low Density Array cards with the purchase of an Applied Biosystems 7900HT Fast Real-Time PCR System. This offer cannot be combined with other promotions or discounts. Offer valid until March 31, 2006. Void where prohibited. This offer is for US customers only — International customers please inquire with your local sales office. Other restrictions may apply. All prices exclude any applicable delivery and/or local tax. Please contact your local Sales Representative for other details of this offer. <http://www.7900HT.com>

For Research Use Only. Not for use in diagnostic procedures. The Applied Biosystems 7900HT Fast Real-Time PCR System is covered by U.S. Patents Nos. 6,563,581 and 6,719,949. The Applied Biosystems 7900HT Fast Real-Time PCR System base unit equipped with its sample block module is an Authorized Thermal Cycler for PCR and may be used with PCR licenses available from Applied Biosystems. Its use with Authorized Reagents also provides a limited PCR license in accordance with the label rights accompanying such reagents. This instrument is licensed under U.S. Patent No. 6,814,934 and corresponding claims in its non-U.S. counterparts and under one or more of U.S. Patents Nos. 5,038,852, 5,656,483, 5,333,675, 5,475,610 or 6,703,236, or corresponding claims in their non-U.S. counterparts, for use in research. Purchase of this instrument does not convey any right to practice the 5' nuclease assay or any of the other real-time methods or rights under any other patent claims or for any other application expressly, by implication, or by estoppel. Applied Biosystems and AB (Design) are registered trademarks and Applied is a trademark of Applied Biosystems Corporation or its subsidiaries in the US and/or certain other countries. TaqMan is a registered trademark of Roche Molecular Systems, Inc. © 2007 Applied Biosystems. All rights reserved.



## What the Scientific Community Can Do

IN HIS EDITORIAL "SHOW US THE MONEY" (8 Dec. 2006, p. 1515), Donald Kennedy suggests that the scientific community should tell the Administration, the public, and Congress what it can accomplish for our society. As chairman and member of the executive committee of the Association of American Universities and as president of Northwestern University, which has made large investments in human and physical capital over the last decade, especially in the life and nano sciences, I want to do just that.

We can list many research-to-bedside accomplishments. A discovery in our chemistry labs by Richard Silverman led to the drug Lyrica, licensed to Pfizer, which has proved an effective neuropathic pain reliever for tens of thousands of patients. Many other universities can also point to new therapies and diagnostics that were discovered or developed in their lab.

The economic benefits of biomedical research are equally striking. One only has to look at the jobs created in the construction industry when we built the Robert H. Lurie

Medical Research Center, the creation of many new biotech companies from our research efforts, or the mobilizing of private-donor support to see the economic benefits. The Chicago area has benefited mightily from our efforts, as Atlanta has benefited from Emory's efforts and Baltimore from those of John Hopkins.

Elias Zerhouni, director of NIH, is correct to note that we in the research community often take for granted the extraordinary return on investments in NIH ("NIH in the post-doubling era: realities and strategies," Policy Forum, 17 Nov. 2006, p. 1088). He refers to scientific and health care benefits. I can also point to the economic returns expressed in job creation and multiple effects of investment from the partnerships among the federal government, private donors, and the research universities.

HENRY S. BIENEN

President, Northwestern University, Evanston, IL 60201, USA.

### TECHNICAL COMMENT ABSTRACTS

#### COMMENT ON "Why Are There So Many Species of Herbivorous Insects in

#### Tropical Rainforests?"

David A. Norton and Raphael K. Didham

Novotny *et al.* (Reports, 25 August 2006, p. 1115) argued that higher herbivore diversity in tropical forests results from greater phylogenetic diversity of host plants, not from higher host specificity. However, if host specificity is related to host abundance, differences in relative host abundance between tropical and temperate regions may limit any general conclusion that herbivore diversity scales directly with host-plant diversity.

Full text at [www.sciencemag.org/cgi/content/full/315/5819/1666b](http://www.sciencemag.org/cgi/content/full/315/5819/1666b)

#### RESPONSE TO COMMENT ON "Why Are There So Many Species of Herbivorous Insects in Tropical Rainforests?"

Vojtech Novotny, Pavel Drozd, Scott E. Miller, Miroslav Kulfan, Milan Janda, Yves Basset, George D. Weiblen

Norton and Didham suggest that differences in plant abundance between tropical and temperate forests may influence the host specificity of herbivores in these forests. We agree in principle but show that this is likely only for very rare plant species in tropical forests. Studies of herbivores hosted by rare plant species would help our understanding of tropical plant-insect interactions.

Full text at [www.sciencemag.org/cgi/content/full/315/5819/1666c](http://www.sciencemag.org/cgi/content/full/315/5819/1666c)

# Science Alerts in Your Inbox

Get daily and weekly E-alerts on the latest breaking news and research!

**Science News This Week**  
Brief summaries of the journal's news content

**ScienceNOW Weekly Alert**  
Weekly headline summary

**Science Express Notification**  
Articles published in advance of print

**Science Posting Notification**  
Alert when weekly issue is posted

**ScienceNOW Daily Alert\***  
Daily headline summary

**Science Magazine TOC**  
Weekly table of contents

**STKE TOC**  
Weekly table of contents

**Editors' Choice**  
Highlights of the recent literature

**This Week in Science**  
Summaries of research content

Get the latest news and research from *Science* as soon as it is published. Sign up for our e-alert services and you can know when the latest issue of *Science* or *Science Express* has been posted, peruse the latest table of contents for *Science* or *Science's* Signal Transduction Knowledge Environment, and read summaries of the journal's research, news content, or Editors' Choice column, all from your e-mail inbox. To start receiving e-mail updates, go to:

<http://www.sciencemag.org/ema>

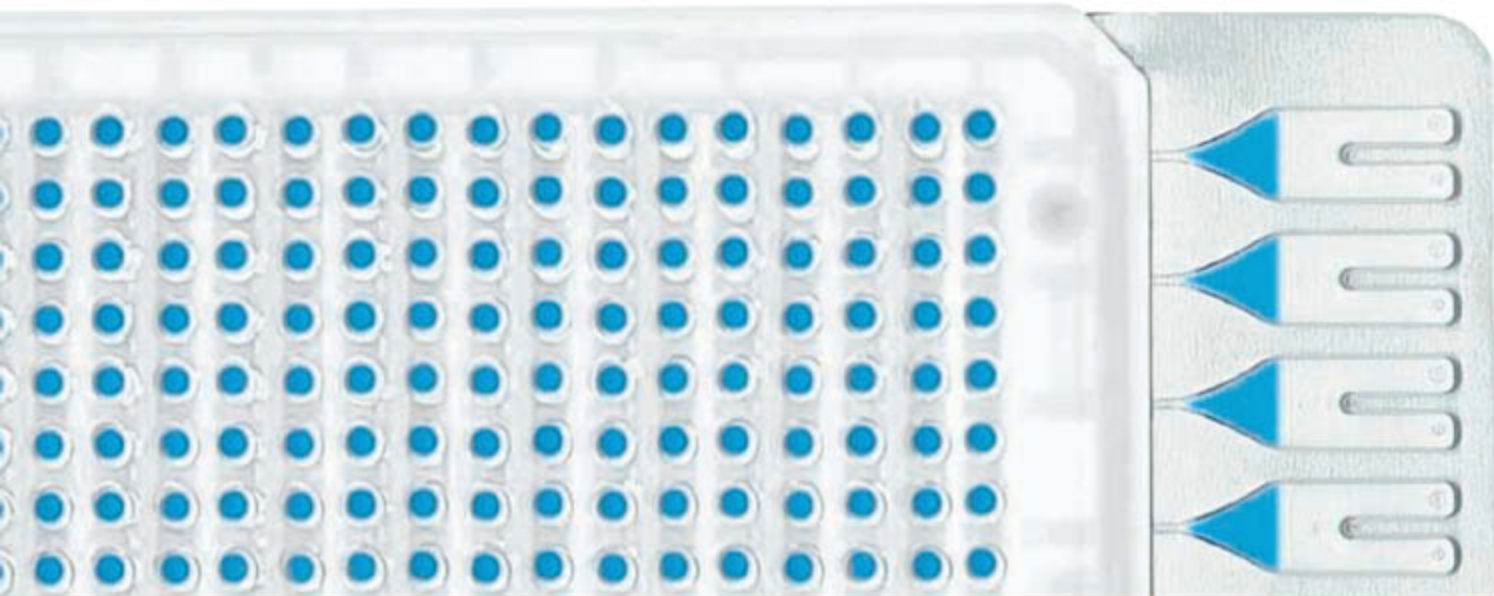




**Now Available!**

Custom panels in smaller, 10-card order sizes.

# 384 Wells. Preloaded for TaqMan® Performance.



**Readily available TaqMan® Arrays deliver speed, accuracy and sensitivity to your real-time PCR gene expression analysis.**

TaqMan® Low Density Array Gene Signature Panels are readily available, expertly-designed, focused gene sets that don't require liquid handling robots or complex pipetting to use. Simply add your cDNA and TaqMan® Universal PCR Master Mix into the eight sample ports of this micro fluidic card and instantly run 384 real-time PCR reactions on the 7900HT Fast Real-Time PCR System. The Gene Signature Panels come pre-loaded with TaqMan® Gene Expression Assays, so you get the accuracy, reproducibility, and specificity that only TaqMan® Assays can provide. It's the fast and affordable way to validate micro-array hits and screen pathways and biomarkers without the worry and difficulty associated with 96-well plates or individual tubes.

**Order from the growing portfolio of TaqMan® Low Density Array Gene Signature Panels:**

- Human or Mouse GPCR Panel
- Human or Mouse Immune Panel
- Human, Mouse, or Rat Endogenous Control Panel
- Human Protein Kinase Panel
- Human Apoptosis Panel
- Human ABC Transporter Panel

**More panels will be available soon! Register to receive new Gene Signature Panel product announcements or suggest a panel of your own at [tlda.appliedbiosystems.com](http://tlda.appliedbiosystems.com)**



The perfect combination: the TaqMan Low Density Array and Applied Biosystems 7900HT Fast Real-Time PCR System.

**AB Applied Biosystems**

Applied Biosystems is committed to providing the world's leading technology and information for life scientists. Applied Biosystems consists of the Applied Biosystems and Celera Genomics businesses. For Research Use Only. Not for use in diagnostic procedures. Practice of the patented 5' Nuclease Process requires a license from Applied Biosystems. The purchase of TaqMan® Low Density Array Gene Signature Panels includes an immunity from suit under patents specified in the product insert to use only the amount purchased for the purchaser's own internal research when used with the separate purchase of an Authorized 5' Nuclease Core Kit. No other patent rights are conveyed expressly, by implication, or by estoppel. For further information on purchasing licenses contact the Director of Licensing, Applied Biosystems, 850 Lincoln Centre Drive, Foster City, California 94404, USA. The TaqMan® Low Density Array is covered by U.S. Patents Nos. 6,514,750 and 6,942,837. Micro Fluidic Card developed in collaboration with 3M Company. Applied Biosystems and AB (Design) are registered trademarks and Applied is a trademark of Applied Biosystems or its subsidiaries in the US and/or certain other countries. TaqMan is a registered trademark of Roche Molecular Systems, Inc. ©2007 Applied Biosystems.



## SOCIAL SCIENCE

## Dealing with Differences

A. Scott Henderson

All societies make decisions about the distribution of goods and services. Despotism allocates them in whatever manner they see fit. Governments based on egalitarian principles, however, cannot act capriciously. Their policies must be predicated on justice and fairness. But how can states create such policies when individuals obviously differ from one another? How, in other words, do societies committed to equality deal with differences among people?

In *The Measure of Merit*, John Carson, a historian at the University of Michigan, offers an informative, exhaustively researched account of how France and America each addressed this challenge. His narrative reveals how positivism, the rise of social science, and cultural beliefs converged to shape our modern notions of intelligence.

Enlightenment-era thinkers scorned the advantages and disadvantages that flowed from one's economic status or family background. They believed that a more rational and just social order could be constructed on the basis of merit or, to use a more historically accurate term, "talents." To express this view, Condillac, Helvétius, Rousseau, and other philosophers systematically analyzed a broad array of human aptitudes. Their discussions were important for two reasons. First, although they did not always agree on the particulars, they tended to define talents as a multivalent phenomenon that could be enhanced by various means, including education. Second, as Carson notes, it was primarily philosophers who undertook the early investigations of intelligence (the term that would replace talents by the mid-19th century).

In perhaps the book's strongest section, Carson examines how positivism transformed the study and perceptions of human intelligence. Associated most closely with the French philosopher Auguste Comte, positivism sought to apply the scientific method to social problems. Comte himself emphasized the need for social theories to be predictive,

empirically verifiable, practical, and materialist (not metaphysical). Emphasizing these criteria, Comte laid the foundations of modern social science. Positivism's legacy, however, would intensify a growing apprehension within the nascent social sciences over experimental methods that departed from strict, almost mechanical, objectivity. This near obsession with objectivity could distort, as well as clarify, the phenomena being examined. (Testing something—intelligence, for example—suggests that there is a tangible entity to examine, sometimes a debatable proposition.)

The French psychologist Alfred Binet did more than any other individual to apply positivism's dictums to the study of intelligence. Binet, with his colleague Theodore Simon, devised the most comprehensive intelligence test to that date. Yet, as Carson insightfully notes, the first version of the test (1905) was never meant to generate a single number to describe an individual's mental acumen. However, for reasons that are not clear, between 1905 and 1911 Binet revised the test by reducing the test administrator's discretion (a certain amount of subjectivity was inevitable) and placing greater emphasis on the instrumental outcomes (the test's ability to precisely locate an individual on an intelligence continuum). Further revisions, including introduction of an "intelligence quotient," by Stanford University psychologist Lewis Terman in 1916, produced a test that envisioned intelligence as biologically determined, unitary, hereditary, and fixed throughout an individual's lifetime.

Carson offers intriguing explanations for why France and America reacted differently to intelligence tests. The French placed less importance on them for several reasons: professional antagonisms, e.g., doctors and teachers were unwilling to cede their authority to psychologists; intellectual trends, French scholars began to emphasize subjectivity (most notably, intuition) over rigid objectivity;



Locating differences in head shapes. Phrenologists, such as William Bally, argued for "cerebral localization of mental functions."

institutional exigencies, the French Army (unlike the American military) never adopted and thus never validated the use of intelligence tests; and the presence of fully functional sorting mechanisms in France (a national system of secondary schools and universities). Americans, on the other hand, confronted different circumstances and were therefore more willing to confer intellectual and practical value on intelligence tests. Also important were anxieties over the increasing heterogeneity of American society and the need, expressed by some, to create intellectual and racial hierarchies to maintain social order. Even so, Carson concludes that Americans have never fully accepted intelligence (as measured by narrowly designed tests) as the only criterion of merit. Although Carson does not fully explicate this ambivalence, he correctly notes it is manifest in current debates over the Scholastic Aptitude Test.

*The Measure of Merit* offers a useful supplement to books by Stephen Jay Gould (1) and Steven Pinker (2). One might wish that Carson had devoted less attention to the 18th century and more to the 20th—especially to political scientist Charles Murray's contentious assertions about the distribution of intelligence (3). Nonetheless, scholars in several disciplines will find Carson's arguments relevant and engaging.

## References

1. S. J. Gould, *The Mismeasure of Man* (Norton, New York, ed. 2, 1996).
2. S. Pinker, *The Blank Slate* (Viking, New York, 2002); reviewed by P. Bateson, *Science* 297, 2212 (2002).
3. R. J. Herrnstein, C. Murray, *The Bell Curve* (Free Press, New York, 1994).

## The Measure of Merit

Talents, Intelligence, and Inequality in the French and American Republics, 1750–1940

by John Carson

Princeton University Press, Princeton, N.J., 2007. 421 pp. \$39.50, £26.95. ISBN 9780691017150.

The reviewer is in the Department of Education, Furman University, 3300 Poinsett Highway, Greenville, SC 29613–1134, USA. E-mail: Scott.Henderson@Furman.edu

10.1126/science.1140436



## PUBLIC HEALTH

## Plumb Crazy

Rebecca Renner

Today, scientists know a great deal about lead. Children and infants are very vulnerable to this neurodevelopmental toxin, which can be harmful even in very small amounts. Paint, dust, and soil are the most common sources of lead. In many places, the lead in soil came from the leaded gasoline that was formerly widely used in automobiles. Water, too, can be a source of lead, and recently some U.S. cities and regions in Brazil, France, and Germany have had problems with high levels of lead in their drinking water.

But a hundred years ago—before leaded gasoline and the widespread use of leaded paint—drinking water contaminated by lead water pipes was the main source of human-ingested lead. In 1900, 85% of large U.S. cities had lead pipes and so did most major European cities. In regions supplied with corrosive waters, such as Massachusetts and northern England, tap water contained hundreds of times more lead than modern standards allow.

Those massive amounts had massive consequences: in *The Great Lead Pipe Disaster*, Werner Troesken concludes they brought illness and frequently death to millions of people. As a point of comparison, Troesken (a historian at the University of Pittsburgh) notes that late-19th-century women trying to abort a baby would often take pills made of lead plaster. In towns with the worst lead problems, a woman could get the same dose of lead by drinking a glass of water. Given these levels of contamination, it is little wonder that in Massachusetts and northern England lead water pipes appeared to increase infant mortality rates and stillbirth rates by up to 25%. By any measure, this was one of the most serious environmental disasters of the past 200 years, and yet few people recognized it at the time and almost no one knows about it now.

Troesken unearths the catastrophe using a combination of historical detective work (focusing on England and Massachusetts) and modern epidemiology. He mines vast amounts

of data and information by digging away at old government reports, scientific papers, court documents, and books. Then he applies modern statistics and knowledge about lead to reveal what happened.

The harmful effects of lead water pipes became apparent almost as soon as cities the world over began to install them. Observant doctors and scientists began attributing sickness and death to lead pipes as early as the 1850s. Early in that decade, Erasmus Fenner, a prominent New Orleans physician, traced an epidemic of colic and convulsions to the city's expanding system of lead water pipes.

The British physician Norman Porritt had an even more sweeping understanding of the problem. Perhaps his personal experience may have piqued his interest in lead's effects, as he twice came down with lead poisoning. Porritt noticed that eclampsia (pregnancy-related seizures and coma) was most common in northern England and Wales, where the water chemistry was likely to dissolve lead. He published on the "cumulative

### The Great Lead Water Pipe Disaster

by Werner Troesken

MIT Press, Cambridge, MA,  
2006. 328 pp. \$29.95, £19.95.  
ISBN 9780262201674.



"Lead helps to guard your health." The illustration for an ad in the November 1923 *National Geographic*, one of a series by the National Lead Company.

effects of infinitesimal doses of lead" (1) and wrote a 1934 book (2) to alert society to this menace. Like Fenner, he was largely ignored. Troesken shows that Porritt was right. Armed with more data, epidemiological models, and statistical methods that can control for confounding factors, he vindicates Porritt. The rates of death from eclampsia were two to three times as high in waters with a greater tendency to dissolve lead.

Troesken notes that there are many reasons why the evidence was ignored and the doctors' warnings went unheeded. Chronic lead exposure produces symptoms that are not unique, and its effects are not so dramatic as the sudden death associated with cholera and other infectious diseases that wracked societies at the

time. In addition, most doctors tended to focus on adults rather than more-vulnerable children. And although the problem was widespread, it was not always associated with lead pipes. For lead to contaminate water, the water needs to corrode lead. The factors that cause water to be corrosive can be subtle and make drawing the causal link more difficult.

But scientific arguments only partly explain the failure of early-20th-century societies to accept the lead pipe problem. There were social factors as well. Municipalities were in denial about the dangers. Lead pipes were an expensive improvement that brought pure water to homes; how could that be wrong? There was even a theory to bolster their disregard: the doctrine of protective

power, which held that over time most lead pipes developed a protective interior coating that inhibited subsequent uptake of lead. The concept has merit in many cases, but cities made the convenient mistake of expecting it to apply universally. The courts compounded the problem when judges decided that customers, not municipalities, were responsible for any contamination that came from pipes installed by the cities.

Over time, the massive levels of lead in drinking water have declined. Engineers have learned how to control the corrosiveness of water, and lead pipes are gradually being replaced. But Troesken's tale is more than an interesting historical footnote. Lead water pipes are still in use, and there are other sources of lead in drinking water, including solder and brass plumbing fixtures. Between 2000 and 2005, Washington, D.C., faced a lead crisis in which thousands of homes had elevated

lead in their drinking water; in the worst cases, the contamination levels approached those seen in the early 1900s. In many ways, Troesken's account in *The Great Lead Water Pipe Disaster* resonates uncannily with Washington's problem. A well-intended change in water treatment had the undesired consequence of increasing the water's corrosiveness. Public officials tried to explain the threat away with a modern version of the doctrine of protective power.

#### References

1. N. Porritt, *Br. Med. J.* 1931, 92 (18 July 1931).
2. N. Porritt, *The Menace and Geography of Eclampsia in England and Wales* (H. Millard, London, 1934).

The reviewer is a science writer in Williamsport, PA, USA.  
E-mail: rrenner@nasw.org

10.1126/science.1139087



# Carbon Trading Over Taxes

William Chameides,<sup>1\*</sup> Michael Oppenheimer<sup>2</sup>

As the United States moves inevitably toward climate legislation, discussion has shifted from the science to the policy options for slowing emissions of carbon dioxide (CO<sub>2</sub>) and other greenhouse gases. Some favor a tax on CO<sub>2</sub> emissions—referred to as a C tax (1). Others favor government subsidies (2). If high enough to alter consumer behavior, a carbon tax would reduce emissions by raising the effective price of carbon-intensive energy relative to carbon-free sources. Subsidies may speed development of specific, targeted low-C technologies.

But a market-based system with an economy-wide cap on emissions and trading of emission allowances would do the same, while having distinct advantages (3). Most important, a cap-and-trade system, coupled with adequate enforcement, assures that environmental goals actually would be achieved by a certain date. Given the potential for escalating damages and the urgent need to meet specific emission targets (4), such certainty is a major advantage. A federal cap-and-trade system could be incorporated into existing emissions trading frameworks and markets, such as the Kyoto Protocol's international market or sub-national ones like the Regional Greenhouse Gas Initiative.

Earth's climate is agnostic about the location and type of CO<sub>2</sub> emissions and is sensitive only to the total burden of CO<sub>2</sub>. It makes sense, therefore, to design a climate policy that taps all possible avenues to limit net CO<sub>2</sub> emissions. Trading of emissions across all sectors of the economy addresses this by allowing emitters to purchase carbon offsets from businesses that are able to lower their own emissions below their allocation. If trading were incorporated into an international system, U.S. firms and consumers could meet emissions targets at reduced costs by substituting less expensive cuts in, for example, developing countries, for expensive emissions cuts in the United States. Because investment would be funneled to



Pollution credits exchanged for cash.

technologies that reduce CO<sub>2</sub> emissions at the least cost, the overall expense of the program would be minimized.

Cutting emissions of pollutants is admittedly not as complicated as cutting CO<sub>2</sub> emissions, and transaction costs can be a factor. Nevertheless, the United States was able to reduce sulfur oxide emissions ahead of schedule and at 30% of the projected cost using a market-based cap-and-trade system (5). Elimination of lead from gasoline and phase-out of ozone-depleting chemicals were also facilitated by emissions trading programs.

Offsetting emissions by storing carbon in soils, forests, and other forms of biomass in the United States has the potential to offset 10 to 20% of U.S. emissions in 2025 at relatively low cost (see chart below and table S1). International opportunities also exist. Deforestation of tropical rainforests is currently estimated to cause more than 7000 million metric tons per year of CO<sub>2</sub> emissions, the equivalent of about 25% of worldwide emissions from fossil fuel burning today; in 2025 the percentage is estimated to be about 15% (table S2). Using an international cap-and-trade market to compensate nations for slowing deforestation would bring a significant block of emissions under management, while preserving irreplaceable ecosystems and providing income to developing economies (6–8).

Ensuring the integrity of such a system will require rigorous monitoring, auditing, and registration. Leakage (e.g., where

Carbon emissions trading ensures not only that targets will be met by a specific date but also fosters international cooperation and development objectives.

reduced timber harvest in one location is replaced by increased harvest elsewhere to meet demand for lumber), the credibility of baselines in capped and uncapped systems, and the full climate effects of enhanced biological growth must be addressed (9–10). However, these problems are manageable (11). Frameworks and methodologies for documenting the size and validity of carbon offsets based on land-management practices are available (12, 13).

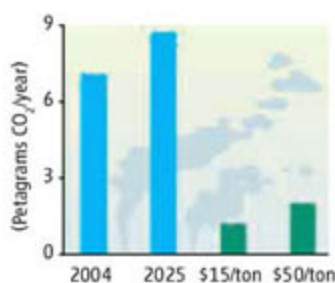
Following such a methodology will not be a trivial exercise. It will involve costs that will affect those hoping to market offsets. But the advantage of a market-based system is that it provides an incentive for innovation—which can translate into inexpensive CO<sub>2</sub> emission reductions. Why would we want to exclude any sector of the economy from this competition, let alone one with such large potential?

## References and Notes

- W. H. Schlesinger, *Science* **314**, 1217 (2006).
- M. I. Hoffert et al., *Science* **298**, 981 (2002).
- C.-J. Yang, M. Oppenheimer, *Clim. Change* **80**, 199 (2007).
- H. J. Schellnhuber, Ed., *Avoiding Dangerous Climate Change* (Cambridge Univ. Press, Cambridge, 2006).
- National Acid Precipitation Assessment Program Report to Congress: An Integrated Assessment (U.S. National Science and Technology Council, Washington, DC, 2005); [www.esrl.noaa.gov/csd/AQRS/reports/napareport05.pdf](http://www.esrl.noaa.gov/csd/AQRS/reports/napareport05.pdf).
- P. Moutinho, S. Schwartzman, Eds., *Tropical Deforestation and Climate Change* (Amazon Institute for Environmental Research, Belém, Pará, Brazil, 2005).
- R. Bonnie, S. Schwartzman, M. Oppenheimer, J. Bloomfield, *Science* **288**, 1763 (2000).
- M. Santilli et al., *Clim. Change* **71**, 267 (2005).
- F. Keppler et al., *Nature* **439**, 187 (2006).
- S. Gibbard et al., *Geophys. Res. Lett.* **32**, L23705 (2005).
- L. Olander, *Do Recent Scientific Findings Undermine the Climate Benefits of Sequestration in Forests?* (Nicholas Institute, Durham, NC, 2006); [www.nicholas.duke.edu/institute/methanewater.pdf](http://www.nicholas.duke.edu/institute/methanewater.pdf).
- Nicholas Institute, *Harnessing Farms and Forests in the Low-Carbon Economy: How to Create, Measure, and Verify Greenhouse Gas Offsets Based on Storing Carbon in Trees and Soil and Reducing Emissions from Land Use* (Duke Univ. Press, Durham, NC, in press).
- J. M. Penman et al., Eds., *Intergovernmental Panel on Climate Change: Good Practice Guidance for Land Use, Land-Use Change, and Forestry* (Institute for Global Environmental Strategies, Hayama, Kanagawa, Japan, 2003); [www.ipcc-nggip.iges.or.jp/public/gpglulucf/gpglulucf.htm](http://www.ipcc-nggip.iges.or.jp/public/gpglulucf/gpglulucf.htm).

## Supporting Online Material

[www.sciencemag.org/cgi/content/full/315/5819/1670/DC1](http://www.sciencemag.org/cgi/content/full/315/5819/1670/DC1)



**Effect of carbon credits.** U.S. greenhouse gas emissions for 2004 and 2025 with business as usual (blue); estimated U.S. land-management offsets in 2025 at \$15 and \$50 per ton of CO<sub>2</sub> (green); 1 petagram = 1 billion tons (table S1).

<sup>1</sup>Environmental Defense, 257 Park Avenue South, New York, NY 10010, USA.

<sup>2</sup>Woodrow Wilson School and Department of Geosciences, Princeton University, Princeton, NJ 08544, USA.

\*Author for correspondence. E-mail: [bcchameides@environmentaldefense.org](mailto:bcchameides@environmentaldefense.org)



## BIOCHEMISTRY

## Balancing Cellular Energy

D. Grahame Hardie

Obesity and type 2 diabetes are disorders of energy balance that are reaching epidemic proportions worldwide. A key target for drug development in this area is the adenosine monophosphate-activated protein kinase (AMPK) complex, which regulates cellular energy balance. For example, AMPK is switched on in muscle during exercise as a result of increased energy demand, triggering metabolic changes such as the switch from storing to consuming fats and carbohydrate. AMPK activation during regular exercise helps to protect against obesity and diabetes, and this protein complex is also the target for antidiabetic drugs such as the biguanides and thiazolidinediones (1). On page 1726 of this issue, Townley and Shapiro (2) describe crystal structures for the core of the AMPK complex from fission yeast. The study provides insights into binding of AMP and adenosine triphosphate (ATP), which may be very helpful in the design of new drugs.

Mammalian AMPK regulates energy balance by monitoring changes in the cellular concentrations of the nucleotides AMP and ATP. An increase in AMP concentration—indicating an energy deficit—switches the kinase on, causing it to attach phosphate to downstream target proteins, thereby switching on proteins involved in ATP-generating pathways and switching off those involved in ATP consumption. Conversely, high ATP concentrations—indicating energy sufficiency—prevent AMP from switching on the kinase by competing for binding at the same site.

AMPK and its relatives in nonmammalian species are composed of a catalytic subunit ( $\alpha$ ) and two regulatory subunits ( $\beta$  and  $\gamma$ ). The nucleotide-binding sites are located in two “Bateman domains,” each of which is formed by two repeats of a pattern of amino acids termed a CBS motif (3). The nucleotide-binding site has been modeled on the basis of the structure of other Bateman domains and on the locations of mutations causing human heart disease that are known to interfere with nucleotide binding (3, 4). Townley and Shapiro now show how the subunits interact in, and how the nucleotides are bound to, the core of the  $\alpha\beta\gamma$  complex from fission yeast.

The author is in the Division of Molecular Physiology, College of Life Sciences, University of Dundee, Dundee DD1 5EH, UK. E-mail: d.g.hardie@dundee.ac.uk

The ability of mammalian AMPK to phosphorylate downstream target proteins is increased >100-fold by attachment of phosphate to its  $\alpha$  subunit by another protein (5, 6). This protein seems to phosphorylate AMPK constantly, but the phosphate is normally rapidly removed by yet another enzyme, so that AMPK immediately returns to the inactive state. Binding of AMP to the  $\gamma$  subunit inhibits this dephosphorylation (7, 8), providing a mechanism for converting the kinase to its active state during times of energy deficit. AMP binding also induces a change in structure that causes an additional activation; the combination of the two effects produces >1000-fold activation (9). However, neither effect of AMP appears to occur with the related protein from budding yeast (8), even though the AMP-binding sites are conserved.

Large multiprotein complexes are often difficult to crystallize because of their complex shape and flexibility. The strategy adopted by Townley and Shapiro was to treat the

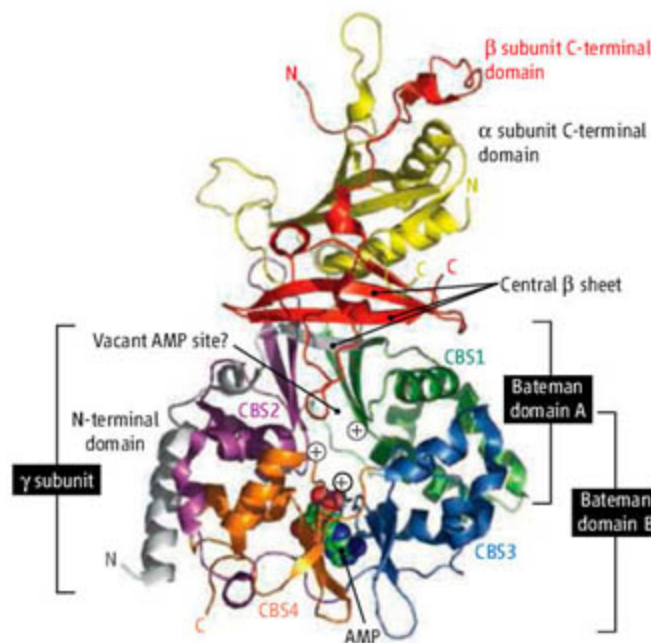
The structure of the core of an enzyme complex that senses and responds to changes in the cell's energy balance has been solved.

human complex with protein-degrading enzymes to generate the more compact and rigid core of the complex. This core contained the entire  $\gamma$  subunit but only the C-terminal domains of the  $\alpha$  and  $\beta$  subunits, which were known to be required for formation of the  $\alpha\beta\gamma$  complex. Bacteria were then programmed to make this core complex by genetic manipulation techniques, but suitable crystals were obtained only with the protein from fission yeast and not with that from humans. This is unfortunate, because little is known about the fission yeast enzyme, although its sequence is more similar to that of the protein from budding yeast than to the one from humans.

In their structure, the C-terminal domain of the  $\alpha$  subunit has a compact shape, with the C-terminal domain of the  $\beta$  subunit snaking around it (see the figure). There is minimal contact between  $\alpha$  and  $\gamma$  but extensive contact between  $\beta$  and  $\gamma$ . The amino acids involved in the  $\beta$ - $\gamma$  interaction tend to be similar in AMPK relatives in all species, which suggests that the subunit interactions will also be similar.

In the structures reported by Townley and Shapiro, the N- and C-terminal Bateman domains (domains A and B) face each other like mirror images. In crystals grown in the presence of AMP or ATP, a molecule of each nucleotide was bound in a very similar manner, but only in domain B. Although crystallized in the presence of  $Mg^{2+}$ , the ATP complex contained no metal. This agrees with findings that ATP binding to the Bateman domains did not require  $Mg^{2+}$  (3). It also helps to explain how AMP can compete effectively for binding with ATP, even though the latter is normally present at 100-fold higher concentrations: Most ATP in the cell is present as the  $MgATP^{2-}$  complex, whereas the concentration of free ATP is much lower and closer to that of AMP.

Bateman domain A was unoccupied by nucleotide, despite high AMP and ATP concentra-



**The core of the complex.** The structures of Townley and Shapiro (2) contain the C-terminal domains of the  $\alpha$  (yellow) and  $\beta$  subunits (red) shown at the top, and the entire  $\gamma$  subunit. The  $\beta$  and  $\gamma$  subunits interact mainly via the central  $\beta$  sheet. Bateman domains A (formed from CBS1 and CBS2) and B (CBS3 and CBS4) face each other like mirror images, with domain B to the front in this view. A single AMP molecule is bound in domain B, with the negatively charged phosphate group (red oxygen atoms) interacting with a positively charged side chain on CBS4. The approximate positions of two equivalent positive side chains in human CBS1 and CBS2 are also indicated; these are not conserved in the yeast enzymes.



tions during crystallization. This was unexpected, because the isolated Bateman domains from the mammalian  $\gamma$  subunits bind two molecules of AMP or ATP (3). This is likely to be a genuine difference between the mammalian and yeast enzymes.

In the new structures, a positively charged side chain in domain B (lowest "+" symbol in the figure) interacts with negatively charged phosphate(s) on AMP or ATP. A mutation of the equivalent side chain in the human enzyme ( $\gamma 2$  variant) that causes severe heart disease also greatly reduces binding of AMP (10). In the human enzyme, mutations in positively charged side chains occupying similar positions in CBS1 and CBS2 (upper "+" symbols in the figure) cause similar effects (3), supporting

the idea that domain A also binds AMP in humans. Recently, my laboratory has provided evidence for a mechanism of activation of the human enzyme by AMP (11) that involves binding of AMP to these side chains. These residues are not conserved in the fission or budding yeast enzymes, which might explain why the latter is not activated by AMP.

Resolving these remaining uncertainties and anomalies will require structures of mammalian complexes in the presence of AMP or ATP, together with other methods to study domain interactions, especially of those domains not present in the structures reported by Townley and Shapiro. The effort will be very worthwhile if it facilitates development of new

drugs aimed at treatment of the epidemic of obesity and diabetes.

#### References

1. D. G. Hardie, *Annu. Rev. Pharmacol. Toxicol.* **47**, 185 (2007).
2. R. Townley, L. Shapiro, *Science* **315**, 1726 (2007).
3. J. W. Scott *et al.*, *J. Clin. Invest.* **113**, 274 (2004).
4. J. Adams *et al.*, *Protein Sci.* **13**, 155 (2004).
5. S. A. Hawley *et al.*, *J. Biol.* **2**, 28 (2003).
6. A. Woods *et al.*, *Curr. Biol.* **13**, 2004 (2003).
7. S. P. Davies, N. R. Helps, P. T. W. Cohen, D. G. Hardie, *FEBS Lett.* **377**, 421 (1995).
8. M. J. Sanders, P. O. Grandin, B. D. Hegarty, M. A. Snowden, D. Carling, *Biochem. J.* **10.1042/BJ20061520** (2006).
9. M. Suter *et al.*, *J. Biol. Chem.* **281**, 32207 (2006).
10. B. Burwinkel *et al.*, *Am. J. Hum. Genet.* **76**, 1034 (2005).
11. J. W. Scott, F. A. Ross, J. K. Liu, D. G. Hardie, *EMBO J.* **26**, 806 (2007).

10.1126/science/1140737

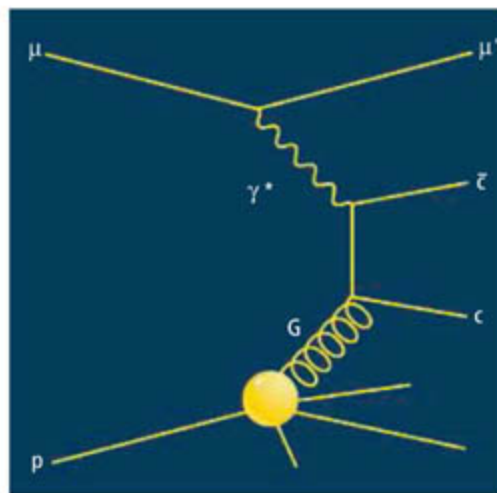
## PHYSICS

# How Does the Proton Spin?

Steven D. Bass

Many particles, such as electrons, protons, and neutrons, behave like spinning tops. Unlike classical tops, however, the spin of these particles is an intrinsic quantum mechanical phenomenon. This spin is responsible for many fundamental properties of matter, including the proton's magnetic moment, the different phases of matter in low-temperature physics, the properties of neutron stars, and the stability of the known universe. In recent experiments, a number of research groups have been seeking to shed some light on the puzzling origin of spin and how this might resolve some large discrepancies between theory and experiment.

Particles such as the proton are actually combinations of more basic entities called quarks and gluons (which bind the quarks together). One of the challenges to physicists over the past 20 years has been to understand how the proton's spin is built up from its quark and gluon constituents. Models of the proton generally predict that about 60% of the proton's spin should be carried by the intrinsic spin of its three quarks, with the rest carried by orbital angular momentum (that is, the quarks flying around inside the proton). However, experiments at CERN (European Organization for Nuclear Research), DESY (Deutsches Elektronen-Synchrotron), and SLAC (Stanford



Linear Accelerator Center) have taught us that the contribution from the spin of the quarks inside is small, only about 30% (1–4). This shortfall offers a substantial challenge to our understanding about the structure of the proton. To sort this out, a vigorous global program has produced about 1000 theoretical papers, and dedicated spin experiments are under way at CERN, DESY, Jefferson Laboratory, and RHIC (Relativistic Heavy Ion Collider) to map individual quark and gluon angular momentum contributions to the proton's spin. These experiments are now yielding exciting results (5).

The proton is described by quantum chromodynamics (QCD, the theory of quarks and gluons) as a bound state of three confined "valence" quarks (6). The quarks have spin 1/2 and interact through the exchange of glu-

Protons are made of quarks and gluons, but their spins don't add up. New experiments may help resolve this discrepancy.

**Spin story.** Physicists use Feynman diagrams such as this to express the sequence of events in a high-energy particle collision. In one type of experiment, a polarized muon ( $\mu$ ) and a polarized proton ( $p$ ) approach each other on the left hand side. As they interact, the muon exchanges a polarized photon ( $\gamma$ ). Pairs of charm-anticharm quark particles ( $c$ - $\bar{c}$ ) are produced; the precise number of these particles created depends on the spin of the gluons ( $G$ ) in the polarized proton, which allows the spin of the gluons to be reconstructed.

ons, which have a spin of 1 (where spin is quoted in units of Planck's constant divided by  $\pi$ ). When we probe deep inside the proton, the strength of quark-gluon and gluon-gluon interactions is small because of "asymptotic freedom." This unusual idea means that, unlike some interactions, such as electrostatic forces, the force between quarks and gluons weakens as they get closer together. If a quark tries to escape, though, the force becomes stronger—so strong, in fact, that the quarks and gluons are always bound inside nuclear particles such as the proton; they are never observed by themselves as free particles.

In low-energy experiments, the proton behaves like a system of three massive "constituent" quarks carrying about 1/3 each of the mass of the proton. When we look deeper inside in high-energy experiments, these constituent quarks dissolve into near massless "current" quarks and a sea of quark-antiquark pairs and gluons.

The spin experiments at CERN, DESY,

The author is at the Institute for Theoretical Physics, Universität Innsbruck, A6020 Innsbruck, Austria. E-mail: sbass@mail.cern.ch



Jefferson Laboratory, and SLAC involve firing high-energy electrons or muons at a target of protons with aligned spins. The incoming electron interacts with a target proton by exchanging a high-energy photon that enables researchers to probe deep inside the proton. The photon can be absorbed by a quark polarized in the opposite direction to the photon but not by one polarized in the same direction as the photon. This allows us to extract information about the spin of the quarks when one controls the spin polarization of both the beam and the proton target. The RHIC spin experiments involve high-energy polarized proton-proton collisions, rather than electron-proton interactions.

In analyzing these collisions, the key questions (7) are: What happens to spin in the transition from current quarks (those probed in high-energy experiments) to constituent quarks (the building blocks of the proton)? How is the spin 1/2 value of the proton built up from the spins and orbital angular momentum of the quarks and gluons inside? Why is the measured quark spin contribution so small compared with quark model predictions? Is the "missing spin" a valence quark effect or attributable to the sea of quarks and antiquarks? Are the excitations of the quark-antiquark sea polarized in the opposite direction to the proton's spin (thus canceling some of the spin)?

The spin of the gluons that bind the proton can screen the spin of the quarks measured in high-energy experiments, making the spin look diminished. This effect is proportional to the gluon polarization  $\Delta g$ . But how large is this gluon polarization? The QCD vacuum is a quantum superposition of an infinite number of states characterized by nontrivial spin structure. When one puts a valence quark in this vacuum, its spin can become delocalized so that the total spin becomes a property of the proton rather than the sum over the individual quarks probed in high-energy experiments. How big is this effect?

Measurements by the COMPASS (Common Muon Proton Apparatus for Structure and Spectroscopy) Collaboration at CERN and the PHENIX (Pioneering High-Energy Nuclear Interaction Experiment) and STAR (Solenoid Tracker at RHIC) experiments at RHIC suggest that the gluon polarization is much too small to explain the difference between the quark model prediction of ~60% for the quark spin contribution and the measured value of ~30%, although it may still make an important contribution to the net spin of the proton (5, 8). The COMPASS and RHIC experiments use different processes to access the gluon polarization. The COMPASS

measurements are extracted from the production of charm particles (see the figure) and charged pions with large transverse-momentum in polarized muon-nucleon collisions. The RHIC measurements are extracted from high-energy particle production in polarized proton-proton collisions. Measurements of the sea polarization by the HERMES (HERA Measurement of Spin, where HERA is the Hadron Elektron Ring Anlage Accelerator at DESY) suggest that this is also small, too small to resolve the spin puzzle, and that the 30% quark spin contribution is approximately saturated by valence quark contributions (9).

New, more precise gluon-polarization measurements will soon be available from the 2006 data taken at COMPASS and RHIC. Independent measurements of the valence and sea-quark contributions will soon be available from COMPASS. It will be interesting to see whether these CERN data confirm the HERMES results. Experiments at Jefferson Laboratory are probing the spin properties of the valence quarks in kinematics, where they are sensitive to the confinement process.

The planned 12-GeV upgrade of the facility will make vital contributions to our understanding of orbital angular momentum contributions to the proton's spin.

Spin measurements have a bright future and continue to challenge our understanding about the structure of the proton and fundamental aspects of quark dynamics. Much exciting progress has been made. The next years promise to be equally exciting.

#### References

1. J. Ashman *et al.* (European Muon Collaboration), *Nucl. Phys.* **B328**, 1 (1989).
2. B. Adeva *et al.* (Spin Muon Collaboration), *Phys. Rev.* **D58**, 112001 (1998).
3. K. Abe *et al.* (SLAC E143 Collaboration), *Phys. Rev.* **D58**, 112003 (1998).
4. A. Aipapetian *et al.* (HERMES Collaboration), *Phys. Rev.* **D75**, 012007 (2007).
5. S. D. Bass, C. A. Aidala, *Int. J. Mod. Phys.* **A21**, 4407 (2006).
6. A. W. Thomas, W. Weise, *The Structure of the Nucleon* (Wiley-VCH, Berlin, 2001).
7. S. D. Bass, *Rev. Mod. Phys.* **77**, 1257 (2005).
8. G. Mallot, [www.arxiv.org/hep-ex/0612055](http://www.arxiv.org/hep-ex/0612055).
9. HERMES Collaboration (A. Airapetian *et al.*), *Phys. Rev. Lett.* **92**, 012005 (2004).

10.1126/science.1140165

## IMMUNOLOGY

# Asymmetry and Immune Memory

Dan R. Littman and Harinder Singh

Asymmetric cell division of lymphocytes ensures that our adaptive immune system maintains a balanced production of two different types of T cells.

**O**ur adaptive immune system is endowed with an enormous repertoire of antigen-specific cells (B and T cells) that respond to and eliminate diverse pathogens. The system can also recall previous infections and respond more rapidly and effectively when reexposed to a pathogen, a feature known as immunological memory. How T cells differentiate into both short-lived effector cells that combat infections and long-lived memory cells that protect us for years has been a central question in immunology (1). On page 1687 in this issue, Chang *et al.* (2) propose that effector and memory T cells are simultaneously generated from the division (mitosis) of a T cell after it responds to a

microbial challenge. T cells appear to have adopted an evolutionarily ancient means of asymmetrically partitioning cell fate determinants, thus ensuring balanced production of both T cell types and avoiding depletion of the T cell repertoire.

When microbial pathogens breach our mucosal barriers (such as the lining of the gastrointestinal or respiratory tract), the innate immune system responds by processing and presenting pathogen components to T cells. Microbial antigens are loaded onto major histocompatibility complex (MHC) molecules on the surface of dendritic cells, and thus interact with antigen receptors on the surface of pathogen-specific T cells. This interaction stimulates formation of an interface known as the immunological synapse (see the figure) and involves redistribution of other T cell surface components to the synapse, including coreceptor molecules CD4 or CD8, adhesion proteins (integrins), and cytokine receptors (3, 4).

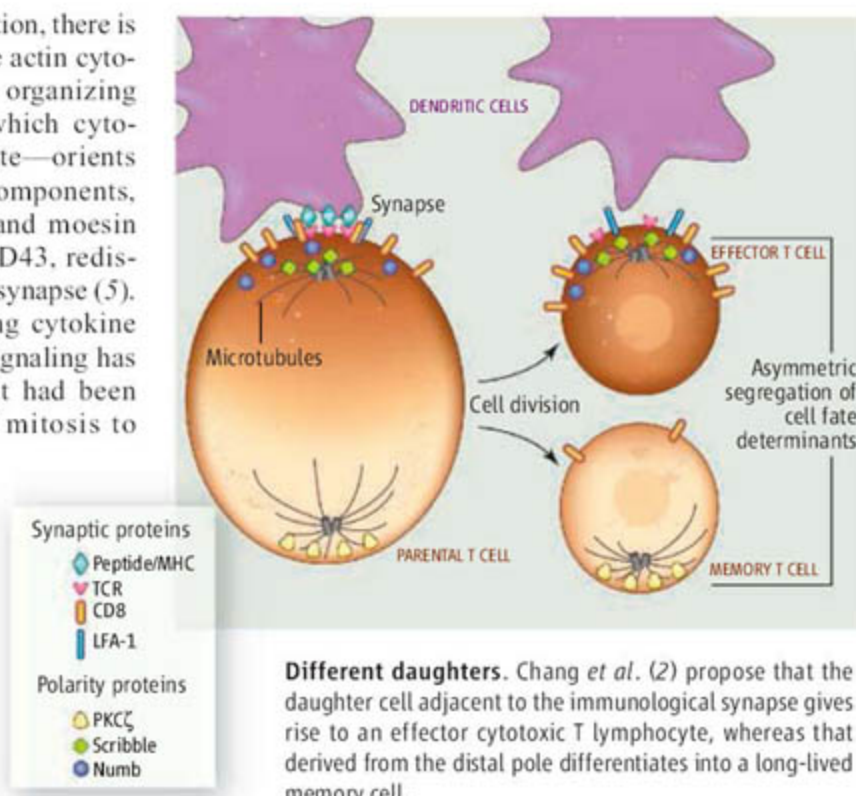
D. R. Littman is in the Howard Hughes Medical Institute, Skirball Institute of Biomolecular Medicine, New York University School of Medicine, New York, NY 10016, USA. H. Singh is in the Howard Hughes Medical Institute, Department of Molecular Genetics and Cell Biology, University of Chicago, Chicago, IL 60637, USA. E-mail: littman@saturn.med.nyu.edu; hsingh@uchicago.edu



Very early in synapse formation, there is localized polymerization of the actin cytoskeleton and the microtubule organizing center—the structure from which cytoskeletal microtubules radiate—orients toward the synapse. Other components, including cytoskeletal ezrin and moesin and the cell surface protein CD43, redistribute to the pole opposite the synapse (5). Synapse function in regulating cytokine secretion and T cell receptor signaling has been intensely studied, and it had been speculated that coupling of mitosis to the cytoplasmic polarization that is induced upon synapse formation could result in an asymmetric cell division (6).

T cells remain in contact with antigen-presenting dendritic cells for several hours, suggesting that contacts could extend through mitosis (7). Chang *et al.* tested the asymmetric cell division hypothesis by analyzing T cells that were engineered to express a T cell receptor specific for a *Listeria monocytogenes* antigen. The T cells were labeled with a fluorescent dye and injected into mice infected with the pathogen. Proliferation of T cells was monitored *ex vivo* by stepwise dilution of the dye. This permitted sorting of undivided yet activated T cells as well as those that had divided once. Polarization of premitotic and mitotic T cells was verified by localization of a microtubule organizing center at the remnants of an immunological synapse that still displayed clustered T cell receptor, CD8, and the integrin LFA-1.

To determine if cytoplasmic polarization could lead to distinct mitotic progeny, the authors analyzed the subcellular distribution of components of an evolutionarily conserved asymmetric cell division pathway. In neuroepithelial cells of *Drosophila melanogaster*, and in the *Caenorhabditis elegans* zygote, this pathway uses a protein complex of Par3, Par6, and atypical protein kinase C (Par pathway) for segregating cell fate determinants to the apical cell pole before mitosis (8). Chang *et al.* found that the atypical protein kinase C  $\zeta$  localizes with a microtubule organizing center at the pole opposite the remnants of the immunological synapse. In addition, Numb (an inhibitor of Notch pathway signaling) segregated away from protein kinase C  $\zeta$ , similar to what had been described in asymmetric mitosis in *Drosophila* epithelial cells (9). Nonmuscle myosin II, which contributes to the exclusion



of Numb from the apical pole in neuroblasts (10), has also been implicated in actin-based segregation of signaling components to the immunological synapse (6). Together, these findings suggest that signaling from the synapse results in an asymmetric mitosis that resembles those in invertebrate systems.

Although it is generally assumed that both effector and memory T cells can be derived from the same progenitor T cell, formal proof for such a lineage relationship has been lacking (1). Chang *et al.* noticed that after activation of the dye-labeled T cells in injected mice, those cells that had divided once could be separated into subpopulations expressing high or low amounts of CD8 (CD8<sup>hi</sup> and CD8<sup>lo</sup>). Presumably, this corresponds to the daughter cells that are generated proximally and distally, respectively, to the synapse forged by the parental T cell and dendritic cell (see the figure). In fact, the CD8<sup>hi</sup> cells had phenotypic markers characteristic of effector T cells, whereas the CD8<sup>lo</sup> cells expressed memory cell markers. When these cells were separated and transferred into recipient mice, both animal populations effectively cleared an acute infection with *L. monocytogenes*. However, when mice were infected 30 days after transfer of the two types of T cells, the CD8<sup>lo</sup> cells were much more effective at clearing the microbe. These results are consistent with activated T cells undergoing an asymmetric division to generate effector and memory daughter cells.

It cannot yet be ruled out that the CD8<sup>hi</sup> and CD8<sup>lo</sup> cells used in the transfer experiments are generated independently rather than derived from the same progenitor T cell. Intravital microscopy with fluorescently labeled proteins could address that issue and perhaps support the asymmetric cell division model. As the generation of a memory CD8 T cell response, but not an effector (cytotoxic) CD8 T cell response, requires CD4 T helper cells (11), the role of T helper cells in the asymmetric division needs to be addressed. Genetic analyses will also be needed to prove that components of the conserved Par pathway are required to generate these distinct T cell fates. Subsequently, it will be important to identify the molecular deter-

minants of effector and memory cell fate and explore how they are asymmetrically segregated during the first cell division, as well as how they promote distinct states of gene expression.

One major mechanism for asymmetrically partitioning cell fate determinants involves polarized transport of RNAs (12), and this may also be used by T cells. The findings of Chang *et al.*, along with those on asymmetric cell division in the mammalian epithelium (13), suggest that the Par pathway may regulate both vertebrate stem cell and cellular differentiation fates in a variety of developmental contexts.

#### References

- V. Kalia, S. Sarkar, T. S. Gourley, B. T. Rouse, R. Ahmed, *Curr. Opin. Immunol.* **18**, 255 (2006).
- J. T. Chang *et al.*, *Science* **315**, 1687 (2007); published online 1 March 2007 (10.1126/science.1139393).
- A. Grakoui *et al.*, *Science* **285**, 221 (1999).
- C. R. Monks, B. A. Freiberg, H. Kupfer, N. Sciaky, A. Kupfer, *Nature* **395**, 82 (1998).
- P. Cullinan, A. I. Sperling, J. K. Burkhardt, *Immunol. Rev.* **189**, 111 (2002).
- M. L. Dustin, A. C. Chan, *Cell* **103**, 283 (2000).
- C. Sumen, T. R. Mempel, I. B. Mazo, U. H. von Andrian, *Immunity* **21**, 315 (2004).
- J. Betschinger, J. A. Knoblich, *Curr. Biol.* **14**, R674 (2004).
- F. Roegiers, Y. N. Jan, *Curr. Opin. Cell Biol.* **16**, 195 (2004).
- F. Yu, C. T. Kuo, Y. N. Jan, *Neuron* **51**, 13 (2006).
- S. M. Kaech, R. Ahmed, *Science* **300**, 263 (2003).
- S. Fuerstenberg, J. Broadus, C. Q. Doe, *Int. J. Dev. Biol.* **42**, 379 (1998).
- T. Lechler, E. Fuchs, *Nature* **437**, 275 (2005).



## GEOPHYSICS

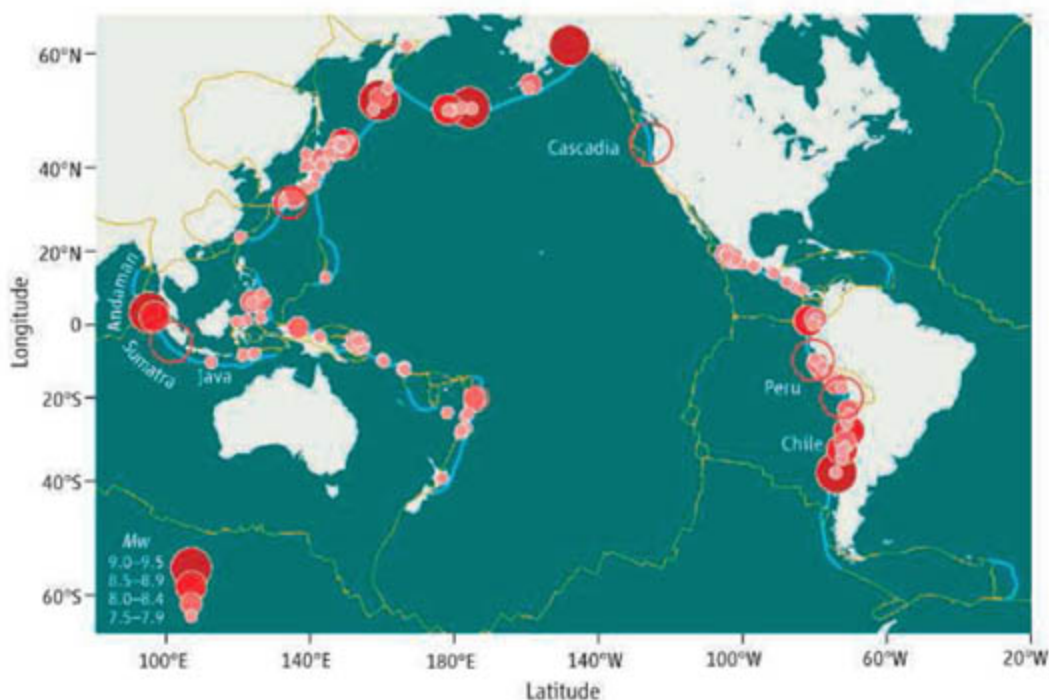
# The Next Great Earthquake

Robert McCaffrey

Earthquakes with a magnitude 9 (M9) or larger occur very infrequently but can cause widespread damage and loss of life, as we saw with the Sumatra-Andaman earthquake in December 2004. Most of these earthquakes occur at the type of tectonic boundaries where one plate slides at a gentle angle beneath another (a process known as subduction). Because they happen mostly beneath the ocean, they often generate destructive tsunami waves.

at 0.02 to 0.10 meters per year; thus, an average time between them is 200 to 1000 years, assuming all the slip is by M9 quakes. If some slip occurs through smaller quakes or creep, the interval will be longer.

From an observational standpoint, this long interval is problematic, because in most places, reliable records of earthquakes date back only a century. Historic accounts and geologic observations can be used to extend the record, but they lack detail.



There are more than 40,000 km of subduction boundaries (see the figure). The rupture of any one contiguous segment ~800 km or more in length can produce an M9 earthquake. Seismologists have long tried to determine which segments are more likely than others to break. Yet, the M9 earthquake of 2004 ruptured a segment that was thought to be among the least likely to go. What governs the frequency of these massive quakes, and are all subduction segments capable of producing one?

Earthquake frequency can be estimated on the basis of plate tectonics. An M9 earthquake accounts for about 20 meters of slip on the boundary between two plates, which converge

In places where long histories are available, the times between great earthquakes appear to be highly irregular. In Cascadia, for example, disturbances of the soft sediments by shaking and deposits of sand by tsunamis, both suggestive of past great earthquakes, show an average time between events of 600 years (1). However, the actual times range from 200 to 1500 years, revealing a very large randomness to when the margin breaks.

The world's major subduction zones can be divided into several segments based on natural geologic changes or earthquake histories (see the figure). Each segment is long enough to produce an M9 quake. Five have had M9 quakes in the past century; many others have not produced quakes greater than M8 in recorded history. In the past few decades, seismologists have focused on trying to correlate this variable earthquake behavior with other

The 2004 Sumatra-Andaman earthquake occurred at a surprising time and place; the lessons learned may help coastal communities in the future.

properties of the different subduction zones. An underlying premise was that, as a result of geologic factors, some subduction zones are intrinsically incapable of generating an M9 quake. If true, this would be important to know.

According to an early idea, the age and speed of the subducting plate were important: If the subducting plate was geologically young (and therefore warm and buoyant), or moving quickly, or both, then its shallow trajectory into the mantle would make it stick more to the plate above it, leading to bigger quakes (2). This idea had empirical support from the 100-year historical earthquake record (3). Other similar suggestions based on

**Danger zones.** Subduction zone segments (blue curves) and tectonic plate boundaries (brown curves) with filled circles showing locations of known earthquakes of M7.5 or greater since 1900. Open circles show incomplete sample of inferred largest earthquakes from 1700 to 1900 (6). Some segments that are free of M9 earthquakes in the past 100 years had them in the previous 200 years.

plate mechanics were that the lateral motion of the subducted plate in Earth's mantle modified stress on the plate boundary (4) and that thick sediments in the trench lubricated the fault (5). The Sumatra-Andaman earthquake occurred in a very unlikely region, according to these explanations (6).

In contrast to mechanical processes, subduction of young, hot lithosphere heats the fault zone, and earthquakes may be inhibited in this setting because high temperatures within Earth promote ductile over brittle deformation (7). Regressions relating earthquake behavior to fault-zone temperatures gave similar statistical fits as the mechanical models (8). However, thermal considerations put the Andaman subduction-zone fault in the high-magnitude class: Its average temperature is probably close to that of central Chile, where the largest known subduction-zone earthquake (M9.5) occurred in 1960 (9).

The rate of convergence between plates can affect the generation of great earthquakes in another way. Theoretically, the frequency of earthquakes of a given size increases with the rate of the relative plate motion (10). If we observe the earthquake process for a finite time, it stands to reason that subduction zones with faster slip rates and, hence, more fre-

The author is in the Department of Earth and Environmental Sciences, Rensselaer Polytechnic Institute, Troy, NY 12180, USA. E-mail: mccafr@rpi.edu



quent M9s will have more M9s than those that are slow. Indeed, the number of M9 earthquakes that have occurred in the past 100 years (five) is within one of those expected at random if we take into account only the rate-predicted intervals between them (11). This recurrence-time concept explains some of the earlier positive correlations of earthquake size with slip rate. However, it differs fundamentally from the mechanical and thermal explanations, in that the latter predict some subduction zones to be incapable of having an M9, whereas the former holds that they are merely improbable.

The Sumatra-Andaman earthquake surprised many Earth scientists by occurring in an unexpected place. Earth gave us a stark reminder of the important difference between improbability and impossibility. Our understanding of where and when the next great earthquake will happen is in its infancy at best. We have not had enough time to decipher M9 earthquake behavior. It will take many more centuries, or many more quakes, or

both, to understand the pattern, if one exists.

For policy purposes, one lesson we should take away from the Sumatra-Andaman earthquake is that every subduction zone is potentially locked, loaded, and dangerous. To focus on some and ignore others may be folly. Several are near densely populated land areas, and the potential impacts of shaking and tsunamis cannot be overstated. We learned that great earthquakes pose a unique hazard to distant coasts: The long rupture generated tsunami waves that traveled over vast oceans with little loss of amplitude due to spreading.

The great reach of the 2004 tsunami (12), and the expected long time interval between such events, requires that these lessons persist over a wide expanse of time and space. A small amount of knowledge in the right place can save many lives, as in the story of the 10-year-old British girl who had learned of tsunamis in school and warned fellow sunbathers in Thailand to run for higher ground, probably saving them (13).

Even while we develop technology-

based global warning systems, we should, by sustained education, embed the lessons of 2004 in the cultural memories of all coastal communities.

#### References

1. C. Goldfinger *et al.*, *Annu. Rev. Earth Planet. Sci.* **31**, 555 (2003).
2. S. Uyeda, H. Kanamori, *J. Geophys. Res.* **84**, 1049 (1979).
3. L. Ruff, H. Kanamori, *Phys. Earth. Planet. Int.* **23**, 240 (1980).
4. C. H. Scholz, J. Campos, *J. Geophys. Res.* **100**, 22103 (1995).
5. L. Ruff, *Pure Appl. Geophys.* **129**, 263 (1989).
6. S. Stein, E. Okal, *Bull. Seismol. Soc. Am.* **97**, 5279 (2007).
7. R. Hyndman, K. Wang, *J. Geophys. Res.* **98**, 2039 (1995).
8. R. McCaffrey, *J. Geophys. Res.* **102**, 22839 (1997).
9. I. Cifuentes, *J. Geophys. Res.* **94**, 665 (1989).
10. P. Molnar, *Bull. Seismol. Soc. Am.* **69**, 115 (1979).
11. R. McCaffrey *et al.*, *Eos Trans. AGU* **87**(52) (Fall Meet. Suppl.) Abstract U518-02 (2006).
12. V. Titov *et al.*, *Science* **309**, 2045 (2005).
13. [http://news.nationalgeographic.com/news/2005/01/0118\\_050118\\_tsunami\\_geography\\_lesson.html](http://news.nationalgeographic.com/news/2005/01/0118_050118_tsunami_geography_lesson.html)

10.1126/science.1140173

#### BOTANY

## A Plant Receptor with a Big Family

Erwin Grill and Alexander Christmann

The largest known family of proteins is also, not surprisingly, involved in a wide range of biological processes in the animal world. Vital physiological functions such as vision, taste, and olfaction recruit G protein-coupled receptors to relay external signals into cells, to elicit the appropriate responses. Likewise, G protein-coupled receptors mediate responses to endogenous signals encoded by peptides, nucleotides, or lipids, to adjust cell growth and differentiation, metabolism, embryogenesis, and development to current physiological demands. The human genome encodes more than 800 G protein-coupled receptors. In contrast to this pervasiveness, plants seem not to have evolved such a dependence on these receptors. The genome of the plant *Arabidopsis thaliana* encodes about 25 "candidate" G protein-coupled receptors—plasma membrane-localized proteins with a seven-transmembrane topology that characterizes this receptor family. Moreover, not a

single ligand for a candidate plant G protein-coupled receptor has been known. Now Liu *et al.*, on page 1712 in this issue (1), report that a candidate G protein-coupled receptor of *Arabidopsis* is the receptor for the phytohormone abscisic acid. This is satisfying not only because it establishes the first functional member of this receptor family in the plant world, but it also identifies a long sought after receptor for an important plant developmental hormone.

Abscisic acid serves as a plant-specific signal during development and in response to environmental stresses such as cold, drought, and high concentrations of salt in the soil. The physiological responses it elicits include the closure of leaf stomatal pores to restrict transpiration, adjustment of metabolism to tolerate desiccation and cold temperatures, and inhibition of seed germination and seedling growth. Biochemical and electrophysiological studies provide evidence for both extracellular and intracellular perception of the hormone (2, 3). Recently, the nuclear RNA-binding protein FCA, which controls flowering time (4), and the Mg-chelatase subunit H located in chloroplasts (5), were identified as intracellular abscisic acid receptors. Liu *et al.*

A hormone that controls plant development and survival acts through a member of a receptor family whose other members are pervasive in animal cells.

now show that GCR2 is a plasma membrane-localized G protein-coupled receptor that specifically binds to naturally occurring abscisic acid, but not to the physiologically inactive isomer (trans-abscisic acid), to control stomatal closure, seed germination, and seedling growth.

In addition to seven-transmembrane domains, a G protein-coupled receptor has a cytosolic domain that acts as a guanine-nucleotide exchange factor for heterotrimeric GTP-binding proteins (G proteins). Upon binding to a ligand, the receptor promotes the exchange of bound GDP for GTP in an associated G protein; this results in receptor dissociation from the G protein. The G protein itself dissociates into  $G\alpha$  and  $G\beta\gamma$  complexes that then target downstream effectors such as guanylyl cyclase, protein kinases, or phospholipases. There is only one canonical  $G\alpha$ , one  $G\beta$ , and two  $G\gamma$  subunits expressed in *Arabidopsis*. Previous functional analysis of plant G protein subunits implicated their involvement in phytohormone responses, including abscisic acid signaling (6). In mutant plants lacking  $G\alpha$  (GPA1), regulation of stomatal movement is impaired and germination is hypersensitive to abscisic acid (7).

The authors are in the Department of Plant Science, Technical University Munich, Am Hochanger 4, 85350 Freising-Weihenstephan, Germany. E-mail: erwin.grill@wzw.tum.de



The identification by Liu *et al.* of a physical interaction between the G protein-coupled receptor GCR2 and the G $\alpha$  subunit GPA1 provides the missing link between a G protein and abscisic acid perception. The authors show that in plants lacking GPA1 and GCR2, responses to abscisic acid are impaired but not abolished. This is consistent with a parallel or redundant hormone response pathway that possibly involves the intracellular hormone receptor in chloroplasts. Analysis of mutant plants deficient in both extracellular and intracellular abscisic acid reception sites should clarify this point. Alternatively, GCR2-related proteins and noncanonical G $\alpha$  subunits might be functionally redundant in relaying an abscisic acid signal. The two known GCR2-related proteins in plants share 42% and 63% identity at the amino acid level with GRC2, and all three proteins are structurally related to the mammalian peptide-modifying lanthionine synthetase C-like protein. Liu *et al.* also found that the insensitivity or hypersensitivity of mutant plants that lack or overexpress GCR2, respectively, to abscisic acid depends on the G $\alpha$  subunit GPA1. This points to a positive regulatory role of GCR2 in abscisic acid signal transduction.

What happens then, when GCR2 is activated by abscisic acid? In the classic paradigm of G protein signaling (6), GPA1-GTP and G $\beta\gamma$  are predicted to dissociate from the receptor upon receptor-abscisic acid interaction. GPA1 and G $\beta\gamma$  subunits then serve as signaling molecules that remain tethered to the plasma membrane (through lipid moieties) (see the figure). G $\beta$  has been linked to several plant hormone responses and shown to inhibit lateral root initiation in response to the hormone auxin. G $\beta$  also negatively regulates abscisic acid signaling during germination and early seedling development (7).

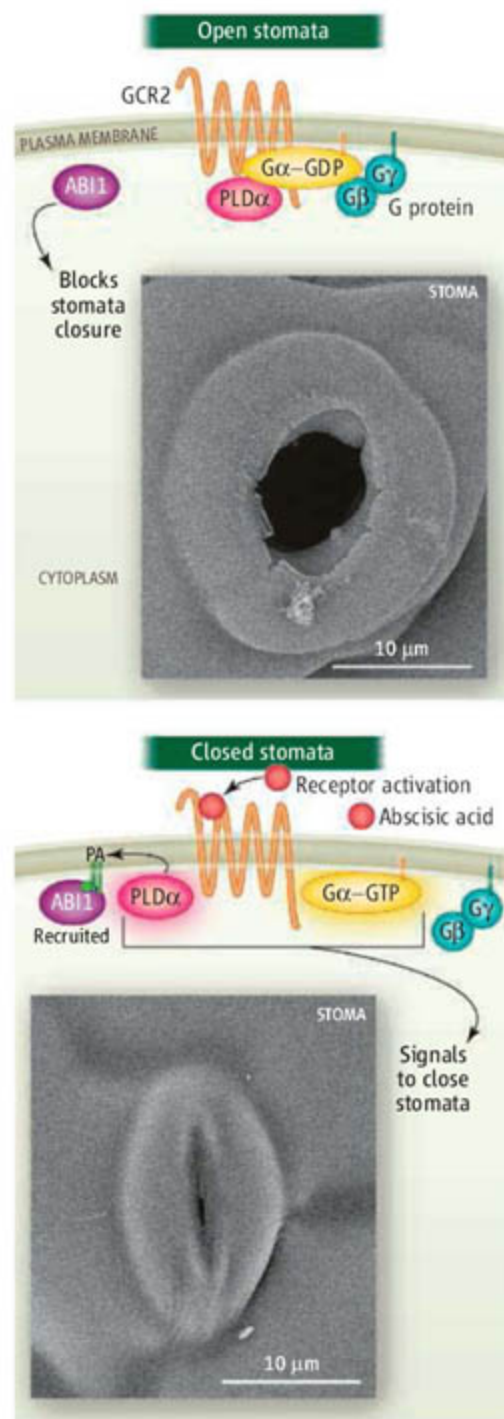
The effects of GPA1 involve proteins that bind to it. These include phospholipase D $\alpha$ 1 (PLD $\alpha$ ), which is involved in stomatal responses, and the cupin-domain protein AtPirin1, which functions downstream of GPA1 in seed germination and early seedling development. In addition, the protein thylakoid formation 1 interacts with GPA1 and links G protein signaling to a sugar-sensing pathway. Abscisic acid-stimulated phospholipid cleavage by PLD $\alpha$  generates the signaling molecule phosphatidic acid in the plasma membrane. Phosphatidic acid further promotes abscisic acid signaling by recruiting ABI1, a negative hormone response regulator (ABI1 interacts with different cellular targets such as the transcription factor AtHB6 to negatively regulate abscisic acid responses), to the plasma membrane; this relocalization of ABI1 blocks its activity (8). The interaction of

GPA1 with PLD $\alpha$  is destabilized when GTP binds the G $\alpha$  subunit (9). This is compatible with an abscisic acid-dependent release of PLD $\alpha$  from the G $\alpha$  subunit.

In animal cells, phosphatidic acid recruits the enzyme sphingosine kinase to the plasma membrane and thereby controls generation of

the lipid sphingosine 1-phosphate. Sphingosine 1-phosphate then acts as an extracellular ligand for G protein-coupled receptors. In plants, sphingosine 1-phosphate promotes GPA1-dependent stomatal closure (10) and may also act via a G protein-coupled receptor. GCR1 of *Arabidopsis* is a candidate G protein-coupled receptor, the ligand of which is unknown. GCR1 interacts directly with GPA1 and functions antagonistically to GCR2 by promoting germination and shortening the time to flowering (11). This indicates a competing interaction with GCR2 for GPA1. Thus, GPA1 appears to represent a node where different signaling pathways converge.

The identification of GCR2 as an abscisic acid receptor brings G protein signaling into the limelight of plant research. To date, studies of plant signaling have focused on leucine-rich repeat receptors. The *Arabidopsis* genome encodes more than 600 leucine-rich repeat receptors, which are involved in pathogen recognition and in regulating numerous developmental processes. In contrast, the analysis of predicted seven-transmembrane proteins has been neglected. G protein-coupled receptor candidates in *Arabidopsis* include the barley mildew resistance locus O and heptahelical proteins that are related to mammalian adiponectin and progesterin receptors (which possess seven-transmembrane domains) (12, 13). It is hard to predict how many different G protein-coupled receptors exist in plants and how they might interact. The limited number of different heteromeric G protein subunits, however, provides an excellent system to functionally elucidate the specificity and integration of G protein-coupled receptor signaling at the level of G proteins.



**Guards on hormones.** (Top) The aperture of a stomatal pore in a leaf is controlled by osmoregulation of two guard cells. When the G protein-coupled receptor GCR2 is inactive, the protein phosphatase ABI1 inhibits stomata closure by attenuating abscisic acid signal transduction. (Bottom) Hyposmotic conditions in guard cells (relative to surrounding tissue) cause stomata to close. This involves activation of GCR2 by abscisic acid, which triggers specific signaling pathways that lead to closed stomata. Scanning electron micrographs of stomata are from (14).

## References

1. X. Liu *et al.*, *Science*, **315**, 1712 (2007); published online 8 March 2007 (10.1126/science.1135882).
2. A. Christmann *et al.*, *Plant Biol.* **8**, 314 (2006).
3. R. R. Finkelstein, S. S. Gampala, C. D. Rock, *Plant Cell* **14** (suppl.), S15 (2002).
4. F. A. Razem, A. El-Kereamy, S. R. Abrams, R. D. Hill, *Nature* **439**, 290 (2006).
5. Y. Y. Shen *et al.*, *Nature* **443**, 823 (2006).
6. A. M. Jones, S. M. Assmann, *EMBO Rep.* **5**, 572 (2004).
7. S. Pandey, J. G. Chen, A. M. Jones, S. M. Assmann, *Plant Physiol.* **141**, 243 (2006).
8. G. Mishra, W. Zhang, F. Deng, J. Zhao, X. Wang, *Science* **312**, 264 (2006).
9. J. Zhao, X. Wang, *J. Biol. Chem.* **279**, 1794 (2004).
10. S. Coursol *et al.*, *Nature* **423**, 651 (2003).
11. L. Perfus-Barbeoch, A. M. Jones, S. M. Assmann, *Curr. Opin. Plant Biol.* **7**, 719 (2004).
12. A. Devoto *et al.*, *J. Mol. Evol.* **56**, 77 (2003).
13. M. H. Hsieh, H. M. Goodman, *J. Exp. Bot.* **56**, 3137 (2005).
14. E. Grill, H. Ziegler, *Science* **282**, 252 (1998).

Published online 8 March 2007;  
10.1126/science.1140761.

Include this information when citing this paper.



## RETROSPECTIVE

## Alan G. MacDiarmid (1927–2007)

Ray H. Baughman

On 7 February 2007, Alan Graham MacDiarmid died in Philadelphia at age 79, after falling when about to depart for a visit to his native New Zealand. He suffered from a blood disease that was expected to soon end his life.

Alan MacDiarmid, who shared the 2000 Nobel Prize in Chemistry with Alan Heeger and Hideki Shirakawa, believed that winning the prize gave him a special obligation for advancing humankind. His indomitable spirit and sense of responsibility never dwindled. Having been close to death 2 months earlier in China, he was back on the road this January to a Department of Energy laboratory and his institute at the University of Texas at Dallas. His planned 10-day trip to New Zealand included a life-sustaining blood transfusion, three keynote lectures, discussions with government ministers, a TV interview, and a likely last farewell to family.

Alan was born in New Zealand on 14 April 1927. The ravages of the Great Depression and long-term unemployment of his engineer father caused Alan to live in poverty during his youth. Yet his family assisted other impoverished families as best they could. This tradition of helping others, which Alan did in so many fields and countries, is an important part of his legacy.

After delivering milk in the early morning on a bicycle, Alan began primary school classes in a two-room school house, where "most of my school chums were Maori boys and girls from whom I learned so much" (1). In honor of the native Maori and his New Zealand heritage, Alan danced the Maori haka at the all-night student celebration ending the Nobel Prize ceremonies, and at many other celebrations with friends.

Alan's love of chemistry began at age 10, when he started to read his father's chemistry textbook from the late 1800s. Alan prematurely left high school to help support his family, and fortunately found a part-time job as lab boy and janitor in the chemistry department of Victoria University College. It was here that he earned his bachelor's and master's degrees. His first published paper, in 1949, was on the cyclic  $S_4N_4$  molecule, which much

later played an indirect role in his Nobel Prize-winning codiscovery of metallic organic polymers.

Alan earned doctorates from the University of Wisconsin and Cambridge University and later became a professor at the University of Pennsylvania, where he made pioneering breakthroughs in silicon chemistry, which earned him the 1971 Frederick Stanley Kipping Award of the American Chemical Society. In 2002, he became professor of chemistry and James Von Ehr Distinguished Chair in Science and Technology at the University of Texas at Dallas.

In the 1970s, there was much excitement about newly discovered kinds of metallic molecular charge-transfer complexes, an area in which Alan Heeger and his group were making landmark discoveries. Many researchers were trying to make insulating organic polymers metallic—but either with the wrong polymer or the wrong dopant. Then, Mort Labes and co-workers at Temple University showed metallic conductivity down to 4 K for the undoped inorganic polymer  $(SN)_x$ , which can be made from  $S_4N_4$ . MacDiarmid and Heeger began to collaborate on  $(SN)_x$  and found that bromine doping produced a 10-fold increase in electrical conductivity. While visiting the Tokyo Institute of Technology in 1975, MacDiarmid showed Hideki Shirakawa golden crystals of  $(SN)_x$ , and Shirakawa showed him films of his silvery polyacetylene  $(CH)_x$ . Sharing a vision of possibly transforming  $(CH)_x$  from an insulator into a polymeric metal, Shirakawa joined Heeger and MacDiarmid at the University of Pennsylvania to make this happen.

The discovery that insulating organic polymers could be converted into metallic conductors by doping earned Heeger, MacDiarmid, and Shirakawa the Nobel Prize in Chemistry. It has had enormous fundamental and practical importance. Realized or proposed products include, for example, antistatic and corrosion-protection materials, electromagnetic shields, light-emitting devices, solar cells,

A. G. MacDiarmid, a chemist who co-discovered metallic organic polymers, had a profound sense of responsibility toward individuals and humankind.

sensors, artificial muscles, transistors, supercapacitors, batteries, and fuel cells.

A graduate student once ran into Alan's office saying that he might have accidentally condensed acetylene, thereby potentially creating a powerful bomb, as the acetylene gas precursor to  $(CH)_x$  becomes highly explosive when liquefied. The fire department was called and the building cleared. Alan volunteered to go alone into harm's way to eliminate the danger. With all others safely behind walls, he tucked a notebook into his trousers to reinforce protection afforded by bomb disposal clothing, and used a fishing rod to open a valve and avert a potential catastrophe.

Alan was a hero in many other ways. He created institutes in New Zealand, China, India, South Korea, Brazil, and Texas, which emphasized finding sustainable solutions for the increasing need for energy. During conference poster sessions, he would focus on the work of young people. He would listen intently to their presentations, ask penetrating questions, and then frequently and sincerely comment that "your work is so very interesting." This and other encouragement from such a great scientist inspired generations of students.

Alan was exuberant, loving, sensitive, and active in responding to individual human needs and those of humankind. His insights and discoveries, both fundamental and applied, were critical for beginning the second age of polymers, where polymers become fully functional electronic materials. There would have been more institutes that he nourished and many more breakthroughs, if he had lived just a little longer. He is survived by his wife, a sister, and two brothers, his four children, and nine grandchildren.

## References and Notes

1. This quote is from Alan's autobiography on the Nobel Web site ([nobelprize.org/nobel\\_prizes/chemistry/laureates/2000/macdiarmid-autobio.html](http://nobelprize.org/nobel_prizes/chemistry/laureates/2000/macdiarmid-autobio.html)).



The author is at the NanoTech Institute, University of Texas at Dallas, TX 75080, USA. E-mail: ray.baughman@utdallas.edu



# Restoration of the Mississippi Delta: Lessons from Hurricanes Katrina and Rita

John W. Day Jr.,<sup>1\*</sup> Donald F. Boesch,<sup>2</sup> Ellis J. Clairain,<sup>3</sup> G. Paul Kemp,<sup>4</sup> Shirley B. Laska,<sup>5</sup> William J. Mitsch,<sup>6</sup> Kenneth Orth,<sup>7</sup> Hassan Mashriqui,<sup>8</sup> Denise J. Reed,<sup>9</sup> Leonard Shabman,<sup>10</sup> Charles A. Simenstad,<sup>11</sup> Bill J. Streever,<sup>12</sup> Robert R. Twilley,<sup>1</sup> Chester C. Watson,<sup>13</sup> John T. Wells,<sup>14</sup> Dennis F. Whigham<sup>15</sup>

Hurricanes Katrina and Rita showed the vulnerability of coastal communities and how human activities that caused deterioration of the Mississippi Deltaic Plain (MDP) exacerbated this vulnerability. The MDP formed by dynamic interactions between river and coast at various temporal and spatial scales, and human activity has reduced these interactions at all scales. Restoration efforts aim to re-establish this dynamic interaction, with emphasis on reconnecting the river to the deltaic plain. Science must guide MDP restoration, which will provide insights into delta restoration elsewhere and generally into coasts facing climate change in times of resource scarcity.

The Mississippi Deltaic Plain (MDP) is a 25,000-km<sup>2</sup> dynamic landscape of water, wetlands, and low upland ridges, formed as a series of overlapping delta lobes. An understanding of how humans and Hurricanes Katrina and Rita affected the MDP in 2005 requires knowledge about the complex processes that formed and sustained the delta for millennia before human impact. The delta emerged about 6000 to 7000 years ago after eustatic sea level stabilized (Fig. 1) (1–3). A variety of processes formed and sustained the delta and increased its overall size (Table 1) (4). Riverine sediments were deposited at river mouths and via overbank flooding, crevasse formation, and older distributaries (2, 3). Crevasses were usually short-lived (<100 years) and formed depositional splays about 10 km wide, as com-

pared to hundreds of kilometers for delta lobes (5). Many former distributaries functioned, either permanently or seasonally, at the beginning of European colonization, around 1700. A skeletal framework of distributary ridges and barrier islands (6) protected interior fresher wetlands from marine forces and saltwater intrusion (Fig. 1).

To survive, the soil surface of coastal wetlands must grow vertically to keep pace with local sea level. This is critical in the MDP, where geologic subsidence causes a relative sea-level rise (RSLR) of about 1 cm/year as compared to ~1.5 mm/year of eustatic SLR. Plant growth contributes organic soils; the rest of the vertical growth comes from mineral sediments (7). Riverine inputs benefit coastal wetlands in several ways: Mineral sediments increase accretion and bulk density, nutrients enhance plant growth, fresh water buffers saltwater intrusion, and iron precipitates toxic sulfides (8, 9). The deposition of older river sediments resuspended from bays and the nearshore Gulf of Mexico or eroded from other wetlands is especially important during winter storms and hurricanes (7, 10, 11). However, most sediment is introduced directly from the river (12).

In the MDP, barrier islands grow and diminish in conjunction with deltaic lobe cycles (Fig. 2) (13). Coarser sediments are deposited at active river mouths, and as the delta advances, sand is transported laterally to form beach ridges. After channel abandonment, delta-front sands are reworked to form erosional headlands attached to marshes behind the barrier. Waves and currents rework and redistribute headland sands laterally to form flanking barrier islands, and the islands move landward as sand is transported in wash-

<sup>1</sup>Department of Oceanography and Coastal Sciences, Louisiana State University, Baton Rouge, LA 70803, USA. <sup>2</sup>University of Maryland Center for Environmental Science, Post Office Box 775, Cambridge, MD 21613, USA. <sup>3</sup>Engineer Research and Development Center, U.S. Army Corps of Engineers, Vicksburg, MS 39180, USA. <sup>4</sup>The Hurricane Center, Louisiana State University, Baton Rouge, LA 70803, USA. <sup>5</sup>Department of Sociology, University of New Orleans, New Orleans, LA 70148, USA. <sup>6</sup>Oleantary River Wetland Research Park, The Ohio State University, 352 West Dodridge Street, Columbus, OH 43202, USA. <sup>7</sup>Institute for Water Resources, U.S. Army Corps of Engineers, 7701 Telegraph Road, Alexandria, VA 22315, USA. <sup>8</sup>Department of Civil and Environmental Engineering, Louisiana State University, Baton Rouge, LA 70803, USA. <sup>9</sup>Department of Geology and Geophysics, University of New Orleans, New Orleans, LA 70148, USA. <sup>10</sup>Resources for the Future, 1616 P Street, NW, Washington, DC 20036, USA. <sup>11</sup>School of Aquatic and Fishery Sciences, Box 355020, University of Washington, Seattle, WA 98015, USA. <sup>12</sup>BP Exploration (Alaska), Post Office Box 196612, Anchorage, AK 99519-6612, USA. <sup>13</sup>Engineering Research Center, Colorado State University, Fort Collins, CO 80523, USA. <sup>14</sup>Virginia Institute of Marine Science, Box 1346, Gloucester Point, VA 23062, USA. <sup>15</sup>Smithsonian Environmental Research Center, Box 28, Edgewater, MD 21037, USA.

\*To whom correspondence should be addressed. E-mail: johnday@lsu.edu

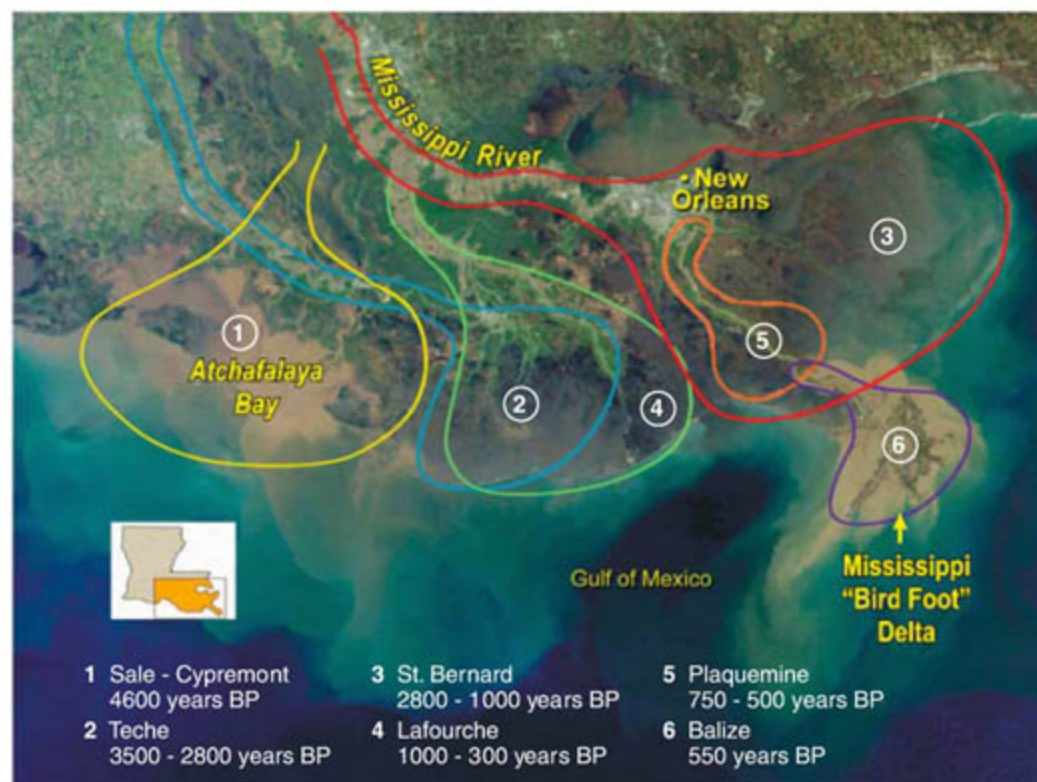


**Fig. 1.** The MDP was formed by a series of overlapping delta lobes as the river occupied different channels. The delta is characterized by current and abandoned river channels, barrier islands, and extensive coastal wetlands. Currently, about two-thirds of flow is discharged via the lower Mississippi directly to the Gulf and one-third is discharged via the Atchafalaya River to a shallow bay where a new delta is forming. The location of levees is shown on the lower river as well as the location of the MRGO. The turbid plume shown on the right results from a river diversion. BP, before the present. [Modified from (66)]



over fans. As wetlands deteriorate, a barrier island arc is formed. Over time, the barriers fragment into smaller islands, and extensive washover terraces or sandy shoals are formed inshore of the islands, eventually producing a submerged complex of shoals and sand sheets. This process continues until another distributary channel forms and the cycle begins again.

#### Deterioration of the MDP

Since 1900, about 4900 km<sup>2</sup> of wetlands in coastal Louisiana have been lost at rates as high as 100 km<sup>2</sup>/year (14, 15). Wetland loss is much lower on the central coast, where the Atchafalaya River, a distributary that carries one-third of the flow of the Mississippi River, discharges into a shallow inshore bay (16). Loss occurs at the wetland edge because of wave erosion and in interior wetlands by submergence as soil accretion fails to keep up with RSLR (17). Most loss was initially internal, but as wetlands opened up, wave erosion has become more important (18). Although a delta grows and decays as a natural outcome of the delta lobe cycle, the MDP experienced an overall net growth for several thousand years after the sea level stabilized. Human activities during the 20th century reversed this trend (15, 17, 19).

The main cause of loss was the isolation of the river from the MDP (17, 19). The river is now almost completely leveed, preventing overbank flooding and crevasse formation, so most of its discharge is into the deep Gulf of Mexico (Fig. 1). With the exception of the Atchafalaya River, all distributaries of the river have been closed. The lower Mississippi is prevented from seeking a shorter course to the Gulf via the Atchafalaya by the Old River Control Structure.

Over 15,000 km of canals have been dredged for navigation, drainage, and logging, but mostly for oil and gas development (17). This and

the construction of impoundments have altered the hydrology that sustains the system (20). Spoil banks associated with canals reduce sheet flow of water through wetlands (21). Deep, straight navigation canals cause saltwater intrusion and the death of freshwater plant communities (17). One of the most notable is the Mississippi River Gulf Outlet (MRGO), a 12-by-300-m canal dredged through the Breton Sound Basin in 1963. Saltwater intrusion via the MRGO killed thousands of hectares of freshwater wetland forests. As Katrina's path crossed Breton Sound, levees along the MRGO were breached and storm surge funneled through the MRGO and into the Gulf Intracoastal Waterway to contribute to the flooding of New Orleans. The withdrawal of oil, natural gas, and formation waters lowered pressures in underlying geologic features, probably causing downfaulting and increasing the rate of subsidence by two to three times during active oil and gas production (22).

The construction of reservoirs in the Mississippi basin dramatically reduced the supply of both suspended and bedload sediments to the delta (6). Inputs of sand are particularly important for maintaining barrier islands; thus, all barrier islands in the deltaic plain are deteriorating (13) because the deterioration phase of the barrier island cycle has accelerated while the development phase has been greatly reduced.

#### Hurricanes and Mississippi Delta Wetlands

Hurricanes are a regular, if episodic, force in the MDP. Thousands of tropical storms affected the delta as it grew over the past 6000 to 7000 years. Under some conditions, runoff generated by hurricane precipitation introduces fresh water and nutrients that reduce salinity and enhance coastal productivity (23). Hurricanes also deposit large amounts of resuspended sediments on

wetland surfaces, helping to offset RSLR, and thus are important for the sustainability of marshes (7, 10). Hurricanes Katrina and Rita were the fourth and fifth most powerful storms to strike the MDP since 1893 with respect to maximum wind speed at landfall, but were more remarkable in both cases for the hundreds of kilometers of the coast affected by a storm surge of more than 3 m. As Katrina progressed across Breton Sound and Lake Borgne as a category 3 storm (sustained winds of 194 km hour<sup>-1</sup>), it generated a storm surge that exceeded 10 m on the Mississippi coast and measured up to 6 m southeast of New Orleans, with up to 2 m of additional wave run-up in the most exposed locations (Fig. 3) (24). In southeast Louisiana, communities unprotected by levees were inundated, and the storm destroyed levees protecting eastern New Orleans and St. Bernard and Plaquemines parishes to the south and east. Floodwalls failed along drainage and navigation canals connected to Lakes Pontchartrain and Borgne, inundating most of the rest of New Orleans. Because much of this area is below sea level, the floodwaters remained for 3 or more weeks while emergency repairs were made and the water was pumped out. More than 1500 people died as a direct or indirect result of Hurricane Katrina, almost 1100 of them in Louisiana.

Katrina and Rita deposited 5 to 10 cm of sediment over large areas of coastal wetlands (11). But about 100 km<sup>2</sup> of wetlands in the Breton Sound Basin lying in the storm path were converted to open water (25). Although some of this area is now 1 m or more deep, most of the damaged area is shallow mud flats interspersed with myriad marsh clumps uprooted by the storm. The disturbance of buoyant low-salinity marshes with low-density organic soils often occurs during hurricanes. The Caemarvon river diversion structure is presently being operated to the maximum extent possible to enhance marsh recovery in the most heavily affected area. Initial observations indicate substantial marsh recovery.

Hurricane Rita made landfall near Sabine Pass at the Louisiana-Texas border on 24 September 2005, generating a storm surge of up to 5 m (Fig. 3) and reflooding parts of New Orleans more than 200 km east of landfall. Coastal communities in Cameron Parish were destroyed, and parts of the city of Lake Charles experienced 2-to-3-m-deep flooding associated with surge propagating up a ship channel. To the east, the 30-to-50-km-wide Chenier Plain wetlands reduced surge inland. Because of the lesser storm surge and lower population densities, fewer than 10 people lost their lives directly as a result of Rita's winds and surge. Rita's surge displaced residents from all Louisiana coastal parishes, however, and drove salt water tens of kilometers inland, killing freshwater wetlands in artificially impounded areas (25).

Hurricane Rita's highest storm surge was nearly as great as the surge confronting the

**Table 1.** A hierarchy of forcings or pulsing events affecting the formation and sustainability of deltas. [Modified from (4)]

Event	Time scale	Impact
Major changes in river channels	500–1000 years	New delta lobe formation (avulsions), major sediment deposition
Major river floods	50–100 years	Avulsion enhancement, major sediment deposition, enhancement of crevasse formation and growth
Major storms	20–25 years	Major sediment deposition, enhanced production
Average river floods	Annual	Enhanced sediment deposition, freshening (lower salinity), nutrient input, enhanced primary and secondary production
Normal storm events (frontal passage)	Weekly	Enhanced sediment deposition, enhanced organism transport, higher net materials transport
Tides	Daily	Marsh drainage, stimulated marsh production, low net transport of water and materials



eastern side of New Orleans during Katrina, but had to cross 30 to 50 km of Chenier Plain wetlands before reaching main population centers, whereas Katrina's surge was less impeded as it traveled through large lagoons, degraded wetlands, and artificial channels. Barrier islands, shoals, and wetlands can reduce storm surge and waves, but the full range of these effects is not well captured at present by most numerical models. Although it has been shown that damage from the 2004 Indian Ocean tsunami was less in communities sheltered by intact mangroves (26), the existence of an extensive barrier island system off of the Mississippi coast did not protect it from a 10-m surge during Katrina. Observations of water levels indicate that Rita's surge was attenuated at an average rate of 4.7 cm per kilometer of wetland landscape where channels were not present. This is similar to previous hurricanes, including Hurricane Andrew in 1992, indicating storm surge attenuation of 7.9 cm per kilometer for intact wetlands along the central Louisiana coast (27–29).

Emergent canopies of forested wetlands can greatly diminish wind penetration, thereby reducing the wind stress available to generate surface waves as well as storm surge (30, 31). The sheltering effect of these canopied areas also affects the fetch over which wave development takes place. Shallow water depths attenuate waves via bottom friction and breaking, whereas vegetation provides additional frictional drag and wave attenuation (32) and also limits static wave setup (33). Extracting energy from waves either by breaking or increased drag reduces destructive wave action on levees. During Katrina, wave-induced run-up and overtopping washed away many miles of turf-covered earthen levees along the MRGO (24). Few wetlands or fast lands protected these levees from high-energy surge currents and waves that broke on the levee face.

Conversely, other earthen levees nearby that were overtopped by the low-velocity surge, but fronted by extensive wetlands, escaped substantial damage (34).

Depending on the rate of RSLR, coastal wetlands maintain a near-sea-level elevation by trapping sediments and forming organic-rich soils. Thus, wetlands play an important role in maintaining elevations near sea level, in contrast to the –3 to –4-m elevations that characterize the

equilibrium depth of large bays along the Louisiana coast. Although the relative effects of shallow open waters versus intertidal wetlands on both waves and storm surges from strong hurricanes remain to be fully resolved, it is clear that the intact barrier islands, wetlands, and ridges that once characterized the coastal landscape of Louisiana afforded substantial protection to New Orleans and other coastal communities that cannot be depended

by large navigation channels, which may now also require elaborate gates and other closure structures.

### The Evolving MDP Restoration Effort

Planning the restoration of the coastal landscape requires the design of sustainable ecosystems that integrate human society with the natural environment (35–37) and work with rather than against natural processes. Such ecological engineering approaches rely primarily on the energies of nature, with human energy being used in the design and control of key processes. Because of the dimensions of the delta's problems, traditional engineering approaches such as levee construction and the placing of dredged sediments are also required. An important goal of MDP restoration is the application of the optimum mix of ecological and standard engineering approaches. With this in mind, four general approaches to restoration are being evaluated, planned, or implemented in the MDP:

(1) Reconnecting the river to the deltaic plain via river reintroductions, the reopening of old distributaries, and crevasse-splay development (35, 37, 38). Over the past two decades, it has become increasingly clear that this will have to be done on a large scale.

(2) Using dredged sediments to create and restore wetlands by pumping them over distances of tens of kilometers. This is expensive, but because dredged sediments can be used to create wetlands quickly, this technique may be useful for restoring wetlands that would soon be lost or quickly creating large areas of wetlands that would then be sustained through river reintroductions (39).

(3) Restoring barrier islands by pumping sands from offshore, constructing groins and breakwaters, placing riprap, and using fences and plantings to stabilize sand dunes (40, 41). Because

MDP barrier islands do not just migrate but deteriorate over time, restoration will require ongoing maintenance. Restoration and maintenance can be justified, however, because islands reduce waves and storm surge and provide important habitats in the coastal landscape. In the future, the remobilization of sand trapped in up-basin reservoirs may become a source of coarse sediments that will aid in maintaining barrier islands.

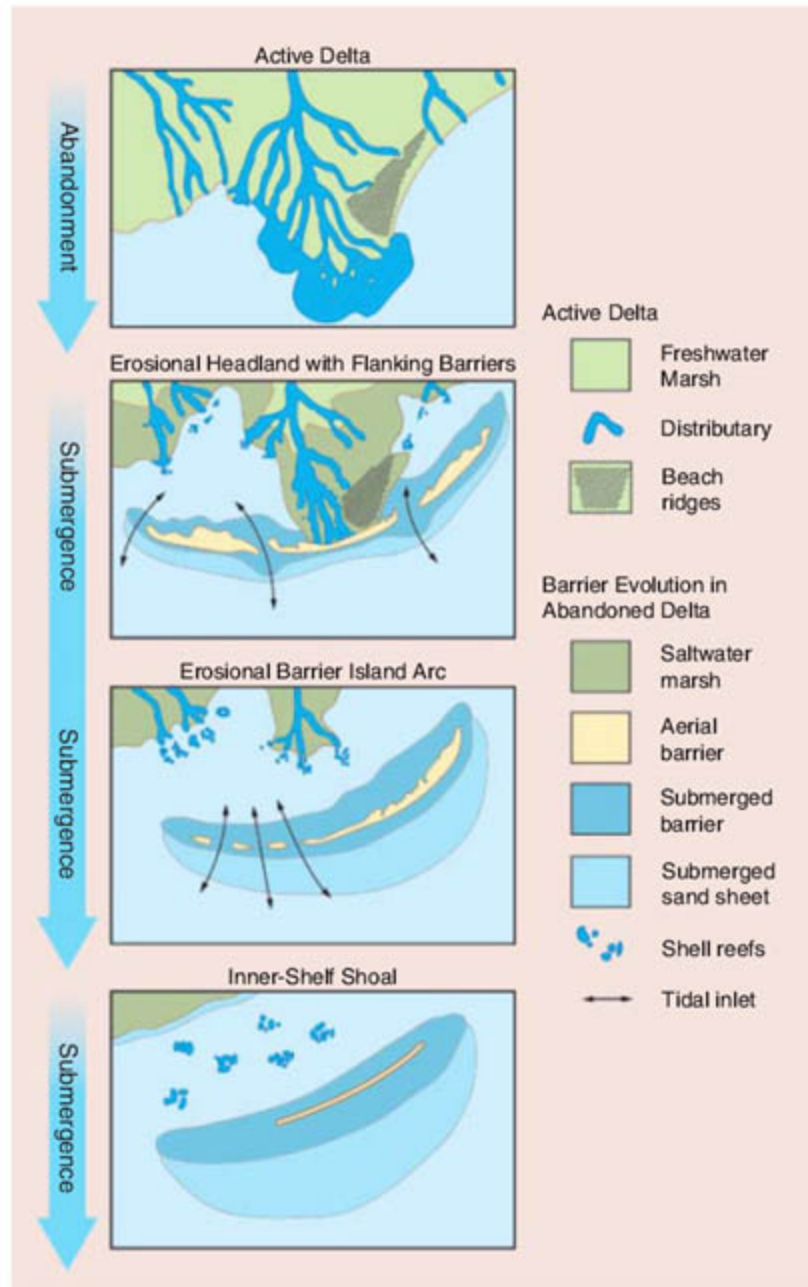
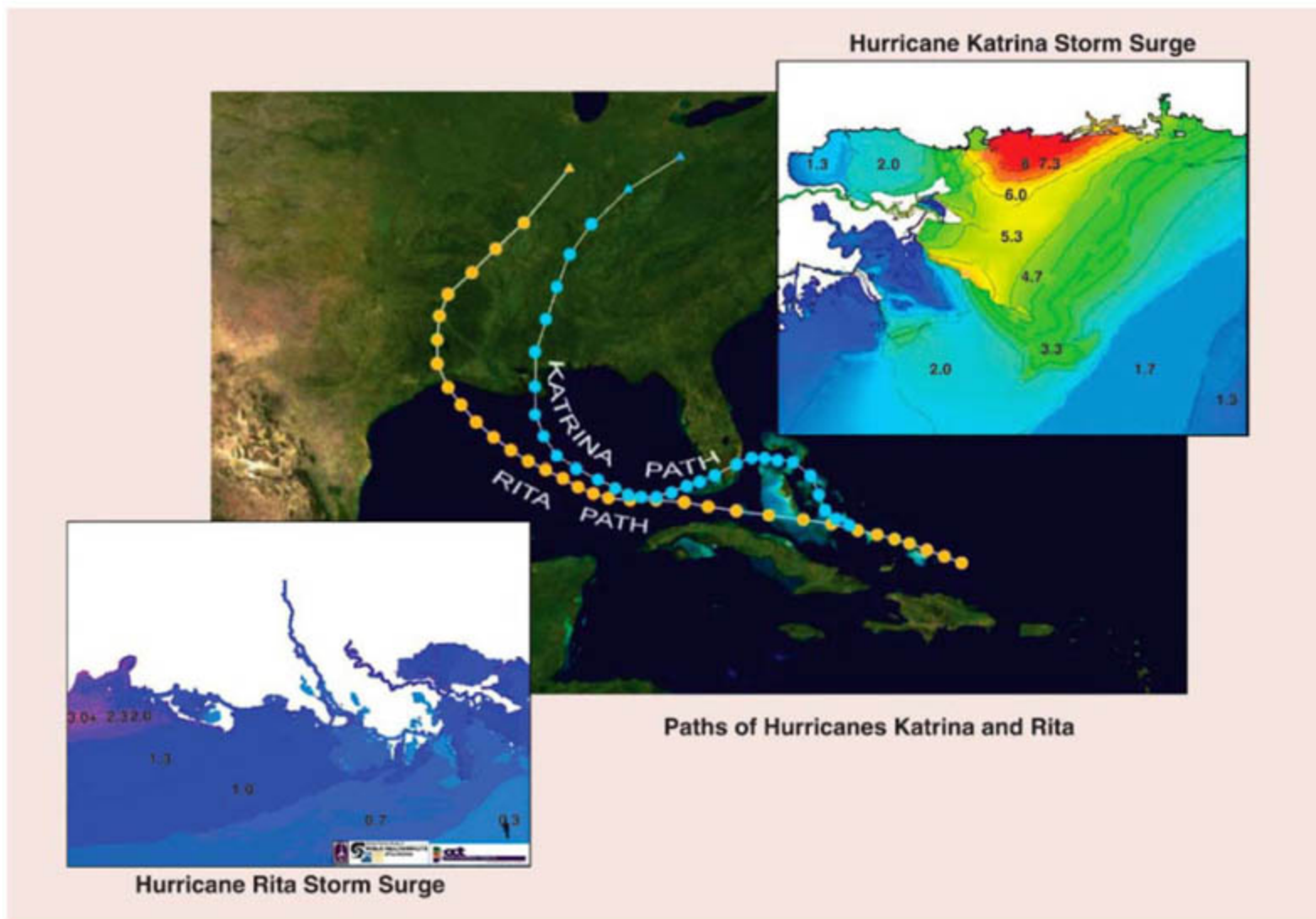


Fig. 2. The barrier island cycle in the MDP. [Modified from (13)]

on today and must be replaced by more massive levees.

Consequently, maintaining and, where possible, using deltaic processes to increase the area of marshes, mangroves, and swamps in strategic locations would provide a self-sustaining complement to the structural protection of levees. Unfortunately, the physical and hydrologic integrity of the wetlands southeast of New Orleans has been greatly compromised





**Fig. 3.** A composite figure showing paths of Hurricanes Katrina and Rita, surge levels [in meters, as estimated by the ADCIRC model (67)], areas flooded, sites of levee failures, and wetland loss due to the hurricane.

(4) Restoring hydrological processes by removing spoil banks, backfilling canals, closing deep navigation channels (such as the MRGO), installing locks (42), trapping sediments (43), and protecting interior shorelines against erosion. Such restoration generally affects a relatively small area, but can be particularly effective if done in conjunction with diversions so that river water is used most effectively.

Even with its bountiful natural resources, it must be remembered that the MDP is a “working coast” (38, 44), and restoration must be integrated with navigation and flood-protection infrastructure, agriculture, urban development, commercial and recreational fishing, and oil and gas production. In turn, these activities will have to adapt to projects, such as diversions, that seek to return the delta to a more natural state. This is a lesson to be learned regarding most deltas.

Coastal restoration will be more effective if it takes into account changes in fresh water supply, suspended sediment, and nutrient fluxes in the Mississippi River Basin (45, 46). It should work cooperatively with efforts to better manage and restore the resources and environments of the basin, including the restoration of the Missouri and Upper Mississippi Rivers, reservoir

management, the reconnection of wetlands and flood plains, and reducing loadings of nutrients from agricultural lands that result in hypoxia in the Gulf of Mexico (47–49).

Global climate change and the availability and cost of energy have important implications for delta restoration (50). Accelerated sea-level rise, changes in precipitation patterns, and changes in the frequency and intensity of hurricanes (51–54) must be taken into account in designing effective restoration strategies. Less energy-intensive restoration techniques that use the energies of nature, rather than dwindling and costly fossil fuels (55, 47), should be emphasized (50).

#### A New Institutional Framework

For most of the 20th century, public decisions and investments in coastal Louisiana focused on flood protection, navigation, oil and gas extraction, or wildlife management. Growing awareness of the dimensions and consequences of wetland loss has resulted in considerable regional advocacy and planning for substantial public investments for restoration of the MDP. The federal Coastal Wetlands, Planning, Protection and Restoration Act (CWPPRA) of 1990

has provided up to \$50 million per year in the United States, but it became apparent that larger-scale restoration efforts were needed (56). A more inclusive ecosystem restoration plan, “Coast 2050—Toward a Sustainable Coastal Louisiana,” was developed in 1998, which included a diverse amalgamation of projects of various sizes and purposes located throughout the coastal zone (57).

To further refine the Coast 2050 Plan, the U.S. Army Corps of Engineers undertook the Louisiana Coastal Area (LCA) Ecosystem Restoration Study (58). The LCA Study produced detailed quantitative analyses of various restoration features and of the cost and effectiveness of suites of various features in achieving ecosystem benefits, ranging in total cost from \$5 billion to 17 billion. The Office of Management and Budget directed the Corps to prepare a scaled-back LCA Plan that was submitted to Congress in January 2005 (38). It recommended authorization of five “near-term critical ecosystem restoration features,” a science and technology program, a demonstration program, beneficial use of dredged materials, and further investigations of other near-term restoration features, at a cost of nearly \$2 billion. The Assistant Secretary of the Army



requested programmatic authorization for elements totaling \$1.12 billion, which currently awaits passage of a Water Resources Development Act or some other statute.

A National Research Council review of the LCA Plan concluded: "although the individual projects in the study are scientifically sound, there should be more and larger scale projects that provide a comprehensive approach to addressing land loss over such a large area. More importantly, the study should be guided by a detailed map of the expected future landscape of coastal Louisiana that is developed from agreed upon goals for the region and the nation." (59, 60). Congress directed the Corps to develop a plan for closure of the MRGO to deep-draft navigation, and in December 2006 the Corps recommended that the channel be permanently blocked and not maintained even for shallow-draft navigation.

Before the hurricanes of 2005, planning and decision-making for delta restoration remained largely separate from that for storm protection and navigation (33). In LCA planning, restoration features were evaluated on the basis of ecosystem benefits and financial costs, so that the most cost-effective array of features could be identified. Benefits did not specifically include the value of storm damage reduction, and costs were only financial outlays by governments, even though the features might impose costs or yield benefits to current ecosystem users (such as fishers and oil and gas and navigation interests). These analytical limitations effectively isolated restoration plan formulation from other potential synergies or conflicts with flood protection, storm damage reduction, and navigation.

It has become clear not only to scientists and engineers (38) but also to a growing segment of the public and political leadership that sustaining a coastal landscape is necessary to ensure the habitability and economic enterprises of the MDP (61, 37). The implications of this new awareness are twofold: First, activities that could further diminish the coastal landscape have to be adjusted so that they are consistent with that sustainability; and second, ecosystem restoration efforts must now include storm damage reduction benefits as a major consideration in the overall restoration plan (38). In the aftermath of the 2005 hurricanes, the Louisiana Legislature created the Louisiana Coastal Protection and Restoration Authority and Congress directed the Corps to undertake the 2-year Louisiana Coastal Protection and Restoration Project (LACPR) in order to identify, describe, and propose a full range of flood control, coastal restoration, and hurricane protection measures for south Louisiana. At this point, the preliminary LACPR report and the preliminary draft State Master Plan (61) deal predominantly with hurricane protection barriers, including coastwise levees with floodgates that could diminish the sustainability of the coastal landscape. Much remains to be done to integrate hurricane pro-

tection and coastal ecosystem restoration in a compatible manner.

Nonetheless, the 2005 hurricanes have also given new impetus to more comprehensive and aggressive coastal ecosystem restoration approaches than those included in the 2005 LCA Plan proposed to Congress. These include larger-scale diversions, the long-distance conveyance of sediment slurries, and reengineering of the navigational access at the mouth of the Mississippi River so that more of the sediment load of the river is retained in the nearshore zone to contribute to constructive and sustaining delta processes. Furthermore, the damage wrought by the hurricanes has lessened some previous social obstacles to these more aggressive approaches by forcing relocation away from the coast, causing losses of resources and/or infrastructure, and lowering public tolerance for obstructions by narrow interests. All of this is evidence that there is a growing recognition that delta restoration and hurricane protection will demand a suite of activities that are much greater in scale and more profound than those considered barely a decade ago.

The Gulf of Mexico Energy Security Act, signed into law in December 2006, gives Louisiana and other Gulf Coast states 37% of the revenues from newly opened oil and gas tracts. Louisiana has constitutionally dedicated these revenues to coastal restoration and protection. Along with other anticipated revenue streams, this could provide approximately \$1 billion per year over 30 years for these purposes. Consequently, the state may have the resources to pursue coastal ecosystem restoration on a scale larger than any other U.S. region. This poses a major challenge to science and science-based planning to develop the most strategic and effective strategies, while minimizing the conflicts and maximizing the synergies in achieving multiple social objectives within a sustainable coastal landscape required for the future of the region. At the same time, the substantial uncertainties must be recognized, accepted, and incrementally reduced through adaptive management approaches that promote learning while executing and enhancing the effectiveness of future decisions—for this must truly be a long-term commitment. That will require substantial improvements in science, engineering, planning, and management capacity, operating with a sense of urgency and purpose.

The restoration of the MDP is important not only in its own right, but because it provides understanding needed to contend with the many other deteriorating delta systems around the world. Moreover, it serves as a model for adaptation to future climate change in coastal ecosystems more generally. Because of high rates of subsidence, the MDP presently has a rate of relative sea-level rise equivalent to that predicted for many coasts toward the end of this century. Human impacts have caused both substantial increases and decreases in freshwater inflow to

parts of the coast. And the area has one of the highest frequencies of tropical cyclone impacts in the world. The management approaches developed to restore and sustain the MDP in the face of present-day forces will undoubtedly influence future adaptation to climate change impacts elsewhere, especially during a period of resource scarcity. In addition, the experience in the MDP indicates that restoration on such large scales requires long time periods and complex stakeholder engagement.

#### References and Notes

- H. N. Fisk, E. McFarlan, C. Kolb, J. Wilbert, *J. Sed. Petrol.* **24**, 76 (1954).
- R. Saucier, *Geomorphology and Quaternary Geologic History of the Lower Mississippi Valley* (U.S. Army Corps of Engineers, Vicksburg, MS, 1994), vol. 1.
- H. H. Roberts, *J. Coastal Res.* **13**, 605 (1997).
- J. W. Day Jr., J. F. Martin, L. Cardoch, P. H. Templet, *Coastal Manage.* **25**, 115 (1997).
- J. Wells, J. Coleman, *Estuar. Coastal Shelf Sci.* **25**, 111 (1987).
- R. H. Kesel, *Environ. Geol. Water Sci.* **13**, 183 (1989).
- D. Cahoon, D. Reed, J. Day Jr., *Mar. Geol.* **128**, 1 (1995).
- I. A. Mendelsohn, J. T. Morris, in *Concepts and Controversies in Tidal Marsh Ecology*, M. P. Weinstein, D. A. Kreeger, Eds. (Kluwer Academic, Boston, 2000), pp. 59–80.
- R. D. DeLaune, S. R. Pezeshki, *Water Air Soil Pollut.* **3**, 167 (2003).
- R. H. Baumann, J. W. Day Jr., C. A. Miller, *Science* **224**, 1093 (1984).
- R. E. Turner, J. J. Boustian, E. M. Swenson, J. S. Spicer, *Science* **314**, 449 (2006).
- J. M. Coleman, H. H. Roberts, G. W. Stone, *J. Coastal Res.* **14**, 698 (1998).
- S. Penland, R. Boyd, J. Suter, *J. Sed. Petrol.* **58**, 932 (1988).
- L. Britsch, J. Dunbar, *J. Coastal Res.* **9**, 324 (1993).
- S. Gagliano, K. Meyer-Arendt, K. Wicker, *Trans. Gulf Coast. Assoc. Geol. Soc. Trans.* **31**, 295 (1981).
- L. Britsch, J. Dunbar, *J. Coastal Res.* **9**, 324 (1993).
- J. W. Day Jr. et al., *Estuaries* **23**, 425 (2000).
- J. A. Barras, P. E. Bourgeois, L. R. Handley, *Landloss in Coastal Louisiana: 1956-90* (Open File Report 94-01, National Biological Survey, National Wetlands Research Center, Lafayette, LA, 1994).
- D. F. Boesch et al., *J. Coastal Res.*, Special Issue **20** (1994).
- R. H. Day, R. K. Holz, J. W. Day Jr., *Environ. Manage.* **14**, 229 (1990).
- E. M. Swenson, R. E. Turner, *Estuar. Coastal Shelf Sci.* **24**, 599 (1987).
- R. A. Morton, N. A. Bster, M. D. Krohn, *Gulf Coast Assoc. Geol. Soc. Trans.* **52**, 767 (2002).
- W. Conner, J. Day, R. Baumann, J. Randall, *Wetlands Ecol. Manage.* **1**, 45 (1989).
- Interagency Performance Evaluation Task Force, *Performance Evaluation of the New Orleans and Southeast Louisiana Hurricane Protection System* (MMTF 00038-06, U.S. Army Corps of Engineers, Vicksburg, MS, 2006).
- National Wetlands Research Center, U.S. Geological Survey ([www.nwrc.usgs.gov/hurricane/katrina.htm](http://www.nwrc.usgs.gov/hurricane/katrina.htm)).
- F. Danielsen et al., *Science* **310**, 643 (2005).
- J. K. Lovelace, *Storm-tide Elevations Produced by Hurricane Andrew along the Louisiana Coast, August 25-27, 1992* (Open File Report 94-371, U.S. Geological Survey, Baton Rouge, LA, 1994).
- E. M. Swenson, *Hurricane Andrew: the Inundation of the Louisiana Coastal Marshes* (Department of Natural Resources contract no. 256081-95-02, report to the Louisiana Department of Natural Resources, Baton Rouge, LA, 1994).
- U. S. Army Corps of Engineers, *Hurricane Study for Morgan City, Louisiana and Vicinity, New Orleans District* (U.S. Army Corps of Engineers, New Orleans, LA, 1963).



30. R. O. Reid, R. E. Whitaker, J. Waterway, *J. Waterw. Harbors Coastal Eng. Div. Am. Soc. Civ. Eng.* **WW1**, 61 (1976).
31. M. R. Raupach, A. S. Thom, *Annu. Rev. Fluid Mech.* **13**, 97 (1981).
32. E. W. Koch, G. Gust, *Mar. Ecol. Prog. Ser.* **184**, 63 (1999).
33. R. G. Dean, C. J. Bender, *Coastal Eng.* **53**, 149 (2006).
34. H. S. Mashriqui *et al.*, in *Coastal Hydrology and Water Quality: Proceedings of the AIH 25th Anniversary Meeting and International Conference*, Y. J. Xu, V. J. Singh, Eds. (American Institute of Hydrology, Baton Rouge, LA, 2006), pp. 481–489.
35. W. J. Mitsch, S. E. Jørgensen, Eds, *Ecological Engineering and Ecosystem Restoration* (Wiley, New York, 2003).
36. S. Laska, *Nat. Haz. Observer* **31**, 2 (2006).
37. R. Costanza, W. J. Mitsch, J. W. Day Jr., *Front. Ecol. Environ.* **4**, 465 (2006).
38. D. Boesch *et al.*, *A New Framework for Planning the Future of Coastal Louisiana after the Hurricanes of 2005* (Univ. of Maryland Center for Environmental Science, Cambridge, MD, 2006).
39. I. A. Mendelsohn, N. L. Kuhn, *Ecol. Eng.* **21**, 115 (2003).
40. I. A. Mendelsohn, M. W. Hester, F. J. Monteferrante, *J. Coastal Res.* **7**, 137 (1991).
41. G. W. Stone, R. A. McBride, *J. Coastal Res.* **14**, 900 (1998).
42. R. E. Turner, B. Streever, *Approaches to Coastal Wetland Restoration: Northern Gulf of Mexico* (SPB Academic Publishing, The Hague, Netherlands, 2002).
43. R. M. J. Boumans, J. W. Day Jr., G. P. Kemp, K. Kilgen, *Ecol. Eng.* **9**, 37 (1997).
44. R. Gramling, R. Hagelman, *J. Coastal Res.* **S144**, 112 (2005).
45. N. N. Rabalais *et al.*, *Estuaries* **17**, 850 (1994).
46. W. Mitsch *et al.*, *Bioscience* **51**, 373 (2001).
47. C. Hall, P. Tharakan, J. Hallock, C. Cleveland, M. Jefferson, *Nature* **426**, 318 (2003).
48. J. Day *et al.*, *Biotechnol. Adv.* **22**, 135 (2003).
49. W. Mitsch, J. Day, *Ecol. Eng.* **26**, 55 (2006).
50. J. Day *et al.*, *Ecol. Eng.* **24**, 253 (2005).
51. Intergovernmental Panel on Climate Change, *Climate Change 2001: The Scientific Basis, Contribution of Working Group I to the Third Assessment Report* (Cambridge Univ. Press, Cambridge, 2001).
52. P. J. Webster, G. J. Holland, J. A. Curry, H.-R. Chang, *Science* **309**, 1844 (2005).
53. K. Emanuel, *Nature* **436**, 686 (2005).
54. C. D. Hoyos, P. A. Agudelo, P. J. Webster, J. A. Curry, *Science* **312**, 94 (2006).
55. K. S. Deffeyes, *Hubbert's Peak: The Impending World Oil Shortage* (Princeton Univ. Press, Princeton, NJ, 2001).
56. Coastal Wetlands Planning, Protection, and Restoration Act, *A Response to Louisiana's Land Loss* (2006) ([www.lacoast.gov/reports/program/program.asp?r=16809](http://www.lacoast.gov/reports/program/program.asp?r=16809)).
57. Louisiana Wetlands Conservation and Restoration Task Force, *Coast 2050: Toward a Sustainable Coastal Louisiana* (1998) ([www.lca.gov/net\\_prod\\_download/public/lca\\_net\\_pub\\_products/doc/2050report.pdf](http://www.lca.gov/net_prod_download/public/lca_net_pub_products/doc/2050report.pdf)).
58. U. S. Army Corps of Engineers, *Louisiana Coastal Area, Louisiana Ecosystem Restoration Study* (2004) ([http://data.lca.gov/lvan6/main/main\\_report\\_all.pdf](http://data.lca.gov/lvan6/main/main_report_all.pdf)).
59. National Research Council, *Drawing Louisiana's New Map: Addressing Land Loss in Coastal Louisiana* (National Academies Press, Washington, DC, 2005).
60. Although the National Research Council report (59) called for a detailed map of expected coastal restoration projects, there is no single agreed-on map of the coastal restoration plan. Rather, a series of maps and plans have been produced over the past 10 to 15 years that depict the evolution of thinking about restoration. The reader is directed to several reports and Web sites describing the evolving coastal restoration effort. These include the CWPPRA programs (56), the Coast 2050 program (57), the LCA project (58), and the Louisiana Comprehensive Coastal Protection Master Plan for Louisiana (62). Two plans have been released for closure of the Mississippi River Gulf Outlet: one by the U.S. Army Corps of Engineers (63) and a second by a group of scientists and environmental groups (64). A group of forested wetland ecologists documented the loss of coastal forested wetlands and discussed management options to sustain these forests (65). Costanza *et al.* (37) provided a series of principles to guide efforts for hurricane protection and delta restoration.
61. S. Laska *et al.*, *J. Coastal Res. Spec. Iss.* **44**, 90 (2005).
62. Coastal Protection and Restoration Authority, *Comprehensive Coastal Protection Master Plan for Louisiana* (2006) ([www.louisianacoastalplanning.org/documents/Comprehensive%20Coastal%20Protection%20Master%20Plan%20for%20Louisiana%20-%20Preliminary%20Draft.pdf](http://www.louisianacoastalplanning.org/documents/Comprehensive%20Coastal%20Protection%20Master%20Plan%20for%20Louisiana%20-%20Preliminary%20Draft.pdf)).
63. U. S. Army Corps of Engineers *Mississippi River Gulf Outlet Deep-Draft De-Authorization* (Interim Report to Congress, 2006) ([www.mvn.usace.army.mil/pao/RELEASES/MRGO\\_Report\\_Congress\\_061214\\_Final.pdf](http://www.mvn.usace.army.mil/pao/RELEASES/MRGO_Report_Congress_061214_Final.pdf)).
64. Lake Pontchartrain Basin Foundation, *Unified Deauthorization Plan Report* (2006) ([www.saveourlake.org/wetlands.htm](http://www.saveourlake.org/wetlands.htm)).
65. Coastal Wetland Forests Conservation and Use Science Working Group, *Conservation, Protection and Utilization of Louisiana's Coastal Wetland Forests* (Final Report to the Governor of Louisiana, 2005) ([www.coastalforestswg.lsu.edu/SWG\\_FinalReport.pdf](http://www.coastalforestswg.lsu.edu/SWG_FinalReport.pdf)).
66. C. R. Kolb, J. R. Van Lopik, in M. L. Shirley, Ed., *Deltas in Their Geological Framework*, M. L. Shirley, Ed. (Houston Geological Society, Houston, TX, 1966), pp. 16–61 and fig. 2.
67. ADCIRC: Advanced Circulation Hydrodynamic Model, U.S. Army Corps of Engineers, Vicksburg, MS.
68. This work resulted from the authors' participation on the National Technical Review Committee as part of the LCA Project (58) and/or the Working Group for Post-Hurricane Planning for the Louisiana Coast (38). We thank C. Izdepski for help in the preparation of the manuscript and the reviewers for comments.

10.1126/science.1137030



# Gene Co-Inheritance and Gene Transfer

Yaniv Brandvain,\* Michael S. Barker, Michael J. Wade

The functional transfer of mitochondrial genes to the nucleus is an enigmatic feature of eukaryotic genome evolution (1). In angiosperms, functional gene transfer is characterized by periods of stasis punctuated with bursts of transfer activity, a large variance in the number of transfers among lineages, and a high frequency of recent and a dearth of ancient transfers (2, 3). Despite extensive documentation of mitonuclear gene transfer in angiosperms, there is no well-supported explanation for this “unfathomable” variation (3). To understand the variation in mitochondrial gene translocation (3) and the evolutionary forces affecting genomic transfer, we examined the association between number of functional mitonuclear gene transfer events and angiosperm reproductive mode.

When a gene moves from the mitochondria to the nucleus, its environment changes from a primarily nonrecombining, haploid, uniparentally inherited mitochondrial genome to a recombining, biparentally inherited nuclear genome. Thus, the evolutionary advantages of recombination may drive mitonuclear gene transfer, because recombination allows mitochondrial genes to escape degradation by Muller's ratchet, the irreversible accumulation of deleterious mutations, or increases the rate of spread of advantageous mutations (4). If either of these selective forces drives mitonuclear gene transfer, more gene transfer should be observed in outcrossing taxa because they experience more effective recombination than selfing or clonal taxa.

Although selfing and clonal reproduction diminish recombination, they increase  $\theta_{MN}$ , the probability that mitonuclear gene pairs in the same individual are inherited together and thus are simultaneously identical by descent. High  $\theta_{MN}$  conserves mitonuclear gene combinations (5) across generations as well as nuclear gene combinations, increasing the effectiveness of selection on mitonuclear and nuclear-nuclear epistasis (6).

The opportunity for functional gene transfer

begins with the incorporation of a mitochondrial gene into a nuclear genome. The transferred gene must then acquire sequences conferring nuclear expression and sequences targeting the gene product to the mitochondrion (1). Lastly, the mitochondrial copy must be silenced or lost from the population while the nuclear copy is retained. Throughout this complex process, high  $\theta_{MN}$  preserves functional gene combinations, whereas reproduction with low  $\theta_{MN}$  breaks apart gene combinations, potentially uniting two nonfunctional complements.

If the process of gene transfer involves coadaptation of mitonuclear gene combinations, heritability of these combinations is necessary for a response to selection. Because adaptive function after transfer requires simultaneous genetic changes in both genomes, it is probable that co-inheritance is also essential to successful functional gene transfer (5). A positive association between co-inheritance and transfer numbers would provide support for this hypothesis.

Alternatively, mitonuclear transfer could be a neutral process, guided by random genetic drift, or an adaptive process, guided by genes with additive effects on fitness regardless of mating system. Neither of these hypotheses makes any prediction concerning the relationship between  $\theta_{MN}$  and the number of transfer events.

We tested these competing hypotheses by examining the relationship between independent mitochondrial gene losses [documented in (2)] and ancestral  $\theta_{MN}$  (ranked as high, intermediate, or low) across 170 angiosperm genera [see Sup-

porting Online Material (SOM) text for criteria, categorization, justification, and reference of each  $\theta_{MN}$ ]. Adams *et al.* (2) inferred loss of essential mitochondrial genes by Southern blots but did not confirm transfer between the mitochondria and nucleus. Sequenced plant mitochondrial genomes show that most inferred losses represent true losses and that functional copies of lost mitochondrial genes are usually found in the nucleus (1, 2), with exceptions removed from our analysis (detailed in SOM text). Similarly, our inference of ancestral reproductive mode is imperfect (SOM text), and thus greater resolution of the timing of gene transfer would facilitate better inference of ancestral  $\theta_{MN}$ , providing a stronger test of our hypothesis.

We found a strong, positive association between  $\theta_{MN}$  and the number of functional gene transfer events (Spearman's  $\rho = 0.233$ , two-tailed  $P = 0.002$ , Fig. 1), consistent with the prediction that gene co-inheritance facilitates functional gene transfer and opposite to predictions that suggest these advantages are due to recombination (4). The range of variation in the number of transfer events and the value of  $\theta_{MN}$  within clades (fig. S1) rules out the possibility that this result is due to a phylogenetic coincidence. Furthermore, a positive association between  $\theta_{MN}$  and gene transfer is consistent with the observed phylogenetic distribution of many recent but few ancient transfers; if selfing and clonal reproduction represent a “dead end” (7), gene transfer in these high  $\theta_{MN}$  groups is followed by their extinction.

Evidence that chloroplast-to-nuclear gene transfers, movement of nuclear genes among chromosomes, or movement of genes between hosts and vertically transmitted endosymbionts are associated with higher  $\theta$  would further support our hypothesis. Overall, these findings and predictions demonstrate that the heritability of gene combinations provides a predictive framework for the evolution of genome architecture.

## References and Notes

1. K. L. Adams, J. D. Palmer, *Mol. Phylogenet. Evol.* **29**, 380 (2003).
2. K. L. Adams, Y. L. Qiu, M. Stouthamer, J. D. Palmer, *Proc. Natl. Acad. Sci. U.S.A.* **99**, 9905 (2002).
3. J. D. Palmer *et al.*, *Proc. Natl. Acad. Sci. U.S.A.* **97**, 6960 (2000).
4. J. L. Blanchard, M. Lynch, *Trends Genet.* **16**, 315 (2000).
5. M. J. Wade, C. J. Goodnight, *Evolution* **60**, 643 (2006).
6. I. Eshel, M. W. Feldman, *Theor. Popul. Biol.* **1**, 88 (1970).
7. G. L. Stebbins, *Am. Nat.* **91**, 337 (1957).
8. Supported by an NSF predoctoral fellowship to Y.B., an NIH training grant to M.S.B., and NIH grant R01GM65414 to M.J.W. Comments from D. McCauley, M. Hahn, L. Delph, J. Palmer, T. Platt, N. Kane, A. Richardson, C. Hertlhy, and members of our lab group improved this manuscript.

## Supporting Online Material

www.sciencemag.org/cgi/content/full/315/5819/1685/DC1

SOM Text

Fig. S1

References

6 September 2006; accepted 20 December 2006

10.1126/science.1134789

Department of Biology, Indiana University, Bloomington, IN 47405, USA.

\*To whom correspondence should be addressed. E-mail: ybrandva@indiana.edu

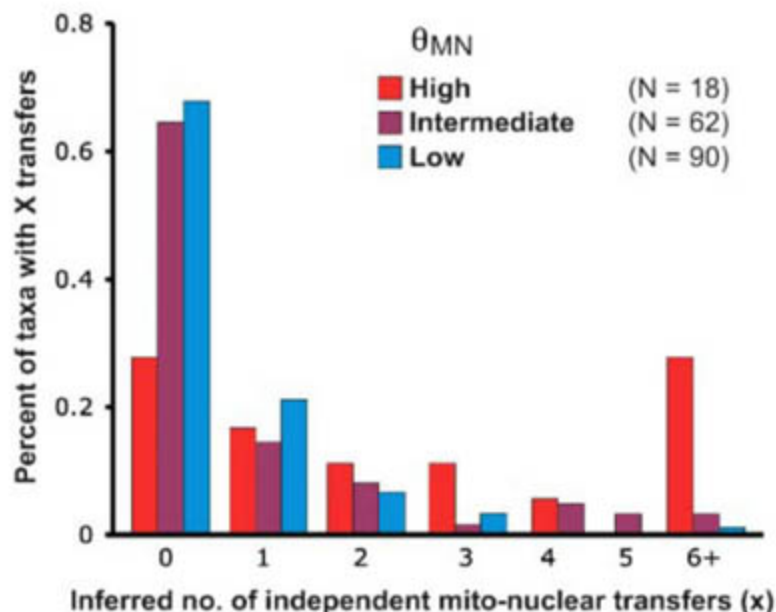


Fig. 1. Distribution of inferred number of gene transfers by  $\theta_{MN}$ .



# Far-Field Optical Hyperlens Magnifying Sub-Diffraction-Limited Objects

Zhaowei Liu,\* Hyesog Lee,\* Yi Xiong, Cheng Sun, Xiang Zhang†

The diffraction limit of light, which is caused by the loss of evanescent waves in the far field that carry high spatial frequency information, limits the resolution of optical lenses to the order of the wavelength of light used to image the object. Projecting a sub-diffraction-limited image into the far field would require recovery of the evanescent waves. A metamaterials-based superlens offers that possibility (1). Although slablike superlenses have demonstrated sub-diffraction-limited resolution (1–4) imaging in the near field, magnification of subwavelength features into the far field has not been possible. It was proposed that a magnifying superlens could be constructed by using cylindrical metamaterials (5, 6).

Recent theoretical studies on an optical hyperlens and a metamaterial crystal superlens have proposed the use of an anisotropic medium with a hyperbolic dispersion such that ordinary evanescent waves propagate along the radial direction of the layered metamaterial (7–9). Microscopically, the large spatial frequency waves propagate through coupled surface plasmon excitations between the metallic layers (10, 11).

We demonstrate a magnifying optical hyperlens consisting of a curved periodic stack of Ag (35 nm) and Al<sub>2</sub>O<sub>3</sub> (35 nm) deposited on a half-cylindrical cavity fabricated on a quartz substrate (Fig. 1A). Sub-diffraction-limited objects were inscribed into a 50-nm-thick chrome

layer located at the inner surface (air side).

The anisotropic metamaterial was designed so that the radial and tangential permittivities have different signs. Upon illumination, the scattered evanescent field from the object enters the anisotropic medium and propagates along the radial direction. Because of the conservation of angular momentum, the tangential wave vectors are progressively compressed as the waves travel outward, resulting in a magnified image at the outer boundary of the hyperlens (7). Once the magnified feature is larger than the diffraction limit, it can then be imaged with a conventional optical microscope. We calculated the electromagnetic field in a metamaterials hyperlens by using the actual metal loss (Fig. 1A).

In our experiment, the object imaged with the hyperlens was a pair of 35-nm-wide lines spaced 150 nm apart (Fig. 1B). The magnified image (350-nm spacing) can be clearly

resolved with an optical microscope [numerical aperture (NA) = 1.4], thus demonstrating magnification and projection of a sub-diffraction-limited image into the far field. In a control experiment, the line pair object was imaged without the hyperlens. The line pair could not be resolved because of the diffraction limit ( $\lambda/NA = 260$  nm) (Fig. 1, B and C). Because the hyperlens supports the propagation of a very broad spectrum of wave vectors, it can magnify arbitrary objects with sub-diffraction-limited resolution. The recorded image of the letters “ON” shows the fine features of the object (Fig. 1D). The subdiffraction resolution of 130 nm was achieved (fig. S1). Although this work deals with the cylindrical hyperlens, it should be possible to design a spherical hyperlens that can magnify in three dimensions. Unlike near-field optical microscopy that uses a tip to scan the object, our optical hyperlens magnifies a sub-diffraction-limited image and projects it into the far field.

This experiment demonstrates the capability of a hyperlens for sub-diffraction-limited imaging. The hyperlens magnifies the object by transforming the scattered evanescent waves into propagating waves in the anisotropic medium, projecting a high-resolution image into the far field. The optical hyperlens opens up exciting possibilities in applications, such as real-time biomolecular imaging and nanolithography.

## References and Notes

1. J. B. Pendry, *Phys. Rev. Lett.* **85**, 3966 (2000).
2. N. Fang, H. Lee, C. Sun, X. Zhang, *Science* **308**, 534 (2005).
3. T. Taubner, D. Korobkin, Y. Urzhumov, G. Shvets, R. Hillenbrand, *Science* **313**, 1595 (2006).
4. D. O. S. Melville, R. J. Blaikie, *Opt. Express* **13**, 2127 (2005).
5. J. B. Pendry, S. A. Ramakrishna, *J. Phys. Condens. Matter* **14**, 8463 (2002).
6. J. B. Pendry, *Opt. Express* **11**, 755 (2003).
7. Z. Jacob, L. V. Alekseyev, E. Narimanov, *Opt. Express* **14**, 8247 (2006).
8. A. Salandrino, N. Engheta, *Phys. Rev. B* **74**, 075103 (2006).
9. A. A. Goyadzinov, V. A. Podolskiy, *Phys. Rev. B* **73**, 115108 (2006).
10. D. R. Smith, D. Schurig, *Phys. Rev. Lett.* **90**, 077405 (2003).
11. B. Wood, J. B. Pendry, D. P. Tsai, *Phys. Rev. B* **74**, 115116 (2006).
12. The authors thank E. Narimanov and Z. Jacob for fruitful discussions and sharing their theoretical hyperlens paper, which motivated this experiment. This work was supported by the Army Research Office Multidisciplinary University Research Initiative (MURI) program (grant no. 50432-PH-MUR), Air Force Office of Scientific Research MURI (grant no. FA9550-04-1-0434), and the NSF NSEC under award number DMI0327077.

## Supporting Online Material

www.sciencemag.org/cgi/content/full/315/5819/1686/DC1  
Materials and Methods

Fig. S1

9 November 2006; accepted 8 February 2007

10.1126/science.1137368

5130 Etcheverry Hall, NSF Nanoscale Science and Engineering Center (NSEC), University of California, Berkeley, CA 94720–1740, USA.

\*These authors contributed equally to this work.

†To whom correspondence should be addressed. E-mail: xiang@berkeley.edu

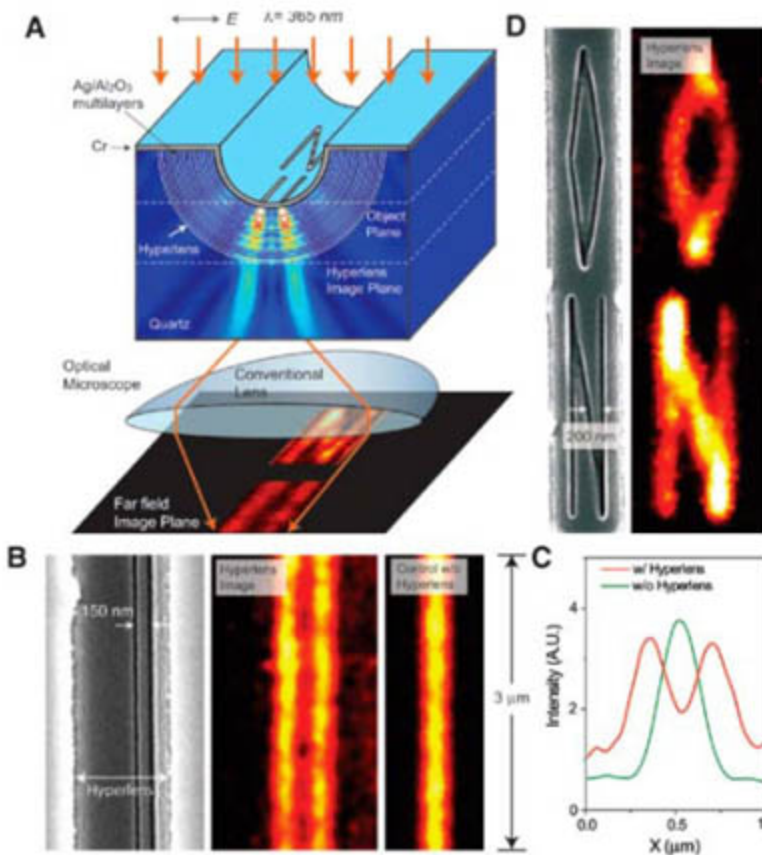


**Fig. 1.** Magnifying optical hyperlens. (A) Schematic of hyperlens and numerical simulation of imaging of sub-diffraction-limited objects. (B) Hyperlens imaging of line pair object with line width of 35 nm and spacing of 150 nm. From left to right, scanning electron microscope image of the line pair object fabricated near the inner side of the hyperlens, magnified hyperlens image showing that the 150-nm-spaced line pair object can be clearly resolved, and the resulting diffraction-limited image from a control experiment without the hyperlens. (C) The averaged cross section of hyperlens image of the line pair object with 150-nm spacing (red), whereas a diffraction-limited image obtained in the control experiment (green). A.U., arbitrary units. (D) An arbitrary object “ON” imaged with subdiffraction resolution. Line width of the object is about 40 nm. The hyperlens is made of 16 layers of Ag/Al<sub>2</sub>O<sub>3</sub>.



# Asymmetric T Lymphocyte Division in the Initiation of Adaptive Immune Responses

John T. Chang,<sup>1\*</sup> Vikram R. Palanivel,<sup>1\*</sup> Ichiko Kinjyo,<sup>1</sup> Felix Schambach,<sup>1</sup> Andrew M. Intlekofer,<sup>1</sup> Arnob Banerjee,<sup>1</sup> Sarah A. Longworth,<sup>1</sup> Kristine E. Vinup,<sup>1</sup> Paul Mrass,<sup>2</sup> Jane Oliaro,<sup>3</sup> Nigel Killeen,<sup>4</sup> Jordan S. Orange,<sup>5</sup> Sarah M. Russell,<sup>3,6</sup> Wolfgang Weninger,<sup>2</sup> Steven L. Reiner<sup>1†</sup>

A hallmark of mammalian immunity is the heterogeneity of cell fate that exists among pathogen-experienced lymphocytes. We show that a dividing T lymphocyte initially responding to a microbe exhibits unequal partitioning of proteins that mediate signaling, cell fate specification, and asymmetric cell division. Asymmetric segregation of determinants appears to be coordinated by prolonged interaction between the T cell and its antigen-presenting cell before division. Additionally, the first two daughter T cells displayed phenotypic and functional indicators of being differentially fated toward effector and memory lineages. These results suggest a mechanism by which a single lymphocyte can apportion diverse cell fates necessary for adaptive immunity.

The clonal selection theory of adaptive immunity suggests that proliferation of a single lymphocyte should provide sufficient function for acute defense (effector cells), as well as the regenerative capacity to maintain the selected lineage (memory cells). Throughout metazoan development and homeostasis, a conserved mechanism is used to confer disparate fates among daughter cells. This mechanism, known as asymmetric cell division, involves polarized alignment of determinants of cell fate perpendicular to the mitotic spindle, thus ensuring the unequal inheritance of critical molecules and divergence of daughter cell fates (1). Asymmetric cell division could thus represent a potential mechanism to ensure that appropriate diversity of cell fate arises from the clonal descendants of a single lymphocyte during an immune response.

T cell interaction with antigen-presenting cells is characterized by orientation of the actin and tubulin cytoskeleton and asymmetric segregation of signaling and adhesive proteins toward the site of intercellular contact (2). With sustained signaling to the T cell, intercellular conjugation can last for hours in vitro (3). Although the immunological synapse has not been fully resolved in vivo (4, 5), recent time-lapse imaging of lymphoid

tissue suggests that an activated T cell undergoes sustained interaction with antigen-bearing dendritic cells (DCs) during the interval preceding its first cell division (5–11).

If synapse-like polarity occurs during the prolonged contact with DCs that precedes the first T cell division, it is possible that asymmetry might ensue. Stable orientation of the original microtubule organizing center (MTOC) in a synapse-proximal position through the time of mitosis would result in the duplicate centrosome moving to the distal pole during prophase. If segregation of signaling components was also maintained during the interval of sustained contact, then their orientation at a pole of the mitotic spindle would fulfill the hallmarks of asymmetric division. Consequently, we explored the possibility that asymmetric cell division can initiate differentiation associated with the adaptive immune response of T cells.

**Segregation of immune receptors and ancestral polarity proteins in mitotic T cells.** Whether initial cytokinesis of naïve T cells occurs during contact with DCs, or after dissociation from DCs, has not been resolved (5, 8, 12, 13). We therefore tested the potential for asymmetric division by isolating T cells that appeared to be preparing for their first division in vivo and examining their subcellular characteristics ex vivo (14). Naïve mouse CD8<sup>+</sup> T cells transgenic for the P14 T cell receptor were labeled with carboxyfluorescein diacetate succinimidyl ester (CFSE) and adoptively transferred into wild-type recipients. These recipients had been infected 24 hours previously with intravenous recombinant *Listeria monocytogenes* bacteria expressing a specific antigenic gp33-41 peptide epitope (gp33-*L. monocytogenes*) (14). At 32 hours after transfer, undivided donor T cells (represented by the brightest CFSE peak)

were sorted by flow cytometry and examined by confocal microscopy. This approach ensured that we were examining T cells preparing for their first division.

Undivided (parental) T cells were stained with antibodies against  $\beta$ -tubulin and various T cell signaling proteins and readily identified as activated blasts by their increased cell size (fig. S1). Most of the blasts contained a single MTOC, indicating that they were activated, but premitotic, cells (Fig. 1A, far left). In more than 90% of such cells, the centrosome colocalized with a polarized patch containing leukocyte function-associated antigen-1 (LFA-1), CD8, and CD3 (Fig. 1A, far left). This polarity was not a direct result of the adoptive-transfer process, because transferred naïve T cells that had not been exposed to antigen exhibited diffuse staining of the same receptors (fig. S2). In contrast to the polarity exhibited by components known to participate in immunological synapse formation, the localization of CD90, a nonsynaptic transmembrane receptor, was found to be diffuse in T cells from infected recipients (Fig. 1A).

Although much less frequent than the premitotic blasts, mitotic cells (those in prophase through anaphase) could be identified by the presence of two oppositely facing MTOCs (Fig. 1A). Like their premitotic counterparts, these mitotic T cells exhibited pronounced polarized distribution of LFA-1, CD8, and CD3 (Fig. 1A). As with premitotic blasts, the synaptic components colocalized with one MTOC, which consequently represented one of the two poles of the mitotic spindle (Fig. 1A). The initial cell divisions we observed in this experimental setting of CD8<sup>+</sup> T cell responses were, therefore, characterized by partitioning of signaling proteins perpendicular to the mitotic spindle, a morphology reminiscent of asymmetric cell division.

We next examined if asymmetric T cell division could also be detected in CD4<sup>+</sup> helper T cell responses. *Leishmania*-specific T cell receptor (TCR) transgenic CD4<sup>+</sup> T cells were labeled with CFSE and adoptively transferred into wild-type recipients that had been infected 24 hours earlier with *L. major* (14). At 32 hours after the transfer, undivided blasts were examined for the localization of LFA-1, CD4, and the receptor for interferon- $\gamma$  (IFN $\gamma$ R), which polarizes to the immunological synapse during activation of CD4<sup>+</sup> T cells in vitro (15). All three receptors colocalized with the MTOC of premitotic blasts and remained asymmetrically partitioned in mitotic CD4<sup>+</sup> T cells in vivo (Fig. 1C). Asymmetric segregation of signaling molecules may, thus, be a feature of both major T cell subsets undergoing the first division during an immune response.

On the basis of their suggested role during T cell migration and activation in vitro (16), we next examined the localization of ancestral regulators of asymmetric cell division, protein kinase C- $\zeta$  (PKC $\zeta$ ) and Scribble, in CD8<sup>+</sup> T cells preparing for division. PKC $\zeta$  is a mamma-

<sup>1</sup>Abramson Family Cancer Research Institute and Department of Medicine, University of Pennsylvania, Philadelphia, PA 19104, USA. <sup>2</sup>Immunology Program, The Wistar Institute, Philadelphia, PA 19104, USA. <sup>3</sup>Immune Signalling Laboratory, Peter MacCallum Cancer Centre, East Melbourne, Victoria 2002, Australia. <sup>4</sup>Department of Microbiology and Immunology, University of California, San Francisco, CA 94143, USA. <sup>5</sup>Department of Pediatrics, University of Pennsylvania, Philadelphia, PA 19104, USA. <sup>6</sup>Center for MicroPhotonics, Faculty of Engineering and Industrial Sciences, Swinburne University of Technology, Victoria 3122, Australia.

\*These authors contributed equally to this work.

†To whom correspondence should be addressed. E-mail: sreiner@mail.med.upenn.edu



lian homolog of atypical PKC, a component of an essential cell polarity complex containing Par-3 and Par-6 (1, 17). Scribble is a signature component of another key polarity complex that is often positioned opposite the atypical PKC-containing complex (17). In premitotic T cell blasts, PKC $\zeta$  was observed to localize opposite the MTOC and persisted into mitosis at this asymmetric position at the putative distal pole (Figs. 1A and 2). In contrast, Scribble colocalized with the MTOC at the putative synaptic pole of premitotic blasts (fig. S3), and this, too, persisted into mitosis (Fig. 2). Thus, an ancestral polarity network appeared to be established before mitosis and persisted into M phase with characteristic orientation at opposite poles of the mitotic spindle.

**Sustained synapsis required for asymmetry during mitosis.** To determine whether the asymmetry we observed in the initial mitotic T cell

was related to its sustained contact with pathogen-associated DC before division, we examined two alternative stimuli eliciting cell division in vivo. In the first, transgenic T cells were transferred into lymphopenic RAG1-deficient recipients to initiate cell division in the absence of pathogen. This form of division is called acute homeostatic proliferation and does not depend on specific recognition of foreign antigen by T cells, but instead is initiated in response to self-antigen in an environment devoid of other lymphocytes (18). In the second model, a foreign microbial stimulus was used, but in recipients lacking intercellular adhesion molecule 1 (ICAM1) and so unable to support LFA-1-dependent interactions between T cells and DCs (19). This mutation was chosen because such integrin-cadherin interactions have been shown to be critical for organizing asymmetric cell division in mammalian skin (20) and because DCs lacking ICAM1

do not support the sustained intervals of T cell contact that characterize productive immune responses (21).

In both the uninfected lymphopenic mice and the infected ICAM1-deficient recipients, vigorous cell division of the transferred T cell population was supported (Fig. 3C, fig. S4). There was, however, a substantial loss of asymmetry in mitotic T cells retrieved from the mutant mice, with diffuse distribution of synaptic and polarity proteins and no apparent orientation of these proteins to the mitotic spindle (Fig. 1, A and B). These findings suggest that events during the prolonged contact between T cell and DC preceding the first T cell division, rather than general mitogenic signaling, are required to establish asymmetry.

**Asymmetric inheritance of fate determinants in the first daughter cells.** To determine if asymmetric segregation of synaptic proteins

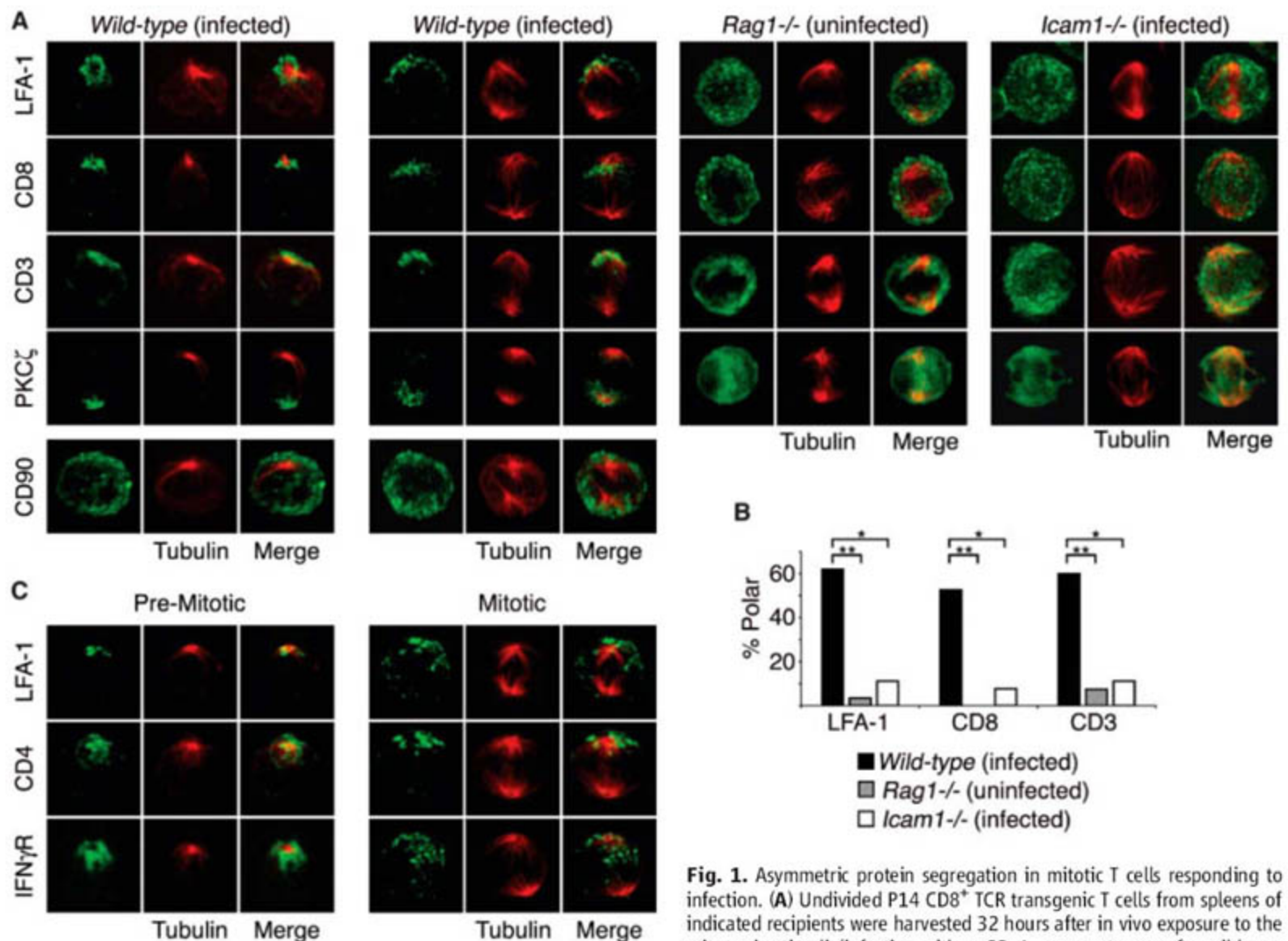


**Fig. 1.** Asymmetric protein segregation in mitotic T cells responding to infection. (A) Undivided P14 CD8<sup>+</sup> TCR transgenic T cells from spleens of indicated recipients were harvested 32 hours after in vivo exposure to the mitogenic stimuli (infection with gp33-*L. monocytogenes* for wild-type and *Icam1*<sup>-/-</sup> mice; lymphopenia for *Rag1*<sup>-/-</sup> mice) and examined by confocal microscopy after staining for  $\beta$ -tubulin (red) and LFA-1, CD3, CD8, PKC $\zeta$ , or CD90 (green). Panels are representative of nine or more mitotic cells per group. Far left panels are premitotic blasts from infected wild-type recipients (large cell, but single MTOC); all remaining panels are mitotic cells (dual, oppositely facing MTOCs). (B) Quantification of polarized receptors on mitotic CD8<sup>+</sup> T cells represented in (A). The number of mitotic cells examined for each receptor (per group of wild-type, *Rag1*<sup>-/-</sup>, and *Icam1*<sup>-/-</sup> mice, respectively) was as follows: LFA-1 (21, 30, 9); CD8 (19, 27, 13); CD3 (15, 27, 9). \* $P \leq 0.025$ ; \*\* $P \leq 0.001$ . (C) Undivided donor *Leishmania*-specific CD4<sup>+</sup> TCR transgenic T cells from infected wild-type recipients were harvested from draining lymph nodes after 32 hours and stained with antibodies against  $\beta$ -tubulin (red) and LFA-1, CD4, or IFN $\gamma$ R (green). Polarity of LFA-1, CD4, and IFN $\gamma$ R was observed in 60% ( $n = 15$ ), 78% ( $n = 9$ ), and 71% ( $n = 14$ ) of mitotic cells, respectively.



persists through mitosis, we examined cells undergoing cytokinesis. Sorted, undivided T cells that had already responded to various *in vivo* stimuli were cultured in media containing cytochalasin B, to inhibit actin polymerization, before imaging (14). This resulted in the arrest of cytokinesis in parent T cells attempting to divide, yielding conjoined twin daughter sets. Costaining of CD8 and PKC $\zeta$  revealed unequal protein inheritance in daughter T cells subsequent to the *in vivo* immune response (Fig. 3A). CD8 and PKC $\zeta$  consistently segregated to opposite daughters, in accord with the synapse-distal localization of PKC $\zeta$  in premitotic and mitotic blasts. In contrast, cells undergoing acute homeostatic proliferation, representing non-antigen-driven cell division, displayed uniform inheritance of CD8 and PKC $\zeta$  to both daughters (Fig. 3A). Similar results were obtained from cytokinetic cells examined directly *ex vivo* that were not cultured in cytochalasin B (fig. S5).

The asymmetric segregation of CD8 between conjoined twin daughter cells suggested that it might be possible to measure flow cytometric evidence for this receptor disparity in nascent daughter populations. In infected wild-type recipients, bimodal distribution of CD8 and LFA-1 staining was evident in bulk populations of daughter T cells (Fig. 3B). In contrast, daughter T cells that had emerged from homeostatic proliferation exhibited a unimodal distribution of co-receptor staining (Fig. 3C). The bimodal staining evident in the first T cell division of the immune response may, thus, have represented proximal and distal daughter populations, with a greater and lesser abundance of synaptic receptors, respectively. However, why the putative distal daughter was not observed to proliferate substantially beyond the first division (Fig. 3, B and C) is not evident and remains to be explored.

To ascertain whether signaling pathways involved in cell fate might be asymmetrically partitioned in CD8<sup>+</sup> T cells, we examined IFN $\gamma$ R in cells responding to gp33-*L. monocytogenes*. Consistent with its proximal location in blasts (fig. S6), preferential inheritance of IFN $\gamma$ R was observed in the putative proximal daughter of conjoined twin sets, based on its segregation away from the putative distal daughter, which inherits the greater portion of PKC $\zeta$  (Fig. 4). Early in the immune response, the ligand for IFN $\gamma$ R might be secreted by CD8<sup>+</sup> T cells themselves (fig. S6), neighboring natural killer cells, or DCs (22). In activated CD8<sup>+</sup> T cells, IFN- $\gamma$  signaling induces the key transcription factor, T-bet (fig. S7), which is preferentially expressed in effector cells compared to the memory lineage (23, 24). It is thus conceivable that differences in IFN- $\gamma$  signaling could directly or indirectly influence fate-associated gene expression in the first daughter T cells during an immune response.

Unequal inheritance of Numb, an inhibitor of Notch signaling, is another ancestral hallmark of asymmetric cell division (1). In conjoined twin cells, we observed preferential inheritance of Numb in the proximal daughter, based on its cosegregation to daughters that inherited greater CD8 (Fig. 4). Inheritance of Numb by proximal daughters was consistent with its reported localization at the immunological synapse *in vitro* (25). Disparity in Notch signaling could contribute to initial fate divergence, because Notch ligands have been found to be induced on pathogen-stimulated DCs (26). Like the asymmetric inheritance seen for IFN $\gamma$ R, that of Numb appeared specific to daughter cells responding to infection, because only symmetric segregation of these proteins was detected in the conjoined twin sets arising from acute homeostatic division (Fig. 4). Segregation of critical compo-

nents of two fate-determining signaling pathways thus provides a possible mechanism for asymmetric T cell division to generate intracloonal diversity during the immune response.

**Asymmetric division yielding effector- and memory-fated progeny.** Consistent with the predicted role for asymmetric cell division in specifying different daughter fates, we observed a pronounced disparity in phenotypic markers of effector and memory cells between the putative proximal and distal daughters, respectively. The putative proximal daughters (possessing more abundant CD8) were larger in size, had increased granularity, and expressed low levels of CD62L but higher levels of CD69, CD43, CD25, and CD44 (Fig. 5A, fig. S8), a profile consistent with the effector lineage (27). In contrast, distal daughters (those with less abundant CD8) had a profile more consistent with the central memory lineage (27); these cells were smaller, less granular, and expressed high levels of CD62L but lower levels of CD69, CD43, CD25, and CD44 (Fig. 5A, fig. S8). We also observed coordinate functional disparity in proximal and distal daughters. Proximal daughters exhibited greater expression of the effector gene products, IFN- $\gamma$  and Granzyme B (Fig. 5B), whereas distal daughters exhibited greater expression of interleukin-7 receptor  $\alpha$  (IL-7R $\alpha$ ) mRNA (Fig. 5C), a marker of early memory precursors (28).

A prediction of these observations is that the effector-fated daughters will terminally differentiate, without substantial regenerative capacity. In contrast, memory-fated daughters would retain long-term developmental plasticity to both self-renew and terminally differentiate, consistent with the recognized features of memory T cells (29). Consequently, both effector and memory precursors should be capable of protection against an acute challenge, whereas delayed challenge should be better controlled by the memory-like precursors (28). To test this prediction, we sorted putative proximal and distal daughters from primary recipients and transferred them to a new set of naïve secondary recipients that were challenged immediately or at 30 days after transfer with gp33-*L. monocytogenes* to assess protection (14). At 30 days after transfer, distal daughters were indeed found to provide measurably better protection than was found with proximal daughter T cells (Fig. 5D). However, proximal daughters provided equal or better protection than their distal counterparts when challenged immediately after transfer (Fig. 5D). The functional properties of the first two daughters were thus consistent with our assignment as effector and memory precursors on the basis of phenotypic and functional markers.

**Discussion.** The function of the immunological synapse, as it has been studied *in vitro*, has remained enigmatic (30). The emerging recognition that the parent T cell and DC undergo prolonged contact *in vivo* relatively late after initial activation (5–11) prompted us to consider the possibility of a previously unknown function

**Fig. 2.** Bipolar segregation of conserved regulators of asymmetric cell division during mitosis. Cells from infected wild-type recipients were harvested as in Fig. 1A and stained for CD3 (green),  $\beta$ -tubulin (blue), and LFA-1, PKC $\zeta$ , or Scribble (red). Colocalization of CD3 with LFA-1 and Scribble was observed in 94% ( $n = 16$ ) and 100% ( $n = 10$ ) of cells, respectively. PKC $\zeta$  was polarized opposite CD3 in 90% ( $n = 10$ ) of cells.

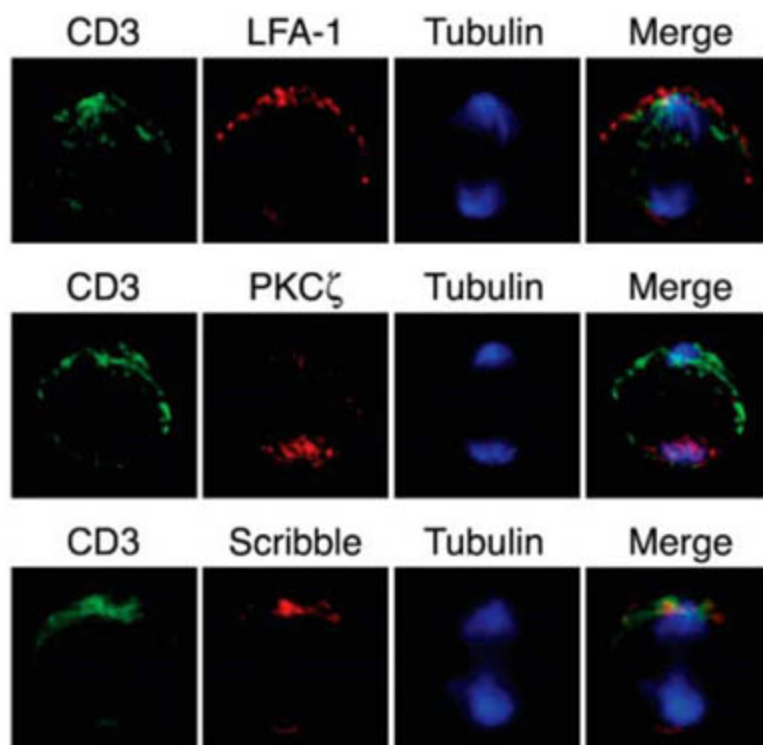




**Fig. 3.** Disparity in synaptic and polarity protein inheritance of daughter CD8<sup>+</sup> T cells. (A) Undivided P14 transgenic CD8<sup>+</sup> T cells from infected wild-type or uninfected *Rag1*<sup>-/-</sup> recipients were cultured in media containing cytochalasin B for 4 hours at 37°C to arrest cytokinesis. Cells were then stained for CD8 (green), PKC $\zeta$  (red),  $\beta$ -tubulin (blue), and DNA (grayscale). Cells undergoing cytokinesis were identified by pronounced cytoplasmic cleft by brightfield and dual nuclei and were scored for asymmetric segregation of staining between conjoined daughter cells. Merges of CD8 with PKC $\zeta$  were superimposed onto both the tubulin and brightfield images (fourth and seventh columns, respectively). Asymmetric segregation of CD8 in wild-type versus *Rag1*<sup>-/-</sup> mice occurred in 69% ( $n = 29$ ) versus 14% ( $n = 35$ ) of twin sets, respectively. The percent asymmetric segregation of PKC $\zeta$  was 62% ( $n = 34$ ) in wild-type and 14% ( $n = 29$ ) in *Rag1*<sup>-/-</sup> mice. For both molecules, the incidence of asymmetry was significantly greater in cells from wild-type compared to *Rag1*<sup>-/-</sup> mice ( $P \leq 0.001$ ). In costaining experiments where both molecules asymmetrically partitioned, CD8 and PKC $\zeta$  segregated to opposite daughters in 100% ( $n = 9$ ) of wild-type twin sets. (B) Differential abundance of synaptic proteins in the first daughter T cells responding to infection. CFSE-labeled transgenic CD8<sup>+</sup> T cells from infected wild-type recipients were analyzed by flow cytometry 48 hours after infection. Division, represented by CFSE dilution (x axis), and receptor abundance (y axis) of all transferred cells (left upper panel) and CD8<sup>+</sup>

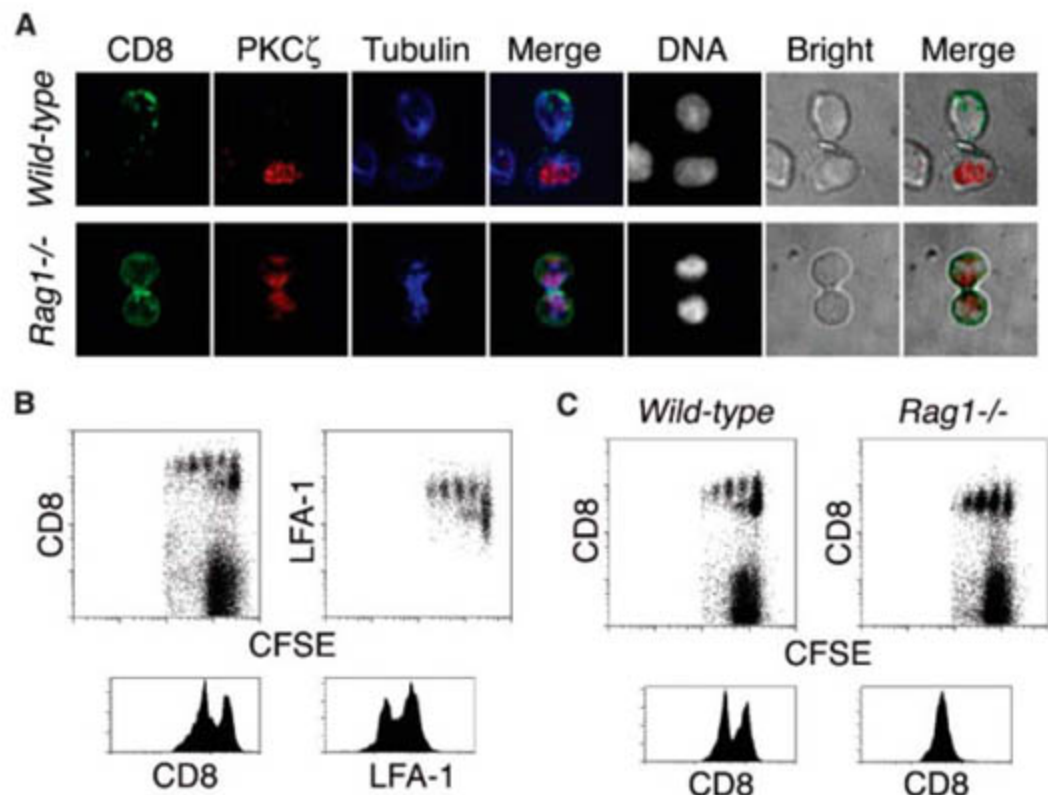
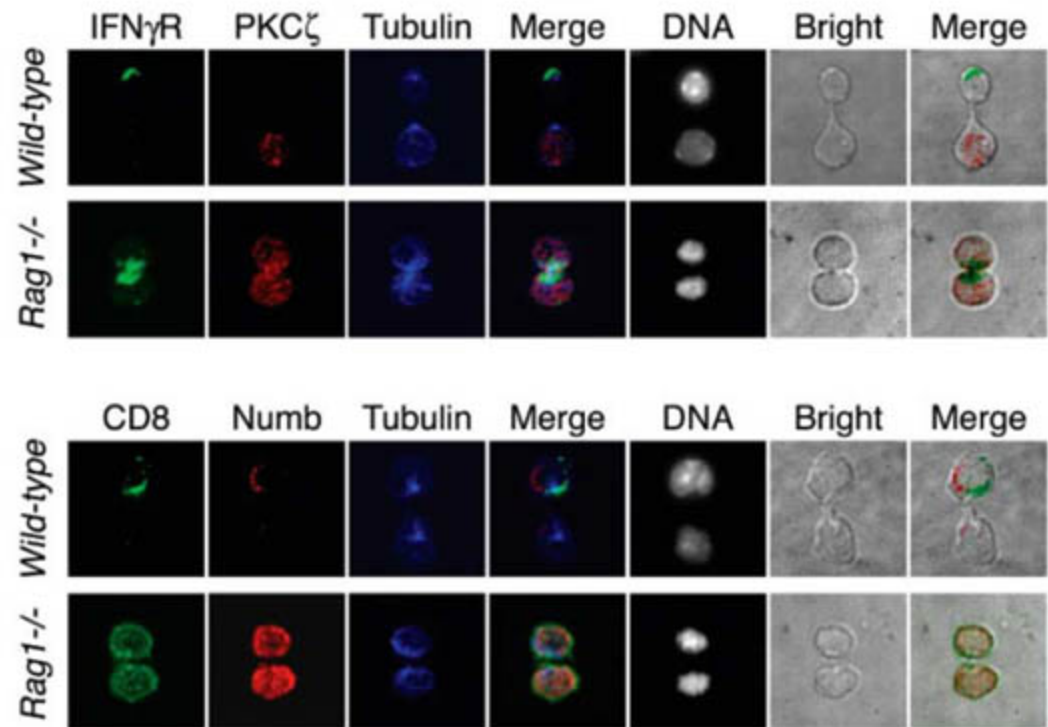


**Fig. 4.** Asymmetric inheritance of fate determinants in the first daughter T lymphocytes. Cells obtained and analyzed as in Fig. 3A were costained for IFN $\gamma$ R and PKC $\zeta$  (upper rows) or CD8 and Numb (lower rows), plus  $\beta$ -tubulin and DNA. Asymmetric segregation of IFN $\gamma$ R in wild-type versus *Rag1*<sup>-/-</sup> mice occurred in 77% ( $n = 13$ ) versus 7% ( $n = 14$ ) of twin sets, respectively. The percent asymmetric segregation of Numb was 67% ( $n = 18$ ) in wild-type and 13% ( $n = 15$ ) in *Rag1*<sup>-/-</sup> mice. For both IFN $\gamma$ R and Numb, the incidence of asymmetry was significantly greater in cells from wild-type compared to *Rag1*<sup>-/-</sup> mice ( $P \leq 0.001$ ). In costaining experiments where both molecules asymmetrically partitioned, IFN $\gamma$ R and PKC $\zeta$  segregated to opposite daughters in 100% ( $n = 5$ ) of wild-type twin sets, while CD8 and Numb segregated to the same daughter in 100% ( $n = 8$ ) of wild-type twin sets.

transferred cells (right upper panel) are shown. Receptor abundance (x axis) of electronically gated daughter cells (second brightest CFSE peak only) is displayed below. (C) Comparison of CD8 abundance in daughter cells arising after infection (left) versus acute homeostatic division (right).



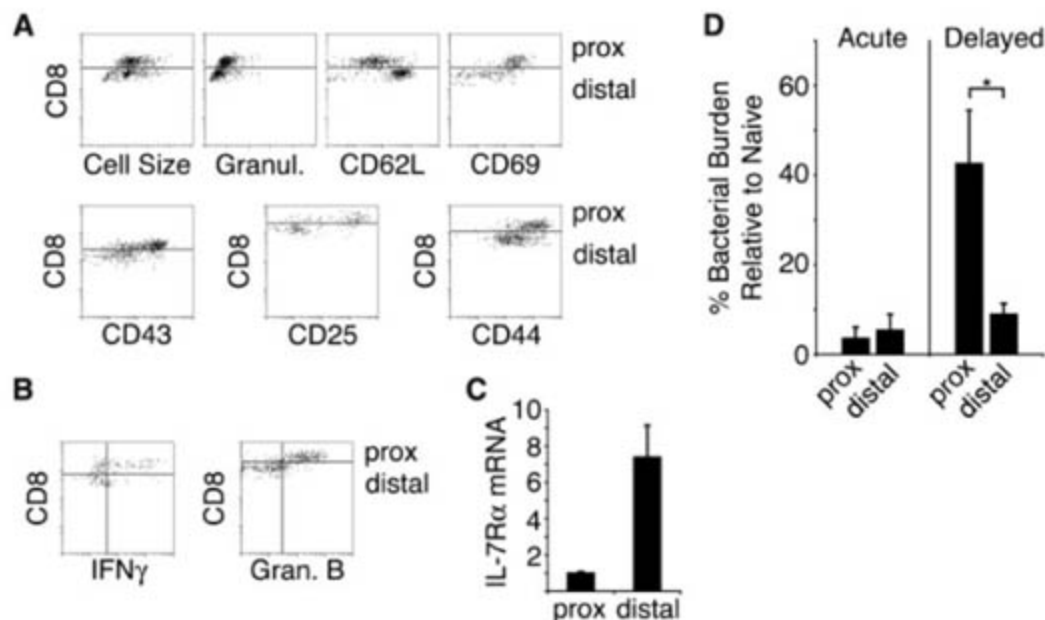
for the synapse; namely, that it helps coordinate asymmetric cell division. At its simplest level, a mechanism for asymmetric cell division might provide a solution to an essential problem facing adaptive immunity. If an immune response were to begin from the activation and proliferation of a single antigen-specific naïve T cell, simultaneous assignment of effector and memory properties to two different daughters would ensure acute elimination of the microbe, while preserving

the useful clone through a memory lineage in the event that all effector cells die. After resolution of infection, the slow, cytokine-driven proliferation of memory T cells might then involve symmetric divisions to maintain stable numbers of similarly fated daughter cells. This might be akin to the symmetric homeostatic division we observed for naïve T cells transferred to antigen-free, lymphopenic mice. Upon secondary exposure to the pathogen, antigen-presenting DCs might

then coordinate another episode of asymmetry in the memory T cell, leading to a terminally differentiated effector lineage, as well as a self-renewing memory lineage. Such a model is consistent with the stem cell-like features that have been proposed for memory T cells (29, 31) and is one that we are currently investigating by examining the morphology and phenotype of memory T cells and their daughters in the response to a secondary challenge. Whether the



**Fig. 5.** Daughter CD8<sup>+</sup> T cells acquiring disparate fates during immunity. **(A)** CFSE-labeled CD8<sup>+</sup> T cells were analyzed as in Fig. 3, B and C, with antibodies against CD8 and one of the following molecules: CD62L, CD69, CD43, CD25, or CD44. Phenotypic markers of effector and memory cells (x axis) and CD8 abundance (y axis) of electronically gated daughter cells (second brightest CFSE peak only) are shown. Cell size represents forward light scatter; granularity represents side light scatter. Fluorescence intensity of surface receptor staining is listed in fig. S8. **(B)** Cells were analyzed as in (A), with antibodies to detect intracellular IFN- $\gamma$  or Granzyme B. **(C)** IL-7R $\alpha$  mRNA was measured by means of real-time reverse transcription–polymerase chain reaction from sorted proximal and distal daughters. **(D)** Sorted proximal and distal daughters were transferred into new naïve recipients. Untransferred control and recipient mice were challenged with *L. monocytogenes* either immediately (Acute) or 30 days (Delayed) after transfer. Four days after infection, quantitative bacterial burdens in spleens were determined. Mean bacterial burden of recipient mice (left to right,  $n = 3, 4, 4, 4$ ) is expressed as a percentage relative to the burden of untransferred control mice. All groups were significantly protected relative to untransferred controls ( $P \leq 0.006$ ). After delayed challenge, distal daughters afforded significantly better protection than proximal daughters ( $*P = 0.03$ ).



asymmetric daughters of naïve T cells are actually fated to become specialized subsets other than effector and memory cells, moreover, cannot be excluded at this time.

Although the progeny of a newly activated CD8<sup>+</sup> T cell may be capable of dividing and differentiating without further exposure to antigen (32, 33), it has been suggested that efficient CD4<sup>+</sup> T cell responses may require continued exposure to antigen by the initial daughter cells (12, 34), raising the possibility that more than one round of asymmetric division might occur. Reiterative rounds of asymmetry during the initial clonal expansion of a CD4<sup>+</sup> T cell might, thus, facilitate the diversification of effector choices [T helper cell 1 (T<sub>H</sub>1), T<sub>H</sub>2, and T<sub>H</sub>17] in addition to, or instead of, simply generating effector and memory progeny. In this way, the spectrum of CD4<sup>+</sup> T cell effector fates, which arise only after cell division (35), might all be represented in the initial clonal burst. Thereafter, only the most useful of the diverse progeny might undergo further selection, on the basis of the type of pathogen encountered. Indeed, the determinants that are segregated in the initial CD8<sup>+</sup> T cell division are also presumptive regulators of CD4<sup>+</sup> T<sub>H</sub>1–T<sub>H</sub>2 lineage choice (15, 26, 36–39). With ever-improving methodology for in vivo imaging and lineage tracing, it may soon be possible to construct a detailed fate map of a single T cell clonal burst during a variety of immune challenges. For now, however, the role of asymmetric cell division in diversifying CD4<sup>+</sup> T cell fate remains to be formally evaluated.

Although information from the environment is essential in choice of cell fate, the facultative milieu of a migrating cell has often made it difficult to identify the most critical signals. It is tempting to speculate that the prolonged interlude with the antigen-presenting cell, which seemingly coordinates the asymmetry of T cell division,

might be mirrored in the behavior of other dividing lymphocytes and in the interactions of metastatic cancer cells with the cellular or extracellular components of their provisional niche. There remain numerous avenues to formally test the prevalence and importance of asymmetric cell division in adaptive immunity and in mammalian development and homeostasis. Extensions of the framework presented here might, thus, expand the principle of asymmetric cell division to various stages of B and T lymphocyte immunity, or provide insight into the elusive circumstances preceding asymmetric division of hematopoietic and neoplastic stem cells (40, 41).

#### References and Notes

- J. Betschinger, J. A. Knoblich, *Curr. Biol.* **14**, R674 (2004).
- C. R. Munks, B. A. Freiberg, H. Kupfer, N. Sciaky, A. Kupfer, *Nature* **395**, 82 (1998).
- J. B. Huppa, M. Gleimer, C. Sumen, M. M. Davis, *Nat. Immunol.* **4**, 749 (2003).
- P. Reichert, R. L. Reinhardt, E. Ingulli, M. K. Jenkins, *J. Immunol.* **166**, 4278 (2001).
- S. Stoll, J. Delon, T. M. Brotz, R. N. Germain, *Science* **296**, 1873 (2002).
- M. J. Miller, S. H. Wei, I. Parker, M. D. Cahalan, *Science* **296**, 1869 (2002).
- P. Bousso, E. Robey, *Nat. Immunol.* **4**, 579 (2003).
- T. R. Mempel, S. E. Henrickson, U. H. Von Andrian, *Nature* **427**, 154 (2004).
- S. Hugues *et al.*, *Nat. Immunol.* **5**, 1235 (2004).
- M. J. Miller, O. Safrina, I. Parker, M. D. Cahalan, *J. Exp. Med.* **200**, 847 (2004).
- G. Shakhbar *et al.*, *Nat. Immunol.* **6**, 707 (2005).
- S. Celli, Z. Garcia, P. Bousso, *J. Exp. Med.* **202**, 1271 (2005).
- M. Hommel, B. Kyewski, *J. Exp. Med.* **197**, 269 (2003).
- Materials and methods are available as supporting material on Science Online.
- R. A. Maldonado, D. J. Irvine, R. Schreiber, L. H. Glimcher, *Nature* **431**, 527 (2004).
- M. J. Ludford-Menting *et al.*, *Immunity* **22**, 737 (2005).
- A. Suzuki, S. Ohno, *J. Cell Sci.* **119**, 979 (2006).
- A. W. Goldrath, M. J. Bevan, *Immunity* **11**, 183 (1999).
- M. L. Dustin, T. A. Springer, *Nature* **341**, 619 (1989).
- T. Lechler, E. Fuchs, *Nature* **437**, 275 (2005).
- S. Amigorena, personal communication.
- D. M. Frucht *et al.*, *Trends Immunol.* **22**, 556 (2001).
- A. M. Intlekofer *et al.*, *Nat. Immunol.* **6**, 1236 (2005).
- N. Takemoto, A. M. Intlekofer, J. T. Northrup, E. J. Wherry, S. L. Reiner, *J. Immunol.* **177**, 7515 (2006).
- A. C. Anderson *et al.*, *J. Immunol.* **174**, 890 (2005).
- D. Amsen *et al.*, *Cell* **117**, 515 (2004).
- N. Manjunath *et al.*, *J. Clin. Invest.* **108**, 871 (2001).
- S. M. Kaech *et al.*, *Nat. Immunol.* **4**, 1191 (2003).
- D. T. Fearon, P. Manders, S. D. Wagner, *Science* **293**, 248 (2001).
- J. Lin, M. J. Miller, A. S. Shaw, *J. Cell Biol.* **170**, 177 (2005).
- C. J. Luckey *et al.*, *Proc. Natl. Acad. Sci. U.S.A.* **103**, 3304 (2006).
- S. M. Kaech, R. Ahmed, *Nat. Immunol.* **2**, 415 (2001).
- M. J. van Stipdonk, E. E. Lemmens, S. P. Schoenberger, *Nat. Immunol.* **2**, 423 (2001).
- R. Obst, H. M. van Santen, D. Mathis, C. Benoist, *J. Exp. Med.* **201**, 1555 (2005).
- J. J. Bird *et al.*, *Immunity* **9**, 229 (1998).
- M. Afkarian *et al.*, *Nat. Immunol.* **3**, 549 (2002).
- A. A. Lighvani *et al.*, *Proc. Natl. Acad. Sci. U.S.A.* **98**, 15137 (2001).
- P. Martin *et al.*, *Proc. Natl. Acad. Sci. U.S.A.* **102**, 9866 (2005).
- L. Tu *et al.*, *J. Exp. Med.* **202**, 1037 (2005).
- S. J. Morrison, J. Kimble, *Nature* **441**, 1068 (2006).
- J. C. Wang, J. E. Dick, *Trends Cell Biol.* **15**, 494 (2005).
- We thank M. Birnbaum and E. Williamson for the generous use of and assistance with the confocal microscope; and N. Takemoto, J. Northrup, A. Pasam, K. Pham, L. Ng, S. Daxini, and J. Laverty for assistance and discussion. Supported by NIH grants AI042370, AI053827, and AI061699 and the Abramson Family (S.L.R.); NIH grants CA114114 and AI069380 (W.W.); NIH training grants DK007066 (J.T.C.), AI055428 and GM007170 (V.R.P.), AI007532 (A.M.I.), and CA87812 (A.B.); and the Peter MacCallum Cancer Centre, National Health and Medical Research Council, and Australian Research Council (S.M.R.).

#### Supporting Online Material

www.sciencemag.org/cgi/content/full/1139393/DC1

Materials and Methods

Figs. S1 to S8

References

28 December 2006; accepted 8 February 2007  
Published online 1 March 2007;  
10.1126/science.1139393  
Include this information when citing this paper.



# Enhanced Bonding of Gold Nanoparticles on Oxidized TiO<sub>2</sub>(110)

D. Matthey, J. G. Wang, S. Wendt, J. Matthiesen, R. Schaub, E. Lægsgaard, B. Hammer, F. Besenbacher\*

We studied the nucleation of gold clusters on TiO<sub>2</sub>(110) surfaces in three different oxidation states by high-resolution scanning tunneling microscopy. The three TiO<sub>2</sub>(110) supports chosen were (i) reduced (having bridging oxygen vacancies), (ii) hydrated (having bridging hydroxyl groups), and (iii) oxidized (having oxygen adatoms). At room temperature, gold nanoclusters nucleate homogeneously on the terraces of the reduced and oxidized supports, whereas on the hydrated TiO<sub>2</sub>(110) surface, clusters form preferentially at the step edges. From interplay with density functional theory calculations, we identified two different gold-TiO<sub>2</sub>(110) adhesion mechanisms for the reduced and oxidized supports. The adhesion of gold clusters is strongest on the oxidized support, and the implications of this finding for catalytic applications are discussed.

The discovery of distinctive catalytic properties of dispersed gold nanoparticles on oxide supports (1, 2) has stimulated extensive research activities (2–5), and a general consensus now exists on several aspects of this system. The size of the gold particles substantially affects the catalytic activity, and the gold clusters must be smaller than 5 nm for high catalytic activity to occur (6–8). The choice of the oxide support influences the catalytic activity, so there is a strong “support effect” in addition to the “size effect” (2, 4, 9), and reducible oxides are advantageous as compared to nonreducible ones (9, 10). However, the relation of the adhesion properties of nano-sized gold with catalytic activity is still unresolved. A number of studies (mainly catalysis work done on high area support materials) have reported that slightly oxidized gold (Au<sup>+δ</sup>), in addition to metallic gold (Au<sup>0</sup>), is important to achieve high activity of dispersed Au catalysts (2, 4, 11–16). In parallel, several surface science studies of model systems favored an interpretation where oxygen vacancies have been invoked as being responsible for the stabilization and activity of Au clusters on the support (17–20).

We studied the fundamental mechanisms of metal oxide–support adhesion by means of scanning tunneling microscopy (STM) and density functional theory (DFT) calculations. We compare the nucleation of Au clusters on one support material that had been prepared in different oxidation states. We chose rutile TiO<sub>2</sub>(110) as the model support because numerous studies exist on the Au/TiO<sub>2</sub> model system, and Au/TiO<sub>2</sub> is a good catalyst for CO oxidation at low

temperatures, as shown in the pioneering studies by Haruta (1, 6), Goodman (7, 18), and the work of others (21–23).

The TiO<sub>2</sub>(110) surface consists of alternating rows of fivefold-coordinated Ti (5f-Ti) atoms and protruding, twofold-coordinated bridging oxygen (O<sub>br</sub>) atoms. The Ti atoms underneath the O<sub>br</sub> atoms are sixfold coordinated as any other Ti atom in stoichiometric rutile. An Ar<sup>+</sup> sputtered and vacuum-annealed TiO<sub>2</sub>(110) crystal is an n-type semiconductor, and its surface has a number of O<sub>br</sub> vacancies (5). The STM images of the TiO<sub>2</sub>(110) surface are dominated by electronic effects (i.e., bright rows correspond to the Ti troughs), whereas geometrically protruding O<sub>br</sub> atoms appear dark (5). Accordingly, the faint spots that connect the bright Ti troughs arise from O<sub>br</sub> vacancies (Fig. 1A) (24).

Starting with a clean, reduced TiO<sub>2</sub>(110) [*r*-TiO<sub>2</sub>(110)] surface, we prepared two further well-defined TiO<sub>2</sub>(110) surfaces under ultrahigh vacuum conditions (24, 25). First, we produced a hydrated TiO<sub>2</sub>(110) [*h*-TiO<sub>2</sub>(110)] surface with H adatoms, capping some of the O<sub>br</sub> atoms by letting water dissociate in O<sub>br</sub> vacancies (Fig. 1B). The capping H atoms form bridging hydroxyls (OH<sub>br</sub>) that appear as brighter protrusions

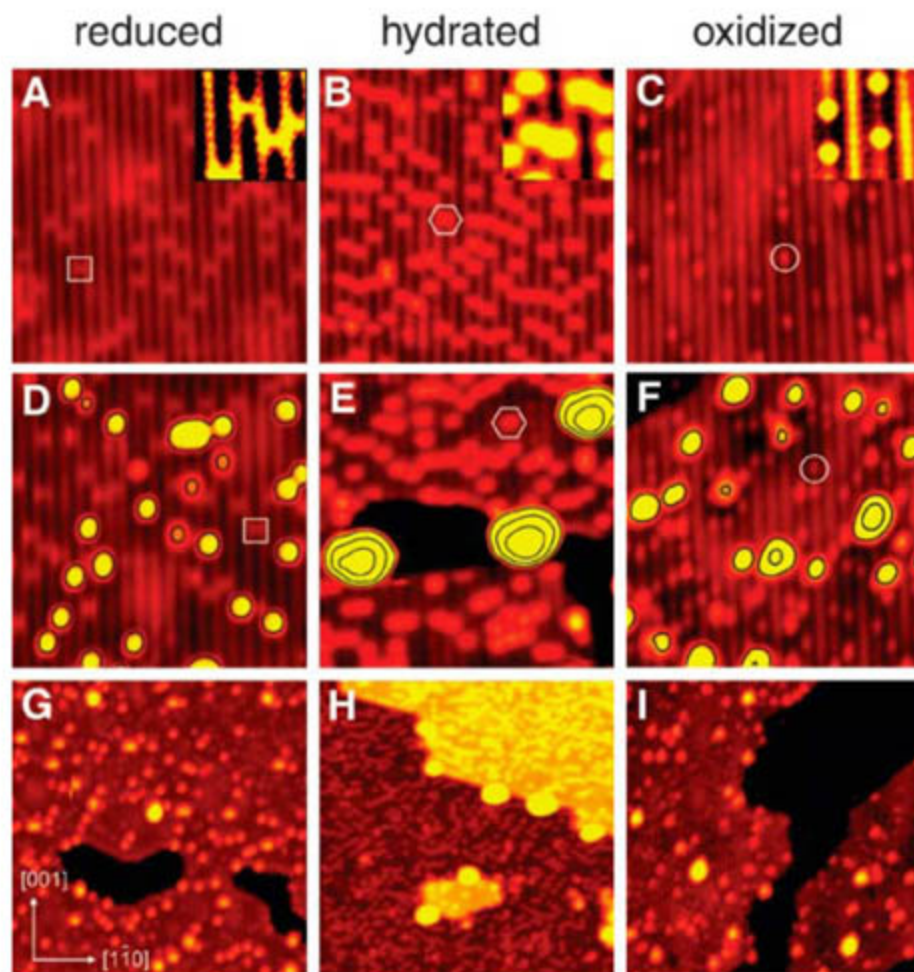


**Fig. 1.** STM images of *r*- (A), *h*- (B), and *o*- (C) TiO<sub>2</sub>(110) surfaces before Au exposure (130 × 130 Å<sup>2</sup>). Symbols indicate O<sub>br</sub> vacancies (square), H adatoms on O<sub>br</sub> sites (hexagon), and O<sub>ot</sub> atoms in the Ti troughs (circle). Insets (30 × 30 Å<sup>2</sup>) show the point defects of interest enlarged. For the detailed preparation recipes, see (25). (D to I) STM images after 3% ML Au exposure at RT [1 ML is defined as 1.387 × 10<sup>15</sup> atoms per cm<sup>2</sup> corresponding to Au(111)]. Image sizes are 130 × 130 Å<sup>2</sup> [(D) to (F)] and 350 × 350 Å<sup>2</sup> [(G) to (I)], respectively. In [(D) to (F)], the heights of the Au clusters are given by contour lines at 1.2, 3.2, and 5.2 Å above the terrace. Directions are as indicated in (G), and tunnel parameters (tunneling current *I*<sub>t</sub> ≤ 0.1 nA, tunneling voltage *V*<sub>t</sub> = 1.2 V) are identical throughout the paper.

Interdisciplinary Nanoscience Center (iNANO) and Department of Physics and Astronomy, University of Aarhus, DK-8000 Aarhus C, Denmark.

\*To whom correspondence should be addressed. E-mail: fbe@inano.dk



sions between the Ti rows than those associated with the  $O_{br}$  vacancies (24, 26). Second, we prepared an oxidized  $TiO_2(110)$  [ $o$ - $TiO_2(110)$ ] surface by letting  $O_2$  dissociate in  $O_{br}$  vacancies (24, 27), resulting in an  $o$ - $TiO_2(110)$  surface characterized by perfect  $O_{br}$  rows and by a number of O adatoms ( $O_{ot}$ ) located in the Ti troughs (Fig. 1C). These  $O_{ot}$  atoms show up in the STM images as protrusions distributed along the Ti troughs and are located on top of 5f-Ti sites (24, 26).

After exposing these three different  $TiO_2(110)$  surfaces to Au [3% of a monolayer (ML)] at room temperature (RT), we observed quite different Au cluster morphologies. In case of the  $r$ - $TiO_2(110)$  surface, numerous rather small Au clusters are distributed homogeneously on the terraces (Fig. 1, D and G). In contrast, on the  $h$ - $TiO_2(110)$  surface, we found fairly large Au clusters that preferentially decorate the step edges of the substrate, and no small Au clusters on the terraces are seen (Fig. 1, E and H).

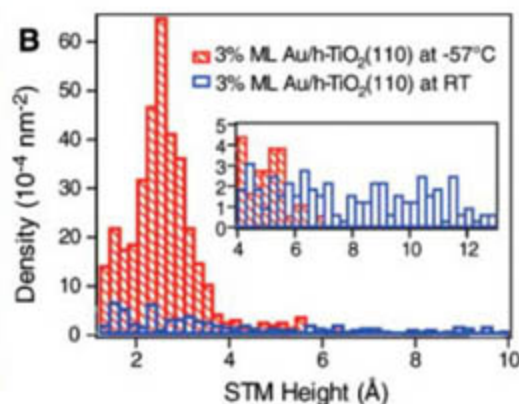
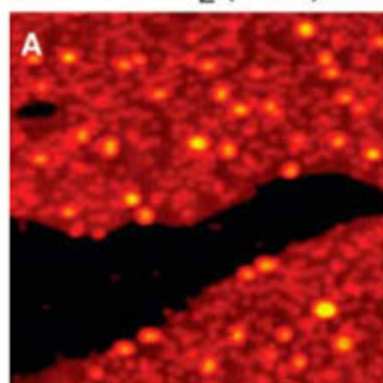
However, on the  $o$ - $TiO_2(110)$  surface, we again found Au clusters to nucleate homogeneously on the terraces (Fig. 1, F and I).

The absence of homogeneously distributed small Au nanoclusters on the  $h$ - $TiO_2(110)$  surface implies that monomeric Au ( $Au_1$ ) and small Au nanoclusters diffuse readily at RT on this surface. This finding is in agreement with previous RT-STM studies addressing Au/ $TiO_2(110)$  (7, 17, 28, 29), where sintering of incoming  $Au_1$  has been reported. In the present work, we found homogeneously distributed small Au clusters also on the terraces of the  $h$ - $TiO_2(110)$  surface when we cooled the substrate down to  $-57^\circ\text{C}$  before exposure (Fig. 2, A and B). According to these results, we infer that the interaction between Au clusters and the  $h$ - $TiO_2(110)$  surface is fairly weak (30). On the contrary, both for the  $r$ - $TiO_2(110)$  surface (with  $O_{br}$  vacancies) and the  $o$ - $TiO_2(110)$  surface (with  $O_{ot}$  atoms), the results presented in Fig. 1 imply that, on these two  $TiO_2(110)$  surfaces, stronger Au- $TiO_2$  interactions occur than on the  $h$ - $TiO_2(110)$  surface.

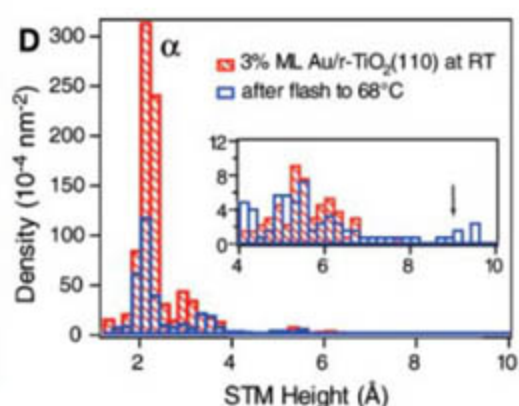
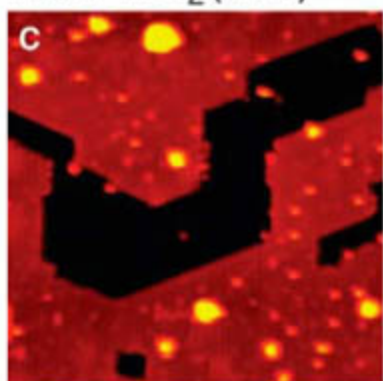
Given the stronger interactions with the  $r$ - and the  $o$ - $TiO_2(110)$  surfaces, we explored the effect of heating on the Au cluster morphologies on these two  $TiO_2$  surfaces (Fig. 2, C to F). Starting points in these experiments were  $r$ - and  $o$ - $TiO_2(110)$  surfaces that we exposed to 3% ML Au at RT (Fig. 1, D and G and Fig. 1, F and I, respectively). After subsequent heating of the samples to  $68^\circ\text{C}$ , Au sintering is clearly evident for  $Au/r$ - $TiO_2(110)$  (Fig. 2C) but not for  $Au/o$ - $TiO_2(110)$  (Fig. 2E). The different stabilities of the Au clusters against sintering on the two  $TiO_2(110)$  surfaces considered are even more obvious when looking at the corresponding Au height histograms (Fig. 2, D and F). For reference, we also show the height histograms obtained on the Au exposed surfaces before heating (hatched red bars). After the heating of the  $Au/r$ - $TiO_2(110)$  surface (blue bars in Fig. 2D), the sharp feature at Au cluster heights of 1.8 to 2.6 Å (labeled "α") is almost three times less intense than before. Because the "α" peak corresponds to  $Au_1$  trapped in  $O_{br}$  vacancies (see below), this result indicates that about two-thirds of the  $Au_1$  clusters have coalesced with other  $Au_n$  clusters. The sintering of  $Au_1/Au_n$  clusters on the  $r$ - $TiO_2(110)$  surface leads to the formation of large  $Au_n$  clusters with STM heights up to 10 Å (Fig. 2D, inset). Nothing in the STM data points to the occurrence of a ripening mechanism. Instead, our data are consistent with coalescence of  $Au_n$  clusters as the prevailing sintering mechanism.

On the  $o$ - $TiO_2(110)$  surface, the Au height histograms (Fig. 2F) show pronounced peaks of identical intensities at STM heights between 1.2 and 3.4 Å (labeled "a") both before and after heating of the sample. The characteristic "a" peak found for the  $Au/o$ - $TiO_2(110)$  surface is less intense but broader than the narrow  $a$  peak typical for  $Au_1$  on the  $r$ - $TiO_2(110)$  surface. This result can be explained by the

### Au/ $h$ - $TiO_2(110)$



### Au/ $r$ - $TiO_2(110)$



### Au/ $o$ - $TiO_2(110)$

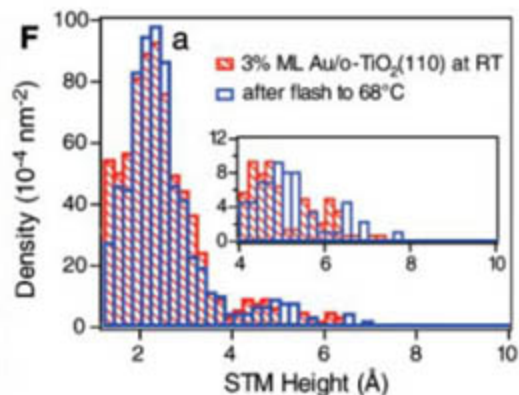
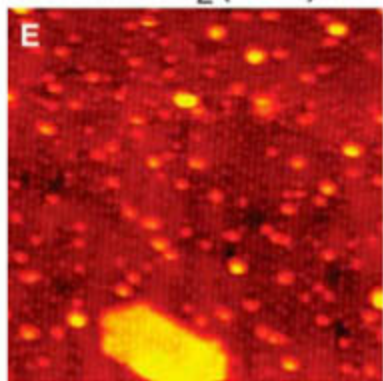


**Fig. 2.** (A) STM image of the  $h$ - $TiO_2(110)$  surface after 3% ML Au exposure at  $-57^\circ\text{C}$  ( $350 \times 350 \text{ \AA}^2$ ), and (B) Au height histograms corresponding to  $Au/h$ - $TiO_2(110)$  surfaces for substrate temperatures of  $-57^\circ\text{C}$  (hatched red bars) and RT (blue bars). The histograms rely on scanned areas of  $\sim 10^4 \text{ nm}^2$  each ( $\sim 1000$  Au clusters per histogram). A threshold of 1.2 Å above the terrace was chosen to ensure that exclusively Au clusters are considered for the histograms. (C) STM image of the  $Au/r$ - $TiO_2(110)$  surface ( $350 \times 350 \text{ \AA}^2$ ) prepared by 3% ML Au deposition at RT followed by heating up to  $68^\circ\text{C}$ . (D) Au height histograms corresponding to  $Au/r$ - $TiO_2(110)$  before (hatched red bars) and after (blue bars) heating of the sample. In (D), the peak indicated by "α" corresponds to  $Au_1$  trapped in  $O_{br}$  vacancies. The arrow in the inset indicates large  $Au_n$  clusters that are a result of sintering. (E and F) Like (C) and (D) but for the  $Au/o$ - $TiO_2(110)$  surface. In (F), the peak indicated by "a" corresponds to  $Au_n$  clusters of one layer height. No sintering was observed.



existence of many stable  $Au_n$  cluster configurations on the  $o$ - $TiO_2(110)$  surface, whereas only few stable  $Au_n$  cluster configurations seem to exist on the  $r$ - $TiO_2(110)$  surface. The clear dependence of the Au height distribution on  $r$ - $TiO_2(110)$  as opposed to the invariance of the distribution on  $o$ - $TiO_2(110)$  upon heating to 68°C reveals that the  $Au_n$  clusters bind more strongly to the O-rich oxide support.

To rationalize the obtained Au cluster distributions after Au exposure at RT, we compared the diffusion of  $Au_1$  on the three different  $TiO_2(110)$  surfaces of interest by means of DFT calculations (31). In some distance of the point defects, all three surfaces can be considered as being stoichiometric [ $s$ - $TiO_2(110)$ ]. In this case, the diffusion barriers are found to be very low (i.e.,  $Au_1$  readily diffuses at RT). Diffusion of  $Au_1$  on  $s$ - $TiO_2(110)$  is possible not only in the [001] direction but also in the [1 $\bar{1}$ 0] direction (Fig. 3A). Previous DFT calculations likewise indicate facile diffusion of small Au particles on stoichiometric oxide surfaces (20, 32–34).

For the  $h$ - $TiO_2(110)$  surface, we reached identical conclusions because the diffusion barriers are almost unchanged (Fig. 3B). However, the Au monomers can be trapped at point defects on the terraces of the  $r$ - and  $o$ - $TiO_2(110)$  surfaces (right side of Fig. 3, C and D, respectively). In these cases, the barriers are high enough to prevent diffusion events at RT. These calculations are fully in line with our STM observations of homogeneously distributed small Au nanoclusters exclusively on the  $r$ - and  $o$ - $TiO_2(110)$  surfaces and sintering of Au clusters on the

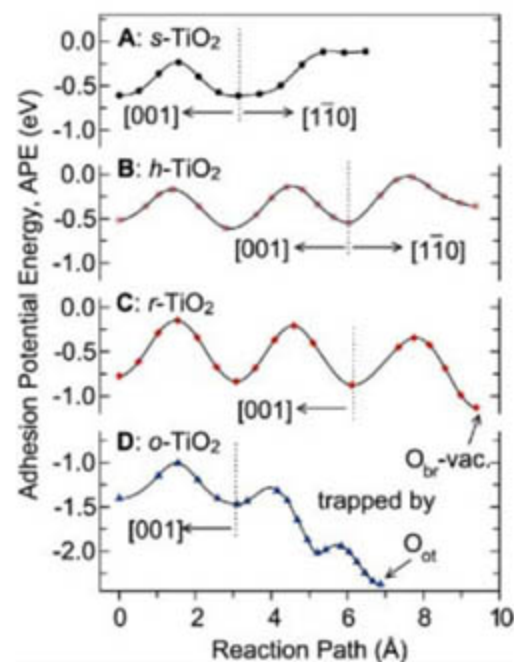


**Fig. 3.** Potential energy profiles for  $Au_1$  cluster diffusion on  $s$ - (A),  $h$ - (B),  $r$ - (C), and  $o$ - (D)  $TiO_2(110)$ . The minima at which  $Au_1$  is trapped at the point defects on  $r$ - and  $o$ - $TiO_2(110)$  are indicated (arrows; vac. means vacancy). On  $s$ - and  $o$ - $TiO_2(110)$ ,  $Au_1$  diffuses along the  $O_{br}$  rows, whereas, on  $h$ - and  $r$ - $TiO_2(110)$ ,  $Au_1$  diffuses along the Ti troughs.

$h$ - $TiO_2(110)$  surface after Au exposure at RT (Fig. 1).

In Fig. 4, we compare the energetically most favorable Au structures found in DFT calculations with the high-resolution STM images of most abundant small  $Au_n$  clusters. On  $r$ - $TiO_2(110)$ , the smallest Au-related protrusions (Fig. 4D) arise from  $Au_1$  in  $O_{br}$  vacancies, because the density of these smallest protrusions increases upon Au exposure at the expense of the density of the faint protrusions arising from  $O_{br}$  vacancies (17, 28). The second smallest protrusions found (Fig. 4, E and F) originate from linear Au trimers ( $Au_3$ ). This assignment relies on the following: (i) Au dimers ( $Au_2$ ) are calculated to adhere less strongly to the support than  $Au_3$  clusters (Table 1), and (ii) DFT calculations of two  $Au_3$  configurations, either symmetrically (Fig. 4B) or asymmetrically (Fig. 4C) attached to the  $O_{br}$  vacancy, precisely reproduce the two most abun-

dant protrusions in this size range revealed in the STM measurements.

On the  $o$ - $TiO_2(110)$  surface, we observed a different distribution of protrusions of  $Au_n$  clusters (Fig. 4, J to L), where some of the smallest Au topographies are depicted. Because the  $O_{ot}$  atoms serve as nucleation sites for incoming  $Au_1$  (Fig. 3D), the  $O_{ot}$  atoms are probably incorporated into the  $Au_n$  clusters. A one-to-one assignment of measured protrusions to certain  $Au_n$ - $O_{ot}$  clusters is not trivial, but the distinct height distribution of the Au clusters on the  $o$ - $TiO_2(110)$  surface allows us to distinguish between  $Au_n$  clusters consisting of one, two, or even three Au layers (fig. S2).

The DFT results of a more complete survey for stable  $Au_n$  clusters with  $1 \leq n \leq 5$  and  $n = 7$  on the three  $TiO_2(110)$  surfaces of interest are summarized in Table 1. As reference, we also considered  $s$ - $TiO_2(110)$ , although this surface was not studied experimentally. The most stable con-

**Fig. 4.** (Top) Most favorable structures found in DFT calculations for  $Au_1$  trapped in an  $O_{br}$  vacancy (A),  $Au_3$  symmetrically attached on an  $O_{br}$  vacancy (B), and non-symmetrically attached  $Au_3$  (C). (D to F) Zoom-in STM images ( $40 \times 40 \text{ \AA}^2$ ) showing  $Au_n$  clusters that are ascribed to the calculated  $Au_n$  cluster configurations. Corresponding line profiles to these measurements are shown in fig. S1. (Bottom) Most favorable structures found in DFT calculations for  $Au_1$  (G),  $Au_4$  (H), and  $Au_7$  (I) on  $o$ - $TiO_2(110)$ . (J to L) Zoom-in STM images ( $40 \times 40 \text{ \AA}^2$ ) of  $Au_n$  clusters attached in the vicinity of  $O_{ot}$  atoms that are tentatively assigned to the calculated  $Au_n$  cluster configurations.

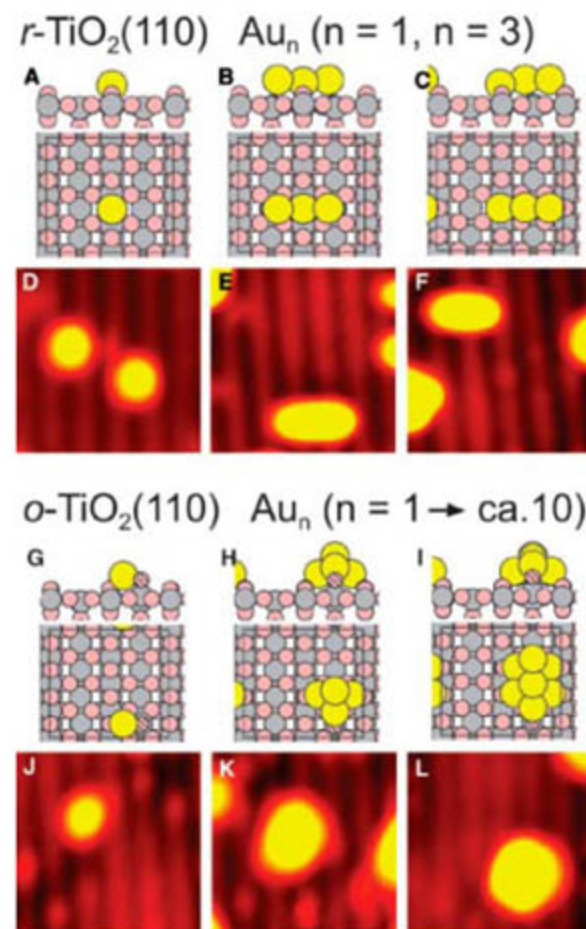


**Table 1.** DFT-based APEs in eV (per  $Au_n$  cluster) of the most stable  $Au_n$  clusters with  $1 \leq n \leq 5$  and  $n = 7$  on  $r$ -,  $h$ -,  $s$ -, and  $o$ - $TiO_2(110)$  surfaces, respectively. Some of these numbers are plotted in Fig. 5E (see also figs. S3 to S7).

Gold cluster	$r$ - $TiO_2(110)$	$h$ - $TiO_2(110)$	$s$ - $TiO_2(110)$	$o$ - $TiO_2(110)$
$Au_1$	-1.14	-0.54	-0.61	-2.38
$Au_2$	-0.71	-0.05	-0.10	-1.94
$Au_3$	-1.41	-1.26	-1.36	-3.09
$Au_4$	-0.57	-0.64	-0.97	-4.04
$Au_5$	-0.31	-1.04	-1.32	-3.57
$Au_7$	-0.52	-0.87	-1.18	-3.83



figurations on *s*-TiO<sub>2</sub>(110) are two-dimensional (2D) structures that are attached via the O<sub>br</sub> atoms and thus are aligned in the [001] direction. As reported previously, these structures adhere only weakly (35). On the *h*-TiO<sub>2</sub>(110) surface, we found even smaller adhesion potential energies (APEs) for the most stable configurations. In contrast, on the *r*-TiO<sub>2</sub>(110) surface, Au<sub>1</sub> and Au<sub>3</sub> bind relatively strongly in O<sub>br</sub> vacancies, whereas Au<sub>2</sub>, Au<sub>4</sub> (Au tetramers), Au<sub>5</sub> (Au pentamers), and Au<sub>7</sub> (Au septamers) bind very weakly. For the *o*-TiO<sub>2</sub>(110) surface, we found extraordinarily strong bonding of all Au<sub>*n*</sub> clusters considered.

According to the DFT results addressing *r*- and *o*-TiO<sub>2</sub>(110), the energy for Au<sub>*n*</sub> cluster detachment from the defects on the *r*-TiO<sub>2</sub>(110) surfaces decreases rapidly with cluster size but not on the *o*-TiO<sub>2</sub>(110) surface, where the detachment energy remains high. This means that, for a given Au dispersion, a higher persistence against sintering upon heating is likely to exist on the *o*-TiO<sub>2</sub>(110) surface as compared to the situation on the *r*-TiO<sub>2</sub>(110) surface. Thus, the DFT results presented in Table 1 corroborate the STM findings shown in Fig. 2, C to F.

To gain insight into why the Au<sub>*n*</sub> clusters bind much more strongly on the *o*-TiO<sub>2</sub>(110) surface than on the *r*-TiO<sub>2</sub>(110) surface, we compared electron charge density difference maps for two selected Au<sub>*n*</sub> clusters (Fig. 5, A and C). For the *r*-TiO<sub>2</sub>(110) surface, we chose an Au<sub>3</sub> cluster symmetrically attached in an O<sub>br</sub> vacancy, because we observed this cluster with the STM (Fig. 4E). Analyzing the bonding qualitatively in three dimensions (Fig. 5A), we found that electron charge accumulates (red isosurfaces) between the Au atoms and the substrate 5f-Ti upon adsorption, indicating the formation of covalent bonds. A more quantitative analysis, where we only considered the charge redistribution perpendicular to the support, shows that the Au atoms primarily experience charge polarization upon adsorption (Fig. 5B).

On the *o*-TiO<sub>2</sub>(110) surface, we studied the extraordinarily stable Au<sub>4</sub> cluster in the vicinity of an O<sub>ot</sub> atom. In this case, charge redistribution is seen along the Au–O bond axes (Fig. 5C), indicating that the Au–O bonds contribute to the attachment of the Au<sub>4</sub> cluster. The quantitative analysis (Fig. 5D) reveals that electron charge has

indeed been transferred to the surface O atoms, whereby the Au<sub>4</sub> cluster has become cationic. This means that the bonding of Au<sub>4</sub> on the *o*-TiO<sub>2</sub>(110) surface is partially ionic.

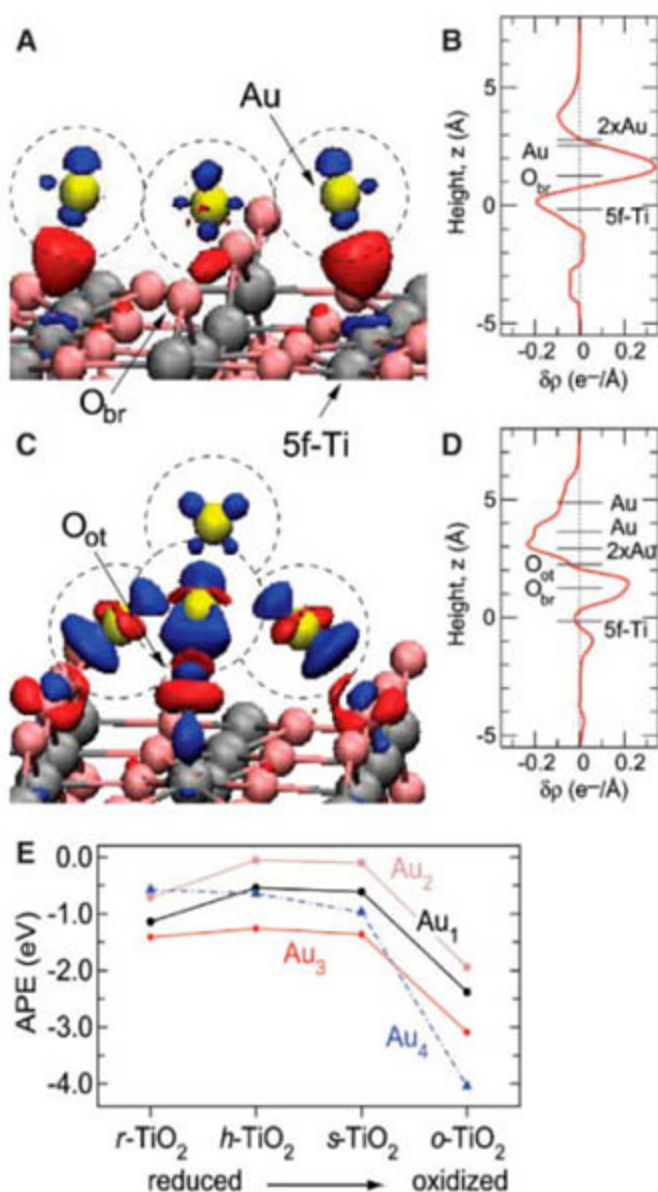
Contribution of ionic bonding in the case of Au<sub>4</sub> on *o*-TiO<sub>2</sub>(110) is consistent with the calculated atomic Au 5d populations upon adsorption of Au<sub>3</sub> and Au<sub>4</sub> on the *r*- and *o*-TiO<sub>2</sub>(110) surfaces, respectively. As compared to Au<sub>3</sub> and Au<sub>4</sub> in the gas phase, the total 5d population is reduced by 0.24 and 0.56 e<sup>-</sup> for Au<sub>3</sub>/*r*-TiO<sub>2</sub>(110) and Au<sub>4</sub>/*o*-TiO<sub>2</sub>(110), respectively (36). The larger reduction of the 5d populations for Au<sub>4</sub>/*o*-TiO<sub>2</sub>(110) can be traced back mainly to the single Au atom that binds directly to the O<sub>ot</sub> atom, because this Au atom contributes 0.22 of the 0.56 e<sup>-</sup>.

The different bond mechanisms of the considered Au<sub>*n*</sub> clusters (Fig. 5, A to D) reflect that the reduced *r*- and *h*-TiO<sub>2</sub>(110) surfaces are electron rich (formally having two and one excess electrons per O<sub>br</sub> vacancy and OH<sub>br</sub> species, respectively), whereas the *o*-TiO<sub>2</sub>(110) surface is electron deficient (formally missing two electrons per O<sub>ot</sub> atom). As a function of the surface oxidation state, the Au<sub>*n*</sub>-TiO<sub>2</sub>(110) adhesion is nonmonotonic for *n* = 1, 2, and 3 with the lowest adhesion strengths on the *h*- and *s*-TiO<sub>2</sub>(110) surfaces (Fig. 5E). For these small Au<sub>*n*</sub> clusters, the adhesion strength increases on *r*-TiO<sub>2</sub>(110), because the covalent bonds between Ti and Au form more readily when not all of the Ti atoms are in their fully oxidized state. However, an adhesion mechanism involving cationic Au occurs when the surface is oxidized [*o*-TiO<sub>2</sub>(110)], which leads to a much stronger Au<sub>*n*</sub>-support bonding than that on the *r*-TiO<sub>2</sub>(110) surface.

In light of the presented experimental and computational results, we doubt that O vacancies on oxide surfaces are relevant at all for the stabilization of dispersed Au particles under real reaction conditions with usually high oxygen pressures. Instead, our results suggest that, even under slightly oxidizing conditions as used here, the Au particles are stabilized via Au–O–M bonds (where M represents a metal atom of the supporting oxide). This interpretation is in line with recent reports on cationic Au species for Au supported on magnesia (11), ceria (12, 15), and iron oxide (14).

In all of the model studies addressing Au supported on titania where the catalytic activity of the systems considered was shown, very high oxygen exposures had been used to prepare or to “activate” the catalysts (7, 8, 18, 23). This observation is an additional reason why we question previously proposed structure models, including our own (17, 35), where it was implied that in O vacancies attached Au clusters cause the catalytic activity in “real” catalysts (i.e., at high pressure). We propose that Au particles dispersed on reducible oxides are better catalysts than those supported on nonreducible ones, because reducible oxides are more capable

**Fig. 5.** (A) Charge density difference map of an Au<sub>3</sub> cluster attached to an O<sub>br</sub> vacancy. Yellow spheres and dashed circles mark positions of Au atoms. Blue and red isosurfaces indicate depletion and addition, respectively, of 0.05 e<sup>-</sup> per Å<sup>3</sup>. (C) Charge density difference map of Au<sub>4</sub> attached on *o*-TiO<sub>2</sub>(110). Iso-surfaces are defined as in (A). (B and D) Electron charge density difference ( $\delta\rho$ ) for the same systems as in (A) and (C), respectively, but integrated over the *x* and *y* dimensions of the super cell. The *z* positions of O and Au atoms are given with respect to the 5f-Ti atoms (*z* = 0), whereby the label “2 × Au” is used to indicate the *z* positions of the two Au atoms that have identical *z* values in the two Au<sub>*n*</sub> clusters considered. (E) Plot of the calculated APEs for the most stable small Au<sub>*n*</sub> clusters (*n* = 1 to 4) as a function of the “TiO<sub>2</sub>(110) oxidation state” (compare with Table 1).





of forming O-rich Au-support interfaces. Note that O-rich surface terminations have been identified not only for titania (24, 37) but also for several other reducible oxides, including vanadium and iron oxide (38).

A much stronger Au oxide-support adhesion exists on O-rich Au-support interfaces than on O-poor oxide-support surfaces. For catalytic applications, this result suggests the occurrence of cationic gold at the Au-support interface as a general feature. For the  $r$ -TiO<sub>2</sub>(110) surface, we found that O<sub>br</sub> vacancies allow for the stabilization of gold monomers and gold trimers, but larger gold clusters cannot be sufficiently stabilized. We emphasize that our approach of studying the oxide support in a range of oxidation states is applicable to numerous other model systems.

#### References and Notes

- M. Haruta, N. Yamada, T. Kobayashi, S. Iijima, *J. Catal.* **115**, 301 (1989).
- G. C. Bond, D. T. Thompson, *Gold Bull.* **33**, 41 (2000).
- F. Cosandey, T. E. Madey, *Surf. Rev. Lett.* **8**, 73 (2001).
- R. Meyer, C. Lemire, Sh. K. Shaikhutdinov, H.-J. Freund, *Gold Bull.* **37**, 72 (2004).
- U. Diebold, *Surf. Sci. Rep.* **48**, 53 (2003).
- G. R. Bamwenda, S. Tsubota, T. Nakamura, M. Haruta, *Catal. Lett.* **44**, 83 (1997).
- M. Valden, X. Lai, K. Luo, Q. Guo, D. W. Goodman, *Science* **281**, 1647 (1998).
- S. Lee, C. Fan, T. Wu, S. L. Anderson, *J. Am. Chem. Soc.* **126**, 5682 (2004).
- M. M. Schubert *et al.*, *J. Catal.* **197**, 113 (2001).
- S. H. Overbury *et al.*, *Catal. Lett.* **95**, 99 (2004).
- J. Guzman, B. C. Gates, *J. Am. Chem. Soc.* **126**, 2672 (2004).
- Q. Fu, H. Saltsburg, M. Flytzani-Stephanopoulos, *Science* **301**, 935 (2003).
- L. Fu *et al.*, *J. Phys. Chem. B* **109**, 3704 (2005).
- G. J. Hutchings *et al.*, *J. Catal.* **242**, 71 (2006).
- J. Guzman, S. Carrettin, A. Corma, *J. Am. Chem. Soc.* **127**, 3286 (2005).
- J. G. Wang, B. Hammer, *Phys. Rev. Lett.* **97**, 136107 (2006).
- E. Wahlström *et al.*, *Phys. Rev. Lett.* **90**, 026101 (2003).
- M. S. Chen, D. W. Goodman, *Science* **306**, 252 (2004).
- I. N. Remediakis, N. Lopez, J. K. Nørskov, *Angew. Chem. Int. Ed.* **44**, 1824 (2005).
- A. S. Wörz, U. Heiz, F. Cinquini, G. Pacchioni, *J. Phys. Chem. B* **109**, 18418 (2005).
- F. Bocuzzi, A. Chiorino, *J. Phys. Chem. B* **104**, 5414 (2000).
- B. Schumacher, V. Plzak, M. Kinne, R. J. Behm, *Catal. Lett.* **89**, 109 (2003).
- T. S. Kim, J. S. Stiehl, C. T. Reeves, R. J. Meyer, C. B. Mullins, *J. Am. Chem. Soc.* **125**, 2018 (2003).
- S. Wendt *et al.*, *Surf. Sci.* **598**, 226 (2005).
- Materials and methods are available as supporting material on Science Online.
- O. Bikondoa *et al.*, *Nat. Mater.* **5**, 189 (2006).
- W. S. Epling, C. H. F. Peden, M. A. Henderson, U. Diebold, *Surf. Sci.* **412-413**, 333 (1998).
- When we compared the herein-presented comprehensive data set with previous data from our group (17), it became apparent that, in (17), Au was evaporated onto TiO<sub>2</sub>(110) surfaces of various character. For the low-temperature experiments in (17), the starting point was a clean  $r$ -TiO<sub>2</sub>(110) surface. For the Au exposures at higher temperatures, however, unintentionally  $h$ -TiO<sub>2</sub>(110) surfaces were used. Taking this into account, there is full agreement between the STM results in (17) and the present work. In both data sets, ~80% of the Au clusters were found at the step edges after Au exposure onto  $h$ -TiO<sub>2</sub>(110) at RT.
- X. Tong *et al.*, *J. Am. Chem. Soc.* **127**, 13516 (2005).
- C. T. Campbell, S. C. Parker, D. E. Starr, *Science* **298**, 811 (2002).
- The Au<sub>n</sub> APES on the various TiO<sub>2</sub>(110) supports were calculated according to  $APE = E_{tot}(Au_n + support) - E_{tot}(Au_n) - E_{tot}(support)$ , where  $E_{tot}(Au_n + support)$ ,  $E_{tot}(Au_n)$ , and  $E_{tot}(support)$  are the total energies of the combined systems, the most stable gas phase Au<sub>n</sub> 2D clusters, and the TiO<sub>2</sub>(110) surface in a certain oxidation state, respectively. Negative APES indicate stable adhesion of the Au<sub>n</sub> clusters. For details, see (25).
- A. Del Vitto, G. Pacchioni, F. Delbecq, P. Sautet, *J. Phys. Chem. B* **109**, 8040 (2005).
- H. Iddir, S. Ögüt, N. D. Browning, M. M. Disko, *Phys. Rev. B* **72**, 081407(R) (2005).
- H. Iddir, S. Ögüt, N. D. Browning, M. M. Disko, *Phys. Rev. B* **73**, 039902(E) (2006).
- L. M. Molina, M. D. Rasmussen, B. Hammer, *J. Chem. Phys.* **120**, 7673 (2004).
- Changes in the Au 6s and 6p populations also occur and must be in the order of 0.25 e<sup>-</sup> accumulation per Au cluster for Au<sub>n</sub>-TiO<sub>2</sub>(110) in order to conform with Fig. 4D, where only charge polarization and no net charging is shown. The changes in the Au 6s and 6p populations cannot be quantified because these orbitals overlap substantially with other orbitals originating from neighboring atoms.
- T. J. Beck *et al.*, *Phys. Rev. Lett.* **93**, 036104 (2004).
- M. Abu Haija *et al.*, *Surf. Sci.* **600**, 1497 (2006), and references therein.
- We acknowledge financial support from the Danish Ministry of Science, Technology, and Innovation through iNANO, the Danish Research Councils, and the Danish Center for Scientific Computing. D.M. acknowledges support from the Swiss National Science Foundation. We thank D. W. Goodman for fruitful discussions.

#### Supporting Online Material

www.sciencemag.org/cgi/content/full/315/5819/1692/DC1  
Materials and Methods

Figs. S1 to S7  
References

2 October 2006; accepted 9 February 2007  
10.1126/science.1135752

## An Atomic Seesaw Switch Formed by Tilted Asymmetric Sn-Ge Dimers on a Ge (001) Surface

K. Tomatsu,<sup>1</sup> K. Nakatsuji,<sup>1</sup> T. Iimori,<sup>1</sup> Y. Takagi,<sup>2</sup> H. Kusunohara,<sup>3</sup> A. Ishii,<sup>3</sup> F. Komori<sup>1</sup>

When tin (Sn) atoms are deposited on a clean germanium (Ge) (001) surface at room temperature, buckled dimers originating from the Sn atoms are formed at the Ge-dimer position. We identified the dimer as a heterogeneous Sn-Ge dimer by reversing its buckling orientation with a scanning tunneling microscope (STM) at 80 kelvin. An atomic seesaw switch was formed for one-dimensional electronic conduction in the Ge dimer-row direction by using the STM to reversibly flip the buckling orientation of the Sn-Ge dimer and to set up standing-wave states.

Considerable effort has been devoted to the switching of electronic conduction through the movement of atoms. Atomic switches have been formed between two electrodes (such as a metal tip and a metal surface) by controlling the surface migration of atoms or the formation and annihilation of an atomic bridge

(1–5). A molecular conformation change has been proposed to create another type of nanoscale switch (a molecular switch) (6–11). However, the direct observation of different conducting pathways with atomic resolution has been difficult to achieve. One difficulty in correlating changes in atomic positions with changes in conductivity is that in most of the systems that have been studied, the conducting pathway is perpendicular to the direction that can be imaged with scanning probe methods, or the switching between conducting and nonconducting configurations is not reversible. We now report the observation of switching

between conducting and nonconducting states of one-dimensional (1D) rows of dimers on a semi-conducting Ge (001) surface on which a sparse coverage of Sn atoms had been deposited. These adatoms incorporate into the dimer rows to create buckled Sn-Ge dimers that can adopt two different configurations that can be switched reversibly with a scanning tunneling microscope (STM) tip. We find that one of these configurations maintains the conductive free-electron state, whereas the other reflects the conduction electrons and sets up a standing-wave state.

On a clean Ge (001) surface, two atoms form a dimer with multiple bonds of  $\pi$  and  $\sigma$  conjugations. The dimer tilts (buckles) from the surface plane, and the bonding  $\pi$  and antibonding  $\pi^*$  states localize on the upper and lower atoms of the dimer, respectively (12). The Ge dimers align in the [110] direction, forming a dimer row. The neighboring dimers in the same dimer row are buckled in the opposite configuration, and the  $\pi^*$  electron behaves like a 1D free electron along the dimer row (13). It was recently shown that the buckling orientation of the Ge dimer can be reversibly controlled by a surface bias voltage of the STM (14). This conformation change is induced by inelastic scattering of injected carriers from the STM tip to the surface under the electric field, as a result of the bias voltage.

<sup>1</sup>Institute for Solid State Physics, University of Tokyo, 5-1-5 Kashiwanoha, Kashiwa-shi, Chiba 277-8581, Japan. <sup>2</sup>RIKEN Harima Institute at Spring-8, 1-1-1 Kouto, Mikazuki-cho, Sayo-gun, Hyogo 679-5148, Japan. <sup>3</sup>Department of Applied Mathematics and Physics, Tottori University, 4-101 Minami, Koyama, Tottori 680-8552, Japan.



When we deposited submonolayer coverages [ $<0.4$  monolayer (ML) (15)] of Sn atoms onto the Ge (001) surface above room temperature (RT), a buckled dimer (X dimer), in which the electronic states were different from those of the Ge dimers, was observed at the substrate Ge-dimer positions in STM measurements at RT (16, 17). Successive filled-state images (surface bias voltage  $V_b = -0.4$  V and tunneling current  $I = 1.0$  nA) of the Sn-deposited ( $<0.05$  ML) Ge (001) surface at 80 K are shown in Fig. 1, A to C (18), and Fig. 1, D to F, shows the structural models corresponding to the rectangular area surrounded by solid lines in Fig. 1A. There are two stable superstructures on the clean Ge (001) surface characterized by whether the buckling orientation of the neighboring dimer rows is out of or in phase: a  $c(4 \times 2)$  domain for out-of-phase orientations and a  $p(2 \times 2)$  domain for in-phase orientations (12, 14). In Fig. 1A, most of the dimer rows buckle into the  $c(4 \times 2)$  domain, except for one X dimer, which appears higher in the image than the other Ge dimers and is observed at the substrate Ge-dimer position indicated by the dotted circle.

The  $c(4 \times 2)$  and  $p(2 \times 2)$  domains on the clean Ge (001) surface can be reversibly exchanged by STM below 80 K (14). When we applied a pulse bias voltage  $V_b \geq +0.7$  V from  $-0.4$  V in the  $c(4 \times 2)$  domain, the buckling orientation of the dimers in the dimer row just under the tip apex was reversed, and a  $p(2 \times 2)$  domain elongating in the dimer-row direction appeared. When we scanned over this surface at  $V_b \leq -0.6$  V, the  $p(2 \times 2)$  domain in the scanned area was erased, and the  $c(4 \times 2)$  domain reappeared. When the bias voltage was  $-0.6$  V  $< V_b < +0.7$  V, the surface superstructure remained the same.

After observing the surface shown in Fig. 1A, we applied a pulse voltage of  $+0.8$  V for 500 ms, with the tip height fixed at the position indicated by the white cross in Fig. 1B. The feedback loop of the STM control was cut at  $V_b = -0.4$  V and  $I = 1.0$  nA to fix the tip height. A  $p(2 \times 2)$  domain was created by reversing the buckling orientation of

the dimers in the dimer rows including the X dimer, as shown in Fig. 1B. At this stage, the image of the X dimer became the same as that of the Ge dimer. After taking the image in Fig. 1B, we subsequently scanned all of the imaged area at  $V_b = -1.2$  V and  $I = 1.0$  nA three times, which returned the created  $p(2 \times 2)$  domain back to the  $c(4 \times 2)$  domain. This process also reversed the buckling orientation of the X dimer back to the original position, and its image height resumed, as shown in Fig. 1C. On the same surface, we found that the X dimers were imaged higher than the Ge dimer in the  $p(2 \times 2)$  domain for  $V_b = -0.4$  V. Their apparent height became the same as that of the Ge dimers for the same  $V_b$  when the domain structure was changed to  $c(4 \times 2)$ . Thus, the surface superstructure does not govern the apparent height of the X dimer.

These results give critical information on the composition of the X dimer. If the X dimer is a chemically symmetric dimer, such as a pure Sn dimer, it should be imaged in the same manner, irrespective of its buckling orientation.

Hence, we can identify the X dimer as a chemically asymmetric dimer, a Sn-Ge dimer. Here we define the dimer imaged higher than the Ge dimer in the filled-state image as a U dimer, and that imaged like the Ge dimer as an L dimer.

In order to determine which atom of the Sn-Ge dimers is at the upper- or lower-atom position, we measured the bias-voltage dependence of these dimers. In the filled-state images (Fig. 2, A and C), the upper atoms (where the  $\pi$  states localize) are imaged as protrusions, and in the empty-state images (Fig. 2, B and D), the lower atoms (where the  $\pi^*$  states localize) are seen. The U dimer was imaged higher than the Ge dimer in both filled- and empty-state images (Fig. 2, A and B), whereas the L dimer was imaged similarly to the Ge dimer in the filled-state image and higher than the Ge dimer in the empty-state image (Fig. 2, C and D). In the STM observation at RT, most of the X dimers exhibit the same bias-voltage dependence as that of the U dimer (16, 17). Thus, the U dimer is more stable than the L dimer.

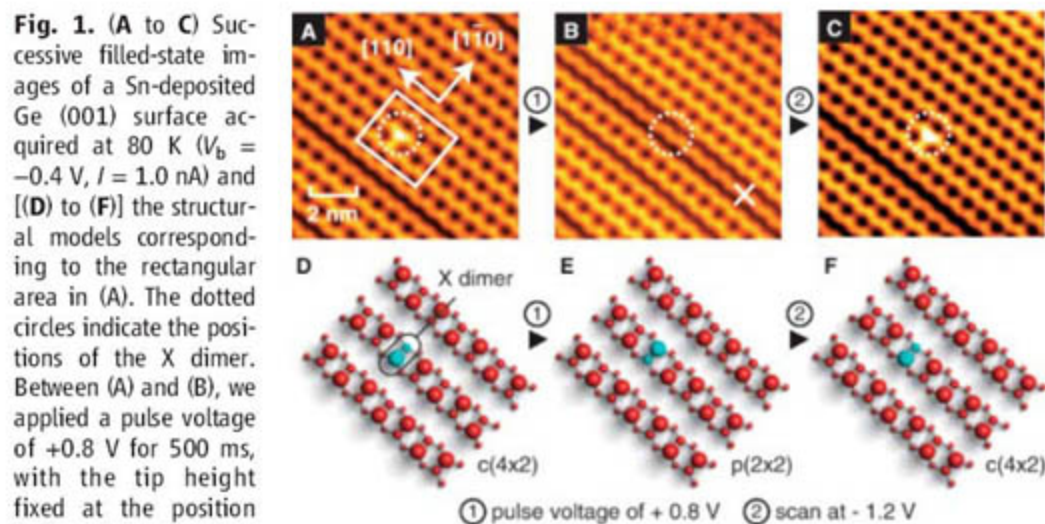
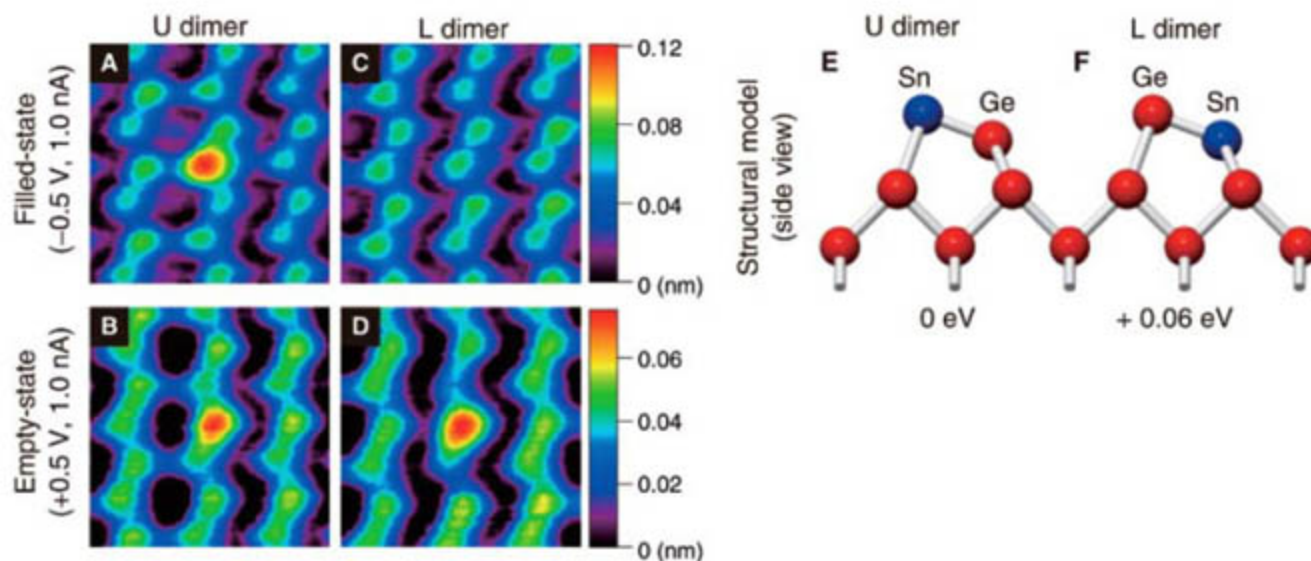


**Fig. 1.** (A to C) Successive filled-state images of a Sn-deposited Ge (001) surface acquired at 80 K ( $V_b = -0.4$  V,  $I = 1.0$  nA) and [(D) to (F)] the structural models corresponding to the rectangular area in (A). The dotted circles indicate the positions of the X dimer. Between (A) and (B), we applied a pulse voltage of  $+0.8$  V for 500 ms, with the tip height fixed at the position indicated by the white cross in (B). Between (B) and (C), we scanned the imaged area at  $V_b = -1.2$  V and  $I = 1.0$  nA. The blue spheres in the structural models represent the X dimers.

**Fig. 2.** (A and B) Empty- and filled-state images of the U dimer and [(C) and (D)] those of the L dimer. (E and F) Structural models of the U and L dimers.





We next examined the energies of these two kinds of Sn-Ge dimers, on the basis of density-functional calculations (17). The Sn-Ge dimer with a Sn atom at the upper-atom position (Fig. 2E) was found to be 0.06 eV more stable than that with a Sn atom at the lower-atom position (Fig. 2F). We also calculated the energy of the Ge dimer with a Sn atom in the second layer. This dimer was 0.12 eV less stable than was the Sn-Ge dimer with a Sn atom at the upper-atom position. This result rules out the possible substitution of Sn atoms into the second layer. Hence, the U and L dimers refer to the position of the Sn atom (Fig. 2, E and F).

On the clean Ge (001) surface, a 1D free-electron system in the dimer-row direction is formed by the empty  $\pi^*$  electrons, and each dimer row can be regarded as an atomic wire. In order to investigate the conduction of the 1D electronic state, we observed standing waves caused by the reflection at the Sn-Ge dimers in differential ( $dI/dV$ ) images. The  $dI/dV$  signal is proportional to the local density of states at a specific energy level that corresponds to the bias voltage.

Empty-state (Fig. 3A) and  $dI/dV$  (Fig. 3B) images of the same dimer row in the  $p(2 \times 2)$  domain with the L dimer reveal an electronic standing wave (19). Its wavelength increased as the bias voltage decreased, and we confirmed that the band dispersion agrees well with that of the  $\pi^*$  band on the clean Ge (001) surface (13).

**Fig. 3.** (A and B) Empty-state and  $dI/dV$  images ( $V_b = +0.7$  V,  $I = 1.0$  nA) of a dimer row including the L dimer and [(C) and (D)] those including the U dimer in the  $p(2 \times 2)$  domain (19). (E) Line profiles along the dimer row including the L or U dimer in the  $dI/dV$  images. The dotted circles in the empty-state images indicate the L- and U-dimer positions.

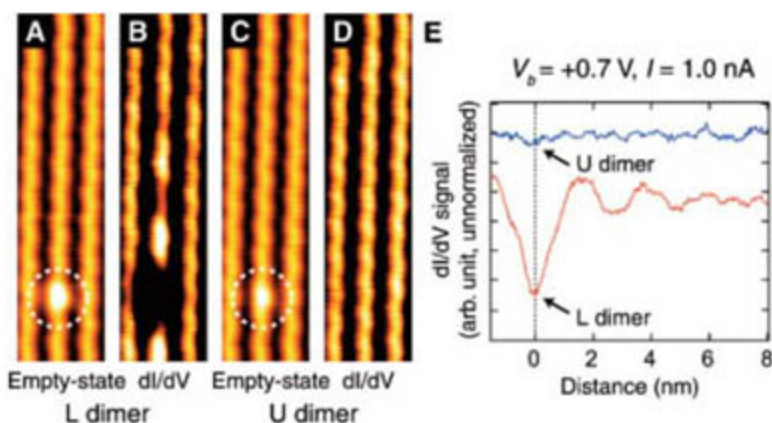
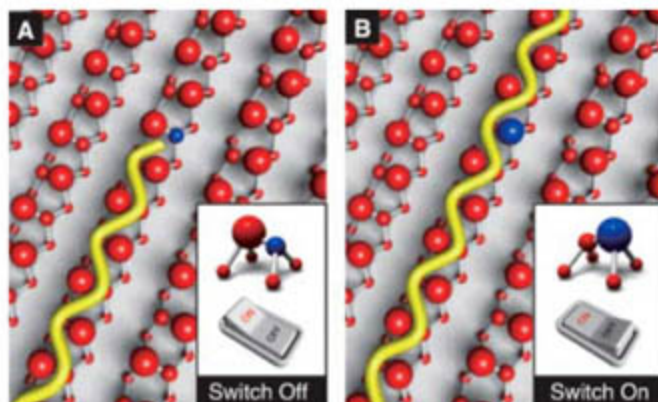


**Fig. 4.** Schematics of propagation of the  $\pi^*$  electrons around (A) the L and (B) the U dimers. The red and blue atoms represent Ge and Sn atoms, respectively, and the yellow curve shows a conduction pathway for the  $\pi^*$  electron. The  $\pi^*$  electrons are reflected at the L dimer because the Sn atom is located on their pathway. In contrast, most of the  $\pi^*$  electrons pass through the U dimer because the lower atoms are always Ge atoms throughout the dimer row.



Thus, the  $\pi^*$  electrons were reflected at the L dimer. In contrast, empty-state (Fig. 3C) and  $dI/dV$  (Fig. 3D) images of the same dimer row with the U dimer, acquired under the same condition as the L dimer, did not reveal the presence of any standing waves at the bias voltage we used ( $V_b = 0.4$  to 1.2 V). This means that most of the  $\pi^*$  electrons passed through the U dimer without reflection. The large difference in the reflection probability between the U and L dimers (Fig. 3E) also appeared in the  $c(4 \times 2)$  domain.

These phenomena can be qualitatively understood by structural and electronic differences between the U and L dimers (Fig. 4). On the clean Ge (001) surface, the  $\pi^*$  band exhibiting free-electron character is mainly composed of the atomic orbitals of the lower-dimer atoms (12, 13). In other words, the  $\pi^*$  electrons propagate along the dimer row through the lower-atom side. The L dimer in the dimer row has a Sn atom at the lower-atom position (Fig. 2F); that is, the Sn atom is located on the  $\pi^*$  electron path. The  $\pi^*$  electrons propagating along the dimer row meet the Sn atom at the L dimer, which can reflect the  $\pi^*$  electrons. However, the U dimer in the dimer row has a Sn atom at the upper-atom position (Fig. 2E), and the lower atoms are always Ge atoms throughout the dimer row. Thus, the  $\pi^*$  electrons can be scattered weakly by the U dimer. The electronic states of the Ge atom, however, should

be perturbed by those of the Sn atom because the Ge lower atom chemically bonds with the Sn upper atom. The negligible reflection can be attributed to the weak antibonding interaction of  $\pi$  conjugation.

The U and L dimers can be reversibly exchanged by STM, and such exchange does not occur when the bias voltage is  $-0.6$  V  $< V_b < +0.7$  V (Fig. 1). The results in Fig. 3 show that an atomic switch can be formed for 1D electronic conduction on the dimer row. Unlike conventional atomic switches (1–5), this atomic switch is not accompanied by the mass transport of atoms, but uses reversible conformation change—that is, reversals of the dimer-buckling orientation of a chemically asymmetric dimer. In this sense, we can regard this switch as an atomic seesaw switch, as illustrated in the insets of Fig. 4 and in movie S1 (17).

### References and Notes

- D. M. Eigler, C. P. Lutz, W. E. Rudge, *Nature* **352**, 600 (1991).
- D. P. E. Smith, *Science* **269**, 371 (1995).
- F.-Q. Xie, L. Nittler, Ch. Obermair, Th. Schimmel, *Phys. Rev. Lett.* **93**, 128303 (2004).
- J. A. Stroscio, R. J. Celotta, *Science* **306**, 242 (2004).
- K. Terabe, T. Hasegawa, T. Nakayama, M. Aono, *Nature* **433**, 47 (2005).
- C. P. Collier *et al.*, *Science* **285**, 391 (1999).
- C. P. Collier *et al.*, *Science* **289**, 1172 (2000).
- Z. J. Donhauser *et al.*, *Science* **292**, 2303 (2001).
- G. K. Ramachandran *et al.*, *Science* **300**, 1413 (2003).
- Y. Yasutake, Z. Shi, T. Okazaki, H. Shinohara, Y. Majima, *Nano Lett.* **5**, 1057 (2005).
- M. Lastapis *et al.*, *Science* **308**, 1000 (2005).
- M. Needels, M. C. Payne, J. D. Joannopoulos, *Phys. Rev. B* **38**, 5543 (1988).
- K. Nakatsuji, Y. Takagi, H. Kusunohara, A. Ishii, F. Komori, *Phys. Rev. B* **72**, 241308 (2005).
- Y. Takagi, Y. Yoshimoto, K. Nakatsuji, F. Komori, *Surf. Sci.* **559**, 1 (2004).
- ML is defined as the number density of the Ge atoms on the Ge (001) surface (1 ML =  $6.25 \times 10^{14}$  atoms/cm<sup>2</sup>). Under these conditions, a few X dimers are formed per 20-by-20-nm area.
- K. Tomatsu, K. Nakatsuji, T. Iimori, F. Komori, *Surf. Sci.*, in press; preprint available at <http://arxiv.org/abs/cond-mat/0701517>.
- STM images of the X dimer at RT, details of our calculation setup, and movie S1 demonstrating conductance switching with the buckled Sn-Ge dimer are available as supporting material on Science Online.
- The STM measurements were performed at 80 K under ultra-high-vacuum conditions ( $<1 \times 10^{-9}$  Pa). Sn was deposited onto a clean substrate at RT. The average Sn coverage was less than 0.05 ML.
- The  $dI/dV$  images were acquired by the lock-in technique with the tip feedback turned on. The bias voltage was modulated by 80 mV (peak to peak) at 3.0 kHz.
- We thank M. Yamada and Y. Binghai for fruitful discussion. This work was carried out by joint research at the Institute for Solid State Physics at the University of Tokyo.

### Supporting Online Material

[www.sciencemag.org/cgi/content/full/315/5819/1696/DC1](http://www.sciencemag.org/cgi/content/full/315/5819/1696/DC1)  
Materials and Methods

Fig. S1

References

Movie S1

21 November 2006; accepted 8 February 2007  
10.1126/science.1137848



# Magnifying Superlens in the Visible Frequency Range

Igor I. Smolyaninov,\* Yu-Ju Hung, Christopher C. Davis

We demonstrate a magnifying superlens that can be integrated into a conventional far-field optical microscope. Our design is based on a multilayer photonic metamaterial consisting of alternating layers of positive and negative refractive index, as originally proposed by Narimanov and Engheta. We achieved a resolution on the order of 70 nanometers. The use of such a magnifying superlens should find numerous applications in imaging.

Optical microscopy is an invaluable tool for studies of materials and biological entities. Imaging tools with ever-increasing spatial resolution are required if the current rate of progress in nanotechnology and microbiology is to continue. However, the spatial resolution of conventional microscopy is limited by the diffraction of light waves to a value on the order of 200 nm. Thus, viruses, proteins, DNA molecules, and many other samples are impossible to visualize with a regular microscope. One suggested way to overcome this limitation is based on the concept of a superlens (1), which relies on the use of materials or metamaterials that have negative refractive index in the visible frequency range. Near-field superlens imaging was recently demonstrated (2, 3), but the technique is limited by the fact that the magnification of the planar superlens is equal to 1. Thus, a thin planar superlens cannot be integrated into a conventional optical microscope to image objects smaller than the diffraction limit.

We describe the realization of a magnifying superlens (Fig. 1A) and demonstrate its integration into a regular far-field optical microscope. Our design is based on the theo-

retical proposals of an "optical hyperlens" (4) and "metamaterial crystal lens" (5) and on the recently developed plasmon-assisted microscopy technique (6), and in particular on the unusual optics of surface plasmon polaritons (SPPs). The properties of these two-dimensional optical modes and convenient ways to excite them are described in detail in (7). The wave vector of the SPPs is defined by the expression

$$k_p = \frac{\omega}{c} \left( \frac{\epsilon_d \epsilon_m}{\epsilon_d + \epsilon_m} \right)^{1/2} \quad (1)$$

where  $\epsilon_m(\omega)$  and  $\epsilon_d(\omega)$  are the frequency-dependent dielectric constants of the metal and the dielectric, respectively, and  $c$  is the speed of light. Above the resonant frequency  $\omega$  described by the condition

$$\epsilon_m(\omega) \approx -\epsilon_d(\omega) \quad (2)$$

the SPP group and phase velocities may have opposite signs (Fig. 1B). The internal structure of the magnifying superlens (Fig. 2A) consists of concentric rings of poly(methyl methacrylate) (PMMA) deposited on a gold film surface. For the SPP dispersion law for the gold-vacuum and gold-PMMA interfaces (Fig. 1B) in the frequency range marked by the box, PMMA has negative refractive index  $n_2 < 0$  as perceived by plasmons (the group velocity is opposite to the

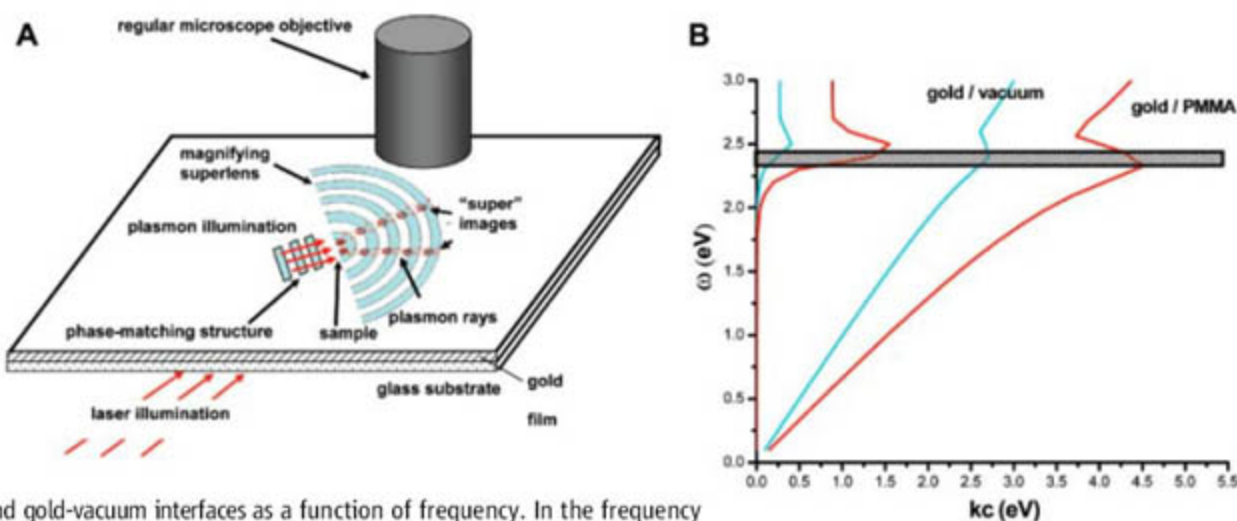
phase velocity). The width of the PMMA rings  $d_2$  is chosen so that  $n_1 d_1 = -n_2 d_2$ , where  $d_1$  is the width of the gold-vacuum portions of the interface. Although the imaging action of our lens is based on the original planar superlens idea, its magnification depends on the fact that all the rays in the superlens tend to propagate in the radial direction when  $n_1 d_1 = -n_2 d_2$  (Fig. 1A). This behavior was observed in the experiment upon illumination of the lens with  $\lambda = 495$  nm laser light (bottom portion of Fig. 2B) for which  $n_1 d_1 = -n_2 d_2$ . The narrow beam visible in the image is produced by repeating self-imaging of the focal point by the alternating layers of materials with positive and negative refractive index. On the other hand, if 515-nm light is used, the lens becomes uncompensated and the optical field distribution inside the lens reproduces the field distribution in the normal "plasmonic lens" as described in (8) (top portion of Fig. 2B). However, in the complete theoretical description of the magnifying superlens, the ray optics picture presented in Fig. 1A may need to be supplemented by the anisotropic effective medium theory presented in (4, 5).

The magnifying action of the superlens is demonstrated in Figs. 3 and 4. Rows of two or three PMMA dots were produced near the inner ring of the superlens (Fig. 3, B and C). These rows of PMMA dots had 0.5- $\mu\text{m}$  periodicity in the radial direction, so that phase matching between the incident laser light and surface plasmons could be achieved (Fig. 1A). Upon illumination with an external laser, the three rows of PMMA dots in Fig. 3B gave rise to three radial divergent plasmon "rays," which are clearly visible in the plasmon image in Fig. 3D obtained with a conventional optical microscope. The cross-sectional analysis of this image across the plasmon "rays" (Fig. 3F) indicates resolution of at least 70 nm, or  $\sim\lambda/7$ . The lateral separation between these rays increased by a factor of 10 as the rays reached the outer rim of the superlens. This increase allowed visualization of the triplet by conventional microscopy. In

Department of Electrical and Computer Engineering, University of Maryland, College Park, MD 20742, USA.

\*To whom correspondence should be addressed. E-mail: smoly@eng.umd.edu

**Fig. 1.** (A) Schematic of the magnifying superlens integrated into a conventional microscope. The plasmons generated by the phase-matching structure illuminate the sample positioned near the center of the superlens. The lateral distance between the images produced by the alternating layers of materials with positive and negative refractive index grows with distance along the radius. The magnified images are viewed by a regular microscope. (B) Real and imaginary parts of the surface plasmon wave vector  $k$  at the gold-PMMA and gold-vacuum interfaces as a function of frequency. In the frequency range marked by the box, PMMA has negative refractive index as perceived by plasmons, whereas the gold-vacuum interface looks like a medium with positive refractive index.





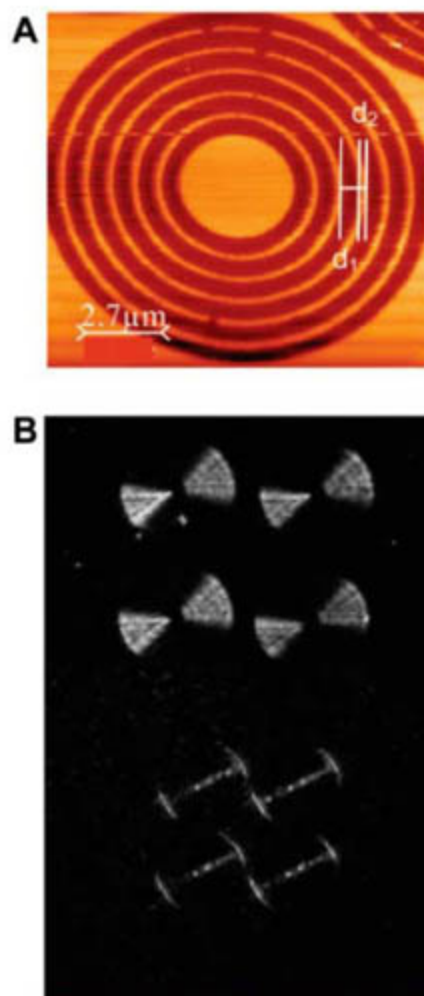


**Fig. 2.** (A) AFM image of the magnifying superlens made of PMMA rings on the gold film surface. (B) Optical field distribution in the magnifying superlens illuminated by external laser in the frequency ranges where  $n_1 d_1 \neq -n_2 d_2$  (top) and  $n_1 d_1 = -n_2 d_2$  (bottom).

a similar fashion, the two radial rows of PMMA dots shown in Fig. 3C gave rise to two plasmon rays, which are visualized in Fig. 3E.

The composite image in Fig. 4 is a superposition of the atomic force microscopy (AFM) image from Fig. 3A and the corresponding optical image obtained by conventional optical microscopy. It illustrates the imaging mechanism of the magnifying superlens: The passage of plasmon rays through the concentric alternating layers of materials with positive and negative refractive index increases the lateral separation of the three rays (marked by arrows at lower right). Near the edge of the superlens, the separation is large enough to be resolved with a conventional optical microscope, thus demonstrating a magnifying superlens in the visible frequency range.

The theoretical resolution of such a microscope may reach the nanometer scale (1, 4). It thus has the potential to become an invaluable tool in medical and biological imaging, where far-field optical imaging of individual viruses and DNA molecules may become a reality. It allows very simple, fast, robust, and straightforward image acquisition.

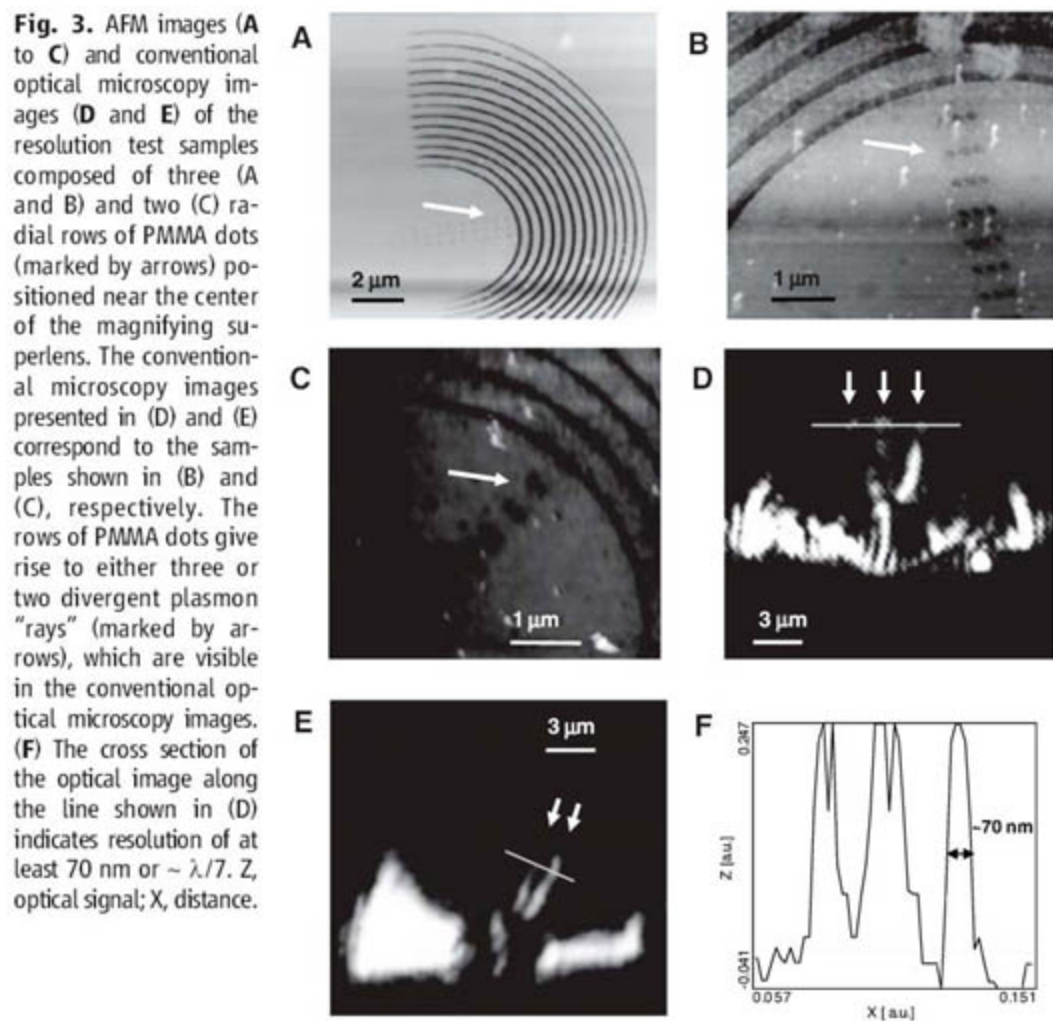


**Fig. 3.** AFM images (A to C) and conventional optical microscopy images (D and E) of the resolution test samples composed of three (A and B) and two (C) radial rows of PMMA dots (marked by arrows) positioned near the center of the magnifying superlens. The conventional microscopy images presented in (D) and (E) correspond to the samples shown in (B) and (C), respectively. The rows of PMMA dots give rise to either three or two divergent plasmon "rays" (marked by arrows), which are visible in the conventional optical microscopy images. (F) The cross section of the optical image along the line shown in (D) indicates resolution of at least 70 nm or  $\sim \lambda/7$ . Z, optical signal; X, distance.

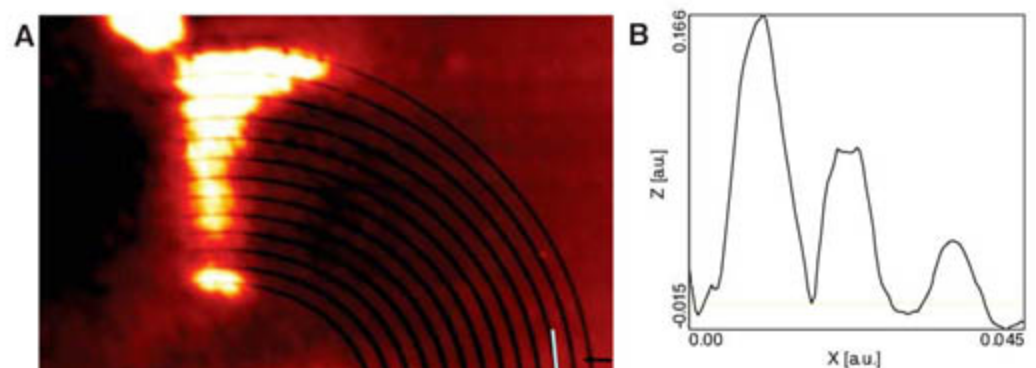


**Fig. 4.** (A) Composite of the AFM image from Fig. 3A superimposed onto the corresponding image obtained by conventional optical microscopy, illustrating the imaging mechanism of the magnifying superlens. Near the edge of the superlens, the separation of three rays (marked by arrows) is large enough to be resolved using a conventional optical microscope. (B) The cross section of the optical image along the line shown in (A) indicates the three rays.

We expect that unusual optical metamaterials may be designed and implemented using the principle of our magnifying superlens. Because  $(d_1 + d_2)$  and the  $d_1/d_2$  ratio (Fig. 2A) are easy to vary locally, the effective anisotropic refractive index of the multilayer material may be varied continuously from large negative to large positive values. Thus, unusual nanophotonic devices may be created in the visible

frequency range, such as the recently suggested (9, 10) and demonstrated (11) "invisibility cloak."

#### References and Notes

1. J. B. Pendry, *Phys. Rev. Lett.* **85**, 3966 (2000).
2. N. Fang, H. Lee, C. Sun, X. Zhang, *Science* **308**, 534 (2005).
3. D. O. S. Melville, R. J. Blaikie, *Opt. Express* **13**, 2127 (2005).



4. Z. Jacob, L. V. Alekseyev, E. Narimanov, *Opt. Express* **14**, 8247 (2006).  
 5. A. Salandrino, N. Engheta, *Phys. Rev. B* **74**, 075103 (2006).  
 6. I. I. Smolyaninov, C. C. Davis, J. Elliott, A. V. Zayats, *Phys. Rev. Lett.* **94**, 057401 (2005).  
 7. A. V. Zayats, I. I. Smolyaninov, A. A. Maradudin, *Phys. Rep.* **408**, 131 (2005).

8. Z. Liu, J. M. Steele, H. Lee, X. Zhang, *Appl. Phys. Lett.* **88**, 171108 (2006).  
 9. J. B. Pendry, D. Schurig, D. R. Smith, *Science* **312**, 1780 (2006); published online 24 May 2006 (10.1126/science.1125907).  
 10. U. Leonhardt, *Science* **312**, 1777 (2006); published online 24 May 2006 (10.1126/science.1126493).

11. D. Schurig *et al.*, *Science* **314**, 977 (2006); published online 18 October 2006 (10.1126/science.1133628).  
 12. Supported by NSF grants ECS-0304046 and CCF-0508213.

12 December 2006; accepted 8 February 2007  
 10.1126/science.1138746

# Coupled Thermal and Hydrological Evolution of Tropical Africa over the Last Deglaciation

Johan W. H. Weijers,<sup>1\*</sup> Enno Schefuß,<sup>2†</sup> Stefan Schouten,<sup>1</sup> Jaap S. Sinninghe Damsté<sup>1</sup>

We analyzed the distribution of branched tetraether membrane lipids derived from soil bacteria in a marine sediment record that was recovered close to the Congo River outflow, and the results enabled us to reconstruct large-scale continental temperature changes in tropical Africa that span the past 25,000 years. Tropical African temperatures gradually increased from  $\sim 21^\circ$  to  $25^\circ\text{C}$  over the last deglaciation, which is a larger warming than estimated for the tropical Atlantic Ocean. A direct comparison with sea-surface temperature estimates from the same core revealed that the land-sea temperature difference was, through the thermal pressure gradient, an important control on central African precipitation patterns.

Continental climate change during the last deglaciation, especially in the tropics, is not as well understood as it is for the oceans (1–3). For Africa, a consensus is emerging on past changes in humidity and their causes based on lake level and pollen studies as well as the deuterium content of plant waxes (4–6), but temperature records for such tropical continental areas remain scarce and incomplete. In contrast to the marine environment, few quantitative temperature proxies exist for the terrestrial environment, and continuous long-term climate archives on land are limited. For instance, pollen-based vegetation studies, a widely used method for environmental reconstructions on land (5), are complicated in the tropics because the effects of changes in temperature are difficult to distinguish from those of changes in precipitation. Temperature estimates based on another method, stable oxygen isotope contents of carbonates and silicates, are widely applied in lacustrine sediments and speleothems. However, although these estimates are appropriate for high-resolution qualitative paleoclimate reconstructions (7, 8), quantification of climate change in terms of paleotemperatures requires tenuous assumptions about the past changes in

parameters that have influenced the source-water composition. The scant paleotemperature data available for the African continent imply a temperature difference of  $\sim 3.5^\circ$  to  $6^\circ\text{C}$  between the Last Glacial Maximum (LGM) and the present day (2, 5, 9, 10), but these data often represent a relatively local signal or are incomplete records. Thus, knowledge on African tropical temperature change over the last deglaciation is rather limited, especially for the vast tropical rainforest area of the Congo Basin. Continuous, high resolution, long-term records of continental-scale temperature change are much needed to improve this knowledge and enable proper comparison with records of marine temperature changes.

To gain better insight into the central African temperature development over the last deglaciation, its relation to global climatic changes, and its effect on the continental hydrological cycle, we used the Methylation index of Branched Tetraethers (MBT) and Cyclization ratio of Branched Tetraethers (CBT) based on branched glycerol dialkyl glycerol tetraethers (GDGTs) (11) present in a marine core recovered close to the Congo River outflow (GeoB 6518-1,  $05^\circ 35.3'S$ ,  $11^\circ 13.3'E$ , water depth of 962 m, Fig. 1). Using the MBT and the CBT, we reconstructed the annual mean air temperature (MAT) of the Congo River basin (12) which could be compared with the sea surface temperature (SST) record obtained from the same core (Fig. 2). Branched GDGTs (fig. S1) are abundant core membrane lipids derived from bacteria that thrive in soils (11, 13, 14). As the soil erodes, the GDGTs are fluviually transported to the ocean. Indeed, they have been shown to be an excellent tracer of the fate of soil organic matter in the Congo deep-sea fan (13) and the Bay of Biscay (15) (fig. S2). The large catchment area of the Congo River ( $3.7 \times 10^6 \text{ km}^2$ ) extends from about  $6^\circ\text{N}$  to  $13^\circ\text{S}$  and from about  $13^\circ$  to  $33^\circ\text{E}$  in central Africa (Fig. 1A), with elevations between 300 and 1200 m except for one small part, located at its eastern boundary, that rises above 2000 m (16). The temperature estimates obtained from our marine core, therefore, represent a catchment-integrated terrestrial temperature signal derived from land of low to intermediate elevation. Analysis of the

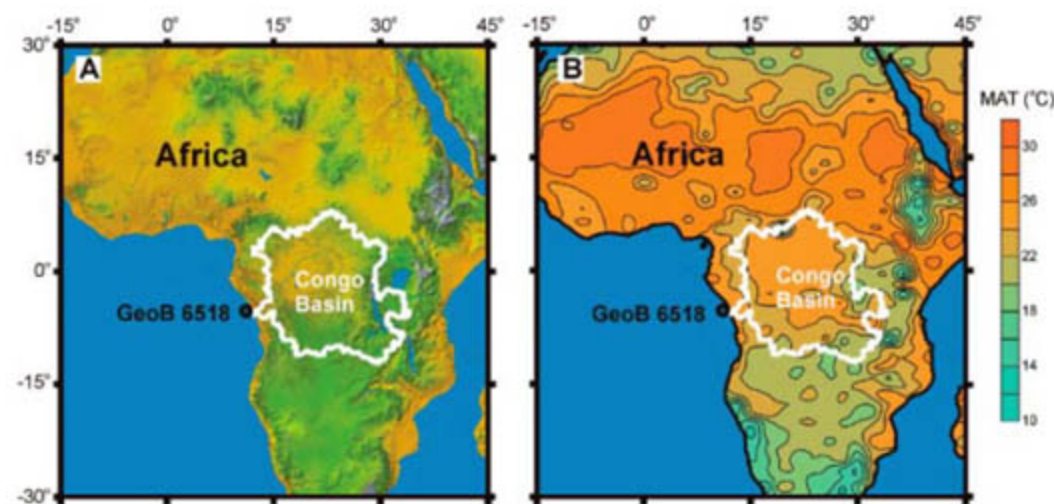


**Fig. 1.** Overview maps of Africa. The position of core GeoB 6518, recovered close to the Congo River outflow from a water depth of 962 m, and the extent of the Congo River drainage basin (white outline) are plotted (A) on a digital elevation map of Africa [picture from NASA Jet Propulsion Laboratory, California Institute of Technology] and (B) on a map showing the annual MAT distribution in Africa [available in the database in (30)].

<sup>1</sup>Royal Netherlands Institute for Sea Research, Department of Marine Biogeochemistry and Toxicology, Post Office Box 59, 1790 AB Den Burg- Texel, Netherlands. <sup>2</sup>Deutsche Forschungsgemeinschaft (DFG)—Research Center Ocean Margins, University of Bremen, Leobener Strasse, 28359 Bremen, Germany.

\*To whom correspondence should be addressed. E-mail: jweijers@nioz.nl

†Present address: Institute for Geosciences, Christian-Albrechts-University Kiel, Ludwig-Meyn-Strasse 10, 28114 Kiel, Germany.



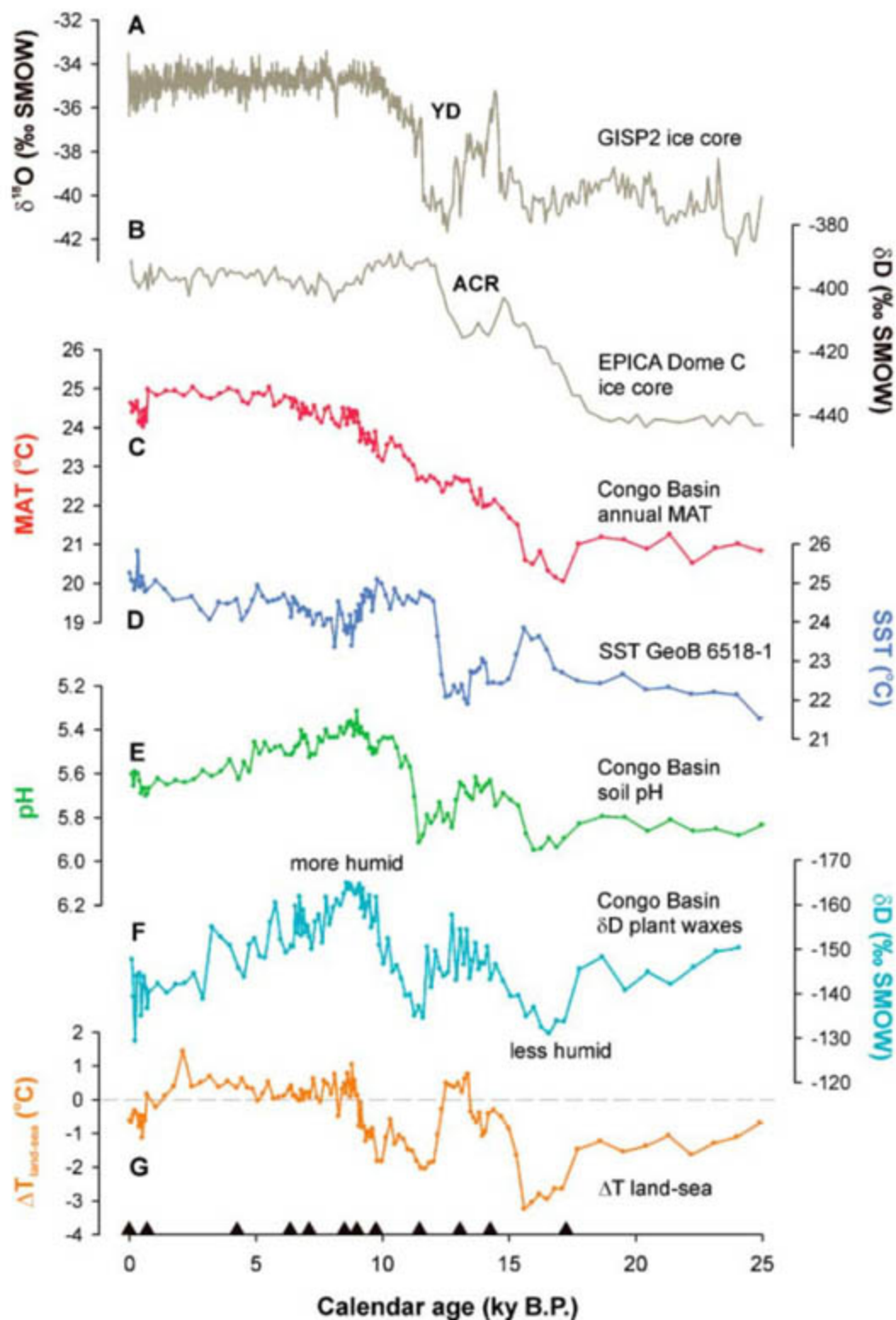


**Fig. 2.** Temperature changes over the past 25,000 years in tropical central Africa compared with African humidity changes and Arctic and Antarctic climate signals. (A) The Greenland Ice Sheet Project 2 (GISP2)  $\delta^{18}\text{O}$  record indicative of Greenland air-temperature fluctuations (31). SMOW, standard mean ocean water. (B) The EPICA Dome C  $\delta\text{D}$  record indicative of Antarctic air-temperature changes (20). (C) The annual MAT record of the Congo Basin based on the MBT index and CBT ratio of the branched GDGT lipids of soil bacteria in core GeoB 6518-1. (D) The SST changes in the equatorial Atlantic Ocean based on alkenone paleothermometry at site GeoB 6518-1 (6). (E) A record of the average soil pH in the Congo Basin based on the CBT ratio of branched GDGT lipids of soil bacteria in core GeoB 6518-1. (F) The  $\delta\text{D}$  record of  $\text{C}_{29}$  *n*-alkane plant waxes in core GeoB 6518-1 reflecting humidity changes in tropical central Africa (6). (G) The land-sea temperature gradient between central tropical Africa and the tropical Atlantic Ocean based on records (C) and (D). Black triangles on the age scale indicate the  $^{14}\text{C}$  accelerator mass spectrometry radiocarbon dates derived from mixed planktonic foraminifera used for establishing the chronology of core GeoB 6518-1 (6). YD, Younger Dryas; ACR, Antarctic Cold Reversal.

stable carbon isotopic content ( $\delta^{13}\text{C}$ ) of plant-wax *n*-alkanes has shown that the Congo River mainly drained rainforest-vegetated areas over the past 20,000 years (6).

The main advantages of our record compared with previous climate records are its relatively high temporal resolution (~200 years), continuous nature, and large geographical coverage (i.e., central tropical Africa). The nature of our data allowed us to gain detailed insight into the general development of tropical African temperature over the last deglaciation. The annual MAT record of the Congo Basin reveals an overall warming since the LGM [~24,000 to 18,000 calibrated years before present (~24 to 18 cal ky B.P.)] of 4° to 4.5°C (Fig. 2C). This is consistent with scant data on paleotemperatures from a few other locations in tropical Africa outside the Congo Basin. Pollen-based temperature reconstructions suggest an LGM that had been 4° to 4.5°C cooler than today—that is, ~4°C cooler in the Burundi highlands (5) and ~4.5°C cooler in the southern Lake Tanganyika basin (17). Furthermore, LGM temperatures that were ~3.5°C lower than today have been reported based on TEX<sub>86</sub> (tetraether index of tetraethers consisting of 86 carbon atoms) lake surface temperature reconstructions for northern Lake Malawi (10). Larger differences between LGM and present-day temperatures have been reported based on analyses of stalagmite stable isotopes and groundwater noble gases. Such analyses indicated that temperatures were ~5.7°C cooler in a South African speleothem (18) and 5° to 6°C cooler in groundwater aquifers in Namibia and South Africa (9, 19), but these data were derived from sites substantially farther south of the equatorial Congo Basin. Our record indicates that deglacial warming has been of similar magnitude for the whole of tropical Africa, from the western and central lowlands to the eastern highlands.

The onset of postglacial warming in our record at about 17 cal ky B.P. (Fig. 2C) is in line with the Southern Hemispheric climate development, with the European Project for Ice Coring in Antarctica (EPICA) Dome C Deuterium record showing the onset of warming at about 17.5 cal ky B.P. (20) (Fig. 2B) and about 17 cal ky B.P. in a stalagmite  $\delta^{18}\text{O}$  record from South Africa (18). Recent work based on  $^{10}\text{Be}$  exposure dating of moraines (3) has shown that in the mid-latitudes of both hemispheres, the onset of the last deglaciation was near synchronous at about 17.2 cal ky B.P.; a similar timing of 17.3 cal ky B.P. was inferred for the onset of the last deglaciation in the South American tropics of Peru and Bolivia. Our tropical temperature record shows that the postglacial warming in tropical central Africa started at the same time, after a short cooling episode between 18 and 17 cal ky B.P., providing strong evidence for a globally synchronous onset of the last deglaciation.

With values of 20.5° to 21°C, temperatures were rather constant during the LGM. The rate



of subsequent deglacial warming was highest between 17 and 13.5 cal ky B.P. and between 11.5 and 9 cal ky B.P., with an average warming of  $\sim 0.7^\circ\text{C ky}^{-1}$ . During the intervening period from 13.5 to 11.5 cal ky B.P., temperatures remained relatively stable at about  $22.5^\circ\text{C}$  and were, notably, not influenced by the Antarctic Cold Reversal in the Southern Hemisphere or by the Younger Dryas cold episode in the Northern Hemisphere. From 9 to 5.5 cal ky B.P., temperatures only rose slowly by  $\sim 0.3^\circ\text{C ky}^{-1}$ , reaching maximum values of  $25^\circ\text{C}$ . During the second part of the Holocene, temperatures remained about  $25^\circ\text{C}$ , except for the last 0.7 ky when the temperature decreased slightly again by  $0.5^\circ$  to  $1^\circ\text{C}$ . The  $24.5^\circ\text{C}$  reconstructed from the core-top sediment is similar to the present-day annual MAT of the Congo River basin, about  $23.7^\circ\text{C}$ , based on weather station data (21) (Fig. 1B).

Our record also enables a more detailed comparison of tropical continental temperature change with global climate development and SST records, in particular from the tropical Atlantic Ocean. SST reconstructions based on alkenone paleothermometry indicate  $\sim 1.7^\circ\text{C}$  lower SSTs for the Indian Ocean and  $\sim 2.7^\circ\text{C}$  lower SSTs for the tropical Atlantic Ocean during the LGM relative to Holocene temperatures (22). This agrees well with the  $\sim 2.5^\circ\text{C}$  alkenone-based LGM-Holocene SST range at this site (Fig. 2D), representative for the eastern tropical Atlantic Ocean (6). Thus, compared with the ocean, the reconstructed continental deglacial warming of  $4^\circ$  to  $4.5^\circ\text{C}$  is considerably stronger. This difference between continental and oceanic deglacial warming in the tropics is in agreement with climate model studies, which suggest that the average continental deglacial warming in the tropics was about 1.5 times stronger than the deglacial warming of the tropical oceans (23, 24). This amplified continental warming may have been because the continents cool more during glacial times. At high and mid-latitudes, the presence of a changed and often reduced vegetation cover during glacials results, through increased albedo, in enhanced cooling of the land surface. However, in tropical areas, this effect is counteracted by a negative feedback from reduced evaporation, which results from decreased tropical rainforest area. The reduced evaporation leads to a decreased loss of latent heat and thus relatively warmer surface temperatures. As a result, vegetation changes in tropical Africa are thought to result eventually in a negligible temperature effect (25). A more likely explanation for the enhanced glacial cooling of the continental tropics may thus be an increased pole-to-equator temperature gradient, resulting in a strengthened and enlarged Hadley Cell circulation (26) and, consequently, an increase in relatively cool air that flows from higher toward lower latitudes.

Because central Africa seasonally receives airflow from both the Northern Hemisphere,

when the Intertropical Convergence Zone (ITCZ) is in its southernmost position, and the Southern Hemisphere, when the ITCZ is in its northernmost position (4), its temperature evolution is likely related to climate changes in both hemispheres. This coupling to both hemispheres supports the idea that the onset of the deglacial warming in our record at about 17 cal ky B.P. is global in character. It also might explain the lack of clear temperature signals related to the Antarctic Cold Reversal and the Younger Dryas, which were asynchronous deglacial cold events in the Southern and Northern hemispheres, respectively (27). Compensation of these cooling events by warmer air from the opposite hemisphere in the tropical realm apparently resulted in the observed period of relatively stable annual MAT over equatorial tropical Africa from 13.5 to 11.5 cal ky B.P.

Notably, the difference in deglacial warming between the continent and the ocean should have had an impact on continental hydrology through the land-sea thermal gradient. Present-day African rainfall variability is in large part associated with SST distributions in the South Atlantic Ocean in that the thermal pressure gradient differs between the African continent and the ocean surface (28). A large negative land-sea temperature gradient—that is, relatively warm sea and cool continent—will result in a generally off-land air flow, preventing moist air from the ocean from flowing onto the continent. An advantage of reconstructing continental African temperatures from a marine core is the possibility of comparing the results with SSTs derived from the same core (6) (Fig. 2D); we used this comparison to reconstruct the thermal gradient between central Africa and the eastern equatorial Atlantic Ocean over the past 25,000 years ( $\Delta T_{\text{land-sea}}$ ; Fig. 2G). During glacial times, the  $\Delta T_{\text{land-sea}}$  record generally shows values of  $-1^\circ$  to  $-3^\circ\text{C}$ , which disappear rather quickly after the onset of the deglaciation. Negative values down to  $-2^\circ\text{C}$  return at about 12 cal ky B.P., coincident with a fast SST increase in the eastern equatorial Atlantic Ocean, and gradually disappear again at the start of the Holocene. During the Holocene, the land-sea temperature gradient was rather stable, with values just greater than  $0^\circ\text{C}$ .

The influence of the land-sea thermal gradient on continental hydrology can be evaluated by comparison with central African humidity changes reflected in the Deuterium content ( $\delta\text{D}$ ) of plant-wax *n*-alkanes from the same record (6) and with the soil pH record derived from the CBT ratio of the branched GDGT membrane lipids (Fig. 2, E and F). Large-scale soil pH changes are assumed to reflect changes in precipitation intensity given that in the long term, soil-leaching processes result in either stronger or weaker soil acidification as precipitation increases or decreases, respectively (29). Indeed, the large negative values in the  $\Delta T_{\text{land-sea}}$  record correspond to relatively dry periods reflected in

the  $\delta\text{D}$  record and relatively high soil pH values (Fig. 2, E to G). Smaller negative or even positive values, indicating weak off-land or even on-land air flow, correspond to wetter conditions and lower soil pH values. Thus, the land-sea thermal gradient apparently exerts a strong control on central African precipitation patterns. The discrepancy between the  $\Delta T_{\text{land-sea}}$  record and the humidity records during the second part of the Holocene might be due to a very weak land-sea temperature gradient in this time interval that allowed other forcing mechanisms to become predominant.

It has been suggested that the meridional tropical-subtropical SST gradient in the South Atlantic Ocean exerts a strong control on central African precipitation changes (6). This mechanism works in the same direction as the land-sea thermal gradient: A relatively warm tropical ocean will result in stronger meridional winds as well as off-land winds, both preventing moist air from flowing from the oceans onto the continent. Before the Holocene, the land-sea thermal gradient was large and apparently exerted a dominant control, whereas during the Holocene, when the land-sea thermal gradient remained weak, the meridional SST gradient increased and became dominant in controlling precipitation in central tropical Africa, thereby causing increasingly dry conditions (6). Hence, the combined evolution of land temperature and SST in different parts of the Atlantic Ocean controlled precipitation patterns in central Africa during the past 25,000 years.

#### References and Notes

1. E. Bard, *Science* **284**, 1133 (1999).
2. I. Farrera et al., *Clim. Dyn.* **15**, 823 (1999).
3. J. M. Schaefer et al., *Science* **312**, 1510 (2006).
4. F. Gasse, *Quat. Sci. Rev.* **19**, 189 (2000).
5. R. Bonnefille, J. C. Roeland, J. Guiot, *Nature* **346**, 347 (1990).
6. E. Schefuß, S. Schouten, R. R. Schneider, *Nature* **437**, 1003 (2005).
7. M. J. Leng, J. D. Marshall, *Quat. Sci. Rev.* **23**, 811 (2004).
8. F. McDermott, *Quat. Sci. Rev.* **23**, 901 (2004).
9. J. T. Kulogowski, D. R. Hilton, E. T. Selaolo, *Geophys. Res. Lett.* **31**, L10204 (2004).
10. L. A. Powers et al., *Geophys. Res. Lett.* **32**, L08706 (2005).
11. J. W. H. Weijers, S. Schouten, J. C. van den Donker, E. C. Hopmans, J. S. Sinninghe Damsté, *Geochim. Cosmochim. Acta* **71**, 703 (2007).
12. Materials and methods are available as supporting material on Science Online.
13. E. C. Hopmans et al., *Earth Planet. Sci. Lett.* **224**, 107 (2004).
14. J. W. H. Weijers et al., *Environ. Microbiol.* **8**, 648 (2006).
15. G. Ménot et al., *Science* **313**, 1623 (2006).
16. S. N. Kazadi, F. Kaoru, *J. Geophys. Res. Atm.* **101**, 21351 (1996).
17. F. Chalie, *C. R. Acad. Sci. Paris* **320**, 205 (1995).
18. K. Holmgren et al., *Quat. Sci. Rev.* **22**, 2311 (2003).
19. T. H. E. Heaton, A. S. Talma, J. C. Vogel, *Quat. Res.* **25**, 79 (1986).
20. L. Augustin et al., *Nature* **429**, 623 (2004).
21. Royal Netherlands Meteorological Institute, World Climate Information (WIKI 2.0); available online ([www.knmi.nl/klimatologie/nomalen1971-2000/wiki.html](http://www.knmi.nl/klimatologie/nomalen1971-2000/wiki.html)).
22. A. Rosell-Melé et al., *Geophys. Res. Lett.* **31**, 1 (2004).
23. B. L. Otto-Bliesner et al., *J. Clim.* **19**, 2526 (2006).
24. S. I. Shin et al., *Clim. Dyn.* **20**, 127 (2003).



25. U. Wyputta, B. J. McAvaney, *Clim. Dyn.* **17**, 923 (2001).
26. G. Ramstein, Y. Serafini-Le Treut, H. Le Treut, M. Forichon, S. Joussaume, *Clim. Dyn.* **14**, 233 (1998).
27. T. Blunier *et al.*, *Geophys. Res. Lett.* **24**, 2683 (1997).
28. P. Camberlin, S. Janicot, I. Pocard, *Int. J. Climatol.* **21**, 973 (2001).
29. D. W. Johnson, P. J. Hanson, D. E. Todd, R. B. Susfalk, C. F. Trettin, *Water Air Soil Pollut.* **105**, 251 (1998).
30. C. J. Willmott, S. M. Robeson, *Int. J. Climatol.* **15**, 221 (1995).
31. M. Stuiver, P. M. Grootes, *Quat. Res.* **53**, 277 (2000).
32. We thank R. R. Schneider for providing samples from core GeOB 6518-1 and E. C. Hopmans for analytical support with the high-performance liquid chromatography/mass spectrometry instrument. This research was supported by the Earth and Life Sciences Council of the Netherlands Organization for Scientific Research and the Deutsche Forschungsgemeinschaft.

## Supporting Online Material

www.sciencemag.org/cgi/content/full/315/5819/1701/DC1  
Materials and Methods  
SOM Text  
Figs. S1 and S2  
References

29 November 2006; accepted 22 February 2007  
10.1126/science.1138131

## A Vestige of Earth's Oldest Ophiolite

Harald Furnes,<sup>1\*</sup> Maarten de Wit,<sup>2,3</sup> Hubert Staudigel,<sup>4</sup>  
Minik Rosing,<sup>5</sup> Karlis Muehlenbachs<sup>6</sup>

A sheeted-dike complex within the ~3.8-billion-year-old Isua supracrustal belt (ISB) in southwest Greenland provides the oldest evidence of oceanic crustal accretion by spreading. The geochemistry of the dikes and associated pillow lavas demonstrates an intraoceanic island arc and mid-ocean ridge–like setting, and their oxygen isotopes suggest a hydrothermal ocean-floor–type metamorphism. The pillows and dikes are associated with gabbroic and ultramafic rocks that together make up an ophiolitic association: the Paleoarchean Isua ophiolite complex. These sheeted dikes offer evidence for remnants of oceanic crust formed by sea-floor spreading of the earliest intact rocks on Earth.

Ophiolites represent sections of oceanic crust that were generated by sea-floor spreading and later emplaced onto continental margins (1). Originally, ophiolites were assumed to represent oceanic crust formed at mid-ocean ridges, but this view has changed radically, and it is becoming clear that the majority of ophiolites are generated in supra-subduction-zone environments (1). Depending on their tectonic environment of formation and their structural architecture and geochemical affinities, Phanerozoic ophiolites can be classified into different types, but the majority are genetically related to subduction environments (1, 2). A complete ophiolite consists of submarine basaltic volcanic rocks (mainly pillow lavas), sheeted dikes, a plutonic complex, and upper-mantle rocks. However, many ophiolites lack one or more of these components (2). In Archean greenstone belts, the absence of complete ophiolite pseudostratigraphies (in particular, sheeted dikes and gabbros) has led many workers to conclude that ophiolites are not represented in the earliest stages of Earth's history (3–5). The oldest purported example is the 2505-million-year-old Dongwanzi ophiolite complex in the North China craton (6), which is a disputed claim (7).

It has been suggested that several Archean greenstone belts host dismembered ophiolites (8, 9). Nonetheless, the question of whether Archean

oceanic crust formed by sea-floor spreading was related to Phanerozoic-like plate tectonics has so far remained conjectural because of the absence of compelling kinematic evidence to discriminate between origins through the horizontal motion of plates at divergent plate boundaries or through vertical motion above mantle plumes. Sheeted dikes provide an answer to these questions because they form by sea-floor spreading and accretion during horizontal movement at divergent plate boundaries, and they are considered to be crucial components of ophiolites. Here we report the discovery of a sheeted-dike complex within the Paleoarchean Isua supracrustal belt (ISB). This and the associated rocks, together with their compositions, make up a ~3.8-billion-year-old ophiolite, which in turn has strong

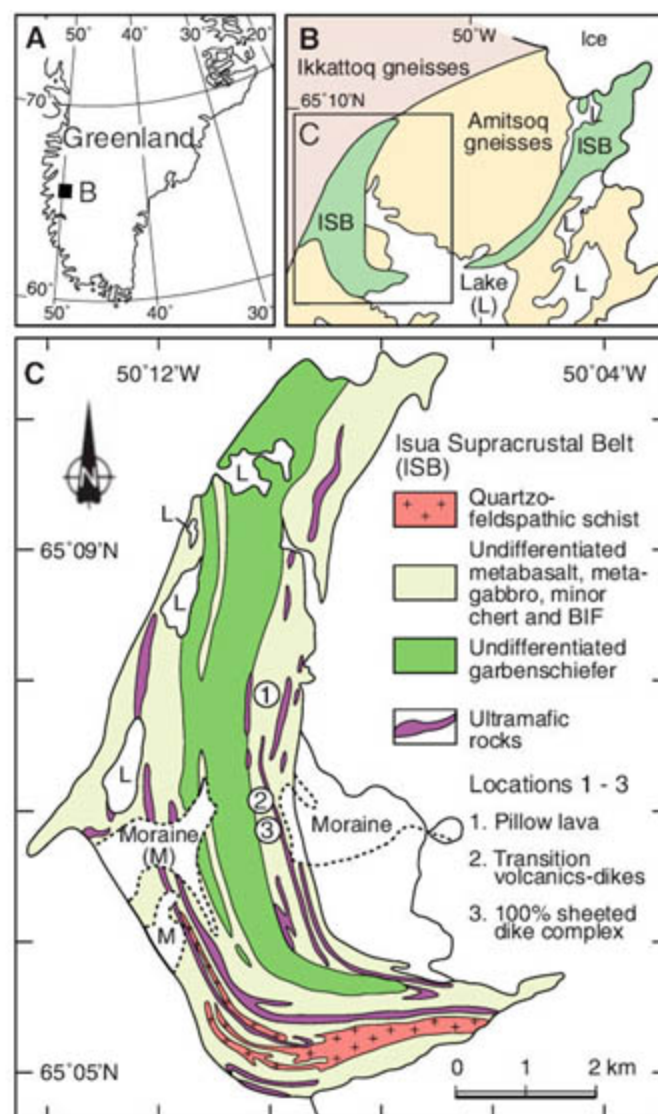


**Fig. 1.** (A) Location of the ISB in southwestern Greenland. The black square shows the location of the area detailed in (B). (B) ISB and adjacent gneisses. (Inset) Location of the area detailed in (C). (C) Simplified geological map of the western arm of the ISB, showing locations (1 to 3) of the 100% sheeted-dike complex (3: latitude 65.05.335°N, longitude 50.10.661°W) grading into dikes and volcanic rocks (2: latitude 65.07.033°N, longitude 50.09.769°W) and volcanic rocks (1: latitude 65.07.889°N, longitude 50.09.835°W). The geological maps [(B) and (C)] are modified from (10, 13, 15).

<sup>1</sup>Centre for Geobiology and Department of Earth Science, University of Bergen, Bergen, Norway. <sup>2</sup>Africa Earth Observatory Network (AEON) and Department of Geological Sciences, University of Cape Town, Rondebosch 7700 South Africa. <sup>3</sup>GeoForschungsZentrum (GFZ)–Potsdam, Telegrafenberg, Potsdam, Germany. <sup>4</sup>Scripps Institution of Oceanography, University of California, San Diego, La Jolla, CA 92093-0225, USA. <sup>5</sup>Nordic Centre for Earth Evolution and Geological Museum, University of Copenhagen, 1350, København K, Denmark. <sup>6</sup>Department of Earth and Atmospheric Sciences, University of Alberta, Edmonton, Alberta T6G 2E3, Canada.

\*To whom correspondence should be addressed. E-mail: harald.furnes@geo.uib.no



implications about the early tectonic and geochemical evolution of Earth.

The ISB, situated in southwestern Greenland (Fig. 1A), defines an arcuate belt ~35 km long and 2.5 km thick (Fig. 1B) that contains a variety of igneous and sedimentary rocks (10, 11). In general, the rocks are strongly deformed and metamorphosed to amphibolite facies, and primary features are scarce. The main lithologies of the ISB are metabasalts (amphibolites), metagabbros and ultramafics associated with metapelites, cherts, banded iron formations (BIFs), and felsic rocks (11), now preserved as enclaves within the surrounding plutons (Ikattoq and Amitsoq gneisses) (Fig. 1B).

Pillow structures and associated hyaloclastites are common within the amphibolites (12, 13) and provide unequivocal evidence of submarine lavas. Another major component (~50%) of the ISB, a unit described as "garbenschiefer," was

first considered to be derived from mafic intrusions (10), but has been reinterpreted as a volcano-sedimentary sequence containing gabbro sills (11, 13, 14). It has been suggested that together these assemblages represent oceanic-like crust that may have been obducted within an accretionary wedge ~3.7 billion years ago, as a result of plate tectonic-like processes (12).

Radiometric dating (U/Pb and Pb/Pb) has shown that the ISB formed between ~3800 and 3700 million years ago (Ma) (14). Whole-rock Sm-Nd isochrons define ages of  $3779 \pm 81$  Ma from metasediments and enclosing garbenschiefer (15) and  $3777 \pm 44$  Ma from pillow lavas and metagabbro (16). The latter date is partly based on samples collected from location 1 of this study (Fig. 1C).

We examined a number of sections in the eastern part of the western arm of the ISB, mapped as variegated schists (10) and amphibolites (13, 17)

within the area around locations 1 to 3 (Fig. 1C). Location 1 shows well-preserved metabasaltic pillow lava (Fig. 2A), in places with small triangular pockets of interpillow hyaloclastite (Fig. 2A). Locally, the pillows contain felsic ocelli (Fig. 2B) and rare amygdalae. The rocks are homogeneously deformed and contain a cleavage that is subparallel to the lithological layering. Deformed ocelli (originally spherical) indicate deformation with 80 to 90% shortening perpendicular to the cleavage and 200 to 250% extension along a well-defined lineation plunging 72°S. At location 2, ~1.5 km south of location 1 (Fig. 1C), the sequence consists of tabular subparallel dikes with intervening centimeter- to decimeter-thick zones of lenticular-to-irregular screens of volcanic material (Fig. 2, C and D, and fig. S1), and locally, plagiogranite occurs [Fig. 2D and supporting online material (SOM)]. Approximately 500 m further south, at location 3, the mixed dike/volcanic sequence changes structurally downward into a sheeted complex consisting of 100% tabular dikes (Fig. 2E and fig. S2), which to the west is in tectonic contact with metagabbro and ultramafic sheets. Individual dikes range in width from 2 to 50 cm. Dikes have both one- and (mostly) two-way fine-grained chilled planar margins (Fig. 2E). Cross-cutting dikes are also observed (Fig. 2F). We examined a number of sections across a 30- to 50-m-wide subvertical sequence of dikes, which we interpret as part of a sheeted-dike complex with an estimated predeformation width of >200 m.

Petrographically, the central parts of the dikes consist of fine-grained (~300  $\mu$ m) plagioclase, amphibole (predominant), and biotite with relic subophitic texture (Fig. 2G). The dark green (commonly schistose) marginal zones, inferred to represent chilled margins (Fig. 2E), consist of dense (~100  $\mu$ m) monomineralic zones of amphibole (Fig. 2H). These chilled margins of the dikes are texturally and mineralogically similar to the margins of the pillows.

Mafic gneisses interpreted as metagabbros occur as scattered outcrops within an area of ~100 by 100 m in the southwestern part of the ISB. They are uniform amphibolites characterized by centimeter-scale discontinuous layers and lenses of plagioclase in a hornblende-quartz-plagioclase matrix (fig. S3), representing a highly deformed and metamorphosed gabbroic texture. This contrasts with most Isua amphibolites, which typically consist of lithological units <1 m across strike (Fig. 2, C and D). Felsic dikes of the Amitsoq gneisses crosscut the metagabbros and define the early Archean age of the Isua supracrustals.

The ultramafic rocks (fig. S4), which occur mainly along the boundaries of the western belt of the ISB, have been variably transformed to serpentinites and calc-silicate rocks by metasomatic processes (11). These layered meta-ultramafic rocks are associated with the sheeted-dike complex (Fig. 1C) and metagabbro, sometimes with uninterrupted transitions from layered ultramafic sequence into gabbros (18).

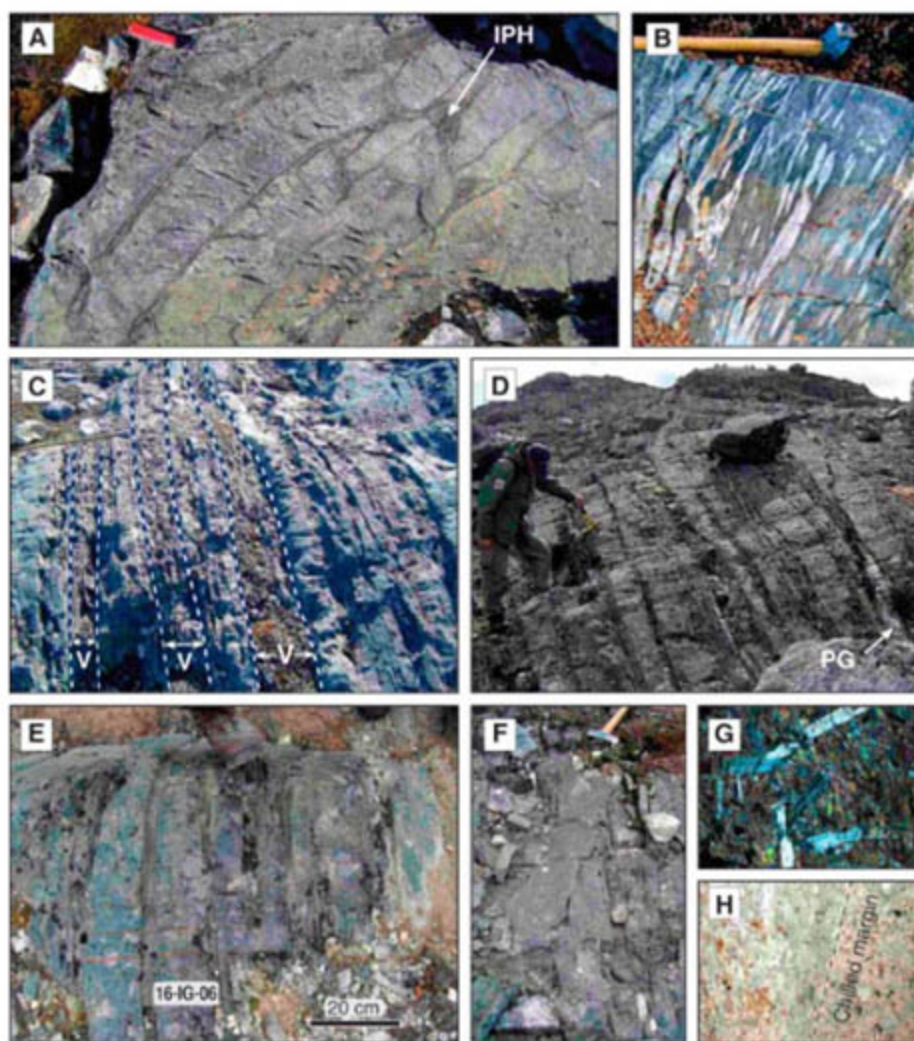


**Fig. 2.** (A) Well-preserved pillow lava exhibiting chilled margins (dark selvages) and pockets of interpillow hyaloclastite (IPH). (B) Ocelli-bearing pillows. The pale gray ocelli, originally spheres, give a measure of the deformation that the rocks have suffered. (A) and (B) are from location 1. (C) Dikes with intervening layers of volcanic rocks (V). (D) Nearly 100% sheeted dikes with minor amounts of interdike volcanic material. Dikes can be traced along strike for more than 20 m. The white lens (bottom right) is a plagiogranite (PG). (C) and (D) are from location 2. (E) 100% sheeted-dike complex. The weathered-out zones are amphibole schist, originally chilled margins. (F) Two crosscutting layers (just below the hammer head). (E) and (F) are from location 3. [(G) and (H)] Photomicrographs of the central part of the dike (G), showing relic subophitic texture (plane-polarized light image), and chilled margin of the dike (H), consisting predominantly of fine-grained amphibole (plane light image).



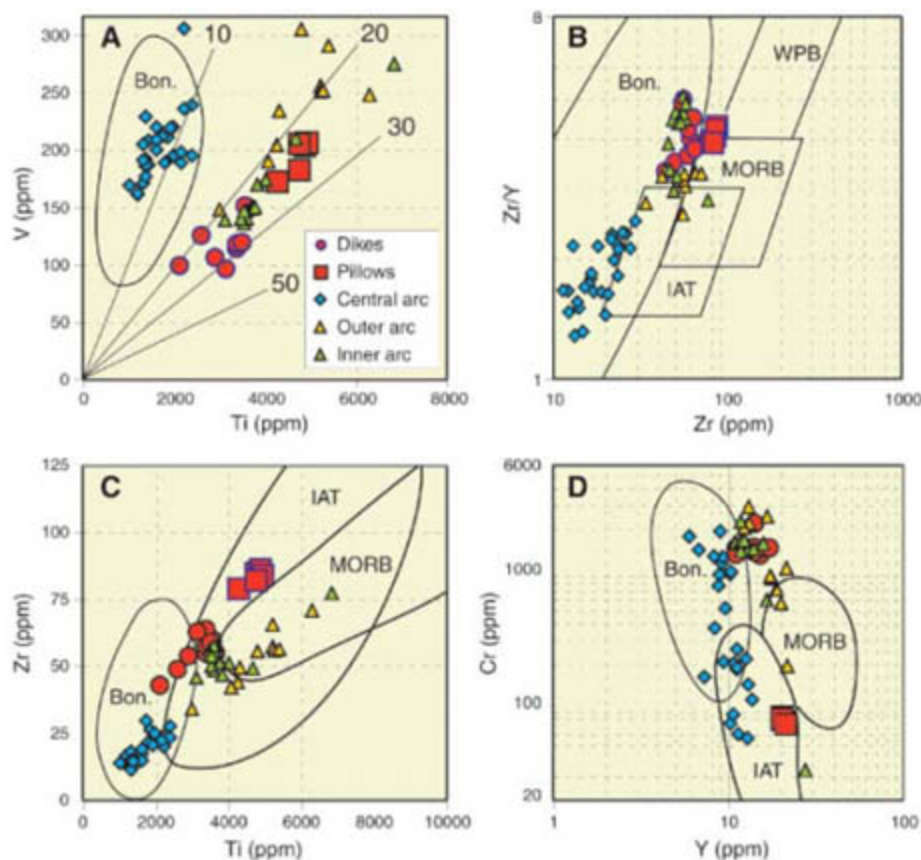


**Fig. 3.** (A) Ti-V, (B) Zr-Zr/Y, (C) Ti-Zr, and (D) Y-Cr discrimination diagrams (1). The geochemical data from the central-, outer-, and inner-arc tectonic domains (undifferentiated metabasalts) are from (17, 19). The new geochemical data of this study are shown in red. The boninite data are from (21). The Ti/V ratios in (A) are characteristic of the following: 10 to 20, island arc; 20 to 50, MORB; 20 to 30, mixed MORB and island arc; and 10 to 50, back-arc basins. Bon, boninites; IAT, island-arc tholeiite; and WPB, within-plate basalt.

The geochemistry of pillow lava and dikes from locations 1 and 3 (Fig. 1C), as well as that of the least altered samples of previous studies (17, 19), has been plotted in discriminant diagrams with various combinations of the relatively immobile elements Ti, V, Cr, Y, and Zr (1). The new geochemical data (table S1 and SOM) demonstrate intraoceanic island arc and mid-ocean ridge basalt (MORB) affinities (Fig. 3), as previously concluded (19). Furthermore, the similarities in the concentrations of incompatible elements (Ti, V, Zr, and Y) and their ratios (Zr/Y) strongly suggest that the pillow lavas and the dikes are cogenetic, supporting our field observations regarding their spatial and temporal relationships. It has been demonstrated that the metabasalts of the central garbenschiefer unit are geochemically similar to boninites (17) (Fig. 3). The presence of boninites is important in the evaluation of the tectonic environment, because they are generally associated with modern intraoceanic island arcs and are thought to be related to proto-arc and back-arc spreading (20–22). This magmatic progression suggests that ophiolites are geochemically heterogeneous and that their tectonic evolution may have involved initial sea-floor spreading, followed by subduction initiation and one or more episodes of arc splitting and basin opening (20, 21).

Oxygen isotope data from locations 1 and 3 (Fig. 1C) show that the pillows are more enriched in  $^{18}\text{O}$  than the dikes (Table 1 and SOM). Although the  $\delta^{18}\text{O}$  values of the central part of the pillows range between 6.5 and 9.9 (average, 7.2), the dikes show a narrower range between 5.7 and 6.9 (average, 6.3). These rocks do not record primary magmatic oxygen isotope values but may record alteration by 0 to +2 of the  $\delta^{18}\text{O}$  value of seawater at a spreading ridge. The pillows are more enriched in  $^{18}\text{O}$  because they altered at lower temperatures than did the dikes, and oxygen isotope fractionation decreases in magnitude with increasing temperature (23). Collectively, these data and the relic subophitic textures in the sheeted dikes are consistent with the seawater/rock interaction during ocean-floor metamorphism that takes place at modern spreading ridges (SOM) and which has been documented in most ophiolites of Phanerozoic and Proterozoic ages (24, 25). This finding is also consistent with fluid-inclusion studies on amygdales in the ISB pillow breccias that indicate alteration during early sea-floor-like hydrothermal metamorphism (26).

We provide three robust lines of evidence for an Isua ophiolite complex as a vestige of Archean supra-subduction-zone oceanic crust. First, the sheeted-dike complex and cogenetic pillow lavas represent the upper-crustal section of a dismem-

**Table 1.** Summary of  $\delta^{18}\text{O}$  results.

Sample	Type	$\delta^{18}\text{O}$ (standard mean ocean water)*
03-3.5	Pillow core	9.9
03-3.13	Pillow core	6.8
03-3.22	Pillow core	7.3
03-3.23	Pillow core	6.9
03-3.31	Pillow core	6.7
03-3.39	Pillow core	6.5
03-3.40	Pillow core	6.6
1A2-IG-06	Pillow core	6.8
1B4-IG-06	Pillow core	6.8
2A-IG-06	Pillow core	6.9
2B2A-IG-06	Pillow core	7.1
3A2A-IG-06	Pillow core	6.8
5B1-IG-06	Pillow core	7.9
5C-IG-06	Pillow core	7.6
6B-IG-06	Pillow core	6.8
7-IG-06	Dike	5.9
8-IG-06	Dike	6.0
9-IG-06	Dike	6.1
16A-IG-06	Dike	6.0
16C-IG-06	Dike	6.3
16E-IG-06	Dike	6.9
16G-IG-06	Dike	6.9
17A-IG-06	Dike	5.8
17B-IG-06	Dike	5.7

\*See SOM.

bered ophiolite. The sheeted-dike complex provides compelling structural evidence of horizontal extension by dike injection at a spreading ridge (SOM). Second, we reject the scenario of dike injection above a plume head in a non-plate tectonic environment, given the oceanic island arc and MORB geochemical characteristics of the pillow lavas and dikes reported here, together with the data from (19). Further, the boninitic affinity of the central garbenschiefer (17) is similar to that of Phanerozoic supra-subduction-zone ophiolites with a protracted tectonomagmatic evolution history (20, 22). Third, the oxygen isotope compositions of the pillow lavas and dikes and their petrographic textures are compatible with sea-floor hydrothermal metamorphism at a spreading ridge. Although the strain history of these rocks is not yet sufficiently well known to permit a detailed reconstruction of the Isua ophiolite complex, we contend that the ISB preserves vestiges of Earth's oldest ophiolite and oceanic crust. This implies that sea-floor spreading and subduction processes of Phanerozoic-like plate tectonics were operating ~3.8 billion years ago, as proposed by Komiya *et al.* (12).

#### References and Notes

1. J. A. Pearce, *Geol. Soc. Am. Spec. Pap.* 373 (2003), p. 269.
2. Y. Dilek, *Geol. Soc. Am. Spec. Pap.* 373 (2003), p. 1.
3. M. J. Bickle, E. G. Nisbet, A. Martin, *J. Geol.* 102, 121 (1994).
4. W. B. Hamilton, *Geol. Soc. Am. Today* 13, 4 (2003).



5. R. J. Stern, *Geology* **33**, 557 (2005).
6. T. M. Kusky, J.-H. Li, R. D. Tucker, *Science* **292**, 1142 (2001).
7. M. Zhai, G. Zhao, Q. Zhang, *Science* **295**, 923a (2002).
8. T. M. Kusky, Ed., *Precambrian Ophiolites and Related Rocks* (Elsevier, Amsterdam, 2004).
9. M. J. de Wit, in *Developments in Precambrian Geology*, vol. 13, T. M. Kusky, Ed. (Elsevier, London, 2004), pp. 599–614.
10. A. P. Nutman, *Greenland Geol. Surv. Bulletin* 154 (1986).
11. M. T. Rosing, N. M. Rose, D. Bridgwater, H. S. Thomsen, *Geology* **24**, 43 (1996).
12. T. Komiyama et al., *J. Geol.* **107**, 515 (1999).
13. J. S. Myers, *Precambrian Res.* **105**, 129 (2001).
14. A. P. Nutman, V. C. Bennett, C. R. L. Friend, M. T. Rosing, *Chem. Geol.* **141**, 271 (1997).
15. M. T. Rosing, *Science* **283**, 674 (1999).
16. M. Boyet et al., *Earth Planet. Sci. Lett.* **214**, 427 (2003).
17. A. Polat, A. W. Hofmann, M. T. Rosing, *Chem. Geol.* **184**, 231 (2002).
18. A. P. Nutman, V. R. McGregor, C. R. L. Friend, V. C. Bennett, P. D. Kinny, *Precambrian Res.* **78**, 1 (1996).
19. A. Polat, A. W. Hofmann, *Precambrian Res.* **126**, 197 (2003).
20. Y. Dilek, M. J. F. Flower, *Geol. Soc. London Spec. Publ.* **218**, 43 (2003).
21. A. J. Crawford, Ed., *Boninites* (Unwin Hyman, London, 1989).
22. R. B. Pedersen, H. Furnes, *J. Geodyn.* **13**, 183 (1991).
23. K. Muehlenbachs, *Chem. Geol.* **145**, 263 (1998).
24. D. S. Stakes, H. P. Taylor Jr., *J. Geophys. Res.* **97**, 7043 (1992).
25. C. Holmden, K. Muehlenbachs, *Science* **259**, 1733 (1993).
26. J. L. R. Touret, *Precambrian Res.* **126**, 219 (2003).
27. Comments by Y. Dilek, B. Robins, N. McLoughlin, and two anonymous reviewers improved the manuscript. Financial support was provided by the Norwegian Research Council, the Geological Museum of Copenhagen, the GFZ-Potsdam, the Agouron foundation, and the National Sciences and Engineering Research Council of Canada. This is AEON contribution no. 31.

#### Supporting Online Material

www.sciencemag.org/cgi/content/full/315/5819/1704/DC1

SOM Text

Figs. S1 to S4

Table S1

References

21 December 2006; accepted 7 February 2007

10.1126/science.1139170

# Bottom-Up Determination of Air-Sea Momentum Exchange Under a Major Tropical Cyclone

Ewa Jarosz,\* Douglas A. Mitchell,† David W. Wang, William J. Teague

As a result of increasing frequency and intensity of tropical cyclones, an accurate forecasting of cyclone evolution and ocean response is becoming even more important to reduce threats to lives and property in coastal regions. To improve predictions, accurate evaluation of the air-sea momentum exchange is required. Using current observations recorded during a major tropical cyclone, we have estimated this momentum transfer from the ocean side of the air-sea interface, and we discuss it in terms of the drag coefficient. For winds between 20 and 48 meters per second, this coefficient initially increases and peaks at winds of about 32 meters per second before decreasing.

The air-sea momentum exchange under a tropical cyclone determines the oceanic response to its winds. An accurate estimation of the exchange hence is required for correctly forecasting storm track and intensity, as well as for accurately predicting storm surges, ocean currents, and waves, and for making hurricane risk assessments, particularly because the frequency and intensity of tropical cyclones are reportedly increasing (1). Conventional methods of determining the air-sea momentum transfer are from the atmospheric side of the interface and are based on measurements of wind profiles near the ocean surface or of wind turbulence (2). These methods, however, cannot work reliably for the extreme high-wind conditions of a major tropical cyclone, because wind measurements near the ocean interface are inevitably contaminated from intense breaking-wave activities and sea spray (3).

Most available field measurements of surface stress are for wind speeds ranging from 4 to

20  $\text{m s}^{-1}$ . The techniques employed estimate the interface momentum exchange as a wind stress,  $\tau_s$ , given by

$$\tau_s = \rho_{\text{air}} C_D |\mathbf{W}|^2 \quad (1)$$

where  $\rho_{\text{air}}$  is the air density,  $C_D$  is the drag coefficient, and  $|\mathbf{W}|$  is the velocity magnitude of the wind at a reference height (usually 10 m).

In open ocean conditions, as the wind becomes stronger the range of surface waves, which travel at slower speeds than the wind, widens. Accordingly,  $C_D$  increases as wind speed increases (3). This pattern of variability in  $C_D$  is commonly used in wave, surge, and circulation numerical models, which incorporate a monotonic increase of the drag coefficient with wind speed even under extreme wind conditions. Such an assumption may result in an overestimation of the air-sea momentum transfer and lead to unrealistic model predictions or, perhaps even worse, model tuning using bad physical justifications.

Recently, limited meteorological observations, theory, and experiments (3–8) suggest a reduction in the drag coefficient at high wind speeds, generally greater than 30  $\text{m s}^{-1}$ . All these efforts to evaluate the air-sea momentum exchange have been made through meteorological measurements, or theories and models developed

for the atmospheric boundary layer (“top-down” determination). Estimation of this exchange can also be done from the other side of the interface with full water-column ocean current observations. This method directly determines the stress at the interface based on ocean currents and provides a very reliable and accurate direct determination of the air-sea momentum transfer under high winds (3). However, this type of “bottom-up” determination imposes the almost impossible requirements of deploying instruments in the ocean directly under the highly unpredictable path of a major tropical cyclone and then having the instruments survive the enormous forces generated by the cyclone.

On 15 September 2004, the center of Hurricane Ivan (at category 4 strength) passed directly over six current and wave/tide gauge moorings on the outer continental shelf in the northeastern Gulf of Mexico (9–12) (Fig. 1). The instrumentation survived and measured nearly full ocean current velocity profiles directly under the cyclone. The resulting data set allows direct “bottom-up” determination of the air-sea momentum exchange under extreme wind conditions.

Extreme winds of a tropical cyclone elicit a four-stage response when passing over ocean waters (9, 13). The first three stages make up the “forced stage” response, whereas the fourth stage is the “relaxation stage.” Over the open ocean, the forced stage response is primarily baroclinic (depth-dependent), with a weak barotropic (depth-independent) response consisting of a trough in sea surface height and an associated geostrophic current that are set up almost instantly (13). Over the continental shelf, however, the forced response is quite different (9). It consists of a strong barotropic component that is not geostrophically balanced and a much weaker baroclinic response. Thus, the directly forced response on the continental shelf should be well described to the first order by the linear time-dependent depth-integrated horizontal momentum equations. Scaling analysis of current velocity measurements recorded in the northeastern Gulf of Mexico (Fig. 1) under Hurricane Ivan supports this assumption, especially for the along-

Naval Research Laboratory, Stennis Space Center, MS 39529–5004, USA.

\*To whom correspondence should be addressed. E-mail: ewa.jarosz@nrlssc.navy.mil

†Present address: Exxon Mobil Upstream Research Company, Houston, TX 77027–6019, USA.



**Fig. 1.** Regional map and instrument locations. Bathymetry (in meters) is shown for the north-eastern Gulf of Mexico. Acoustic Doppler current profiler (ADCP) moorings are denoted by black dots (M1 to M6). The yellow triangle is Buoy 42040, National Data Buoy Center. Hurricane Ivan's path is indicated by the dashed red line. Two inserts in the expanded map are a colored infrared image of Hurricane Ivan taken by the National Oceanic and Atmospheric Administration's Geostationary Operational Environmental Satellite-12 satellite (lower right) and a Barny mooring containing the ADCP current meter (upper right).

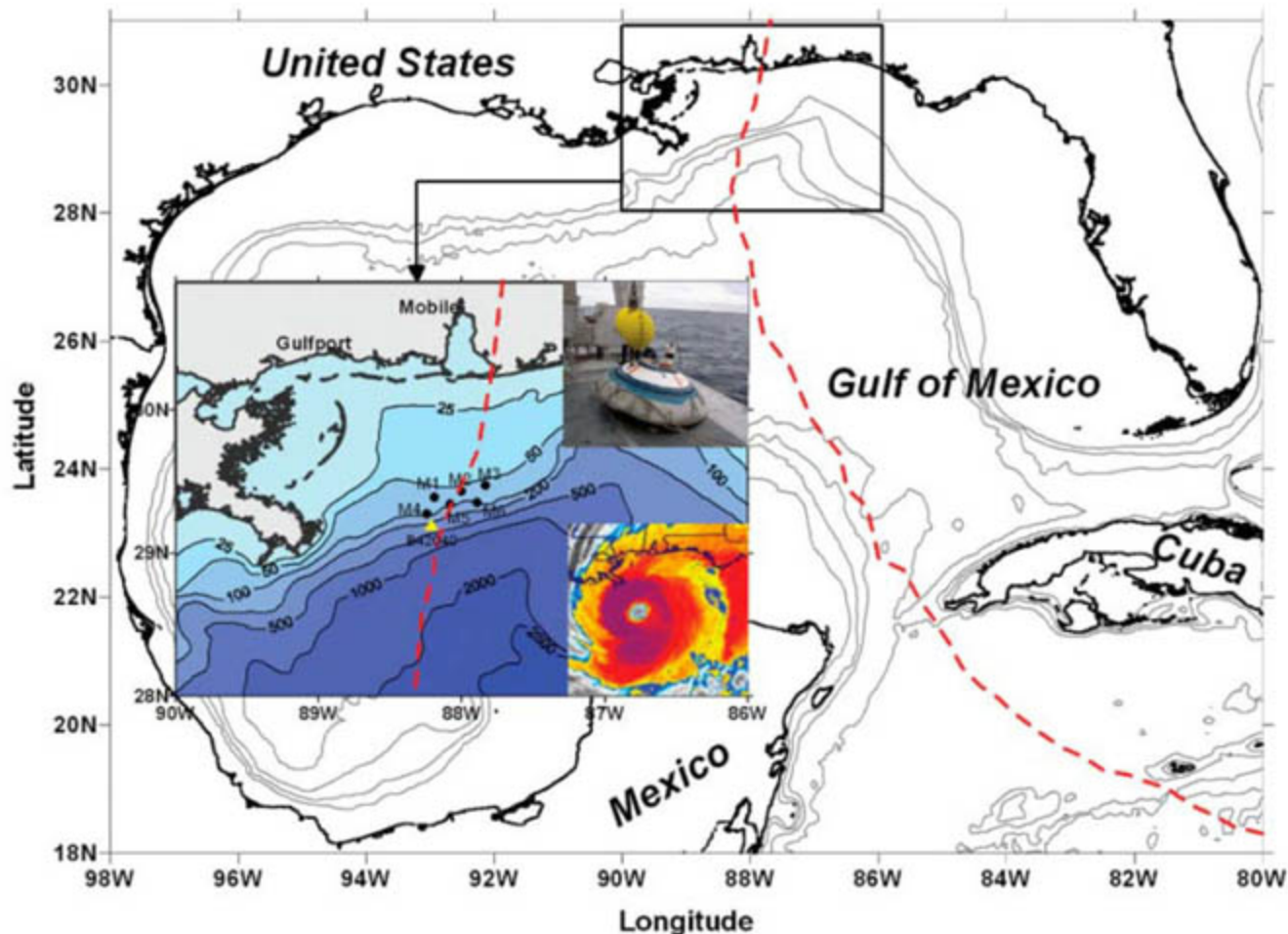
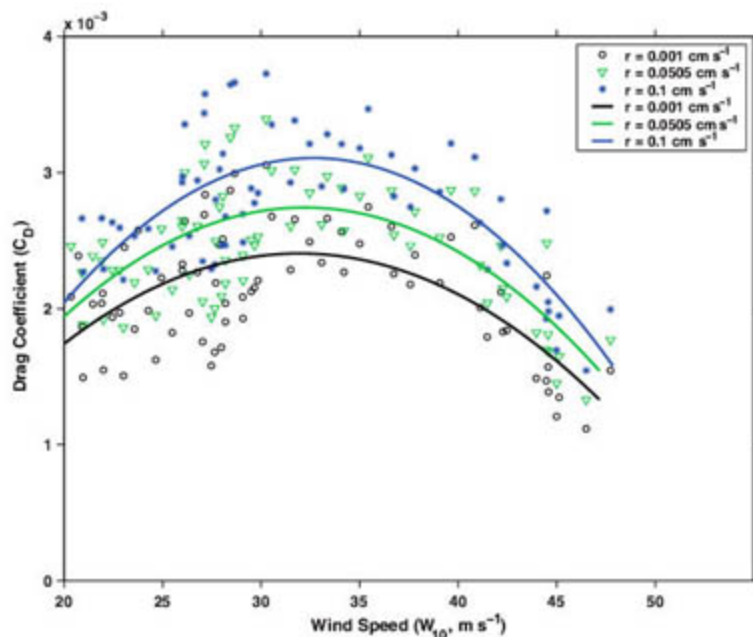


**Fig. 2.** Drag coefficient for several resistance coefficients.  $C_D$  is shown as a function of the wind speed at 10 m ( $W_{10}$ ) for several different resistance coefficients  $r$  (open black circles –  $r = 0.001 \text{ cm s}^{-1}$ ; green triangles –  $r = 0.0505 \text{ cm s}^{-1}$ ; blue asterisks –  $r = 0.1 \text{ cm s}^{-1}$ ). The solid lines represent quadratic curves fitted to the evaluated  $C_D$  separately for each  $r$ .



shelf momentum [more discussion concerning the along-shelf momentum balance is in (14)] given by

$$\frac{\partial U}{\partial t} - fV = \frac{\tau_{sx}}{\rho H} - \frac{rU}{H} \quad (2)$$

where  $\rho$  is a reference density ( $1025 \text{ kg m}^{-3}$ ),  $f$  is the Coriolis parameter ( $0.71 \times 10^{-4} \text{ s}^{-1}$ ),  $U$  and  $V$  are the depth-integrated along-shelf and cross-shelf velocity components,  $H$  is the water depth,  $r$  is a constant resistance coefficient at

the sea floor, and  $\tau_{sx}$  is the along-shelf wind stress.

The simplified dynamics given by Eq. 2 may not hold under all conditions. For instance, in this case, the momentum balance breaks down once the eye of the storm has passed over the moorings and the wind vectors rapidly rotate  $180^\circ$ . When this happens, the water column cannot respond and change direction as rapidly as the wind, and these dynamics no longer hold. Additionally, the momentum balance may not hold for a rapidly moving tropical cyclone or for a cyclone with an

erratic path for similar reasons. However, many cyclones move slowly and steadily enough over the shelf for such an approximation to hold.

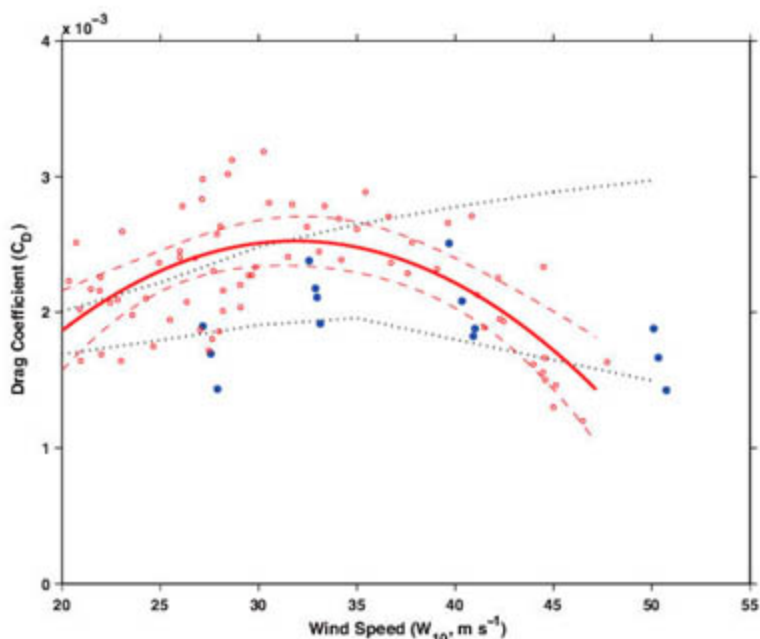
The air-sea momentum transfer, expressed in terms of  $\tau_{sx}$ , is estimated from Eq. 2 using our ocean current observations. In atmospheric studies, this exchange is commonly discussed in terms of the drag coefficient ( $C_D$ ). Wind stress ( $\tau_{sx}$ ) can be also defined as  $\tau_{sx} = \rho_{\text{air}} C_D |W| W_x$ , where  $W_x$  is the along-shelf wind velocity component. Thus, for comparison with other studies, we can determine  $C_D$  by inserting the formula for  $\tau_{sx}$  into Eq. 2.

$$C_D = \frac{\rho H}{\rho_{\text{air}} |W| W_x} \left( \frac{\partial U}{\partial t} - fV + \frac{rU}{H} \right) \quad (3)$$

Results produced from evaluation of Eq. 3 are shown in Figs. 2 and 3. The drag coefficient was derived for several different values of the resistance coefficient ( $r$ ) ranging between  $0.001 \text{ cm s}^{-1}$  and  $0.1 \text{ cm s}^{-1}$ . These values of  $r$  are similar to those used in other studies investigating shelf currents (15–18). Figure 2 displays estimates of  $C_D$  for minimum ( $0.001 \text{ cm s}^{-1}$ ), mean ( $0.0505 \text{ cm s}^{-1}$ ), and maximum ( $0.1 \text{ cm s}^{-1}$ ) values of  $r$  used in Eq. 3, whereas Fig. 3 shows results for  $r = 0.02 \text{ cm s}^{-1}$ , that is, the resistance coefficient that was determined from observations for the northeastern shelf of the Gulf of Mexico (15). The results, especially for the wind



**Fig. 3.** Drag coefficient as a function of wind speed.  $C_D$  is shown for an observation-based resistance coefficient,  $r = 0.02 \text{ cm s}^{-1}$ . The red open circles are the evaluated  $C_D$  from the current and wind observations, the solid red line is a fitted quadratic curve to the  $C_D$  estimates, and the red dashed lines are the 95% confidence limits for this quadratic curve. The black dotted lines represent the window for  $C_D$  reported in (6), whereas the blue dots represent  $C_D$  reported in (4).



speeds below  $30 \text{ m s}^{-1}$ , are somewhat noisy as a result of measurement uncertainty and the need to calculate a velocity derivative, which tends to enhance noise. However, they consistently show a decreasing trend of  $C_D$  for wind speeds greater than  $32 \text{ m s}^{-1}$ , the lower threshold for a category 1 hurricane on the Saffir-Simpson Scale. It is also apparent that the  $C_D$  values are weakly dependent on the choice of the resistance coefficient and are larger for increasing values of  $r$ . The drag coefficient estimates evaluated for  $r = 0.1 \text{ cm s}^{-1}$  are, on average, 20% greater than those calculated for  $r = 0.001 \text{ cm s}^{-1}$  from Eq. 3.

To produce the best representation of  $C_D$  for each  $r$ , a second-order curve (a function of the wind speed) was fitted by a least-squares technique to all estimated values of  $C_D$ . The curves are displayed in Figs. 2 and 3. Additionally, the 95% confidence limits for the fitted curve are shown in Fig. 3. The pattern of the relationship between  $C_D$  and the wind speed is robust, but the curve coefficients are determined by the value chosen for  $r$  in Eq. 3. However, all curves clearly show an initial increase of the drag coefficient and monotonic decrease as found by recent studies (3–8) after reaching a maximum value at  $\sim 32 \text{ m s}^{-1}$ . Some of these studies (3, 19) imply that the decreasing drag at high winds seems to be related to the spray, foam, and bubbles from breaking waves that reduce the drag and allow the hurricane to slip over the sea.

With the nearly full water-column ocean current measurements, the only unknown term left in the simplified equation of motion is the wind stress. Thus, the behavior of the drag coefficient ( $C_D$ ) can easily be estimated for a range of strong winds. Despite the fact that the drag coefficient is evaluated differently here, estimates of  $C_D$  determined “bottom-up” reasonably replicate the values determined “top-down” in recent studies (3–7). Results from our research show that  $C_D$  peaks at a wind speed near  $32 \text{ m s}^{-1}$  and

then steadily decreases as the wind speed continues to rise. Our values for  $C_D$  are in a range of  $C_D$  values found using meteorological observations (4) for wind speeds greater than  $32 \text{ m s}^{-1}$  but are higher for lower wind speeds. These differences may be attributed to uncertainties in the wind measurements and the applicability of the simplified ocean dynamics at the lower wind speeds.

#### References and Notes

1. K. Emanuel, *Nature* **436**, 686 (2005).
2. S. E. Larsen *et al.*, in *Wind Stress Over the Ocean*, I. S. F. Jones, Y. Toba, Eds. (Cambridge Univ. Press, New York, 2001), chap. 7.
3. M. A. Donelan *et al.*, *Geophys. Res. Lett.* **31**, L18306 10.1029/2004GL019460 (2004).

4. M. D. Powell, P. J. Vickery, T. A. Reinhold, *Nature* **422**, 279 (2003).
5. E. D. Fernandez *et al.*, *J. Geophys. Res.* **111**, C08013 10.1029/2005JC003048 (2006).
6. I. J. Moon, I. Ginis, T. Hara, *J. Atmos. Sci.* **61**, 2334 (2004).
7. J. A. T. Bye, A. D. Jenkins, *J. Geophys. Res.* **111**, C03024 10.1029/2005JC003114 (2006).
8. K. Emanuel, *J. Atmos. Sci.* **60**, 1420 (2003).
9. D. A. Mitchell, W. J. Teague, E. Jarosz, D. W. Wang, *Geophys. Res. Lett.* **32**, L11610 10.1029/2005GL023014 (2005).
10. D. W. Wang, D. A. Mitchell, W. J. Teague, E. Jarosz, M. S. Hulbert, *Science* **309**, 896 (2005).
11. W. J. Teague, E. Jarosz, D. W. Wang, D. A. Mitchell, *J. Phys. Oceanogr.*, in press.
12. W. J. Teague, E. Jarosz, M. R. Carnes, D. A. Mitchell, P. J. Hogan, *Cont. Shelf Res.* **26**, 2559 (2006).
13. J. F. Price, T. B. Sanford, G. Z. Forristall, *J. Phys. Oceanogr.* **24**, 233 (1994).
14. Materials and methods are available as supporting material on Science Online.
15. G. T. Mitchum, W. Sturges, *J. Phys. Oceanogr.* **12**, 1310 (1982).
16. S. T. Lentz, *J. Phys. Oceanogr.* **24**, 2461 (1994).
17. S. J. Lentz, *J. Phys. Oceanogr.* **31**, 2749 (2001).
18. J. M. Pringle, *J. Phys. Oceanogr.* **32**, 3101 (2002).
19. E. L. Andreas, *J. Phys. Oceanogr.* **34**, 1429 (2004).
20. We thank M. S. Hulbert, A. J. Quaid, and W. A. Goode for mooring support. We also thank the crews of the research vessels Seward Johnson I and II. This work was supported by the Office of Naval Research as a part of the Naval Research Laboratory's basic research project “Slope to Shelf Energetics and Exchange Dynamics (SEED)” under program element 0601153N, through the Minerals Management Service Environmental Studies Program Technology, and by the Minerals Management Service Technology Assessment and Research Program on Hurricane Ivan.

#### Supporting Online Material

www.sciencemag.org/cgi/content/full/315/5819/1707/DC1

SOM Text

Fig. S1

References

18 October 2006; accepted 14 February 2007

10.1126/science.1136466

## CRISPR Provides Acquired Resistance Against Viruses in Prokaryotes

Rodolphe Barrangou,<sup>1</sup> Christophe Fremaux,<sup>2</sup> H el ene Deveau,<sup>3</sup> Melissa Richards,<sup>1</sup> Patrick Boyaval,<sup>2</sup> Sylvain Moineau,<sup>3</sup> Dennis A. Romero,<sup>1</sup> Philippe Horvath<sup>2\*</sup>

Clustered regularly interspaced short palindromic repeats (CRISPR) are a distinctive feature of the genomes of most Bacteria and Archaea and are thought to be involved in resistance to bacteriophages. We found that, after viral challenge, bacteria integrated new spacers derived from phage genomic sequences. Removal or addition of particular spacers modified the phage-resistance phenotype of the cell. Thus, CRISPR, together with associated *cas* genes, provided resistance against phages, and resistance specificity is determined by spacer-phage sequence similarity.

**B**acteriophages are arguably the most abundant biological entity on the planet (1). Their ubiquitous distribution and abundance have an important impact on microbial ecology and the evolution of bacterial genomes (2). Consequently, bacteria have developed a variety of natural defense mechanisms that target diverse steps of the phage life cycle, notably blocking adsorption, preventing DNA

injection, restricting the incoming DNA, and abortive infection systems. These antiviral barriers can also be engineered and manipulated to better control phage populations (2, 3).

Numerous bacteria have been selected by humans and used extensively for fermentation and biotechnology processes. Unfortunately, domesticated bacteria used in industrial applications are often susceptible to phage attack, including



genera and species widely used as dairy cultures (4). Accordingly, the industry has devised various strategies to combat phage based on strain diversity, bacteriophage-insensitive mutants, and plasmids bearing phage-resistance mechanisms.

*Streptococcus thermophilus* is a low G+C Gram-positive bacterium and a key species exploited in the formulation of dairy culture systems for the production of yogurt and cheese. Comparative genomics analyses of closely related *S. thermophilus* strains have previously revealed that genetic polymorphism primarily occurs at hypervariable loci, such as the *eps* and *rps* operons, as well as two clustered regularly interspaced short palindromic repeats (CRISPR) loci (5–7). CRISPR loci typically consist of several noncontiguous direct repeats separated by stretches of variable sequences called spacers and are oftentimes adjacent to *cas* genes (CRISPR-associated). Although the function of CRISPR loci has not been established biologically, in silico analyses of the spacers have revealed sequence homology with foreign elements, including bacteriophage and plasmid sequences (7–9). Based exclusively on in silico analyses, several hypotheses have been put forward proposing roles for CRISPR and *cas* genes, which include providing immunity against foreign genetic elements via a mechanism based on RNA interference (10).

We analyzed the CRISPR sequences of various *S. thermophilus* strains, including closely related industrial strains and phage-resistant variants (fig. S1). Differences in the number and type of spacers were observed primarily at the CRISPR1 locus. Notably, phage sensitivity appeared to be correlated with CRISPR1 spacer content. Specifically, spacer content was nearly identical between parental strains and phage-resistant derivatives, except for additional spacers present in the latter. These findings therefore suggest a potential relation between the presence of additional spacers and the differences observed in the phage sensitivity of a given strain. This observation prompted us to investigate the origin and function of additional spacers present in phage-resistant mutants.

First, we tested the hypothesis that CRISPR loci are altered during the natural generation of phage-resistant mutants. A phage-host model system was selected, consisting of a phage-sensitive wild-type *S. thermophilus* strain widely used in the dairy industry, DGCC7710 [wild type (WT)] and two distinct but closely related virulent bacteriophages isolated from industrial yogurt samples, phage 858 and phage 2972 (11).

Nine phage-resistant mutants were generated independently by challenging the WT strain with phage 858, phage 2972, or simultaneously with both (12), and their CRISPR loci were analyzed. Differences were consistently observed at the CRISPR1 locus, where 1 to 4 additional spacers were inserted next to the 32 spacers present in the WT strain (Fig. 1). The addition of new spacers in response to phage infection seemed to be polarized toward one end of the CRISPR1 locus. This is consistent with previous observations of spacer hypervariability at the leader end of the CRISPR locus in various strains (9, 13). Sequence analysis of the additional spacers inserted

in the CRISPR1 locus of the various phage-resistant mutants revealed similarity to sequences found within the genomes of the phages used in the challenge (Fig. 2 and fig. S2). Interestingly, similarities were observed throughout the phage genomes, in most functional modules, both on the coding and noncoding strands. No particular sequence, gene, or functional group seemed to be targeted specifically. These results reveal that, on becoming resistant to bacteriophages, the CRISPR1 locus was modified by the integration of novel spacers, apparently derived from phage DNA.

Surprisingly, we observed that some strains were resistant to both phages, whereas others

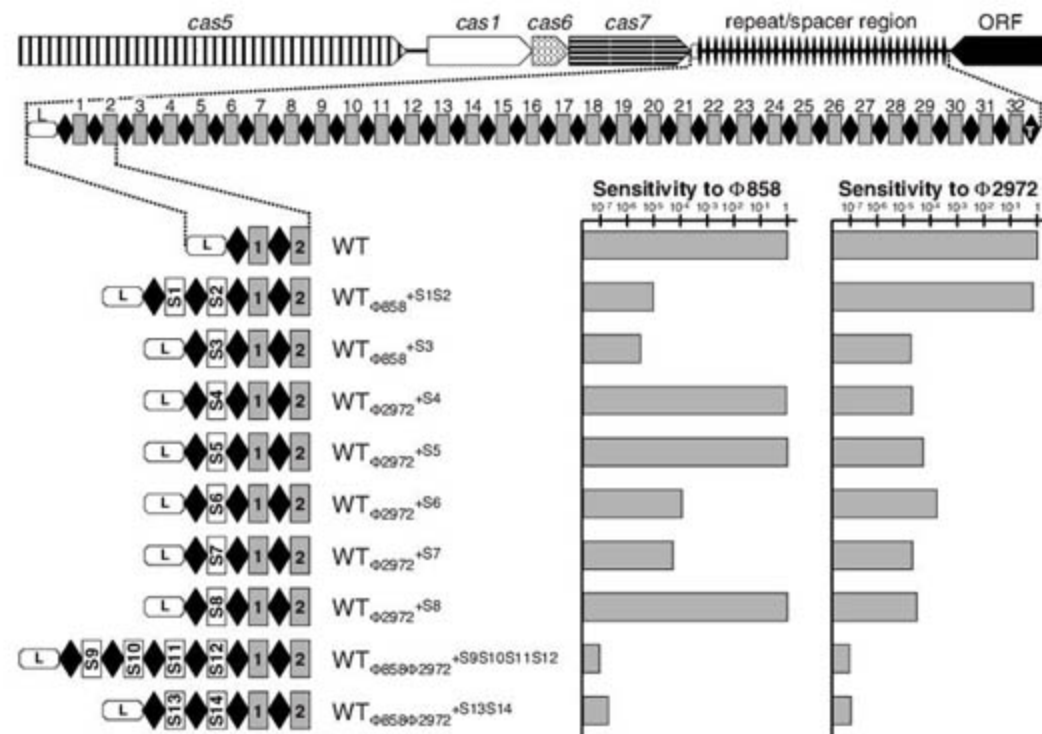


**Fig. 1.** *Streptococcus thermophilus* CRISPR1 locus overview, newly acquired spacers in phage-resistant mutants, and corresponding phage sensitivity. The CRISPR1 locus of DGCC7710 (WT) is at the top. The repeat-spacer region of WT is in the middle: repeats (black diamonds), spacers (numbered gray boxes), leader (L, white box), and terminal repeat (T, black diamond). (Bottom left) The spacer content on the leader side of the locus in phage-resistant mutants is detailed, with newly acquired spacers (white boxes, S1 to S14). (Bottom right) The sensitivity of each strain to phages 858 and 2972 is represented as a histogram of the efficiency of plaquing (EOP), which is the plaque count ratio of a mutant strain to that of the wild-type.

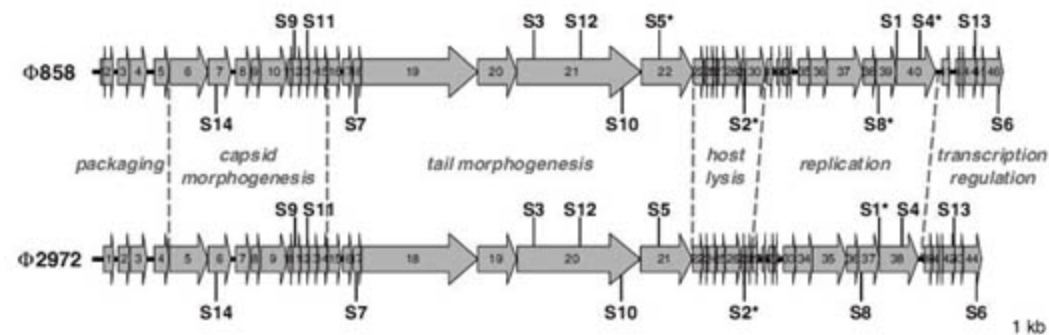


**Fig. 2.** *S. thermophilus* phage genome maps with the position of sequences similar to the acquired CRISPR1 spacers of the phage-resistant mutants. Spacers shown above and below the genome maps indicate that the spacer matches a sequence on the (+) and on the (-) strand, respectively. An asterisk indicates the existence of a SNP between the spacer sequence and that of the phage genome (fig. S1). The genome sequences of phage 2972 (accession number AY699705) and phage 858 are 93% identical.

<sup>1</sup>Danisco USA Inc., 3329 Agriculture Drive, Madison, WI 53716, USA. <sup>2</sup>Danisco France SAS, Boîte Postale 10, F-86220 Dangé-Saint-Romain, France. <sup>3</sup>Département de Biochimie et de Microbiologie, Faculté des Sciences et de Génie, Groupe de Recherche en Ecologie Buccale, Faculté de Médecine Dentaire, Félix d'Hérelle Reference Center for Bacterial Viruses, Université Laval, G1K 7P4 Québec, Canada.

\*To whom correspondence should be addressed. E-mail: philippe.horvath@danisco.com



were resistant only to the phage used in the challenge (Fig. 1). The phage-resistance profile seemed correlated to the spacer content, such that strains with spacers showing 100% identity to sequences conserved in both phages were resistant to both phages, such as spacers S3, S6, and S7. In contrast, when nucleotide polymorphisms were observed between the spacer and the phage sequence [from 1 to 15 single-nucleotide polymorphisms (SNPs) over 29 or 30 nucleotides], the spacer did not seem to provide resistance, such as spacers S1, S2, S4, S5, and S8 (Fig. 1 and fig. S2). In addition, when several spacers were inserted (S9 to S14), phage resistance levels were higher. These findings indicate that the CRISPR1 locus is subject to dynamic and rapid evolutionary changes driven by phage exposure. Altogether, these results reveal that CRISPR loci can indeed be altered during the generation of phage-resistant mutants and also establish a link between CRISPR content and phage sensitivity. These findings suggest that the presence of a CRISPR spacer identical to a phage sequence provides resistance against phages containing this particular sequence.

To determine whether CRISPR spacer content defines phage resistance, we altered the CRISPR1 locus by adding and deleting spacers (12) and tested subsequent strain sensitivity to phages. All constructs were generated and integrated into the *S. thermophilus* chromosome with the system developed by Russell and Klaenhammer (14). We removed the spacers and repeats in the CRISPR1 locus of strain WT<sub>Φ858</sub><sup>+S1S2</sup> and replaced them with a single repeat without any spacer (12). The resulting strain WT<sub>Φ858</sub><sup>+S1S2</sup>ΔCRISPR1 was sensitive to phage 858, which indicated that the phage resistance of the original phage-resistant mutant (WT<sub>Φ858</sub><sup>+S1S2</sup>) was probably linked to the presence of S1 and S2 (Fig. 3).

Further, to address the critical question of whether adding spacers provides novel phage resistance, we replaced the CRISPR1 locus of strain WT<sub>Φ2972</sub><sup>+S4</sup> with a version containing only spacers S1 and S2 (12) and tested whether the phage sensitivity was affected. Remarkably, the resulting strain WT<sub>Φ2972</sub><sup>+S4</sup>::pS1S2 gained resistance to phage 858, which suggested that these two spacers have the ability to provide phage resistance de novo (Fig. 3). Altogether,

these observed modifications establish the link between the CRISPR spacer content and phage resistance.

In the process of generating strain WT<sub>Φ858</sub><sup>+S1S2</sup>ΔCRISPR1, we created WT<sub>Φ858</sub><sup>+S1S2</sup>::pR, a variant that contains the integration vector with a single repeat inserted between the *cas* genes and the native CRISPR1 locus (Fig. 3). Unexpectedly, strain WT<sub>Φ858</sub><sup>+S1S2</sup>::pR was sensitive to phage 858, although spacers S1 and S2 remained on the chromosome (Fig. 3). Similarly, the WT<sub>Φ2972</sub><sup>+S4</sup>::pS1S2 construct lost the resistance to phage 2972, although spacer S4 is present in the chromosome (Fig. 3). These results indicated that spacers alone did not provide resistance, and perhaps, that they have to be in a particular genetic context to be effective.

Although initial work suggested involvement in DNA repair (15), the current hypothesis is that *cas* genes (5, 16) are involved in CRISPR-mediated immunity (10). Consequently, we inactivated two *cas* genes in strain WT<sub>Φ858</sub><sup>+S1S2</sup> (12): *cas5* (COG3513) and *cas7*, which are equivalent to *str0657/stu0657* and *str0660/stu0660*, respectively (6, 7). The *cas5* inactivation resulted in loss of the phage resistance (Fig. 3), and perhaps Cas5 acts as a nuclease, because it contains an HNH-type nuclease motif. In contrast, inactivating *cas7* did not alter the resistance to phage 858 (Fig. 3). Interestingly, we were repeatedly unable to generate CRISPR1 phage-resistant mutants from the *cas7* knock-out, perhaps because Cas7 is involved in the synthesis and/or insertion of new spacers and additional repeats.

When we tested the sensitivity of the phage-resistant mutants, we found that plaque formation was dramatically reduced, but that a relatively small population of bacteriophage retained the ability to infect the mutants. We further analyzed phage variants derived from phage 858 that retained the ability to infect WT<sub>Φ858</sub><sup>+S1S2</sup>. In particular, we investigated the sequence of the genome region corresponding to additional spacers S1 and S2 in two virulent phage variants. In both cases, the genome sequence of the phage variant had mutated, and two distinct SNPs were identified in the sequence corresponding to spacer S1 (fig. S3).

Overall, prokaryotes appear to have evolved a nucleic acid-based "immunity" system whereby specificity is dictated by the CRISPR spacer content, while the resistance is provided by the Cas enzymatic machinery. Additionally, we speculate that some of the *cas* genes not directly providing resistance are actually involved in the insertion of additional CRISPR spacers and repeats, as part of an adaptive "immune" response. Further studies are desired to better characterize the mechanism of action and to identify the specific function of the various *cas* genes. This nucleic acid-based system contrasts with amino acid-based counterparts in eukaryotes through which adaptive immunity is not inheritable.

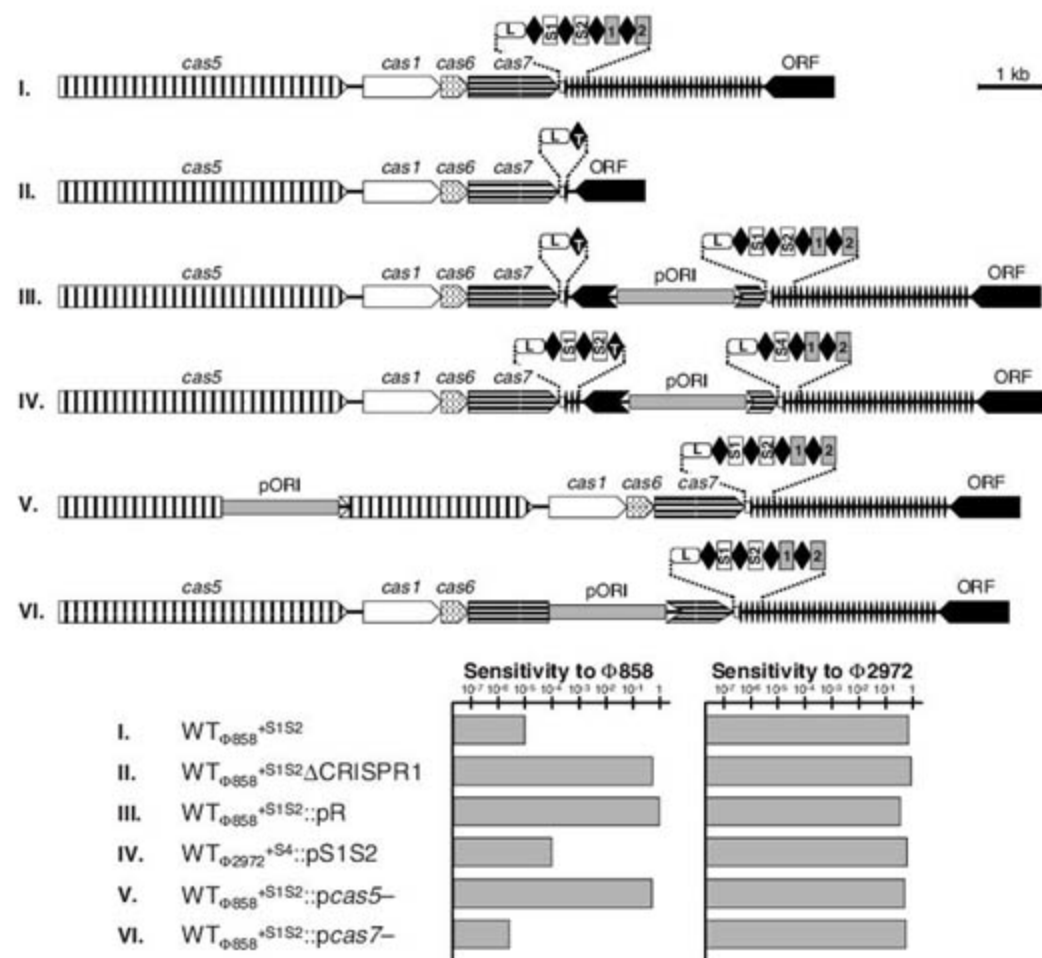


**Fig. 3.** CRISPR spacer engineering, *cas* gene inactivation, and corresponding phage sensitivity. I, mutant WT<sub>Φ858</sub><sup>+S1S2</sup>; II, mutant WT<sub>Φ858</sub><sup>+S1S2</sup>ΔCRISPR1 in which CRISPR1 was deleted; III, mutant WT<sub>Φ858</sub><sup>+S1S2</sup>::pR in which CRISPR1 was displaced and replaced with a unique repeat; IV, WT<sub>Φ2972</sub><sup>+S4</sup>::pS1S2, mutant of strain WT<sub>Φ2972</sub><sup>+S4</sup> in which CRISPR1 was displaced and replaced with a version containing S1 and S2; V, WT<sub>Φ858</sub><sup>+S1S2</sup>::*pcas5*- with *cas5* inactivated; VI, WT<sub>Φ858</sub><sup>+S1S2</sup>::*pcas7*- with *cas7* inactivated. pORI indicates the integrated plasmid (12). The phage sensitivity of each strain to phages 858 and 2972 is represented at the bottom as a histogram of the efficiency of plaquing (EOP).



The inheritable nature of CRISPR spacers supports the use of CRISPR loci as targets for evolutionary, typing, and comparative genomic studies (9, 17–19). Because this system is reactive to the phage environment, it likely plays a significant role in prokaryotic evolution and ecology and provides a historical perspective of phage exposure, as well as a predictive tool for phage sensitivity. The CRISPR-*cas* system may accordingly be exploited as a virus defense mechanism and also potentially used to reduce the dissemination of mobile genetic elements and the acquisition of undesirable traits such as antibiotic resistance genes and virulence markers. From a phage evolution perspective, the integrated phage sequences within CRISPR loci may also provide additional anchor points to facilitate recombination during subsequent phage infections, thus increasing the gene pool to which phages have access (20). Because CRISPR loci are found in the majority of bacterial genera and are ubiquitous in Archaea (5, 13, 21), their study will provide new insights into the relation and codirected evolution between prokaryotes and their predators.

## References and Notes

- M. Breitbart, F. Rohwer, *Trends Microbiol.* **13**, 278 (2005).
- S. Chibani-Chennoufi, A. Bruttin, M.-L. Dillmann, H. Brüssow, *J. Bacteriol.* **186**, 3677 (2004).
- J. M. Sturino, T. R. Klaenhammer, *Nat. Rev. Microbiol.* **4**, 395 (2006).
- H. Brüssow, *Annu. Rev. Microbiol.* **55**, 283 (2001).
- R. Jansen, J. D. A. van Embden, W. Gaastra, L. M. Schouls, *Mol. Microbiol.* **43**, 1565 (2002).
- A. Bolotin *et al.*, *Nat. Biotechnol.* **22**, 1554 (2004).
- A. Bolotin, B. Quinquis, A. Sorokin, S. D. Ehrlich, *Microbiology* **151**, 2551 (2005).
- F. J. M. Mojica, C. Díez-Villaseñor, J. García-Martínez, E. Soria, *J. Mol. Evol.* **60**, 174 (2005).
- C. Pourcel, G. Salvignol, G. Vergnaud, *Microbiology* **151**, 653 (2005).
- K. S. Makarova, N. V. Grishin, S. A. Shabalina, Y. I. Wolf, E. V. Koonin, *Biol. Direct* **1**, 7 (2006).
- C. Lévêque *et al.*, *Appl. Environ. Microbiol.* **71**, 4057 (2005).
- Information on materials and methods for the generation of phage-resistant mutants, engineering of CRISPR spacers (Figs. S4 and S5), and inactivation of *cas* genes is available on Science Online.
- R. K. Lillestøl, P. Redder, R. A. Garrett, K. Brügger, *Archaea* **2**, 59 (2006).
- W. M. Russell, T. R. Klaenhammer, *Appl. Environ. Microbiol.* **67**, 4361 (2001).
- K. S. Makarova, L. Aravind, N. V. Grishin, I. B. Rogozin, E. V. Koonin, *Nucleic Acids Res.* **30**, 482 (2002).
- D. H. Haft, J. Selengut, E. F. Mongodin, K. E. Nelson, *PLoS Comput. Biol.* **1**, e60 (2005).
- P. M. A. Groenen, A. E. Bunschoten, D. van Soolingen, J. D. A. van Embden, *Mol. Microbiol.* **10**, 1057 (1993).
- E. F. Mongodin *et al.*, *J. Bacteriol.* **187**, 4935 (2005).
- R. T. DeBoy, E. F. Mongodin, J. B. Emerson, K. E. Nelson, *J. Bacteriol.* **188**, 2364 (2006).
- R. W. Hendrix *et al.*, *Proc. Natl. Acad. Sci. U.S.A.* **96**, 2192 (1999).
- J. S. Godde, A. Bickerton, *J. Mol. Evol.* **62**, 718 (2006).
- We thank L. Bayer, C. Vos, and A.-C. Couët-Monvoisin of Danisco Innovation, as well as J. Labonté and D. Tremblay of Université Laval for technical support, and E. Bech Hansen for discussions and critical review of the manuscript. Also, we thank T. R. Klaenhammer for providing the integration system. This work was supported by funding from Danisco A/S. Also, S. M. would like to acknowledge support from the Natural Sciences and Engineering Research Council of Canada (NSERC) Discovery Program. Sequences were deposited in GenBank, accession numbers EF434458 to EF434504.

## Supporting Online Material

www.sciencemag.org/cgi/content/full/315/5819/1709/DC1

Materials and Methods

Figs. S1 to S5

References and Notes

29 November 2006; accepted 16 February 2007

10.1126/science.1138140

## A G Protein–Coupled Receptor Is a Plasma Membrane Receptor for the Plant Hormone Abscisic Acid

Xigang Liu,<sup>1,2</sup> Yanling Yue,<sup>1</sup> Bin Li,<sup>3</sup> Yanli Nie,<sup>1</sup> Wei Li,<sup>2</sup> Wei-Hua Wu,<sup>3</sup> Ligeng Ma<sup>1,2\*</sup>

The plant hormone abscisic acid (ABA) regulates many physiological and developmental processes in plants. The mechanism of ABA perception at the cell surface is not understood. Here, we report that a G protein–coupled receptor genetically and physically interacts with the G protein  $\alpha$  subunit GPA1 to mediate all known ABA responses in *Arabidopsis*. Overexpressing this receptor results in an ABA-hypersensitive phenotype. This receptor binds ABA with high affinity at physiological concentration with expected kinetics and stereospecificity. The binding of ABA to the receptor leads to the dissociation of the receptor-GPA1 complex in yeast. Our results demonstrate that this G protein–coupled receptor is a plasma membrane ABA receptor.

Abscisic acid (ABA) is an important hormone that mediates many aspects of plant growth and development, particularly in response to the environmental stresses (1–3). Several components involved in the ABA signaling pathway have been identified (4). Two recent reports have shown that the nuclear RNA binding protein flowering time control protein (FCA) (5) and the chloroplast protein Mg chelatase H subunit (6) are ABA receptors (6).

In contrast, several earlier experiments had suggested that extracellular perception is critical for ABA to achieve its functions (7–9). Thus, other ABA receptors, especially plasma membrane–localized receptors, may be the major players for perceiving extracellular ABA and mediating the classic ABA signaling responses.

Ligand-mediated signaling through G protein–coupled receptors (GPCRs) is a conserved mechanism for the extracellular signal perception at the plasma membrane in eukaryotic organisms (10). The GPCR-mediated signaling pathway plays a central role in vital processes such as vision, taste, and olfaction in animals (11). However, the higher plant *Arabidopsis thaliana* has only one canonical  $G\alpha$  (GPA1) subunit, one  $G\beta$  subunit, and two  $G\gamma$  subunits (12–16). The significance of these subunits in plant systems is poorly understood; only one

*Arabidopsis* putative GPCR protein (GCR1) has been characterized in plants (17–20), and no ligand has been defined for any plant GPCR.

To identify previously unrecognized GPCR proteins in *Arabidopsis*, we started by searching the *Arabidopsis* genome and found a gene (GCR2, GenBank accession code At1g52920) encoding a putative GPCR. Transmembrane structure prediction suggests that GCR2 is a membrane protein with seven transmembrane helices (fig. S1, A and B). The subsequent cellular localization analysis confirmed its plasma membrane localization in the transgenic plant root (fig. S1C). GCR2–yellow fluorescent protein (YFP) is detected in the membrane fraction isolated from the GCR2-YFP transgenic plant. Similar to GCR1 (19), GCR2 is mostly associated with the membrane fraction (fig. S1D). Furthermore, even after washing with detergent or a higher pH buffer, GCR2 is retained with the membrane fraction, suggesting that GCR2 is an integral membrane protein (fig. S1D).

One feature of the GPCR is its ability to interact with G protein to form a complex. To confirm the physical interaction between GCR2 and  $G\alpha$ , we used four different approaches to detect their interaction. We first used surface plasmon resonance spectroscopy to investigate the interaction between GCR2 and GPA1. For this purpose, we expressed and purified recombinant GCR2 and GPA1 proteins in bacteria (fig. S2). This *in vitro* assay clearly indicated that GPA1 is capable of binding to GCR2, whereas no binding activity was detected between GPA1 and bovine serum albumin (BSA) (fig. S3, A and B). The dissociation binding constant ( $K_d$ ) for GCR2 and GPA1 is  $2.1 \times 10^{-9}$  M (fig. S3C).

<sup>1</sup>National Institute of Biological Sciences, 7 Science Park Road, Zhongguancun Life Science Park, Beijing 102206, China.

<sup>2</sup>Laboratory of Molecular and Cellular Biology, Hebei Normal University, Shijiazhuang, Hebei 050016, China. <sup>3</sup>State Key Laboratory of Plant Physiology and Biochemistry, College of Biological Sciences, China Agricultural University, Beijing 100094, China.

\*To whom correspondence should be addressed. E-mail: maligeng@nibs.ac.cn



The commonly used yeast two-hybrid system does not work for the GCR2-GPA1 interaction assay because of their membrane localization, so we used a split-ubiquitin system (21) instead to investigate the GCR2-GPA1 interaction in yeast. This assay confirmed the reported interaction of the full-length GCR1 with GPA1 (19), and the full-length GCR2 also interacted with GPA1 (fig. S4A). The interaction was abolished when the C terminus of the receptor was blocked by fusing the ubiquitin fragment (CubPLV) to the C terminus of GCR2 (fig. S4A). We also found that the C terminus of GCR2 (C<sub>290-401</sub>, containing the free C terminus and the predicted third cytoplasmic loop) interacted with GPA1, whereas the N terminus (N<sub>1-289</sub>) of GCR2 did not (fig. S4, B and C), indicating that the C terminus of GCR2 is necessary and sufficient for its interaction with GPA1.

Bimolecular fluorescence complementation was used to detect the interaction between GCR2 and GPA1 in plant cells. GCR2 and GPA1 interacted in *Arabidopsis* protoplasts (Fig. 1A). Removal of the C terminus of GCR2 (C<sub>290-401</sub>) abolished the interaction (Fig. 1, A and B). This indicated that the interaction between GCR2 and GPA1 is specific and that the C terminus of GCR2 is necessary for its interaction with GPA1. We also confirmed their *in vivo* interaction by a coimmunoprecipitation assay. GCR2 and GPA1 can be coimmunoprecipitated; and we could detect GPA1 in the immunocomplex precipitated with an antibody to FLAG from GCR2-FLAG transgenic plants (Fig. 1C). Thus, results from four distinct assays all supported the interaction between GCR2 and GPA1.

To analyze the function of GCR2 in *Arabidopsis*, we characterized three independent *Arabidopsis* lines harboring the transferred DNA insertions in the *GCR2* locus, *gcr2-1*, *gcr2-2*, or *gcr2-3* (fig. S5). Transcript analysis by reverse transcription polymerase chain reaction (RT-PCR) detected no full-length *GCR2* transcripts in any of the three mutant alleles, but all had the truncated transcripts (fig. S5).

*Arabidopsis* seeds require desiccation or dormancy to prevent premature germination before harvesting. The freshly harvested wild-type seeds seldom germinate; however, freshly harvested seeds from all three alleles of *gcr2* plants germinated well under the same condition (Fig. 2A), indicating that the seeds from *gcr2* mutants lost seed dormancy. The seed dormancy is mainly controlled by phytohormone ABA. This result suggested that *gcr2* mutants are defective in ABA signaling. We therefore reasoned that the mutations in *GCR2* lead to a decreased sensitivity to ABA. We examined other ABA responses in both wild-type and *gcr2* plants. We first checked the effect of *GCR2* mutations on seed germination in the presence of ABA and found that all three *gcr2* mutants were insensitive, whereas the seeds from *GCR2* overexpressor lines were hypersensitive to the ABA-inhibition compared with the wild-type

seeds (Fig. 2B). We also found that the seedling growth inhibition by ABA was substantially reduced in the *gcr2* mutants, but increased in *GCR2* overexpressor lines compared with that of the wild type (Fig. 2C). In the absence of ABA, the *gcr2* seedlings developed normally and were indistinguishable from the wild-type seedlings (Fig. 2C). ABA mediates plant development by controlling the expression of ABA-mediated genes, and we thus compared the expression of ABA marker genes in wild-type and *gcr2* plants. Three well-known ABA marker genes, *RD29A*, *KIN1*, and *ABI5*, were tested. This analysis confirmed that the expression of ABA marker genes was substantially repressed in the *gcr2* mutants (fig. S6).

The ABA-induced closing and ABA-inhibited opening of stomata are classical ABA responses. We observed that both ABA-induced stomata closing and ABA-inhibited stomata opening were insensitive in *gcr2* compared with *gcr2* sensitivity in wild-type plants (Fig. 2, D and E), and the stomata width is larger in *gcr2* plants than in wild-type plants (Fig. 2E). ABA regulates inward K<sup>+</sup> (K<sub>in</sub><sup>+</sup>) channels to control the stomatal aperture (22, 23). To determine whether GCR2 mediates the ABA regulation of K<sub>in</sub><sup>+</sup> channels in stomatal guard cells, we applied patch-clamping techniques to analyze the whole-cell K<sub>in</sub><sup>+</sup> currents in guard cells from wild-type and *gcr2-1* plants. ABA inhibited K<sub>in</sub><sup>+</sup> currents in wild-type guard cells but had no effect on the K<sub>in</sub><sup>+</sup> currents in *gcr2-1* guard cells (Fig. 2F), thus indicating the involvement of GCR2-mediated K<sub>in</sub><sup>+</sup> in ABA-induced stomatal closure. We also found that stomata from *GCR2*-overexpressing plants were hypersensitive to ABA-induced closure

compared with the sensitivity of the wild-type plants (Fig. 2G). The stomata closure defects resulted in a greater water loss in the leaves of the three *gcr2* alleles compared with that in wild-type leaves, whereas water loss was reduced in *GCR2*-overexpressing plant leaves (fig. S7). All of these results indicate that *gcr2* plants are insensitive to ABA, whereas *GCR2*-overexpressing plants are hypersensitive to ABA, demonstrating the involvement of GCR2 in all major ABA responses in *Arabidopsis*.

The *gcr2* plants exhibit all known major ABA defects. The GPA1 null mutant (*gpa1*) is also defective in ABA-induced stomatal opening and inward K<sub>in</sub><sup>+</sup>-channel regulation in guard cells (22). Expression pattern analysis shows that *GCR2* and *GPA1* share a very similar expression pattern (fig. S8, A and B). We also examined the functional significance of GCR2-GPA1 interaction by checking the ABA response in the *gcr2gpa1* or overexpressor of *GCR2* or *GPA1* in different genetic background using stomatal closure as an assay. We found that GPA1 was involved in both ABA-controlled stomatal opening and closing (Fig. 2E and fig. S8, C to E). The defect exhibited by *gcr2gpa1* in ABA-induced stomatal closure was similar to the defect exhibited by *gcr2* or *gpa1* (fig. S8C). Transgenic lines overexpressing *GCR2* or *GPA1* were hypersensitive to the ABA response; however, the effects caused by the overexpression of *GCR2* or *GPA1* were dependent on GPA1 or GCR2, respectively (fig. S8, B, C, and E), indicating that GCR2 and GPA1 function together to transduce the ABA signal.

Given that *gcr2* exhibits defects in all known ABA responses and that GCR2 is a plasma

**Fig. 1.** Physical interaction between GCR2 and GPA1. (A) Bimolecular fluorescence complementation assays indicating the interaction of GCR2: hemagglutinin (HA) with a C-terminal HA tag, but not the corresponding C-terminal deletion construct GCR2IL:HA (N<sub>1-289</sub>) with GPA1 *in vivo*. Auto-, autofluorescence. The scale bar represents 20 μm. (B) The GCR2:HA-YFP<sup>C</sup>, GCR2IL:HA-YFP<sup>C</sup>, and GPA1:cMYC-YFP<sup>N</sup> proteins were expressed in the protoplast. Proteins from *Arabidopsis* protoplasts expressing GCR2:HA-YFP<sup>C</sup>, GCR2IL:HA-YFP<sup>C</sup>, or GPA1:cMYC-YFP<sup>N</sup> were extracted and the sample was analyzed on a 12% SDS-polyacrylamide gel electrophoresis gel. GCR2 or GPA1 was detected with the use of anti-HA for GCR2-YFP<sup>C</sup> or GCR2IL-YFP<sup>C</sup>, or anti-c-Myc for GPA1-YFP<sup>N</sup>. (C) Coimmunoprecipitation (Co-IP) assays verifying the interaction between GCR2 and GPA1 in planta. Total proteins from wild-type (Col-0) and *GCR2:FLAG* transgenic plants were used for *in vivo* Co-IP with antibodies to FLAG. Immunoprecipitated proteins were probed with antibodies (α) to GPA1 and to FLAG. An anti-FLAG cross-reacting band is shown as the loading control.

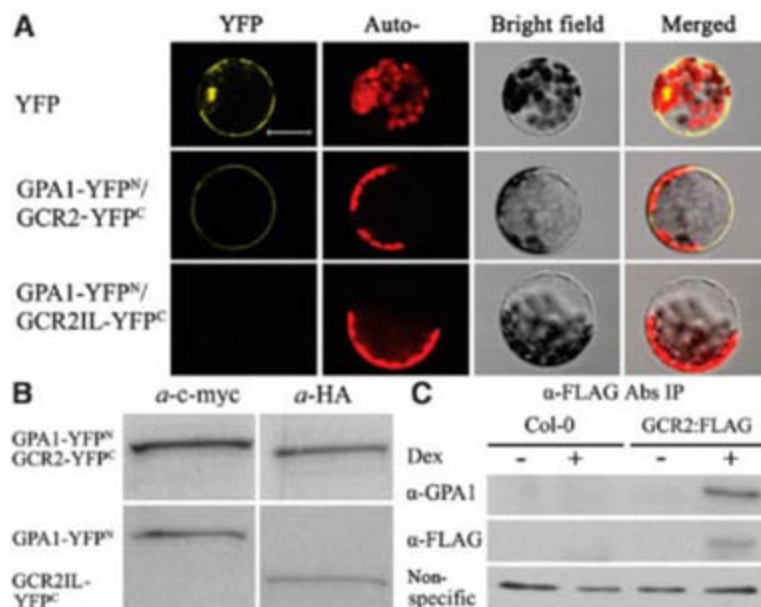
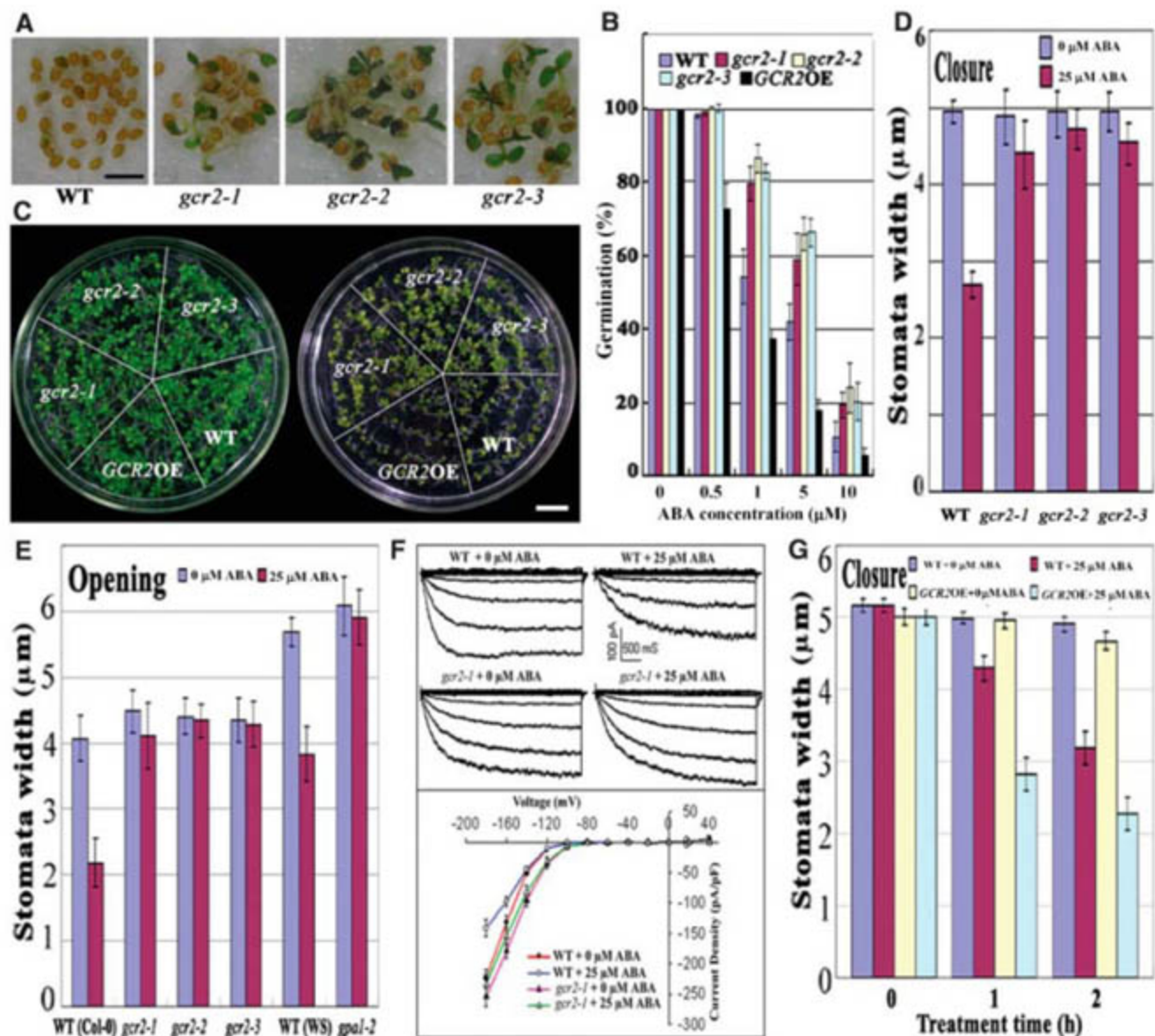




**Fig. 2.** The *gcr2* mutants exhibit all known ABA defects. **(A)** The *gcr2* seeds lose the seed dormancy observed in the wild type (WT). Freshly harvested seeds germinated on water-soaked filter paper for 7 days. The scale bar represents 2 mm. **(B)** The *gcr2* seeds are insensitive to ABA-inhibited seed germination (mean  $\pm$  SD;  $n = 4$ ). The germination percentage was determined 3 days after growing in 1/2 Murashige and Skoog (MS) media. **(C)** The seedling development in *gcr2* is insensitive to ABA. Seeds were grown on 1/2 MS media with (right) or without (left) 0.3  $\mu$ M ABA for 10 days. *GCR2*OE, *GCR2* overexpressor line. The scale bar represents 1 cm. **(D)** The *gcr2* plants show defects in ABA-induced stomatal closure (mean  $\pm$  SD;  $n = 3$ ). **(E)** The *gcr2* and *gpa1* plants are insensitive to ABA for stomatal opening (mean  $\pm$  SD;  $n = 3$ ). WS, Wassilewskija. **(F)** The inward  $K^+$  channel in *gcr2* guard cells is insensitive to ABA. The data in the graph (bottom) are presented as mean  $\pm$  SE ( $n = 4, 3, 5,$  and  $6$  for wild type, wild type+ABA, *gcr2-1*, and *gcr2-1*+ABA, respectively). **(G)** Overexpressor of *GCR2* confers increased ABA sensitivity for stomatal closure (mean  $\pm$  SD;  $n = 3$ ).



membrane receptor, we examined whether *GCR2* is an ABA receptor. For this purpose, we first checked whether *GCR2* could bind ABA. We observed that ABA bound to *GCR2* but did not bind to denatured *GCR2* protein (Fig. 3A). As a positive and negative control, ABA also bound to FCA but not BSA or GPA1 (Fig. 3A). The binding of ABA to *GCR2* protein is dependent on pH, and the optimum pH is between 7.0 and 7.5 (fig. S9). Stereospecificity of *GCR2* binding to the biologically active (+)-ABA was tested in competition assays. Trans-ABA and (-)-ABA analogs did not compete for the *GCR2*-binding site (Fig. 3B).

The specific binding of ABA to purified *GCR2* could be saturated with increasing amounts of ABA (Fig. 3C). Scatchard plot analysis exhibits a linear pattern (Fig. 3D), suggesting a single binding site for ABA in *GCR2*. The equilibrium dissociation constant ( $K_d$ ) for the *GCR2*-ABA complex is 20.1 nM (Fig. 3D), which is consistent with the physiological concentration range of ABA in plants.

Ligand binding to the GPCR induces the dissociation of the GPCR-G protein complex to

release  $G\alpha$  and the  $G\beta\gamma$  dimer, thus activating the downstream signaling events (16, 24). To test whether the binding of ABA to *GCR2* could dissociate the *GCR2*-GPA1 complex, we used the split-ubiquitin system to reconstitute this initial ABA signaling event in yeast. Application of the physiologically active form of ABA [(+)-ABA or (+)-ABA] indeed disrupted the *GCR2*-GPA1 interaction, whereas the physiologically inactive forms of ABA analogs [(-)-ABA or trans-ABA] did not affect the interaction between *GCR2* and GPA1, as indicated in the coimmunoprecipitation assay (Fig. 3E). This result again clearly confirmed that the binding of ABA to *GCR2* is stereospecific.

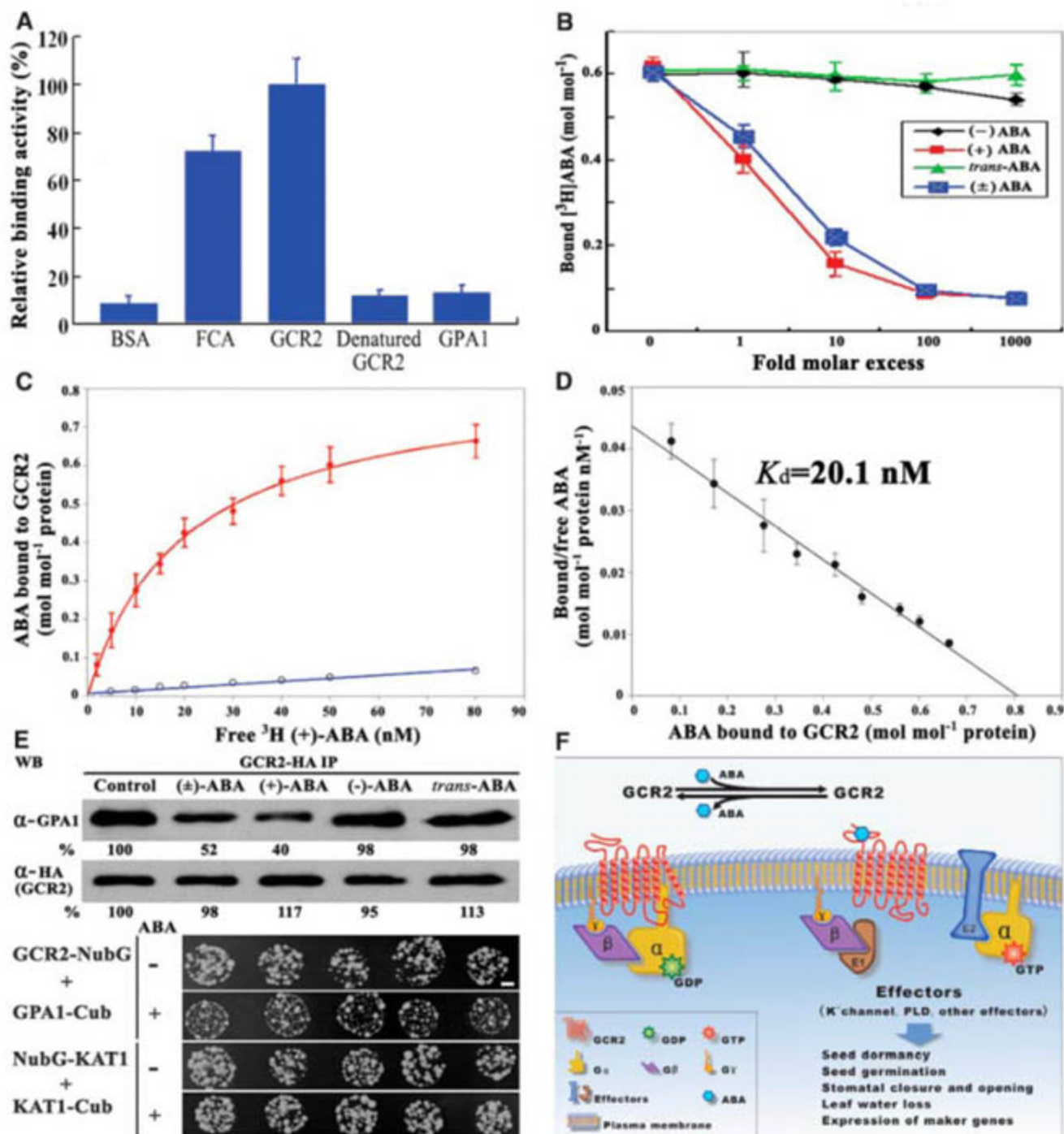
In the split-ubiquitin yeast protein interaction assay, the downstream reporter genes (*HIS3*, *ADE2*, and *lacZ*) were activated if the two assayed proteins interacted with each other (21). We reasoned that the binding of ABA to *GCR2* could repress the expression of reporter genes as a result of the dissociation of *GCR2* and GPA1. This prediction was verified (fig. S10). The addition of a physiologically active

form of ABA repressed *lacZ* expression, whereas physiologically inactive forms of ABA [(-)-ABA or trans-ABA] did not (fig. S10). As a control, ABA did not affect the expression of the reporter gene in a reconstituted  $K^+$  ATPASE1 (*KAT1*)-*KAT1* pathway in the same split-ubiquitin system (fig. S10). In addition, the expression of another two reporter genes, *HIS3* and *ADE2*, was necessary for yeast proliferation in a selection medium. The addition of ABA substantially repressed the proliferation of yeast expressing *GCR2* and GPA1, but did not affect yeast proliferation in expressing *KAT1*-*KAT1* system (Fig. 3E). Together, these results indicated that the effect of ABA on reporter gene expression was specific for the *GCR2*-GPA1 interaction, further supporting that the binding of ABA to *GCR2* results in the dissociation of the *GCR2*-GPA1 complex.

Terrestrial plants are immobile and incapable of escaping unfavorable environmental conditions such as drought or cold. Instead, they rely heavily on ABA to survive these conditions. Thus, how plants perceive and transduce the



**Fig. 3.** Binding of ABA to GCR2. **(A)** ABA binds to the purified GCR2 protein (mean  $\pm$  SD;  $n = 3$ ). **(B)** GCR2 binding of ABA is stereospecific (mean  $\pm$  SD). **(C)** ABA binding to GCR2 behaves according to saturation kinetics. The specific and nonspecific bindings are represented by top and bottom curves, respectively (mean  $\pm$  SD;  $n = 5$ ). **(D)** Scatchard plot analysis of ABA binding shows a linear relationship with the square of the correlation coefficient  $r^2 = 0.99$ , and maximum binding is  $0.8 \text{ mol mol}^{-1}$  protein with  $K_d = 20.1 \text{ nM}$  (mean  $\pm$  SD;  $n = 5$ ). **(E)** ABA disrupts the GCR2-GPA1 interaction in yeast. (Top) Co-IP assay. After  $10 \mu\text{M}$  ABA was added to the medium for 20 min, proteins were isolated. The relative intensity of the immunosignal to the control is indicated by the number below each band. WB, Western blot. (Bottom) Yeast growth assay. The proliferation was observed 7 days after the addition of  $10 \mu\text{M}$  ( $\pm$ )-ABA and  $1 \text{ mM}$  methionine. NubG, ubiquitin N terminus / 13 G mutation. The scale bar represents 2 mm. **(F)** Schematic model for GCR2-mediated ABA signaling pathway. GDP, guanosine diphosphate; GTP, guanosine 5'-triphosphate; PLD, phospholipase D.



ABA signal is a fundamental question. It has been shown that GPA1 was involved in ABA-mediated stomatal response and seed germination (19, 22, 25); a putative GPCR GCR1 interacted with GPA1 to negatively regulate ABA signaling (19). We now describe the characterization of a new GPCR, GCR2, in *Arabidopsis*. We conclude that GCR2 is a major ABA receptor on the basis of the following evidence: (i) Loss-of-function *gcr2* exhibits all known ABA defects; (ii) an overexpressor of GCR2 shows an ABA-hypersensitive phenotype; (iii) GCR2 binds ABA with a high affinity and reasonable dissociation constants, and the binding is stereospecific and abides by receptor kinetics; (iv) GCR2 is localized in the plasma membrane; (v) GCR2 genetically and physically interacts with GPA1; and (vi) the binding of ABA to

GCR2 disrupts GCR2-GPA1 interaction. Notably, the *gcr2* mutants still display ABA responses. This may be due to the weak nature of the mutations (fig. S5) or functional redundancy with GCR2-related proteins, given that there are two other *GCR2* homologous genes in the *Arabidopsis* genome. Consistent with this latter possibility, the semidominant phenotype and partial complementation of *gcr2* by *GCR2* cDNA expression (fig. S11) suggests the possible interference between GCR2 and its homologs.

The following model of ABA signaling can be envisaged. A GPCR, GCR2, which is a plasma membrane-localized ABA receptor, interacts with the  $G\alpha\beta\gamma$  complex. Binding of ABA to GCR2 results in the release of the G protein and dissociation of the heterotrimeric complex into  $G\alpha$  and the  $G\beta\gamma$  dimer to activate downstream ABA ef-

factors and to trigger the ABA responses (Fig. 3F). Thus, our results identified an ABA receptor and its target protein, a heterotrimeric G protein.

#### References and Notes

- R. R. Finkelstein, S. L. Gampala, C. D. Rock, *Plant Cell* **14**, 515 (2002).
- J. Leung, J. Giraudat, *Annu. Rev. Plant Physiol. Plant Mol. Biol.* **49**, 199 (1998).
- J. I. Schroeder, J. M. Kwak, G. J. Allen, *Nature* **410**, 327 (2001).
- J. K. Zhu, *Annu. Rev. Plant Biol.* **53**, 247 (2002).
- F. A. Razem, A. El-Kereamy, S. R. Abrams, R. D. Hill, *Nature* **439**, 290 (2006).
- Y. Y. Shen *et al.*, *Nature* **443**, 823 (2006).
- B. E. Anderson, J. Ward, J. Schroeder, *Plant Physiol.* **104**, 1177 (1994).
- S. Gilroy, R. Jones, *Proc. Natl. Acad. Sci. U.S.A.* **89**, 3591 (1992).
- E. Jeannette *et al.*, *Plant J.* **18**, 13 (1999).



10. K. L. Pierce, R. T. Premont, R. J. Lefkowitz, *Nat. Rev. Mol. Cell Biol.* **3**, 639 (2002).
11. A. M. Spiegel, L. S. Weinstein, *Annu. Rev. Med.* **55**, 27 (2004).
12. H. Ma, M. Yanofsky, E. M. Meyerowitz, *Proc. Natl. Acad. Sci. U.S.A.* **87**, 3821 (1990).
13. H. Ma, *Plant Mol. Biol.* **26**, 1611 (1994).
14. M. G. Mason, J. Botella, *Proc. Natl. Acad. Sci. U.S.A.* **97**, 14784 (2000).
15. M. G. Mason, J. R. Botella, *Biochim. Biophys. Acta* **1520**, 147 (2001).
16. A. M. Jones, S. A. Assmann, *EMBO Rep.* **5**, 572 (2004).
17. S. Plakidou-Dymock, D. Dymock, R. Hooley, *Curr. Biol.* **8**, 315 (1998).
18. G. Colucci, F. Apone, N. Alyeshmerni, D. Chalmers, M. J. Chrispeels, *Proc. Natl. Acad. Sci. U.S.A.* **99**, 4736 (2002).
19. S. Pandey, S. M. Assmann, *Plant Cell* **16**, 1616 (2004).
20. S. M. Assmann, *Science* **310**, 71 (2005).
21. P. Obrdlík et al., *Proc. Natl. Acad. Sci. U.S.A.* **101**, 12242 (2004).
22. X.-Q. Wang, H. Ullah, A. M. Jones, S. M. Assmann, *Science* **292**, 2070 (2001).
23. J. M. Ward, Z. M. Pei, J. I. Schroeder, *Plant Cell* **7**, 833 (1995).
24. S. R. Sprang, *Annu. Rev. Biochem.* **66**, 639 (1997).
25. S. Pandey, J. G. Chen, A. M. Jones, S. M. Assmann, *Plant Physiol.* **141**, 243 (2006).
26. We thank D. Y. Sun for his support; X. W. Deng and J. M. Zhou for their comments and discussion; W. Frommer and P. Obrdlík for making the split-ubiquitin system available; J. Kuala for making the split-YFP system available; J. Chai for his technical assistance and advice for the protein purification; and D. Zhang, Y. Shen, and

F. Razem for their suggestions on the ABA binding assay. This work was supported by the Ministry of Science and Technology of China (to L.M., 2003AA210120), National Science Foundation of China for Outstanding Young Scientists (to L.M., 30025024) and the Chinese National Key Basic Research Project (to W.W., 2006CB100100).

### Supporting Online Material

[www.sciencemag.org/cgi/content/full/1135882/DC1](http://www.sciencemag.org/cgi/content/full/1135882/DC1)

Materials and Methods

Figs. S1 to S11

References

3 October 2006; accepted 24 January 2007

Published online 8 March 2007;

10.1126/science.1135882

Include this information when citing this paper.

## Tunability and Noise Dependence in Differentiation Dynamics

Gürol M. Süel,<sup>1</sup> Rajan P. Kulkarni,<sup>2</sup> Jonathan Dworkin,<sup>3</sup> Jordi Garcia-Ojalvo,<sup>4</sup> Michael B. Elowitz<sup>2\*</sup>

The dynamic process of differentiation depends on the architecture, quantitative parameters, and noise of underlying genetic circuits. However, it remains unclear how these elements combine to control cellular behavior. We analyzed the probabilistic and transient differentiation of *Bacillus subtilis* cells into the state of competence. A few key parameters independently tuned the frequency of initiation and the duration of competence episodes and allowed the circuit to access different dynamic regimes, including oscillation. Altering circuit architecture showed that the duration of competence events can be made more precise. We used an experimental method to reduce global cellular noise and showed that noise levels are correlated with frequency of differentiation events. Together, the data reveal a noise-dependent circuit that is remarkably resilient and tunable in terms of its dynamic behavior.

Three aspects of genetic circuits control dynamic cellular behaviors: the circuit architecture or pattern of regulatory interactions among genetic elements; quantitative parameter values, such as promoter strengths; and stochastic fluctuations, or “noise,” associated with the concentration of cellular components. A fundamental biological question is how these three aspects of genetic circuits combine to determine cellular behavior, its variability, and its potential to evolve (1).

Competence in *B. subtilis* is a stress response that allows cells to take up DNA from the environment (2, 3). Differentiation into competence is transient (Fig. 1A) (4). The genetic basis for this behavior is a circuit involving *comK* and *comS* (Fig. 1B). The transcription factor ComK is necessary and sufficient for differentiation into competence (5, 6). ComK positively autoregulates its

own expression but is degraded by the ClpP-ClpC-MecA protease complex (Fig. 1B) (7–9). ComS competitively inhibits this degradation and is repressed in competent cells, forming a negative feedback loop (4, 10, 11). The circuit operates as

an excitable system in which a relatively small perturbation induces a larger and stereotyped response, as occurs with action potentials in neurons, for example (4, 12). Competence events occur only in a fraction of cells and may be driven by noise in underlying circuit components (4, 7, 8, 13).

Two key characteristics of competence are its probability of initiation,  $P_{\text{init}}$ , and the mean duration of transient competence events,  $\tau_{\text{comp}}$  (Fig. 1A).  $P_{\text{init}}$  denotes the chance per cell division that an individual cell will become competent. Competence events can be quantified by automated time-lapse fluorescence microscopy using fluorescent reporter genes under the control of the ComK-specific *comG* promoter and the *comS* promoter (denoted  $P_{\text{comG}}$  and  $P_{\text{comS}}$ , respectively) (4).

Two parameters that are expected to affect the behavior of the circuit are the basal expression rates of *comK* and *comS*, denoted by  $\alpha_K$  and  $\alpha_S$ , respectively (Fig. 1B and Eq. S1). To manipulate these parameters, we chromosomally integrated an additional copy of either *comS* or *comK* under the control of an inducible promoter, denoted  $P_{\text{hyp}}$ , generating the Hyper- $\alpha_S$  and Hyper- $\alpha_K$

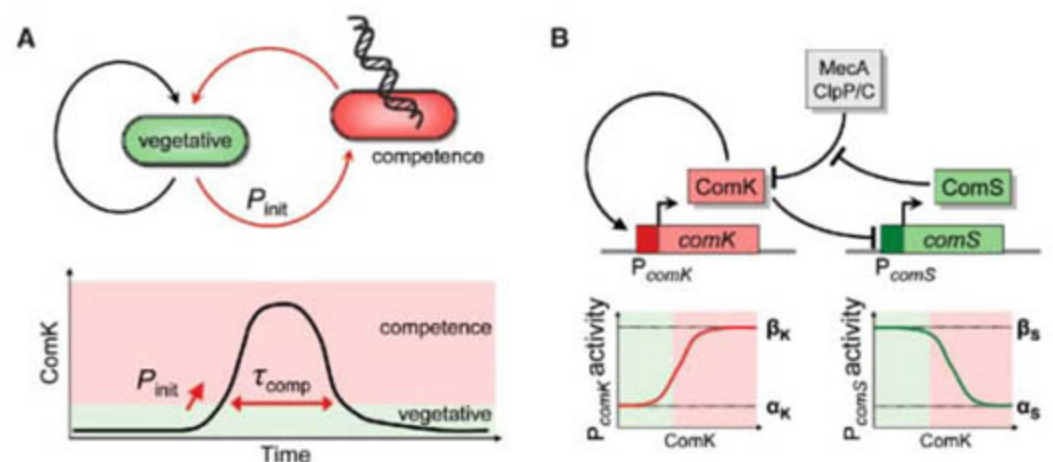


**Fig. 1.** Competence is a probabilistic and transient differentiation process regulated by a genetic circuit. (A) The rate of entering the competent state from the vegetative state is denoted by  $P_{\text{init}}$ . The amount of time spent in the competent state is denoted by  $\tau_{\text{comp}}$ . The ComK transcription factor concentration is high (pink region) when cells are competent and low (green region) when they are growing vegetatively. (B) Map of the core competence circuitry. Key features include positive transcriptional autoregulation of *comK* and a negative feedback loop in which ComK inhibits (possibly indirectly) expression of ComS, which in turn interferes with degradation of ComK. The graphs below the  $P_{\text{comK}}$  and  $P_{\text{comS}}$  promoters define parameters used in the text: Expression rates change from  $\alpha_K$  to  $\beta_K$  and  $\beta_S$  to  $\alpha_S$  respectively, as ComK concentration increases during competence.

<sup>1</sup>Green Center Division for Systems Biology and Department of Pharmacology, University of Texas Southwestern Medical Center, Dallas, TX 75390, USA. <sup>2</sup>Division of Biology and Department of Applied Physics, California Institute of Technology, Pasadena, CA 91125, USA. <sup>3</sup>Department of Microbiology, College of Physicians and Surgeons, Columbia University, New York, NY 10032, USA. <sup>4</sup>Departament de Física i Enginyeria Nuclear, Universitat Politècnica de Catalunya, Colom 11, E-08222 Terrassa, Spain.

\*To whom correspondence should be addressed. E-mail: melowitz@caltech.edu



strains, respectively [see Supporting Online Material (SOM) text]. To systematically scan a range of values for  $\alpha_K$  and  $\alpha_S$ , we made time-lapse fluorescence movies of these strains on media containing different concentrations of the inducer isopropyl- $\beta$ -D-thiogalactopyranoside (IPTG) (Fig. 2, A and B).

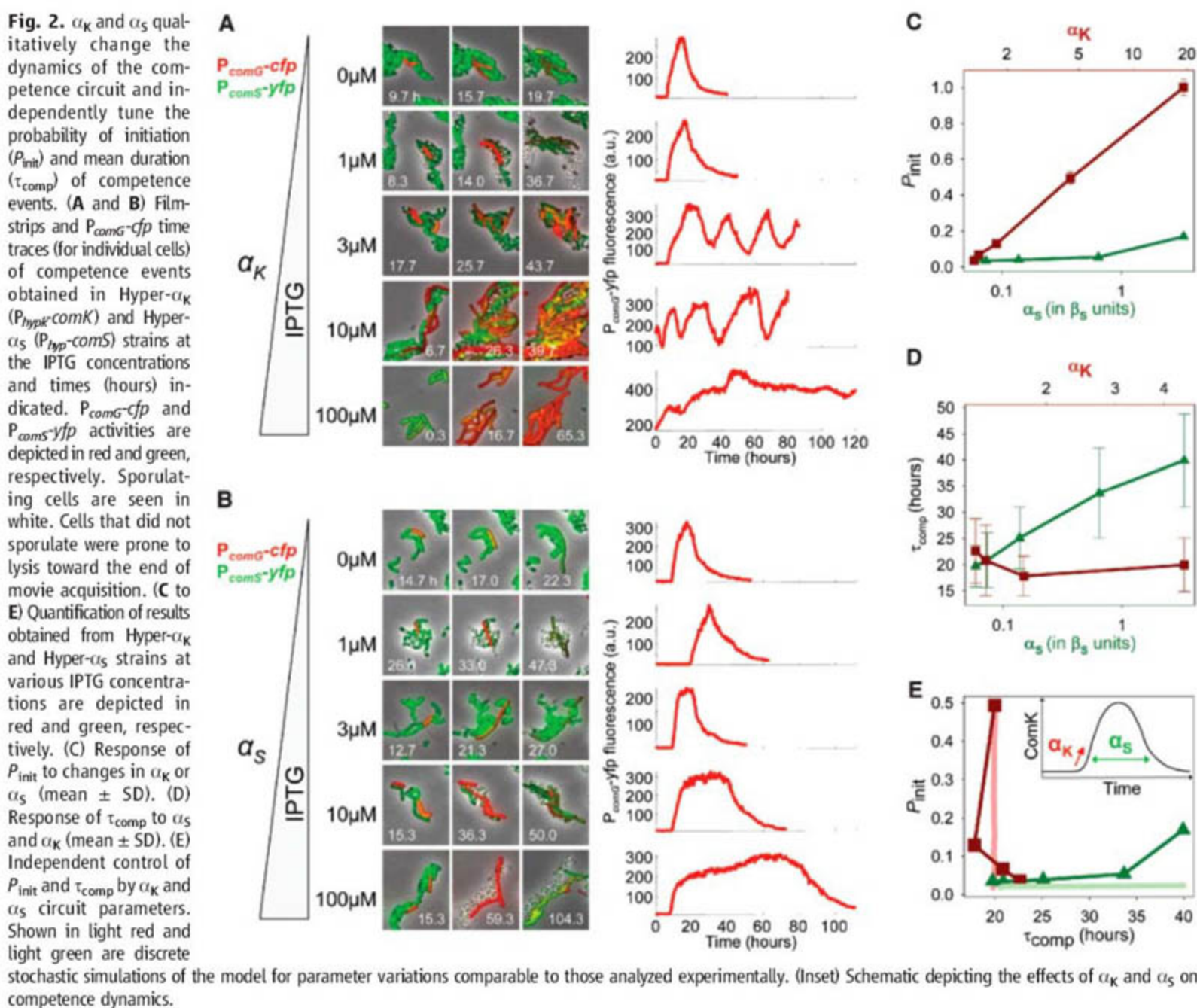
We investigated how  $\alpha_K$  and  $\alpha_S$  combine to regulate  $P_{init}$ . Without IPTG,  $P_{init}$  was  $\sim 3\%$  in the Hyper- $\alpha_K$  strain, unchanged from its wild-type value.  $P_{init}$  increased rapidly with basal *comK* expression (Fig. 2C). Increased expression of *comK* in the Hyper- $\alpha_K$  strain also showed a transition to an oscillatory regime, in which cells repeatedly went in and out of the competent state (Fig. 2A). At  $\alpha_K \sim 20$  times its wild-type value,  $\alpha_K^{wt}$ , all cells entered competence (Fig. 2, A and C). *ComS*, like *ComK*, is necessary for competence. However, expression of *P<sub>hyp-comS</sub>* had a modest effect on initiation, increasing  $P_{init}$  to  $\sim 20\%$  (Fig. 2C). Thus,  $P_{init}$  was predominantly regulated by  $\alpha_K$  rather than  $\alpha_S$ .

We next considered the effects of the same perturbations on  $\tau_{comp}$ . Increasing  $\alpha_K$  up to  $\sim 4.5 \times \alpha_K^{wt}$  caused no increase in  $\tau_{comp}$  (Fig. 2D). On the other hand, in the Hyper- $\alpha_S$  strain,  $\tau_{comp}$  increased with increasing expression of *P<sub>hyp-comS</sub>* (Fig. 2D). Thus,  $\tau_{comp}$  was predominantly regulated by  $\alpha_S$  rather than  $\alpha_K$ . Together, these results show that  $P_{init}$  and  $\tau_{comp}$  can be tuned independently by  $\alpha_K$  and  $\alpha_S$ , respectively (Fig. 2E).

To better understand the effect of *comS* expression on  $\tau_{comp}$ , we constructed a "6 $\times$ S" strain in which *P<sub>comS-comS</sub>* was expressed from a low-copy number plasmid, effectively increasing the activated production rate,  $\beta_S$ , by a factor of 6 over its wild-type value,  $\beta_S^{wt}$ . Unlike *P<sub>hyp-comS</sub>*, this construct retains the regulation found in the wild-type *P<sub>comS</sub>* promoter, including its negligible basal expression rate,  $\alpha_S^{wt}$ . Despite this increase in  $\beta_S$ , excitable behavior was maintained, as  $53 \pm 5\%$  ( $n = 79/151$ ) of competent cells successfully exited the competent state, compared with  $61\% \pm 7\%$  ( $n = 83/136$ ) of wild-type cells. By contrast,

increasing  $\alpha_S$  to  $\sim 3 \times \beta_S^{wt}$  in the Hyper- $\alpha_S$  strain prevented the majority of competent cells from exiting [ $21.3 \pm 5\%$  ( $n = 26/122$ ) of competent cells exited (table S4)]. The repressibility of the natural *P<sub>comS</sub>* promoter is thus critical for maintaining excitability (4). These results show that excitability can be reliably maintained over a broad range of  $\beta_S$  values.

To better understand independent tuning of  $P_{init}$  and  $\tau_{comp}$ , as well as reliable maintenance of excitability, we developed a model of the core interactions in the competence regulation circuitry (Fig. 1B and SOM text). We used stochastic simulations to account for intrinsic noise of biochemical reactions (14). We also analyzed the corresponding continuous model to determine parameter dependence and to identify a biologically reasonable parameter regime in which the discrete model produced results consistent with experiments. We required the continuous model to remain in the excitable regime as the  $\beta_S$  value was varied by a factor of 6





and we required its stochastic counterpart to generate the observed independent tunability of  $P_{init}$  and  $\tau_{comp}$ . We identified a parameter set that accounts for both maintenance of excitability at high  $\beta_S$  and independent tunability by  $\alpha_S$  and  $\alpha_K$ . Analysis of the model is described in detail in the SOM text (15).

Within the model, increasing  $\alpha_K$  increased the probability that vegetative cells reach the minimum concentration of ComK necessary to initiate competence, explaining the strong effect of  $\alpha_K$  on  $P_{init}$  (Fig. S5). Increasing  $\alpha_S$ , on the other hand, did not raise  $P_{init}$  arbitrarily high because initiation of competence is limited by fluctuations in ComK expression (Fig. 2E and fig. S6).

In the model, we also analyzed  $\tau_{comp}$ . Exit from competence requires ComS to be degraded. When the basal production rate of ComK is less than its activated production rate ( $\alpha_K < \beta_K$ ), ComS degradation, and thus  $\tau_{comp}$ , is unaffected. On the other hand, as  $\alpha_S$  is increased from zero, production of ComS offsets its degradation, prolonging competence duration.

Consistent with experimental results, in the model increasing  $\alpha_K$  switches the system from excitable to oscillatory dynamics, further distinguishing  $\alpha_K$  from  $\alpha_S$  (fig. S3). Increasing  $\alpha_S$  takes the system directly from excitability to a bistable regime in which  $P_{init} < 1$ , but, once initiated, most cells remain trapped in the competent state. This behavior was also observed in experiments where no oscillatory behavior was seen at intermediate  $\alpha_S$  values (Fig. 2B).

As in the experiments, cells in the model can become stuck in competence. When the basal production rate of ComK exceeds its activated production rate ( $\alpha_K > \beta_K$ ), ComK levels cannot be reduced in competence, and cells become trapped in the competent state. A similar effect occurs at high  $\alpha_S$  values, because a new stable state arises at competence-maintaining concentrations of ComK (Fig. S7). However, in this case, exit of competence remained possible as a result of noise, which destabilizes the newly formed competent state (see Section S1.4 of SOM text). This is consistent with experimental observations showing that, even at the highest induction levels in the Hyper- $\alpha_S$  strain, ~20% of cells successfully exited competence.

To explore the effects of perturbing the circuit architecture, we reengineered the competence circuit using Rok, a protein that binds to  $P_{comK}$  and represses its expression (16). We inserted a copy of *rok* under the control of  $P_{comG}$ , creating an additional negative feedback loop onto *comK* (Fig. 3A). In this "CompRok" strain, as expected,  $P_{init}$  remained unchanged from its wild-type values (~3%). The mean value of  $\tau_{comp}$ , on the other hand, was reduced, as was its cell-cell variability. In CompRok,  $\tau_{comp} = 13.9 \pm 3.4$  hours (mean  $\pm$  SD,  $n = 30$ ), compared with  $\tau_{comp} = 20.2 \pm 9.9$  hours (mean  $\pm$  SD,  $n = 31$ ) in wild type (Fig. 3B). This reduction in cell-cell variability showed that the precision of  $\tau_{comp}$  can be improved over its wild-type value. In the

model (Fig. 3B, insets), this result can be explained as follows: Exit from competence occurs when the absolute number of ComS molecules is

very low and the relative size of stochastic fluctuations therefore increases. These effects increase the variability in  $\tau_{comp}$ . In the CompRok strain,

**Fig. 3.** Architectural change to the MeKS circuit reduces variability of competence durations ( $\tau_{comp}$ ). (A) Competence circuit was rewired to introduce an additional transcriptional negative feedback loop onto *comK*, generating the CompRok strain. (B) Fluorescence time traces, normalized by their maximum value, from  $P_{comG}$ -*cfp* in the CompRok strain or the wild type. Traces have been aligned with respect to time of initiation of  $P_{comG}$  expression. For each panel, corresponding discrete stochastic simulations of CompRok and wild-type competence circuits are shown as insets.

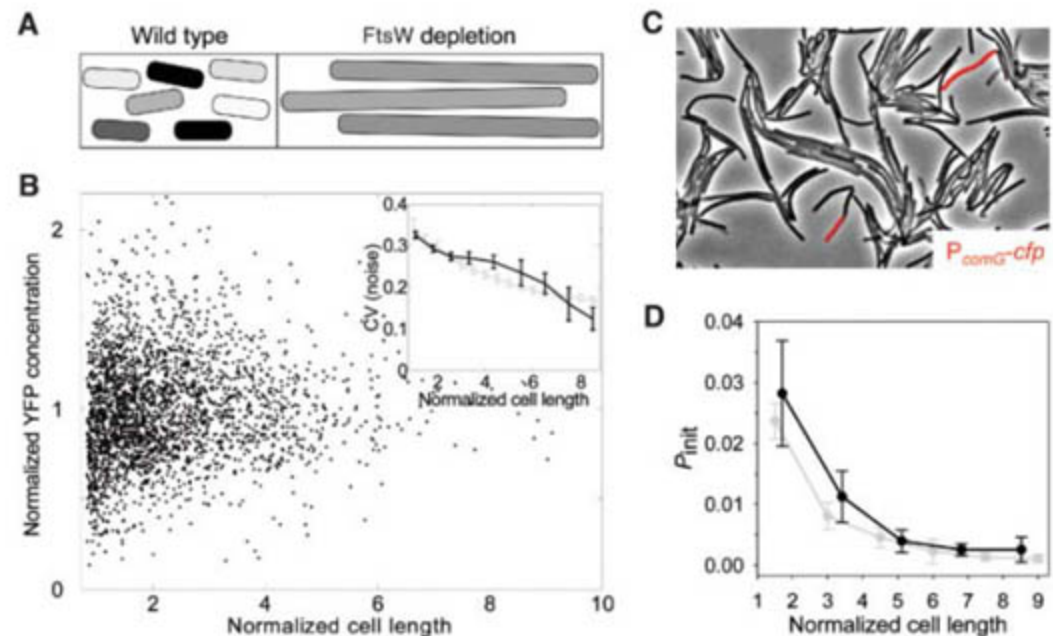
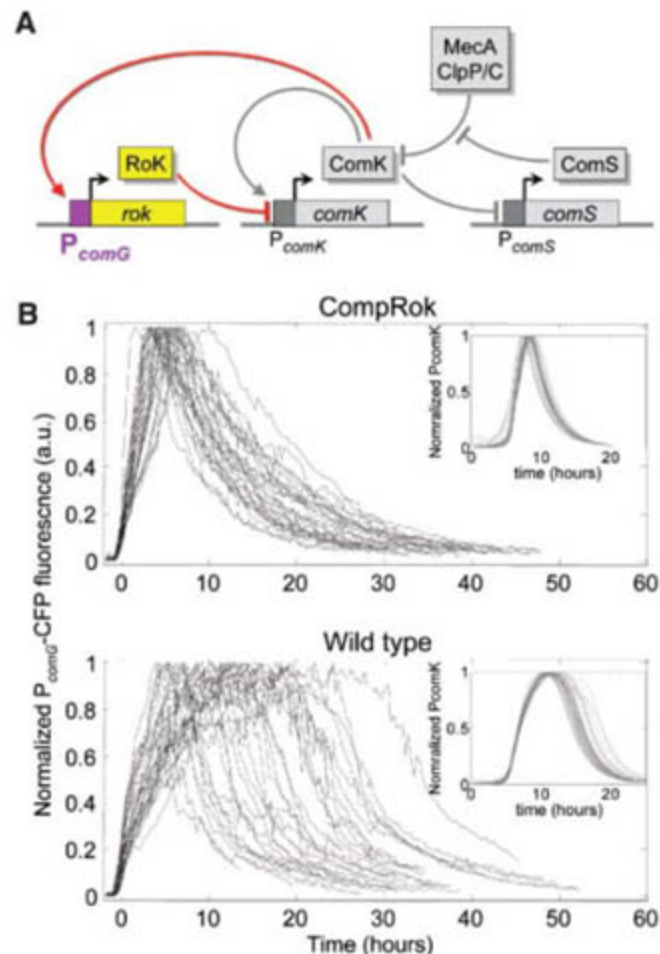


**Fig. 4.** Noise in gene expression and probability of competence initiation ( $P_{init}$ ) decreases with increasing cell length. (A) Cell-cell variation in gene expression (shades of gray) is expected to decrease in elongated conditional *ftsW* mutant cells compared with wild-type cells. (B) Noise decreases with increasing cell length: Dots represent  $P_{hyp-yfp}$  expression (normalized by mean) and length of individual conditional *ftsW* mutant (Fli-H) cells induced with 5  $\mu$ M IPTG. (Inset) Coefficient of variation (CV) of  $P_{hyp-yfp}$  expression as a function of cell length (black) compared with discrete stochastic model prediction (gray). (C) Overlay of phase contrast and  $P_{comG}$ -*cfp* fluorescence (red) snapshots of Fli-SOG cells with increased cell length. (D) Experimentally determined  $P_{init}$  (black line) drops with increasing cell length consistent with discrete stochastic simulations (gray line). Error bars in (C) and (D) denote one SD. (See S3.4 SOM text for details on calculation of  $P_{init}$ .)



however, the additional negative feedback allows exit from competence to occur at higher ComS and Rok concentrations, reducing the sensitivity of  $\tau_{\text{comp}}$  to stochastic fluctuations (fig. S10).

It is not known whether competence initiation is controlled by noise, as in the model. To test the impact of noise on competence initiation, we set out to globally modulate the amount of noise in the cell. We used a *B. subtilis* strain in which the *ftsW* gene, which is necessary for septation, was replaced by an inducible copy. In the absence of inducer, septation was inhibited, resulting in elongated filamentous cells. Each filament was composed of multiple cell units, all sharing cytoplasm. Within a filament, diffusion is expected to effectively average cell contents, reducing noise in gene expression, without affecting mean concentrations of cellular components (Fig. 4A) (17). In some bacterial mutants that have elongated filamentous morphologies, cellular growth, nucleoid density, protein expression, and other physiological characteristics appear normal, even though cellular volume is greatly increased (fig. S12) (18–20). We integrated an inducible  $P_{\text{hyp}}::yfp$  construct and measured the effect of cell length on cell-cell fluctuations in yellow fluorescent protein (YFP) expression (Fig. 4B). We found that noise does indeed decrease with increasing length (Fig. 4B, inset). A simple model of transcription and translation (21–24) that incorporates the continuity of filamentous cell growth produced qualitatively similar results (Fig. 4B, inset, and SOM text). Thus, cell size can in this case be used to modulate gene expression noise.

How does noise affect the probability of initiation of competence? To answer this question, we induced filamentation in the conditional *ftsW* strain at the beginning of, or before, movie acquisition and quantified  $P_{\text{init}}$  as a function of cell length. We determined length distributions of cells at the moment they initiated competence, as detected by  $P_{\text{comG}}$  expression (Fig. 4C). As a comparison, we also measured length distributions for noncompetent cells at a similar distribution of times. We plotted the relative fraction of cells that initiated competence at a given length, compared with the total number of cells at that length. The results showed that  $P_{\text{init}}$  decreased as cells elongated (Fig. 4D and SOM text). A similar decrease in  $P_{\text{init}}$  was observed in corresponding simulations (Fig. 4D). To test if the reduction in  $P_{\text{init}}$  could be due to factors other than diminished noise, we examined two promoters,  $P_{\text{comS}}$  and  $P_{\text{spo0A}}$ , both strongly regulated under these conditions. *Spo0A* is a master regulator of sporulation, a competing starvation response, and high concentrations of *Spo0A* inhibit competence (3). Conversely,  $P_{\text{comS}}$  expression is necessary for competence. Mean expression of both  $P_{\text{comS}}$  and  $P_{\text{spo0A}}$  was unaffected by cell length (fig. S17). This supports the idea that gene expression levels are independent of cell length under these conditions and that  $P_{\text{init}}$  depends on noise.

Noise may play at least three different functional roles in competence. First, noise could be

responsible for the observed variability in duration. Second, noise may be necessary to maintain excitability over a wide parameter range, by inducing escape from states of high ComK concentration. Third, noise appears to have a pivotal role in competence initiation (Fig. 4D) and thus should be considered alongside genetic parameters and circuit architecture to comprehensively understand differentiation at the single-cell level.

Quantitative analysis of a genetic system beyond its normal operating regime, including gene expression strengths, circuit architecture, and noise levels, strongly constrains dynamical models. The competence regulation system maintains excitable behavior over a broad range of parameter values. Experimentally,  $\alpha_K$  and  $\alpha_S$  enable  $P_{\text{init}}$  and  $\tau_{\text{comp}}$  to be tuned independently, allowing the system, in theory, to adapt to independent selective pressures during evolution. The circuit can also access different dynamic regimes, such as oscillation and bistability, indicating its potential to evolve alternative qualitative behaviors.

#### References and Notes

- U. Alon, *An Introduction to Systems Biology: Design Principles of Biological Circuits*. Mathematical and Computational Biology Series, vol. 10 (Chapman & Hall/CRC, Boca Raton, FL, 2006).
- D. Dubnau, *Annu. Rev. Microbiol.* **53**, 217 (1999).
- A. D. Grossman, *Annu. Rev. Genet.* **29**, 477 (1995).
- G. M. Suel et al., *Nature* **440**, 545 (2006).
- R. M. Berka et al., *Mol. Microbiol.* **43**, 1331 (2002).
- D. van Sinderen et al., *Mol. Microbiol.* **15**, 455 (1995).
- H. Maamar, D. Dubnau, *Mol. Microbiol.* **56**, 615 (2005).
- W. K. Smits et al., *Mol. Microbiol.* **56**, 604 (2005).
- K. Turgay et al., *EMBO J.* **17**, 6730 (1998).
- J. Hahn, L. Kong, D. Dubnau, *J. Bacteriol.* **176**, 5753 (1994).
- M. Ogura et al., *Mol. Microbiol.* **32**, 799 (1999).
- C. Koch, *Biophysics of Computation* (Oxford Univ. Press, Oxford, 1999).
- D. Dubnau, R. Losick, *Mol. Microbiol.* **61**, 564 (2006).
- D. T. Gillespie, *J. Phys. Chem.* **81**, 2340 (1977).
- The gene circuit shown in Fig. 18 can be described, in a continuous approximation, by two coupled differential equations that govern the dynamical evolution of the

concentrations of ComK and ComS proteins, denoted  $K$  and  $S$ , respectively. The equation for  $K$  is  $\frac{dK}{dt} = \alpha_K + \frac{\beta_K K^r}{1 + K/\lambda_K} - \frac{\beta_K K}{1 + K/\lambda_K + S/\lambda_S} - \lambda_K K$ , where  $\alpha_K$  and  $\beta_K$  parameterize the strength of constitutive and autoregulated ComK expression, respectively. The third term models degradation through competitive binding of ComK and ComS to MecA. The final term represents linear degradation of ComK. The equation for  $S$  is  $\frac{dS}{dt} = \alpha_S + \frac{\beta_S S^r}{1 + K/\lambda_K + S/\lambda_S} - \lambda_S S$ . Here,  $\alpha_S$  and  $\beta_S$  measure the strength of constitutive and regulated *comS* expression, respectively. The third and fourth terms represent MecA-mediated and linear degradation, respectively. Other parameters are defined in the SOM text. We have also developed a discrete model of the circuit that incorporates intrinsic noise explicitly. The requirement of independent tunability of  $P_{\text{init}}$  and  $\tau_{\text{comp}}$  strongly constrains the allowed parameter values and thus the structure of the phase space. The modeling is described in detail in the SOM text.

- T. T. Hoa et al., *Mol. Microbiol.* **43**, 15 (2002).
- M. B. Elowitz et al., *J. Bacteriol.* **181**, 197 (1999).
- F. Ishino et al., *J. Bacteriol.* **171**, 5523 (1989).
- N. Maki et al., *J. Bacteriol.* **182**, 4337 (2000).
- F. Tetart et al., *Mol. Microbiol.* **6**, 621 (1992).
- H. H. McAdams, A. Arkin, *Proc. Natl. Acad. Sci. U.S.A.* **94**, 814 (1997).
- J. Paulsson, *Nature* **427**, 415 (2004).
- P. S. Swain, M. B. Elowitz, E. D. Siggia, *Proc. Natl. Acad. Sci. U.S.A.* **99**, 12795 (2002).
- M. Thattai, A. van Oudenaarden, *Proc. Natl. Acad. Sci. U.S.A.* **98**, 8614 (2001).
- We thank R. Kishony, B. Shraiman, U. Alon, R. Ranganathan, S. Altschuler, L. Wu, and K. Suel, together with members of the Elowitz laboratory, for thoughtful comments and discussions. This work was supported by grants from NIH (R01 GM079771 to M.B.E. and GM068763 to the Center for Modular Biology), the Searle Scholars Program, the Human Frontiers Science Program, and the Packard Foundation. G.M.S. is supported by California Institute of Technology Center for Biological Circuit Design and the University of Texas Southwestern's Endowed Scholars Program. J.G.O. acknowledges financial support from the Ministerio de Educacion y Ciencia (Spain, project FIS2006-11452) and from the Generalitat de Catalunya.

#### Supporting Online Material

www.sciencemag.org/cgi/content/full/315/5819/1716/DC1

Materials and Methods

SOM Text

Figs. S1 to S17

Tables S1 to S4

References

13 November 2006; accepted 26 February 2007

10.1126/science.1137455

## Temporal Frequency of Subthreshold Oscillations Scales with Entorhinal Grid Cell Field Spacing

Lisa M. Giacomo,<sup>1\*</sup> Eric A. Zilli,<sup>1</sup> Erik Fransén,<sup>2</sup> Michael E. Hasselmo<sup>1\*</sup>

Grid cells in layer II of rat entorhinal cortex fire to spatial locations in a repeating hexagonal grid, with smaller spacing between grid fields for neurons in more dorsal anatomical locations. Data from *in vitro* whole-cell patch recordings showed differences in frequency of subthreshold membrane potential oscillations in entorhinal neurons that correspond to different positions along the dorsal-to-ventral axis, supporting a model of physiological mechanisms for grid cell responses.

The entorhinal cortex plays an important role in encoding of spatial information (1–3) and episodic memory (4). Many layer II neurons of rat entorhinal cortex are grid cells, firing when the rat is in an array of spatial locations forming a hexagonal grid within the environment

(5–7). The spacing of firing fields in the grid varies with anatomical position of the cell along the dorsal-ventral axis of entorhinal cortex, as measured by distance from the postirhinal border (5). Neurons closer to the dorsal border of entorhinal cortex have shorter distances between firing fields. Computa-



tional models explicitly predict that differences in grid field spacing should correspond to differences in intrinsic frequencies of neurons along the dorsal-to-ventral axis (3, 8). This could provide systematic variation in the gain of a movement-speed signal for path integration (2, 3, 9).

Subthreshold membrane potential oscillations in entorhinal cortical stellate cells (10) arise from a single-cell mechanism involving voltage-sensitive currents (11–13) and could contribute to network

dynamics (14). We recorded subthreshold oscillations from 57 stellate cells in layer II of medial entorhinal cortex (fig. S1) in slices from different anatomical positions along the dorsal-ventral axis by using whole-cell patch clamp techniques (15). The position of each horizontal slice was measured individually relative to the dorsal surface of the brain (Fig. 1A).

Stellate cells in dorsal entorhinal cortex showed higher temporal frequencies ( $f$ ) of subthreshold membrane potential oscillations compared with lower frequencies in cells from more ventral entorhinal slices (Fig. 1B). Dorsal cells ( $n = 30$ ) were defined as cells recorded in slices taken between 3.8 mm [the border with postrhinal cortex (16)] and 4.9 mm from the dorsal surface of the brain. Ventral cells ( $n = 27$ ) were defined as

cells recorded in slices between 4.9 and 7.1 mm from the dorsal surface. Because the group means of the frequency of subthreshold oscillations recorded from these populations (Fig. 1B) can depend upon the mean membrane potential voltage, we performed this analysis separately for data gathered at different approximate holding membrane potentials of  $-50$  mV and  $-45$  mV. The mean frequency in dorsal cells was significantly higher than the mean frequency in ventral cells for measurements at about  $-50$  mV (dorsal mean  $f \pm \text{SEM} = 6.42 \pm 0.40$  Hz and  $n = 28$ ; ventral  $f = 4.23 \pm 0.32$  Hz and  $n = 25$ ;  $P < 0.001$ ) and  $-45$  mV (dorsal mean  $f \pm \text{SEM} = 7.18 \pm 0.50$  Hz and  $n = 14$ ; ventral  $f = 4.88 \pm 0.59$  Hz and  $n = 7$ ;  $P < 0.01$ ). Frequencies were determined by an automated autocorrelation anal-

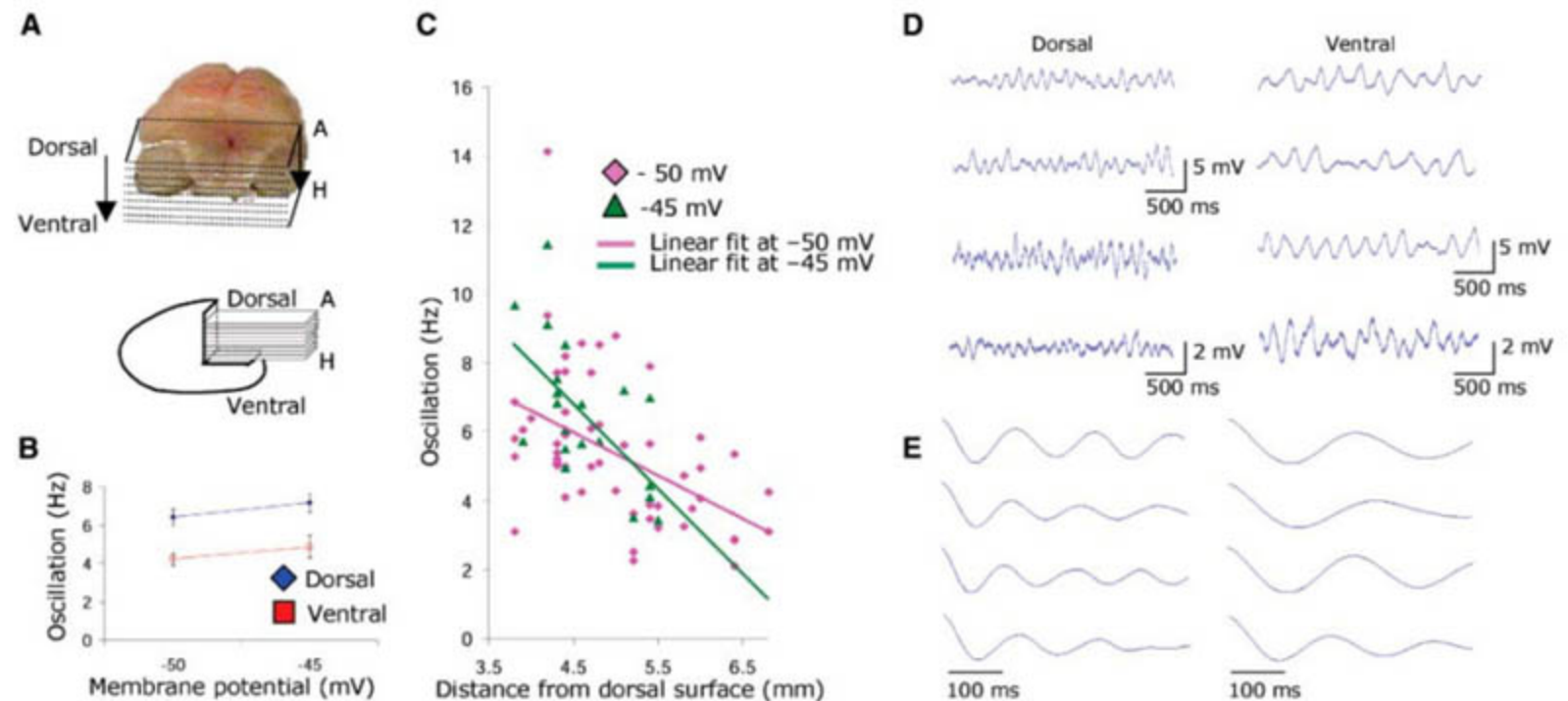


**Fig. 1.** Higher frequency of subthreshold oscillations in dorsal versus ventral entorhinal cortex. (A) Top, dorsal view of brain after slicing. Bottom, sagittal view showing anatomical location of horizontal slices A to H. (B) Mean frequency of subthreshold oscillations for neurons from dorsal slices (3.8 to 4.9 mm bregma) and ventral slices (4.9 to 7.1 mm bregma) at  $-50$  mV and

$-45$  mV. Error bars indicate SEM. (C) Subthreshold oscillation frequency plotted versus anatomical distance from dorsal surface. (D) Examples of subthreshold oscillations at  $-50$  mV in dorsal regions (left) and ventral regions (right). (E) Corresponding autocorrelations used to measure frequency in (D).

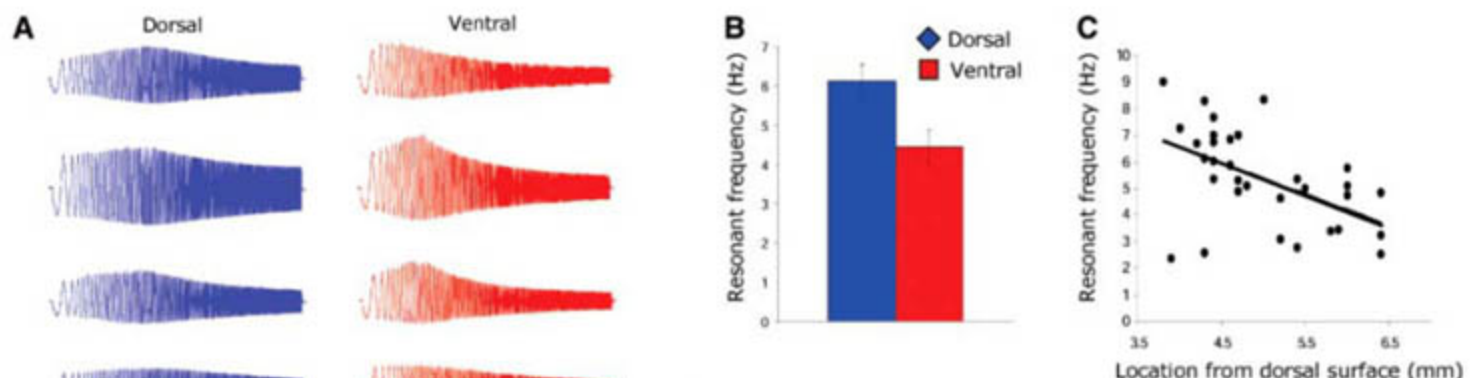


**Fig. 2.** Differences in resonance properties of neurons in dorsal versus ventral entorhinal cortex. (A) Examples of resonance responses of neurons in dorsal (blue) and ventral entorhinal cortex (red) in response to ZAP stimulus (black). (B) Histogram of mean peak resonance frequency for neurons in dorsal versus ventral entorhinal cortex. (C) Resonance frequency plotted versus anatomical distance from the dorsal surface.

<sup>1</sup>Center for Memory and Brain, Department of Psychology, Program in Neuroscience, Boston University, 2 Cummings Street, Boston, MA 02215, USA. <sup>2</sup>School of Computer Science and Communication, Royal Institute of Technology and Stockholm Brain Institute, SE-100 44 Stockholm, Sweden.

\*To whom correspondence should be addressed. E-mail: hasselmo@bu.edu (M.E.H.); giocomo@bu.edu (L.M.G.)



ysis algorithm (15) and were used throughout unless otherwise noted. The significant difference between mean frequencies was replicated with analyses using the peak in the power spectra for data at  $-50$  mV (dorsal  $f = 4.86 \pm 0.37$  Hz and  $n = 28$ ; ventral  $f = 3.44 \pm 0.25$  Hz and  $n = 25$ ;  $P < 0.01$ ) and  $-45$  mV (dorsal  $f = 5.54 \pm 0.49$  Hz and  $n = 14$ ; ventral  $f = 3.76 \pm 0.31$  Hz and  $n = 8$ ;  $P < 0.01$ ) (fig. S2). The resting membrane potential, firing threshold, resistance, and age [dorsal mean age  $\pm$  SEM =  $19.8 \pm 0.4$  days and ventral age =  $19.1 \pm 0.4$  days,  $P$  value not significant (NS)] did not contribute to the difference in the frequency of oscillations observed between neurons from dorsal versus ventral slices (15).

Entorhinal neurons showed a systematic difference in subthreshold oscillation frequency when plotted for different locations along the dorsal-ventral axis (Fig. 1C) for data at  $-50$  mV ( $r = 0.48$ , slope =  $-1.26$ ) and at  $-45$  mV ( $r = 0.60$ , slope =

$-2.48$ ). This pattern resembles the difference in spatial periodicity of grid cells previously recorded from layer II at different positions along the dorsal-ventral-axis in awake, behaving animals (5, 7). Examples of subthreshold oscillations recorded from individual entorhinal neurons illustrate the difference in dorsal versus ventral frequency (Fig. 1D). 500-ms segments of the autocorrelations computed for the same cells in Fig. 1D demonstrate the difference in peak-to-peak wavelength (Fig. 1E).

The frequency of subthreshold oscillations has been shown to correlate with the peak frequency of membrane potential resonance at rest ( $-60$  to  $-64$  mV) in entorhinal neurons (17). We evaluated the resonant frequency of neurons by delivering a 20-s-long impedance amplitude profile (ZAP) stimulus and measuring the input frequency that caused the largest amplitude depolarization of membrane potential. Individual examples of the response to the ZAP stimulus are shown for four

neurons from dorsal entorhinal slices (Fig. 2A) and four neurons from more-ventral slices. The resonant frequency of stellate cells was significantly higher in dorsal cells compared with that in ventral cells (dorsal frequency =  $6.13 \pm 0.41$  Hz and  $n = 18$ ; ventral frequency =  $4.45 \pm 0.40$  Hz and  $n = 14$ ;  $P < 0.01$ ) (Fig. 2B). There was no significant difference in resting potential between the populations used for this analysis (dorsal potential =  $-60.12 \pm 0.26$  mV and  $n = 18$ ; ventral potential =  $-60.11 \pm 0.26$  mV and  $n = 14$ ;  $P$  NS). Resonant frequency was systematically higher in dorsal regions when plotted in relation to anatomical location ( $r = 0.51$ , slope =  $-1.18$ ) (Fig. 2C).

To analyze the relationship of subthreshold oscillations to other intrinsic properties, we measured the change in membrane potential during a hyperpolarizing current injection that usually caused a slow depolarizing shift (a "sag" of the membrane potential). The sag was fit with a dual exponential equation starting just after the trough of the sag and ending near the end of the current injection at steady state potential (Fig. 3, A and B). The faster of the two time constants ( $\tau_1$ ) of the sag was measured for hyperpolarizing current steps that ended at steady-state membrane voltages of  $-69.9$  to  $-65$  mV (V1) and at steady-state membrane voltages of  $-64.9$  to  $-60$  mV (V2). The time constant ( $\tau_1$ ) of the sag increased with depth on the dorsal-ventral axis (at V1,  $r = 0.55$  and slope =  $9.67$ ; at V2,  $r = 0.61$  and slope =  $8.23$ ) (Fig. 3C), with significantly faster values of  $\tau_1$  in more-dorsal portions compared with more-ventral portions at V1 (dorsal  $\tau_1 = 23.37 \pm 1.24$  ms and  $n = 17$ ; ventral  $\tau_1 = 35.52 \pm 1.81$  ms,  $n = 14$ ;  $P < 0.01$ ) and at V2 (dorsal  $\tau_1 = 22.37 \pm 1.60$  ms and  $n = 11$ ; ventral  $\tau_1 = 34.71 \pm 2.68$  ms and  $n = 17$ ;  $P < 0.01$ ). The  $\tau_1$  of the sag correlated with the frequency of subthreshold oscillations (at V1,  $r = 0.63$  and slope =  $-4.32$ ; at V2,  $r = 0.65$  and slope =  $-4.10$ ) (Fig. 3D). Voltage-clamp studies are necessary to confirm underlying currents. A potential candidate is the h current, which has been shown to underlie sag in stellate cells (11, 12).

The differences in temporal frequency shown in this study correspond to differences in spatial periodicity of unit firing observed with extracellular recording in awake, behaving animals (5–7). Neurons at more-dorsal locations show higher intrinsic subthreshold oscillation frequency in vitro and smaller spacing between grid fields in vivo. Plots of the reciprocal of temporal frequency versus anatomical position (Fig. 4A) reveal slopes similar to the slope of grid field spacing ( $G$ ) relative to anatomical position (Fig. 4B).

These data support the prediction of a model (SOM text) (3, 8) related to other models of grid cells and theta phase precession (18–20). In this model, grid cell periodicity arises from an interference pattern generated by intrinsic temporal oscillations in the soma and dendrites of a single cell. During simulated rat movement, cells modulated by head direction and speed (7, 21, 22) shift the frequency of dendritic oscillations (consistent with voltage effects on frequency). The grid pattern is the product of interference by three

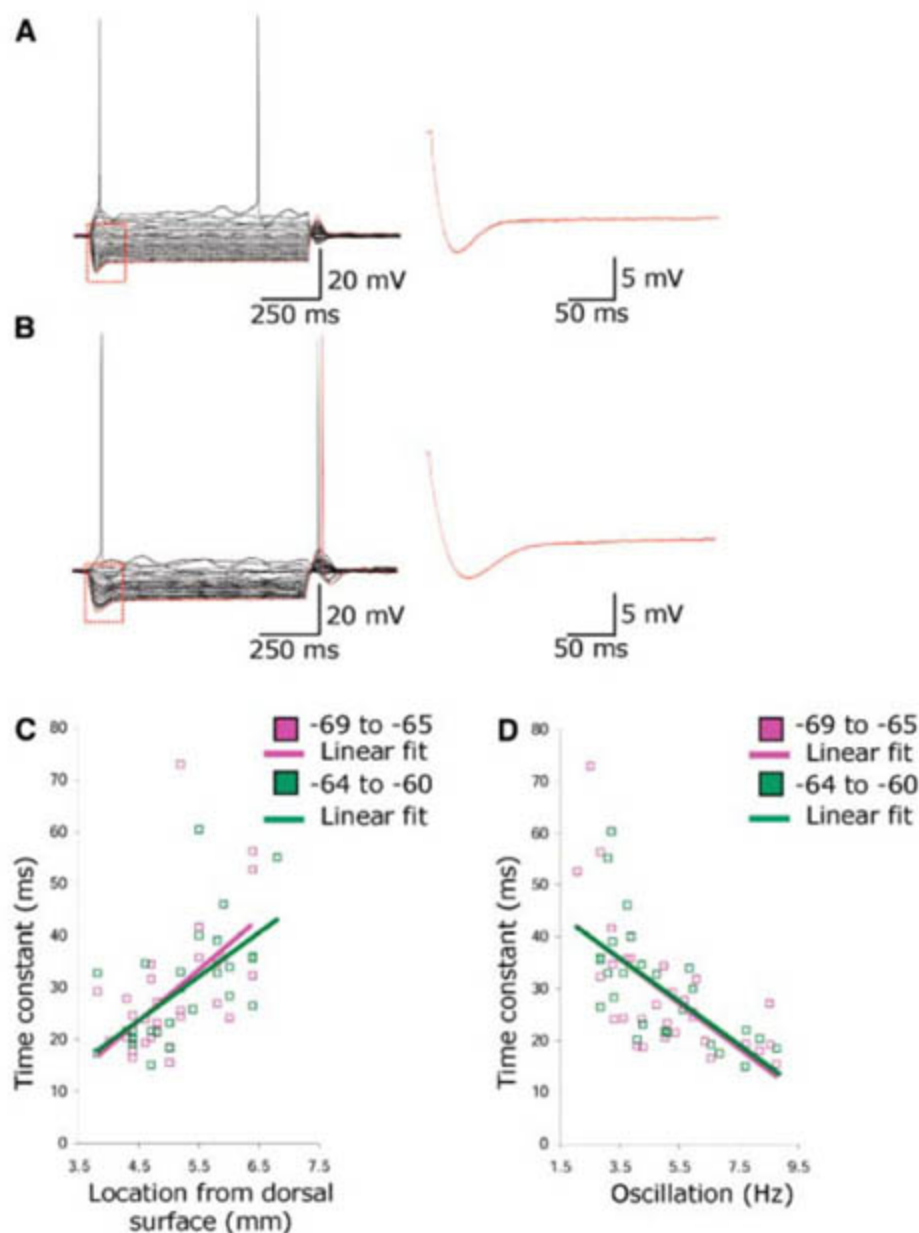


**Fig. 3.** Relationship of subthreshold membrane potential oscillations to sag potential. For single neurons in dorsal (A) and ventral entorhinal cortex (B), traces on left show membrane potential responses to multiple current injection levels. Single traces (right) show sag potentials at higher resolution. (C)  $\tau_1$  of sag potential (ms) plotted versus anatomical location. (D)  $\tau_1$  of sag potential plotted versus subthreshold oscillation frequency.



dendritic oscillations, each receiving a different head direction input, shifting in and out of phase with soma oscillations in proportion to distance moved in the preferred direction of each head direction cell. Spiking occurs when all three dendrites are in phase with the soma, causing oscillations to cross threshold (figs. S4 and S5). Spiking does not alter soma or dendritic phase but occurs with theta rhythmicity, consistent with *in vivo* recordings in entorhinal cortex (5–7) and hippocampus (2, 9, 18) and potentially causing precession relative to field potential oscillations (3, 8, 19, 20).

The model (3, 8) was modified to include shifts in dendritic frequency proportional to soma frequency and to use a scaling factor,  $H = fG$  (fig. S6), determined from the experimental data. Simulations (SOM text) (Fig. 4, C and D) demonstrated that differences in temporal frequency of somatic oscillations result in different grid field spacing. Insertion of the experimentally determined value for subthreshold oscillation frequency ( $f$ ) at a par-

ticular anatomical location resulted in simulated grid cell spacing that matches data (7) on grid cell spacing ( $G$ ) at the same anatomical location (figs. S4 and S7).

The model demonstrates one possible mechanism for path integration (2) and supports the prediction that systematic variation in gain of a movement-speed signal could underlie differences in grid field spacing (2, 9). The model is compatible with maintenance of grid cell representations by persistent firing (23) or attractor dynamics arising from patterned excitatory connectivity (2, 24, 25). Long-term stability of grid fields could require place cell input dependent on external landmarks (3, 8, 26). Differences in intrinsic frequency along the dorsal-ventral axis of entorhinal cortex could contribute to differences in place field size along the septal-to-temporal axis of the hippocampus (9, 27).

The systematic differences in intrinsic temporal frequency may provide multiple scales for

coding of both space and time. Periodic representation of the environment at multiple spatial scales could prove essential to mechanisms of path integration (2, 3, 9, 28), consistent with impairments after entorhinal lesions (1). Coding of continuous dimensions by interacting frequencies could also allow the coding of continuous relative time necessary for episodic memory (29). These results suggest that, beyond simple summation of input, neural processing involves interactions of synaptic input and interference between intrinsic frequencies (8, 9, 18, 19).

References and Notes

1. H. A. Steffenach, M. Witter, M.-B. Moser, E. I. Moser, *Neuron* **45**, 301 (2005).
2. B. L. McNaughton, F. P. Battaglia, O. Jensen, E. I. Moser, M.-B. Moser, *Nat. Rev. Neurosci.* **7**, 663 (2006).
3. J. O'Keefe, N. Burgess, *Hippocampus* **15**, 853 (2005).
4. H. Eichenbaum, N. J. Cohen, *From Conditioning to Conscious Recollection* (Oxford Univ. Press, New York, 2003).
5. T. Hafting, M. Fyhn, S. Molden, M.-B. Moser, E. I. Moser, *Nature* **436**, 801 (2005).
6. M. Fyhn, S. Molden, M. P. Witter, E. I. Moser, M.-B. Moser, *Science* **305**, 1258 (2004).
7. F. Sargolini *et al.*, *Science* **312**, 758 (2006).
8. N. Burgess, C. Barry, J. O'Keefe, *Hippocampus*, in press.
9. A. P. Maurer, S. R. VanRhoads, G. R. Sutherland, P. Lipa, B. L. McNaughton, *Hippocampus* **15**, 841 (2005).
10. A. Alonso, R. R. Llinas, *Nature* **342**, 175 (1999).
11. C. T. Dickson *et al.*, *J. Neurophysiol.* **83**, 2562 (2000).
12. E. Fransen, A. A. Alonso, C. T. Dickson, J. Magistretti, M. E. Hasselmo, *Hippocampus* **14**, 368 (2004).
13. J. A. White, R. Klink, A. Alonso, A. R. Kay, *J. Neurophysiol.* **80**, 262 (1998).
14. C. D. Aker, N. Kopell, J. A. White, *J. Comput. Neurosci.* **15**, 71 (2003).
15. Materials and methods are available on Science Online.
16. G. Paxinos, C. Watson, *The Rat Brain in Stereotaxic Coordinates* (Academic Press, San Diego, CA, 1998).
17. I. Erchova, G. Kreck, U. Heinemann, A. V. Herz, *J. Physiol.* **560**, 89 (2004).
18. J. O'Keefe, M. L. Recce, *Hippocampus* **3**, 317 (1993).
19. M. Lengyel, Z. Szatmari, P. Erdi, *Hippocampus* **13**, 700 (2003).
20. H. T. Blair, A. C. Welday, K. Zhang, *J. Neurosci.*, in press.
21. J. S. Taube, J. P. Bassett, *Cereb. Cortex* **13**, 1162 (2003).
22. P. E. Sharp, H. T. Blair, J. Cho, *Trends Neurosci.* **24**, 289 (2001).
23. E. Fransén, B. Tahvildari, A. V. Egorov, M. E. Hasselmo, A. A. Alonso, *Neuron* **49**, 735 (2006).
24. M. C. Fuhs, D. S. Touretzky, *J. Neurosci.* **26**, 4266 (2006).
25. A. Samsonovich, B. L. McNaughton, *J. Neurosci.* **17**, 5900 (1997).
26. J. J. Knierim, H. S. Kudrimoti, B. L. McNaughton, *J. Neurophysiol.* **80**, 425 (1998).
27. T. Solstad, E. I. Moser, G. T. Einevoll, *Hippocampus* **16**, 1026 (2006).
28. A. D. Redish, D. S. Touretzky, *Hippocampus* **7**, 15 (1997).
29. M. E. Hasselmo, H. Eichenbaum, *Neural Netw.* **18**, 1172 (2005).
30. Thanks to E. Moser, M.-B. Moser, M. Yoshida, K. Lillis, H. Eichenbaum, and J. White for advice and comments. Research supported by National Institute of Mental Health (NIMH) grant MH60013, Silvio O. Conte Center grant NIMH MH71702, NSF Science of Learning Center SBE 0354378, and National Institute on Drug Abuse grant DA16454 (part of the Collaborative Research in Computational Neuroscience program).

Supporting Online Material

www.sciencemag.org/cgi/content/full/315/5819/1719/DC1  
 Materials and Methods  
 SOM Text  
 Figs. S1 to S7

22 December 2006; accepted 23 February 2007  
 10.1126/science.1139207

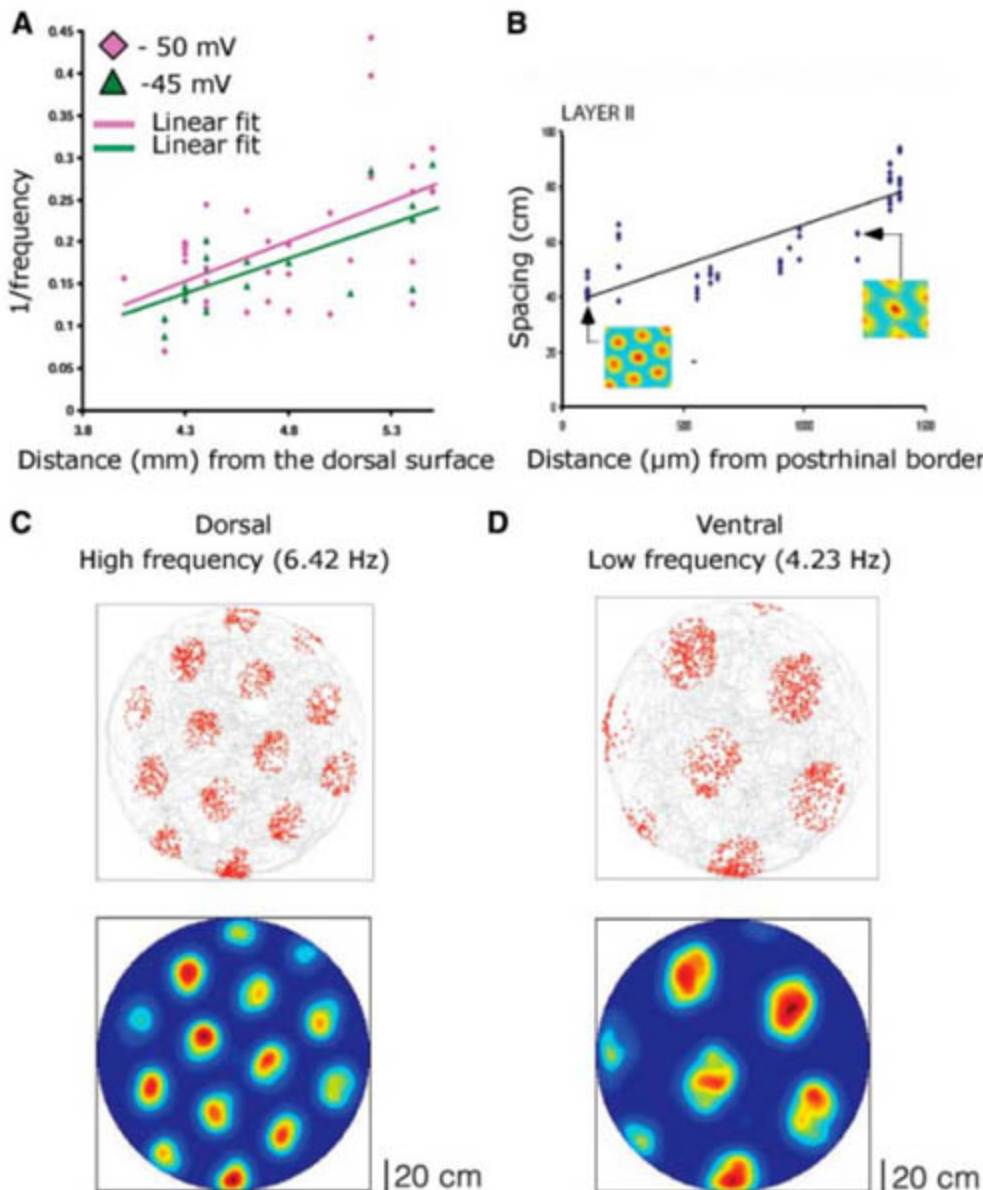


**Fig. 4.** Subthreshold oscillations may underlie differences in grid field spacing. (A) Reciprocal of oscillation frequency plotted versus anatomical depth for anatomical range matching a previous publication (7) as shown in (B). (C and D) Simulations of grid cell model (3, 8). Top, gray indicates trajectory of simulated rat. Red indicates firing locations. Bottom, firing rate map (red, maximum; blue, no spikes). Grid field spacing is small for mean dorsal oscillation frequency of 6.42 Hz (C) and larger for mean ventral frequency of 4.23 Hz (D).



# Emergence of Novel Color Vision in Mice Engineered to Express a Human Cone Photopigment

Gerald H. Jacobs,<sup>1\*</sup> Gary A. Williams,<sup>1</sup> Hugh Cahill,<sup>2,3,4</sup> Jeremy Nathans<sup>2,3,4,5</sup>

Changes in the genes encoding sensory receptor proteins are an essential step in the evolution of new sensory capacities. In primates, trichromatic color vision evolved after changes in X-chromosome-linked photopigment genes. To model this process, we studied knock-in mice that expressed a human long-wavelength-sensitive (L) cone photopigment in the form of an X-linked polymorphism. Behavioral tests demonstrated that heterozygous females, whose retinas contained both native mouse pigments and human L pigment, showed enhanced long-wavelength sensitivity and acquired a new capacity for chromatic discrimination. An inherent plasticity in the mammalian visual system thus permits the emergence of a new dimension of sensory experience based solely on gene-driven changes in receptor organization.

The retinas of most nonprimate mammals contain two classes of cone photopigments that support dichromatic color vision (1). A cone pigment most sensitive to short (S) wavelengths is encoded on an autosome, and a second cone pigment most sensitive to middle (M) or long (L) wavelengths is encoded on the X chromosome. Many primate lineages have added an additional type of M or L pigment, permitting the evolution of trichromacy (2). In Old World primates, the third cone pigment arose by duplication of the ancestral X-chromosomal cone pigment gene (3). By contrast, in most New World monkeys, cone pigment diversity derives from polymorphic variation in a single X-linked gene (4, 5). In heterozygous females, X-chromosome inactivation produces a mosaic of spectrally distinct cone types, which provides the foundation for trichromacy. The polymorphic X-linked pigment genes in New World monkeys may represent the ancestral arrangement for primates, as judged by the observation that the same three amino acid substitutions confer the spectral difference between M and L pigments in all present-day primates (3). Color vision requires both multiple photopigments and appropriate neural wiring, and it has been argued that the organization of the primate retina, and in particular the low-convergence midget bipolar and ganglion cell system, is such that the addition of a new class of cone photoreceptors may be all that is required for comparing M versus L cone signals (6–8).

Our experiments used genetically engineered mice to model the first step in the evolution of primate trichromacy. We asked whether the sud-

den acquisition of an additional and spectrally distinct pigment and its production in a subset of cones suffice to permit a new dimension of chromatic discrimination that would imply that (i) the mammalian brain is sufficiently plastic that it can extract and compare a new dimension of sensory input and (ii) the heterozygous female primate that first inherited an additional X-chromosome allele would have immediately enjoyed a selective advantage with respect to chromatic discrimination. We produced a line of mice in which most of the coding sequences of the normal mouse X-chromosomal M pigment gene [specifying a pigment with wavelength of maximum absorption  $\lambda_{\max}$  ~510 nm, hereafter “M”] was replaced with a human L pigment cDNA (specifying a hybrid pigment with a  $\lambda_{\max}$  of ~556 nm, hereafter “L”) (9). A similar knock-in mouse has recently been produced (10). As in New World monkeys, breeding yields mice with three distinct complements of M/L pigments: Males and homozygous females have either M or L pigments, and heterozygous females have a mixture of the two pigments. Earlier we observed that cones containing the L pigment could transduce light signals with an efficiency roughly equal to that of native M cones, as judged by the electroretinogram (ERG), and that the responses of individual retinal ganglion cells (RGCs) in M/L heterozygotes showed substantial cell-to-cell variability in chromatic sensitivity despite the large number of cones that contribute to the receptive field center of a typical mouse RGC. This functional heterogeneity likely reflects the spatial graininess of M versus L cone territories created by X-chromosome inactivation, which is consistent with the ~50- $\mu$ m average diameters for X-chromosome-inactivation patches in the retina (9).

We first performed an analysis of cone-based spectral sensitivity using ERG flicker photometry (11) [see also supporting online material (SOM)]. The mouse S cone pigment is maximally sensitive in the ultraviolet range (12, 13); we minimized its activation by using lights of relatively long wavelength. Spectral sensitivity functions, obtained from mice whose retinas contained either the M

pigment ( $n = 12$  mice) or the L pigment ( $n = 17$  mice), were fitted with photopigment absorption functions (Fig. 1, A and B). The spectral maxima (512 and 556 nm) are close to those determined by earlier measurements of these pigments (9, 12, 13). Spectral sensitivity functions, similarly obtained from 86 M/L heterozygotes (Fig. 1C), were best fit by linearly summing the spectra from mice with either M or L pigments. On average, there is a twofold larger contribution from the M pigment than from the L pigment (presumably reflecting a bias in the M:L cone ratio), and there is substantial individual variability in this relative weighting (Fig. 1D). The latter likely reflects stochastic variation in X-chromosome inactivation (14).

Although heterozygotes have, on average, greater M than L sensitivity, this is not because the L pigment compromises cone viability or function. First, immunolabeling with antibodies to M/L opsin demonstrated nearly identical densities of M or L cones in retinas from animals expressing only one or the other of these pigments [mean M cone densities  $\pm$ SD = 8129  $\pm$  995 per  $\text{mm}^2$  and mean L cone densities  $\pm$ SD = 8288  $\pm$  952 per  $\text{mm}^2$  ( $n = 2$  mice for each genotype)]. Second, ERG voltage versus intensity ( $V$ -log  $I$ ) functions recorded from M or L retinas are indistinguishable when the intensity of the stimulating light is specified according to its calculated effectiveness for each pigment (Fig. 1E), implying that signals from the L and M pigments activate the ERG with the same efficiency.

To examine whether vision is altered by the added photopigment, we tested mice in a behavioral three-alternative forced-choice discrimination task. In this task, the animal was required to identify which one of the three test panels was illuminated differently from the other two, with the location of the correct choice varying randomly between trials (15). The L pigment has greater sensitivity to long wavelengths than does the M pigment, so one might expect enhanced behavioral sensitivity to such lights in mice whose retinas contain the L pigment. Increment thresholds were determined for 11 mice (four having only M pigment and seven M/L heterozygotes) by briefly adding either of two monochromatic test lights (500 and 600 nm) to one of the three stimulus panels, all of which were continuously illuminated with an achromatic light. The threshold differences between the 500- and 600-nm test lights were significantly smaller for M/L heterozygotes (Fig. 1F), indicating that these mice can extract visual information from L cones.

Color vision implies the ability to discriminate variations in spectral composition irrespective of variations in intensity. To assess this possibility, we derived brightness matches between a monochromatic test light and a series of standard lights of different wavelengths (see SOM) and then asked whether mice could discriminate between a 500-nm test light and two identical standard lights of 600 nm. At each trial, the location of the test light varied randomly among the three panels, and its intensity varied randomly in steps of 0.1 log

<sup>1</sup>Neuroscience Research Institute and Department of Psychology, University of California, Santa Barbara, CA 93106, USA.

<sup>2</sup>Department of Neuroscience, Johns Hopkins Medical School, Baltimore, MD 21205, USA. <sup>3</sup>Department of Ophthalmology, Johns Hopkins Medical School, Baltimore, MD 21205, USA.

<sup>4</sup>Howard Hughes Medical Institute, Johns Hopkins Medical School, Baltimore, MD 21205, USA. <sup>5</sup>Department of Molecular Biology and Genetics, Johns Hopkins Medical School, Baltimore, MD 21205, USA.

\*To whom correspondence should be addressed. E-mail: jacobs@psych.ucsb.edu



units to encompass a range of  $\pm 0.5$  log units around the brightness match. As a control, we first tested a mouse whose retina contained M but not L pigment. As expected, despite extensive testing (totaling  $\sim 15,600$  trials), no significant discrimination was achieved (open circle in Fig. 2A). With the use of the same procedures, two M/L heterozygotes also failed to show evidence of color discrimination (open square and triangle in Fig. 2A;  $\sim 16,000$  trials per subject).

The two M/L heterozygotes that failed in the wavelength discrimination had relatively skewed M:L ratios (78:22 and 65:35). Unbalanced representation of M and L cones has little impact on human color vision (16, 17), but, with smaller numbers of cones, we thought that this might not be true for mice. After extensive training ( $\sim 17,000$  trials), an M/L heterozygote with a more balanced M:L ratio (44:56) successfully discriminated 500-nm from 600-nm lights. The averaged asymptotic performance across the full range of brightness variation at this test wavelength is indicated by the vertical bar and arrow in Fig. 2A. The test wavelength was then progressively displaced in steps of 5 or 10 nm toward 600 nm; the mouse succeeded at each of these discriminations until the test and standard lights were separated by  $\sim 10$  to 15 nm, at which point discrimination failed. This process was repeated for six other standard lights covering the range from 570 to 630 nm, yielding in each case a qualitatively similar result. As an internal control in these experiments, trials in which the test and standard lights were set to the same wavelength were randomly interspersed. The cumulative results of this control procedure (Fig. 2B) show that (i) discrimination failed when both chromatic and brightness cues were eliminated and (ii) the derived brightness matches accurately predict the points of discrimination failure. Two additional M/L heterozygotes also succeeded at the color discrimination task (Fig. 2A).

For the M/L heterozygotes, wavelength discrimination varied across the range tested, being most acute at 590 to 600 nm (Fig. 2C). The U-shaped wavelength discrimination function is qualitatively like those for other dichromatic visual systems (1); in particular, it is similar to wavelength discrimination functions for human tritanopes (18), a dichromatic subtype in which color vision is based only on M and L pigments with peaks at  $\sim 530$  and  $\sim 560$  nm, respectively. At present, we cannot fully explain the variation among M/L heterozygotes in the color discrimination task, but it presumably reflects some combination of individual variation in M:L cone ratio, vagaries in the spatial distribution of cone types vis-à-vis RGC receptive fields, or central factors related to memory, intelligence, or motivation.

To assess dichromatic color matches, we used a test light that was composed of an additive mixture of two monochromatic lights. Using the same brightness control measures as before, we progressively added 620-nm light to 530-nm light to determine what proportions could be discriminated from two monochromatic standard lights

(600 and 580 nm, in successive experiments). Results obtained from the M/L heterozygote with an M:L ratio of 44:56 (solid circles in Fig. 2A) are summarized in Fig. 2, D and E. In both cases, this animal successfully discriminated the combination of test lights when it was composed largely of the 530-nm component. However, as more of the 620-nm component was added, discrimination became more difficult, eventually dropping to chance performance, thereby defining a color match. Dichromatic color matches can be predicted by calculating the proportions of each test light at which the net quantal absorption in the two pigments is equal to the absorption from the standard light. These predicted matches (downward-pointing blue arrows in Fig. 2, D and E) are close to the actual location of discrimination failure, as is also seen for a human equivalently tested (red square and red arrow in Fig. 2D). These results

imply that color vision in this M/L heterozygous mouse is based on a comparison of quantal catches between the M and L pigments.

In primates, midget bipolar and ganglion cells mediate the chromatically opponent M versus L color vision pathway (19, 20). Like many non-primate mammals, the mouse lacks a midget system (21), and thus the color vision documented in M/L heterozygotes must be subserved by other means. Most mouse RGCs have a receptive field center with an antagonistic surround (22), albeit a weak one, and chromatic information could be extracted based on differences in M versus L input to these two regions. In a variation on this idea, chromatic information could also be extracted simply based on variation among RGCs in the total M versus L weightings.

In M/L heterozygous mice and in heterozygous New World monkeys, the stochastic process

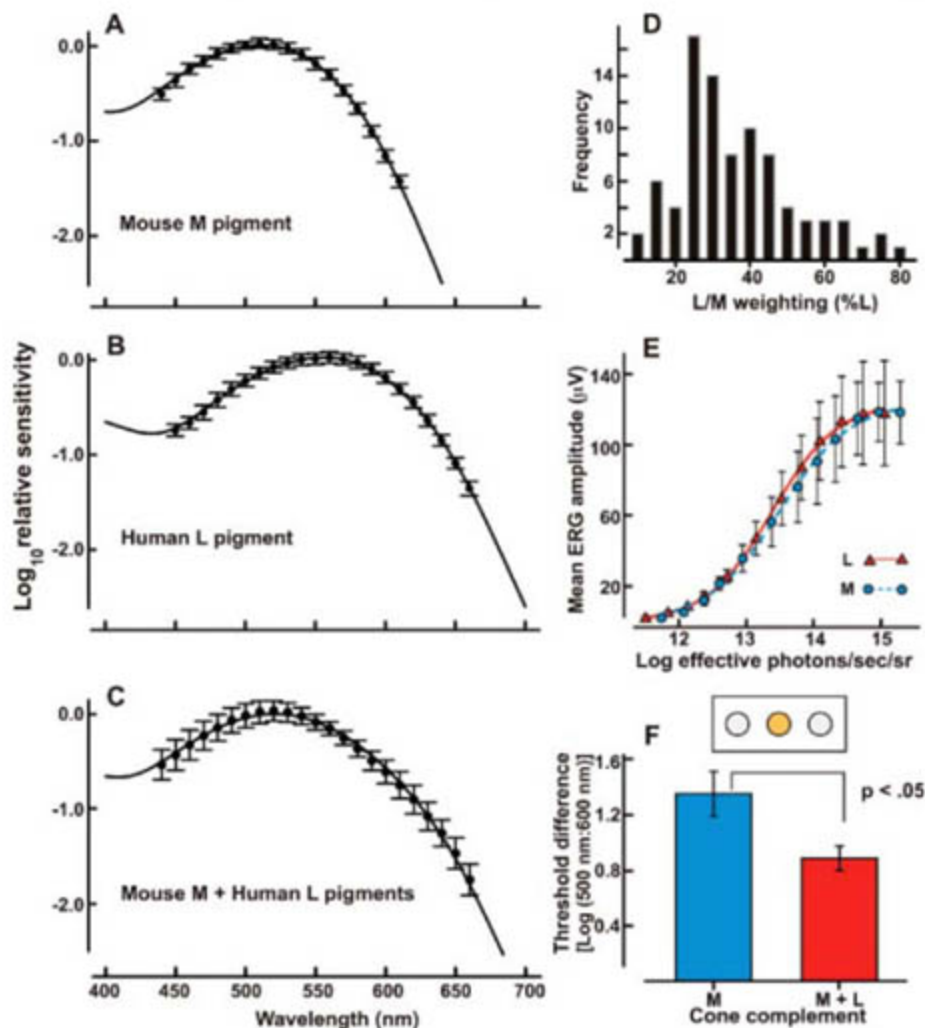


**Fig. 1.** (A) ERG spectral sensitivity for mice expressing the M pigment. Data points are mean values for 12 animals. The curve is that for the best-fitting photopigment absorption function. (B) Mean spectral sensitivity function for 18 mice expressing the human L pigment. (C) Spectral sensitivity for 82 heterozygous mice. The curve is the best-fit linear summation of curves derived from those in (A) and (B). (D) Distribution of the L:M cone weightings required to best fit each of the heterozygous mice represented in (C). (E) Mean  $V\text{-log } I$  functions obtained from activation of either mouse M or human L pigments. Light intensity has been specified according to its calculated effectiveness on each of these pigments. sec, seconds; sr, steradians. For derivation of the fitted functions, see SOM. (F) Increment-threshold measurements. The inset schematizes the discrimination context in which, on each trial, a monochromatic test light was added to any one of the three panels, all of which were steadily illuminated with identical achromatic light. The colored bars depict the difference in the thresholds obtained for 500- and 600-nm test lights for mice whose retinas contained either mouse M ( $n = 4$  mice) or both M and L ( $n = 7$  mice) pigments. Error bars in [(A) to (C)] and [(E) and (F)] indicate 2 SDs.



(X-chromosome inactivation) by which M versus L cone territories are generated and the presumed lack of any molecular distinction between M and L cones other than pigment content have parallels in a recent model for M versus L cone development in Old World primates, in which M versus L pigment gene expression is hypothesized to occur in a stochastic and independent manner in each cell, unaccompanied by any other differences in gene expression (23). The successful acquisition of chromatic discrimination based on X-chromosome

inactivation lends indirect support to this Old World primate model by demonstrating the possibility of behavioral trichromacy in the context of a stochastic process for receptor determination.

These results have general implications for the evolution of sensory systems. In the visual, olfactory, and gustatory systems, genetic manipulations have either added a new receptor protein to the existing complement of receptors or replaced an endogenous receptor protein with a new one (24–27). In each case, the behavioral or electro-

physiological responses show the predicted expansion or modification of sensitivity. However, these earlier experiments were not designed to create an additional class of sensory neurons or to facilitate the emergence of neural circuitry for comparing new and existing sensory responses. In the present experiments, X-chromosome inactivation has provided the means to both express a non-native receptor protein and to localize it to a distinct class of primary sensory neurons. Our observation that the mouse brain can use this information to make spectral discriminations implies that alterations in receptor genes might be of immediate selective value not only because they expand the range or types of stimuli that can be detected but also because they permit a plastic nervous system to discriminate between new and existing stimuli. Additional genetic changes that refine the downstream neural circuitry to more efficiently extract sensory information could then follow over many generations.

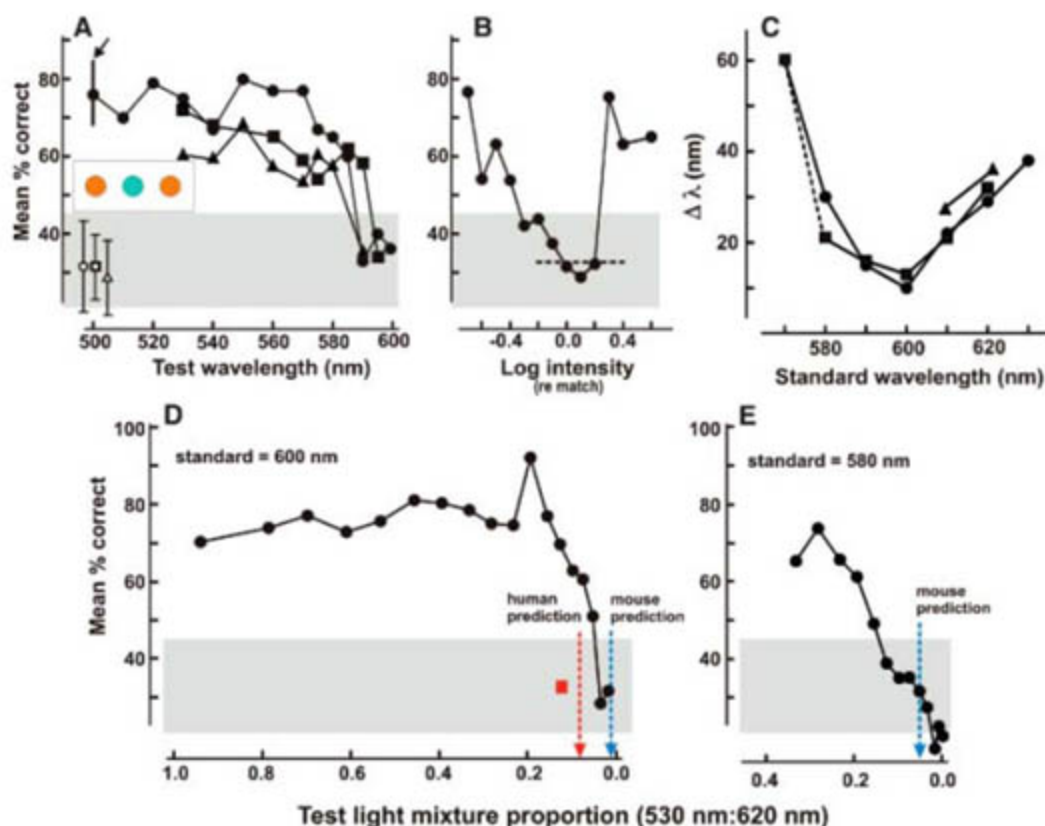


**Fig. 2.** Tests of color vision in mice. **(A)** Wavelength discrimination. The inset symbolizes the context in which the mouse was required to detect which of three stimulus panels was distinctively illuminated; its luminance and position relative to that of the standard wavelength (600 nm) were randomized from trial to trial. Lower left symbols show asymptotic performance levels (for the final 100 trials  $\pm$  1 SD) for three animals at the calculated brightness match (see SOM) and for values  $\pm$  0.1 log units from that point (the open circle indicates the mouse with M pigment; the open square and triangle indicate M/L heterozygotes with M:L ratios of 78:22 and 65:35, respectively). The solid circles connected by lines are the asymptotic performance levels achieved at the calculated brightness match by the M/L heterozygote with an M:L ratio of 44:56. Averaged performance over the full range of luminance variation for a test wavelength of 500 nm (brightness match  $\pm$  0.5 log units) is indicated by the vertical line (arrow). The solid triangles and solid squares show results from two other heterozygous animals (M:L ratios of 46:54 and 53:47, respectively). For the latter animal, the standard wavelength was 610 nm. **(B)** Results from the embedded brightness control test. The circles are asymptotic performance levels for cases where the test and comparison lights were set to the same wavelength and the test light was systematically varied in luminance relative (re) to the value required for a brightness match. The results were cumulated across seven standard wavelengths. The horizontal dashed line indicates chance performance. **(C)** Wavelength discrimination functions for heterozygous knock-in mice. Each point plots the wavelength difference ( $\Delta\lambda$ ) between the test and standard wavelengths that is required for successful discrimination (at the 95% confidence level). Symbols for individual animals are the same as those in (A). The dashed line connecting standard wavelengths of 580 and 570 nm for one female indicates that it failed to successfully discriminate a test light of 510 nm from a standard of 570 nm, and thus  $\Delta\lambda$  for that standard must exceed 60 nm. **(D)** Color-matching data. Plotted are asymptotic levels of performance achieved by an M:L heterozygous mouse (44:56 M:L ratio) at the brightness match where the test light was a variable mixture of 530- and 620-nm lights, and the standard light was 600 nm. The location of the predicted match based on the M and L photopigments is indicated by the blue arrow. The match made by a human trichromat (red square) is shown along with the predicted human match (red arrow). **(E)** Color-matching data. Details are the same as for (D) except that the standard light was 580 nm. The shaded area in [(A) and (B)] and [(D) and (E)] indicates chance performance (at the 95% confidence level).

#### References and Notes

- G. H. Jacobs, *Biol. Rev. Camb. Philos. Soc.* **68**, 413 (1993).
- G. H. Jacobs, *Proc. Natl. Acad. Sci. U.S.A.* **93**, 577 (1996).
- D. M. Hunt et al., *Vision Res.* **38**, 3299 (1998).
- J. D. Mollon, J. K. Bowmaker, G. H. Jacobs, *Proc. R. Soc. London Ser. B Biol. Sci.* **222**, 373 (1984).
- G. H. Jacobs, J. Neitz, *Proc. Natl. Acad. Sci. U.S.A.* **84**, 2545 (1987).
- J. D. Mollon, *J. Exp. Biol.* **146**, 21 (1989).
- H. Wässle, *Nat. Rev. Neurosci.* **5**, 747 (2004).
- B. Boycott, H. Wässle, *Invest. Ophthalmol. Visual Sci.* **40**, 1313 (1999).
- P. M. Smallwood et al., *Proc. Natl. Acad. Sci. U.S.A.* **100**, 11706 (2003).
- A. Onishi et al., *Zool. Sci.* **22**, 1145 (2005).
- G. H. Jacobs, J. Neitz, K. Krogh, *J. Opt. Soc. Am. A* **13**, 641 (1996).
- G. H. Jacobs, J. Neitz, J. F. Deegan II, *Nature* **353**, 655 (1991).
- A. L. Lyubarsky, B. Falsini, M. E. Pennesi, P. Valentini, E. N. Pugh Jr., *J. Neurosci.* **19**, 442 (1999).
- B. R. Migeon, *Cytogenet. Genome Res.* **99**, 8 (2002).
- G. H. Jacobs, G. A. Williams, J. A. Fenwick, *Vision Res.* **44**, 1615 (2004).
- D. H. Brainard et al., *J. Opt. Soc. Am. A* **17**, 607 (2000).
- H. Hofer, J. Carroll, J. Neitz, M. Neitz, D. R. Williams, *J. Neurosci.* **25**, 9669 (2005).
- M. Alpern, *J. Physiol.* **335**, 655 (1953).
- D. M. Dacey, *Prog. Retinal Eye Res.* **18**, 737 (1999).
- B. B. Lee, *Clin. Exp. Optom.* **87**, 239 (2004).
- R. H. Masland, *Nat. Neurosci.* **4**, 877 (2001).
- B. T. Sagdullaev, M. A. McCall, *Visual Neurosci.* **22**, 649 (2005).
- P. M. Smallwood, Y. Wang, J. Nathans, *Proc. Natl. Acad. Sci. U.S.A.* **99**, 1008 (2002).
- E. R. Troemel, B. E. Kimmel, C. I. Bargmann, *Cell* **91**, 161 (1997).
- G. H. Jacobs, J. C. Fenwick, J. B. Calderone, S. S. Deeb, *J. Neurosci.* **19**, 3258 (1999).
- G. Q. Zhao et al., *Cell* **115**, 255 (2003).
- E. A. Hallen, M. G. Ho, J. R. Carlson, *Cell* **117**, 965 (2004).
- We thank J. Fenwick for help with animal testing. This work was supported by grant EY002052 from the National Eye Institute (G.H.J.), the Howard Hughes Medical Institute (J.N.), and the Visual Neurosciences Training Program of the National Eye Institute (H.C.).

#### Supporting Online Material

www.sciencemag.org/cgi/content/full/315/5819/1723/DC1  
Materials and Methods  
References

14 December 2006; accepted 21 February 2007  
10.1126/science.1138838



# Crystal Structures of the Adenylate Sensor from Fission Yeast AMP-Activated Protein Kinase

Robert Townley<sup>1</sup> and Lawrence Shapiro<sup>1,2,3\*</sup>

The 5'-AMP (adenosine monophosphate)-activated protein kinase (AMPK) coordinates metabolic function with energy availability by responding to changes in intracellular ATP (adenosine triphosphate) and AMP concentrations. Here, we report crystal structures at 2.9 and 2.6 Å resolution for ATP- and AMP-bound forms of a core  $\alpha\beta\gamma$  adenylate-binding domain from the fission yeast AMPK homolog. ATP and AMP bind competitively to a single site in the  $\gamma$  subunit, with their respective phosphate groups positioned near function-impairing mutants. Unexpectedly, ATP binds without counterions, amplifying its electrostatic effects on a critical regulatory region where all three subunits converge.

AMPK senses the onset of energy limitation and initiates adaptive responses, including regulation of key enzymes in each of the major branches of metabolism: fatty acid and sterol synthesis, sugar metabolism, protein synthesis, and

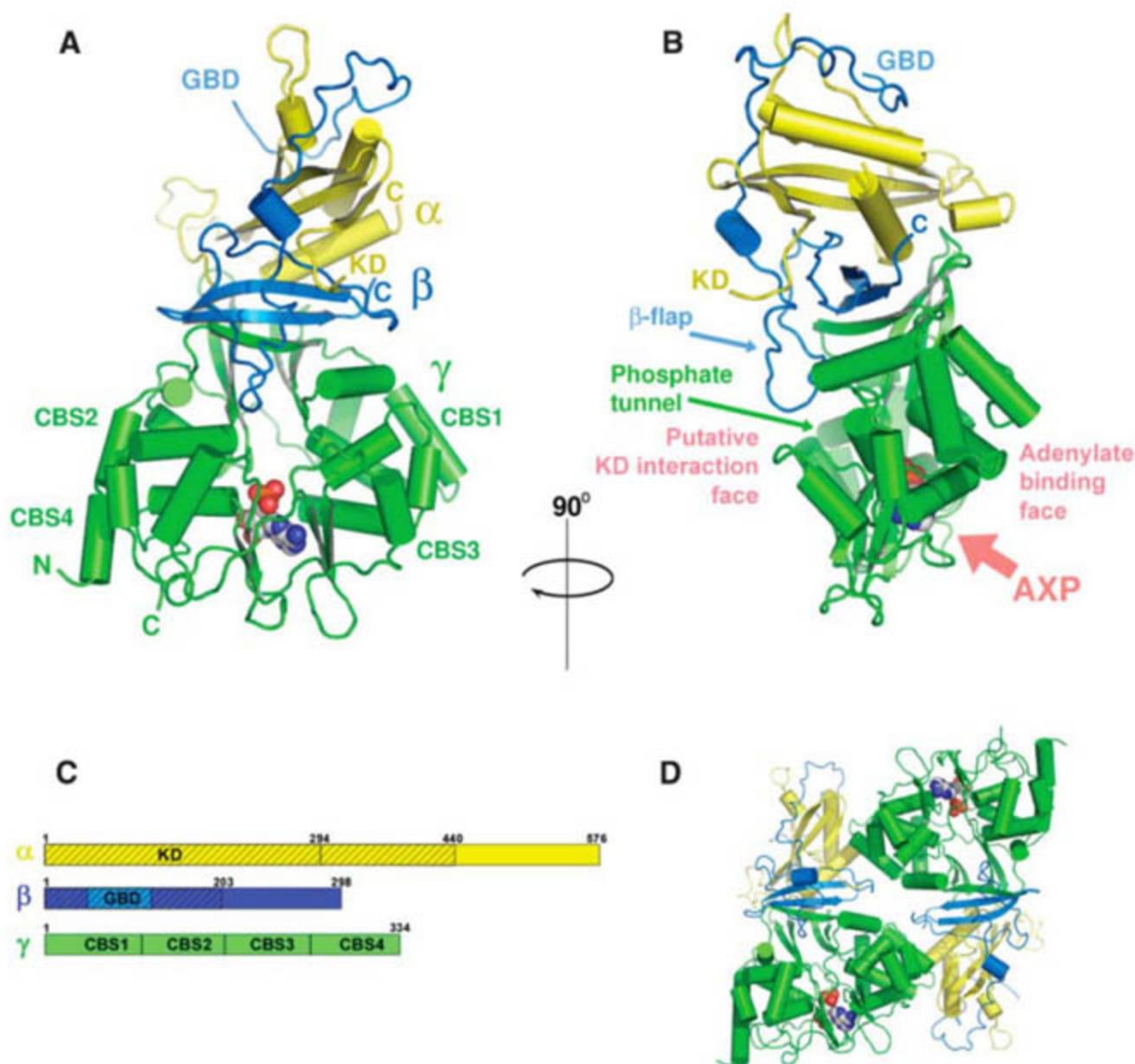
DNA replication (1–3). Long-term regulation by AMPK is controlled by phosphorylation of transcription factors and co-activators that regulate each of these metabolic functions (4). Mammalian AMPK is activated by binding to AMP, but this

activation is inhibited by ATP (1–3). Because cellular adenosine diphosphate (ADP)/ATP ratios remain nearly constant due to the equilibrium maintained by adenylate kinase, it is thought that AMPK activity *in vivo* depends primarily on the ATP/AMP ratio, the primary determinant of cellular energy charge (5). Lowered cellular energy charge can arise either from inhibition of ATP synthesis, for example, in hypoxia or starvation (5), or by increased ATP consumption, as occurs in skeletal muscle during exercise (6, 7). When energy charge is low, active AMPK inhibits numerous ATP-consuming pathways and also activates mobilization of intracellular energy stores to produce ATP. Conversely, when energy charge is high, AMPK inactivation is favored, leading to

<sup>1</sup>Department of Biochemistry and Molecular Biophysics, Columbia University, New York, NY 10032, USA. <sup>2</sup>Edward S. Harkness Eye Institute, Columbia University, New York, NY 10032, USA. <sup>3</sup>Naomi Berrie Diabetes Center, Columbia University, New York, NY 10032, USA.

\*To whom correspondence should be addressed. E-mail: LSS8@columbia.edu

**Fig. 1.** Overall structure of the adenylate binding region from *S. pombe* AMPK with bound AMP. The ATP-bound form is nearly identical (fig. S6) and reveals no global structural changes attributable to nucleotide identity. (A) Ribbon diagram of a single heterotrimer, with  $\alpha$ ,  $\beta$ , and  $\gamma$  subunits colored yellow, blue, and green, respectively. The single molecule of bound AMP is shown in CPK representation, and connections to the GBD and KD at the N-termini of the  $\beta$  and  $\alpha$  subunits, respectively, are indicated. (B) View rotated 90°, highlighting the adenylate binding entrance (AXP) and phosphate binding tunnel, which is capped on the putative KD-interaction surface by a polar flap from the  $\beta$  subunit. The structure corresponds to a heterotrimer defined by limited proteolysis, as indicated in (C): hatched regions were excluded. Each of the two crystal forms reported here includes a dimer of trimers in the asymmetric unit (D). Analytical ultracentrifugation analysis also demonstrates a dimer of trimers configuration.





enhancement of energy storage and use. AMPK also functions in organism-level energy homeostasis by responding to systemically circulating hormones, including leptin (8), adiponectin (9), and resistin (10).

Canonical AMPKs are  $\alpha\beta\gamma$  heterotrimers (1–3). Although gene fusions between the  $\beta$  and  $\gamma$  subunits are found in some plant species, the overall domain architecture of the enzyme is conserved in all eukaryotes (11). In humans, multiple genes encode isoforms of each AMPK subunit ( $\alpha 1$ ,  $\alpha 2$ ,  $\beta 1$ ,  $\beta 2$ ,  $\gamma 1$ ,  $\gamma 2$ , and  $\gamma 3$ ) (1). The  $\alpha$  subunit includes a typical serine-threonine kinase domain near the N terminus and a C-terminal regulatory domain characteristic of AMPKs. AMPK  $\beta$  subunits are required for trimer assembly and subcellular localization of the AMPK complex (12, 13). Many  $\beta$  isoforms include a glycogen-binding domain (GBD), for which structures are now known (14). The heart of AMPK regulation by adenylate binding is thought to reside in  $\gamma$  subunits, which are composed of four repeated cystathionine  $\beta$ -synthase (CBS) domains (15–17). A number of CBS domain crystal structures have been determined (18–20), but only one recent structure included a bound ligand (21). Biochemical and genetic studies have produced an

initial view of interactions among AMPK subunits (1) whereby  $\beta$  subunits play a central role in heterotrimer formation through interactions with both  $\alpha$  and  $\gamma$  subunits. Trimer interaction sites on both  $\alpha$  and  $\beta$  subunits have been mapped to their respective C-terminal regions (22). Nonetheless, the precise molecular architecture of the AMPK heterotrimer has not been defined.

We produced a trimer fragment from the AMPK genes of the yeast *Schizosaccharomyces pombe*, which yielded two distinct crystal forms that diffract x-rays to 2.6 Å (for the AMP complex) and 2.9 Å (for the ATP complex) resolution. The trimer core consists of residues  $\alpha 440$  to  $\alpha 576$ ,  $\beta 205$  to  $\beta 298$ , and the whole of the  $\gamma$  subunit,  $\gamma 1$  to  $\gamma 334$  (Fig. 1). The structure omits two regions of the AMPK complex: the  $\beta$  subunit N-terminal GBD (14) and the N-terminal kinase domain of  $\alpha$ , both of which have been characterized crystallographically (23, 24). Although the enzymology of *S. pombe* homologs has not been investigated, sequence conservation among AMPKs from different species suggests that the structures presented here will be representative for this protein class.

We determined crystal structures by selenomethionine multiwavelength anomalous diffraction (MAD) phasing (25) for both AMP- and

ATP-bound crystal forms that each contained a dimer of trimers in the asymmetric unit (Fig. 1 and table S1). The potential importance of this dimer of trimers is underscored by a human Wolf-Parkinson-White syndrome mutation [human  $\gamma 2$  Asn<sup>488</sup>→Ile<sup>488</sup> (N488I), corresponding to *S. pombe*  $\gamma$ S247 (26)] that maps to the interface. Further, dimerization is consistent with the observation from Marmorstein and co-workers that mutants that disrupt kinase domain (KD) dimerization in vitro fail to disrupt sucrose nonfermenting 1 (SNF1) complex dimerization in vivo, suggesting association through other domains (23). Each AMPK trimer is roughly triangular, with a wide base formed by the  $\gamma$  subunit, which associates with a tight  $\alpha\beta$  complex that forms the narrower apical domain (Fig. 1, A and B). The  $\alpha$  subunit C-terminal domain forms a compact, mixed  $\alpha\beta$  domain (fig. S1) that is topologically related to the kinase-associated domains (KADs) of microtubule affinity-regulating kinase (MARK) kinases (27). The  $\beta$  subunit C-terminal region lacks an independent hydrophobic core (fig. S2) and wraps wholly around the  $\alpha$  KAD (Fig. 1, A and B, and fig. S4), forming extensive hydrophobic contacts. These features suggest an obligate nature for  $\alpha\beta$  complexes.

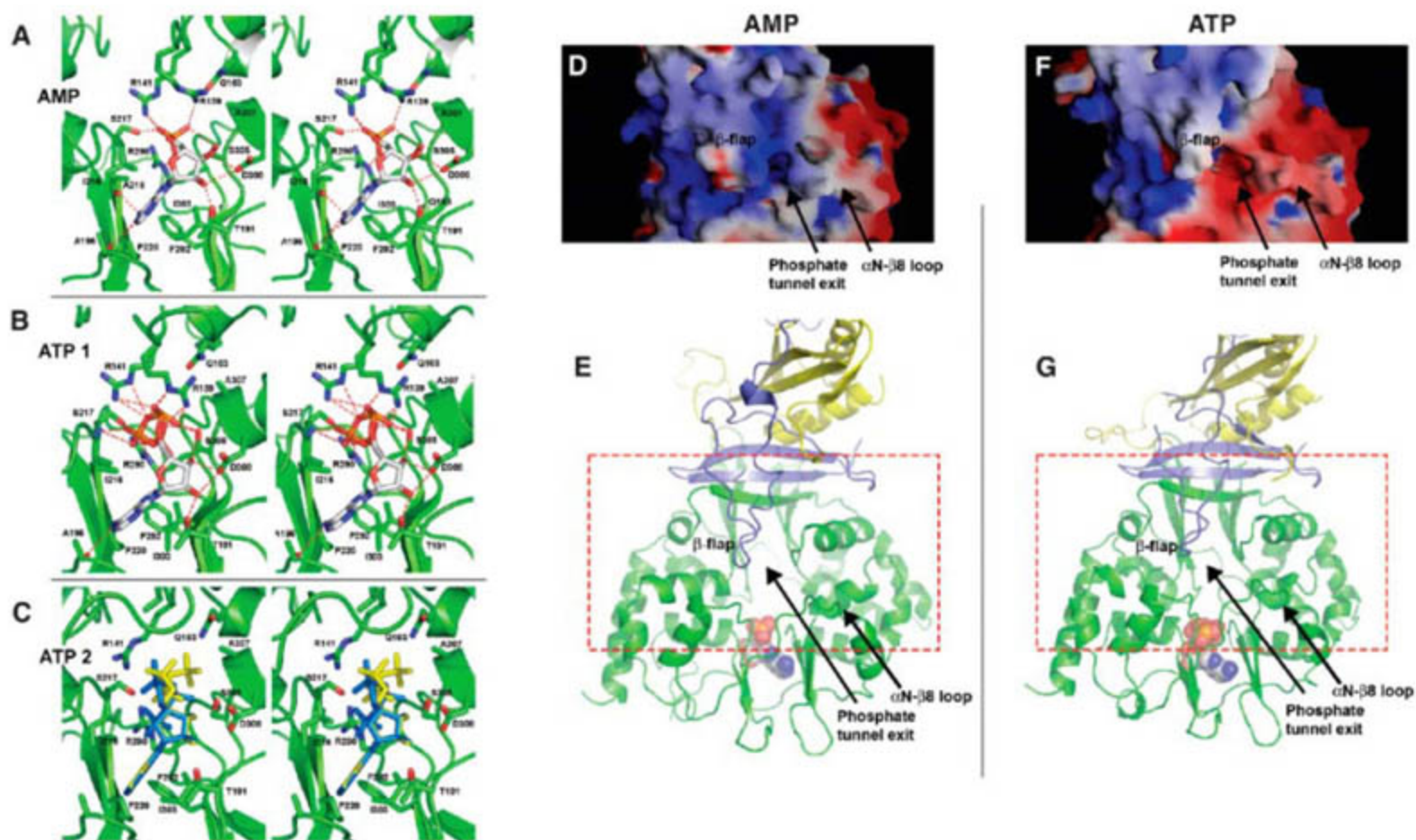


**Fig. 2.** Nucleotide binding. (A) Stereo diagram of AMP bound within the  $\gamma$  subunit. Adenine and ribose moieties are bound by functional groups within the CBS3-CBS4 domain pair; however, the terminal  $\alpha$ -phosphate forms salt bridges with two Arg side chains ( $\gamma$ R139 and  $\gamma$ R141) donated from CBS domain 2. (B) One protomer exhibits a single ATP conformation (ATP 1), whereas the other (C) adopts multiple alternate conformations (ATP 2). ATP

binds through a set of protein ligands identical to those used by AMP, accommodating the  $\beta$  and  $\gamma$  phosphates of ATP by adopting a compact helical structure for the triphosphate group (B). Electrostatic surfaces of the putative kinase-binding face, looking into the phosphate tunnel, show that the charge potential of the tunnel entrance is largely positive (blue) when AMP is bound [(D) and (E)] but negative (red) when ATP is bound [(F) and (G)].



The  $\gamma$  subunit forms an elliptical disk with an aqueous pore in the center. An adenine nucleotide is bound at the interface between CBS domains 3 and 4, positioning the phosphate groups in the pore. CBS domains 1 and 2 form the interface with the  $\alpha\beta$  complex (Fig. 1, A and B, and fig. S5). The  $\gamma$  interface to  $\alpha\beta$  is mediated primarily by interaction of a two-stranded  $\beta$  sheet from the  $\beta$  subunit, which hydrogen bonds with the  $\beta 1$  strand of  $\gamma$  to form a three-stranded intersubunit  $\beta$  sheet (Fig. 1 and fig. S5). This result disagrees with a recent mutagenesis study that concluded that there is no direct binding between  $\beta$  and  $\gamma$  (28). In contrast to the  $\alpha\beta$  complex, very few hydrophobic interactions are formed between  $\beta$  and  $\gamma$ , with this interface formed mainly through hydrogen bonding and salt bridge interactions, suggesting that  $\beta\gamma$  association may not be obligatory.

The  $\gamma$  subunit structures reported here provide initial views of CBS domains binding their regulatory ligands. A single molecule of either ATP or AMP binds at the same site, between  $\beta$  strands 6 and 7 of CBS3 and  $\beta$  strands 9 and 10 of CBS4 (Fig. 2). ATP and AMP bind in nearly identical conformations and use the same set of ligating residues. In addition to these structural elements from CBS3 and CBS4, CBS2 also contributes critical interactions important for binding the nucleotide phosphates. Remarkably, outside the localized nucleotide binding regions, no substantial structural changes attributable to bound nucleotide are observed among these four independent trimers (fig. S6).

In both ATP- and AMP-bound structures, a hydrophobic cleft formed from the side chains

from CBS3 ( $\gamma 1216$  and  $\gamma P220$ ) (26) and CBS4 ( $\gamma 1303$  and  $\gamma F292$ ) sandwich the adenine ring. The N2 ring nitrogen hydrogen bonds to the backbone carbonyl groups of  $\gamma A196$  and  $\gamma A218$ . The ribose moiety is bound in a polar pocket in CBS4, in which the ribose 2' and 3' hydroxyls are hydrogen bonded to side chain atoms of  $\gamma T191$ ,  $\gamma D308$ , and  $\gamma S305$ . In the AMP complex structure (Fig. 2A), the terminal AMP  $\alpha$ -phosphate forms salt bridges with the side chain of the conserved residue  $\gamma R290$  in CBS4 and two residues in CBS2,  $\gamma R139$  and  $\gamma R141$ . Excellent electron density is observed for all AMP atoms in the complex structure (fig. S7). The ATP phosphates are ligated by an identical set of arginine side chains (Fig. 2, B and C); however,  $\gamma R290$  ligates the terminal  $\gamma$ -phosphate, and  $\gamma R139$  and  $\gamma R141$  have poor density and appear to adopt multiple conformations in coordinating the  $\alpha$ - and  $\beta$  phosphates.

In AMPK, unlike the vast majority of ATP-bound protein structures, no electron density for metal counterions is observed bound to ATP. To confirm this observation, we performed experiments with crystals grown in the presence of 2 mM  $GdCl_3$ . The  $Gd^{3+}$  lanthanide ion is known to effectively substitute for  $Mg^{2+}$  in ATP substructures (29) and provides a large anomalous signal for crystallographic experiments. Anomalous difference maps revealed no bound ions (fig. S7). These observations suggest that ATP-bound metal counterions must be stripped before binding to AMPK, where charge balance is provided mainly by the side chains of arginine residues. This agrees with the prior observation from Hardie

and co-workers that  $Mg^{2+}$  is not required for ATP binding by purified  $\gamma$  subunits (16).

Our structural findings are in agreement with the reported relative binding affinities of AMP ( $\sim 100 \mu M$ ) and ATP ( $\sim 400 \mu M$ ) for a protein encoding fragments of the CBS3 and CBS4 domains of the human  $\gamma 2$  subunit (16). However, the apparent absence of regulation by AMP of *S. cerevisiae* AMPK activity (30, 31) raises the possibility that nucleotide-dependent regulation of *S. pombe* AMPK may differ from that of the human enzyme. Cellular ATP concentrations are higher than AMP concentrations, often by an order of magnitude. Even when ATP concentrations fall, leading to AMPK activation, ATP concentrations generally remain higher than AMP. Thus, tighter binding to AMP is a functional requirement for AMPK. The structures presented suggest how AMPK binds ATP more weakly than AMP. This appears to be accomplished, at least in part, through the necessity for stripping ATP of shielding ions for binding to the adenylate sensor. Further, the adenylate binding site is better able to accommodate the smaller AMP ligand: The  $\alpha$  phosphate of AMP and the  $\gamma$  phosphate of ATP are coordinated by the same Arg side chains, and the positions of the two terminal phosphates are nearly the same (Fig. 2 and fig. S6).

The overall orientation of nucleotide binding, for both AMP and ATP, situates the nucleotide phosphates toward an internal cavity that we refer to as the phosphate tunnel, which spans the breadth of the  $\gamma$  subunit disk (Fig. 1B). In both ATP- and AMP-bound forms, the surface-exposed nucleo-

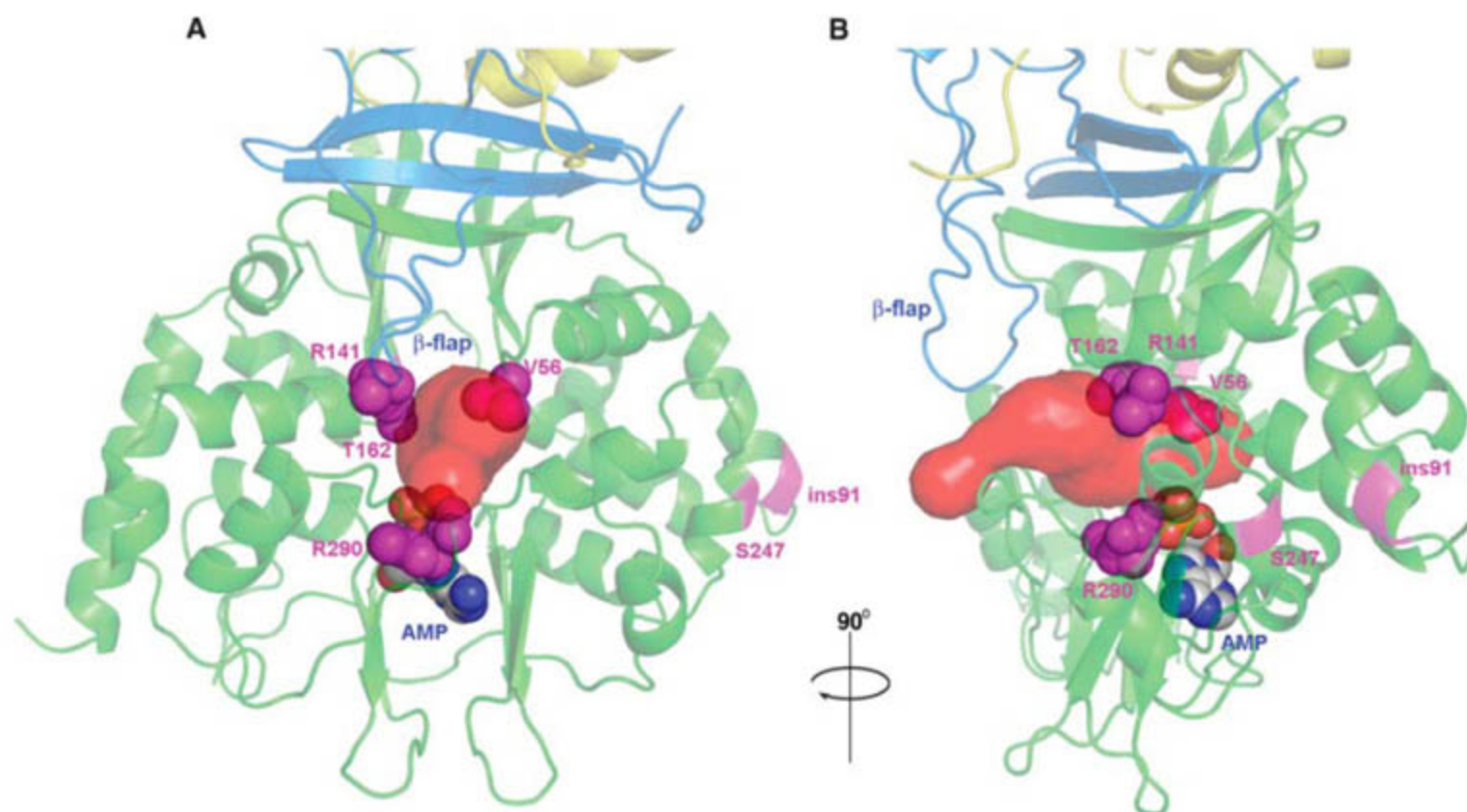


**Fig. 3.** [(A) and (B)] Functional mutations map within the phosphate binding tunnel, a large internal cavity that traverses the  $\gamma$  subunit, shown in red. The majority of known function-impairing mutants map to the

surface of this tunnel, positioned between the terminal phosphate of the bound nucleotide and the putative kinase-binding face. Two orthogonal views are shown.



tide groups include parts of the adenine ring and the phosphate-distal face of the ribose moiety. These surface-exposed groups are identical in both AMP- and ATP-bound structures, suggesting that the nucleotide-binding face of the AMPK regulatory trimer is unlikely to function as the site of activation modulated by adenylate binding. The primary differences between AMP- and ATP-bound forms of the heterotrimer lie within the phosphate tunnel. One substantial difference between the ATP and AMP complexes is in the surface electrostatic potentials at the distal exit of the phosphate tunnel, the putative kinase-interaction face (Fig. 2, D to G). This suggests the possibility that the different effects of these ligands might arise from the charge difference between the mono- and triphosphate groups of AMP and ATP.

Prior studies have identified a number of mutations within the regulatory heterotrimer that lead to impaired function of AMPK, primarily in the  $\gamma$  subunit (*I*). These mutations include an insertion in helix E at position  $\gamma$ 91 (32), and a point mutation at  $\gamma$ S247 (N488I in human  $\gamma$ 2) (33), which is found within the dimer-of-trimers interface region. However, the large majority of functionally important mutations, which include changes to residues  $\gamma$ R290 (human  $\gamma$ 2 R531) (34),  $\gamma$ R141 (human  $\gamma$ 2 H383) (32),  $\gamma$ V56 (human  $\gamma$ 2 R302) (35), and  $\gamma$ T162 (human  $\gamma$ 2 T400N) (33), are all found lining the interior surface of the phosphate tunnel (Fig. 3, A and B). Residues  $\gamma$ R290 and  $\gamma$ R141 coordinate nucleotide phosphates; however, the other mutations, relative to the bound nucleotide phosphate groups, are positioned further toward the protein surface opposite to the nucleotide binding face. This face of the molecule, where  $\alpha$ ,  $\beta$ , and  $\gamma$  subunits meet, may constitute a region for KD interaction, and we thus refer to it as the putative kinase domain interaction face (Figs. 1B and 3).

The phosphate tunnel traverses the  $\gamma$  subunit, defining a large void that is capped on the KD-binding face by a polar loop from the  $\beta$  subunit. We refer to this loop, which includes residues 244 to 255, as the  $\beta$  flap. The region of the  $\beta$  flap that covers the phosphate tunnel includes only polar and charged residues and makes no contacts to the hydrophobic core, suggesting the possibility for structural rearrangement. The  $\beta$  flap appears to be highly mobile (average *B* factors of 84.3 Å<sup>2</sup> in the four independent  $\beta$  subunits, as compared with an overall average *B* factor of 51.6 Å<sup>2</sup> for all protein atoms) and adopts slightly different conformations in the four independent copies of the structures presented here. The majority of  $\gamma$ -subunit mutations that affect AMPK activation are positioned within the phosphate tunnel, between the terminal phosphate of bound AXP and the  $\beta$  flap. Because the difference between the inhibitory (ATP) and activating (AMP) ligands is in the number of phosphates placed within the tunnel and because mutants that affect kinase activation also lie within this tunnel, it appears likely that this represents a critical regulatory region.

We have presented crystal structures that define the core heterotrimeric architecture for

AMPKs. The *S. pombe* AMPK binds either AMP or ATP at a single site, suggesting that activating ligands such as AMP are likely to function by displacing the inhibitory ligand ATP. Nonetheless, possible binding of additional regulatory nucleotides in the context of nucleotide mixtures or the holoenzyme complex cannot be excluded. Although a detailed understanding of the mechanism of AMPK regulation will require structures of the holoenzyme, the structures presented here should provide an entry point for the rational design of AMPK-directed therapeutics.

#### References and Notes

- B. B. Kahn, T. Alquier, D. Carling, D. G. Hardie, *Cell Metab.* **1**, 15 (2005).
- D. G. Hardie, *Endocrinology* **144**, 5179 (2003).
- B. E. Kemp et al., *Biochem. Soc. Trans.* **31**, 162 (2003).
- T. Leff, *Biochem. Soc. Trans.* **31**, 224 (2003).
- D. G. Hardie, S. A. Hawley, J. W. Scott, *J. Physiol.* **574**, 7 (2006).
- S. B. Jørgensen, E. A. Richter, J. F. Wojtaszewski, *J. Physiol.* **574**, 17 (2006).
- N. Musi, H. Yu, L. J. Goodyear, *Biochem. Soc. Trans.* **31**, 191 (2003).
- Y. Minokoshi et al., *Nature* **415**, 339 (2002).
- T. Yamauchi et al., *Nat. Med.* **8**, 1288 (2002).
- R. R. Banerjee et al., *Science* **303**, 1195 (2004).
- V. Lumbrales, M. M. Alba, T. Kleinow, C. Koncz, M. Pages, *EMBO Rep.* **2**, 55 (2001).
- O. Vincent, R. Townley, S. Kuchin, M. Carlson, *Genes Dev.* **15**, 1104 (2001).
- S. M. Warden et al., *Biochem. J.* **354**, 275 (2001).
- G. Polekhina et al., *Structure* **13**, 1453 (2005).
- J. Adams et al., *Protein Sci.* **13**, 155 (2004).
- J. Scott et al., *J. Clin. Investig.* **113**, 274 (2004).
- T. Daniel, D. Carling, *J. Biol. Chem.* **277**, 51017 (2002).
- S. Meyer, R. Dutzler, *Structure* **14**, 299 (2006).
- M. D. Miller et al., *Proteins* **57**, 213 (2004).
- R. Zhang et al., *Biochemistry* **38**, 4691 (1999).
- S. Meyer, S. Savaresi, I. C. Forster, R. Dutzler, *Nat. Struct. Mol. Biol.* **14**, 60 (2007).
- T. J. Iseli et al., *J. Biol. Chem.* **280**, 13395 (2005).

- V. Nayak et al., *Structure* **14**, 477 (2006).
- M. J. Rudolph, G. A. Amodeo, Y. Bai, L. Tong, *Biochem. Biophys. Res. Commun.* **337**, 1224 (2005).
- W. A. Hendrickson, J. R. Horton, D. M. LeMaster, *EMBO J.* **9**, 1665 (1990).
- Single-letter abbreviations for the amino acid residues are as follows: A, Ala; C, Cys; D, Asp; E, Glu; F, Phe; G, Gly; H, His; I, Ile; K, Lys; L, Leu; M, Met; N, Asn; P, Pro; Q, Gln; R, Arg; S, Ser; T, Thr; V, Val; W, Trp; and Y, Tyr.
- N. Tochio et al., *Protein Sci.* **15**, 2534 (2006).
- K. A. Wong, H. F. Lodish, *J. Biol. Chem.* **281**, 36434 (2006).
- X. Zhang et al., *Mol. Cell* **6**, 1473 (2000).
- W. A. Wilson, S. A. Hawley, D. G. Hardie, *Curr. Biol.* **6**, 1426 (1996).
- A. Woods et al., *J. Biol. Chem.* **269**, 19509 (1994).
- E. Blair et al., *Hum. Mol. Genet.* **10**, 1215 (2001).
- M. Arad et al., *J. Clin. Investig.* **109**, 357 (2002).
- M. H. Gollob et al., *Circulation* **104**, 3030 (2001).
- M. H. Gollob et al., *New Engl. J. Med.* **344**, 1823 (2001).
- Coordinates have been deposited in the Protein Data Bank (accession number for AMP complex is 2O0X; for ATP complex, 2O0Y). Crystallographic data were acquired at the New York Structural Biology Center beamline X4A of the National Synchrotron Light Source, Brookhaven National Laboratory. We thank T. Burke and G. Ahlsen for help in biochemical experiments; X. Jin and C. Ciatto for crystallographic help; H. Mu for technical assistance; B. Chait, M. Cadene, and M. Gawinowicz for advice on mass spectrometry analyses; M. Gawinowicz for help in performing them; W. A. Hendrickson and P. D. Kwong for critique of the manuscript; and the reviewers for excellent suggestions. This work was supported in part by a National Institute of Diabetes and Digestive and Kidney Diseases grant and a Jules and Doris Stein Research to Prevent Blindness Foundation professorship award to L.S.

#### Supporting Online Material

www.sciencemag.org/cgi/content/full/1137503/DC1

SOM Text

Figs. S1 to S8

Table S1

13 November 2006; accepted 29 January 2007

Published online 8 February 2007;

10.1126/science.1137503

Include this information when citing this paper.

## Structure of Nup58/45 Suggests Flexible Nuclear Pore Diameter by Intermolecular Sliding

Ivo Melčák, André Hoelz,\* Günter Blobel\*

The nucleoporins Nup58 and Nup45 are part of the central transport channel of the nuclear pore complex, which is thought to have a flexible diameter. In the crystal structure of an  $\alpha$ -helical region of mammalian Nup58/45, we identified distinct tetramers, each consisting of two antiparallel hairpin dimers. The intradimeric interface is hydrophobic, whereas dimer-dimer association occurs through large hydrophilic residues. These residues are laterally displaced in various tetramer conformations, which suggests an intermolecular sliding by 11 angstroms. We propose that circumferential sliding plays a role in adjusting the diameter of the central transport channel.

The nuclear pore complex (NPC) mediates the selective exchange of macromolecules between the nucleus and cytoplasm. The NPC is a ringlike structure with an eight-fold symmetry. A central channel is embraced by rings and spokes that are attached to the pore membrane domain of the nuclear envelope (*1, 2*). Composed of a set of proteins termed nucleoporins (nups), the NPC is one of the largest supramolecular as-

semblies in the eukaryotic cell (~120 megadaltons in vertebrates) (*3*). About 30 different nups are assembled into multiprotein subcomplexes that serve

Laboratory of Cell Biology, Howard Hughes Medical Institute, The Rockefeller University, 1230 York Avenue, New York, NY 10021, USA.

\*To whom correspondence should be addressed. E-mail: hoelza@rockefeller.edu (A.H.), blobel@rockefeller.edu (G.B.)



as the “building blocks” of the NPC (4, 5). Modeling studies have suggested that most nups are constructed from one or two of a small number of structural domains: coiled-coils,  $\alpha$ -helical sole-noids,  $\beta$  propellers, and natively unfolded segments containing phenylalanine-glycine repeats (FG repeats) (6). Current translocation models (5, 7–9) are based on the transient, low-affinity binding of cargo-loaded transport factors to FG repeats (10–12). Large-scale structural rearrangements that occur in response to transport include the constriction and dilation of the central channel, as well as structural alterations of the peripheral assemblies of the NPC (2, 13–16). However, at present, the molecular details of the structural changes of the NPC are unknown.

The central channel of the NPC is lined by the Nup62 complex, which consists of Nup62, Nup58, Nup54, and Nup45 (17). The constituents of the Nup62 complex display a similar domain organization, in which a  $\sim$ 200-residue  $\alpha$ -helical region is flanked by FG repeats (Fig. 1A) (18). Of these two distinct structural elements, the  $\alpha$ -helical regions are likely to form the perimeter of the channel, whereas the flanking, tentacle-like FG repeats sample the space around the channel, entropically occluding it.

The  $\alpha$ -helical regions of all four nups have been predicted to form coiled-coil domains that consist of subdomains separated by short connecting segments (18). Nup58 and Nup45 are alternatively spliced forms that differ only in their unstructured region (19). The yeast homologs are essential for cell viability (20–22) and for the formation of a functional “minimal” NPC (23).

We assembled a *Rattus norvegicus* Nup62 complex that contains the predicted structured regions of Nup62 (residues 322 to 525), Nup54 (residues 115 to 510), and Nup58 (residues 239 to 415). Through monitoring the formation and stability of complexes, a series of N- and C-terminal deletion constructs was designed. We identified a stable Nup62 complex core that is composed of residues 322 to 525 of Nup62, residues 346 to 494 of Nup54, and residues 327 to 415 of Nup58 (Fig. 1, A and B). The minimal core domains of Nup58 and Nup45 are identical, and therefore, we refer to Nup58 and Nup45 as Nup58/45, using the residue numbering of Nup58 in the text below.

Reconstituted Nup62 complexes form concentration-dependent dynamic assemblies, as judged by size-exclusion chromatography (Fig. 1C). In addition, we analyzed the behavior of a Nup58/45 fragment containing residues 327 to 399 (fig. S1). As do the Nup62 complexes, the Nup58/45 fragment exhibited substantial concentration-dependent mobility, again indicating a dynamic, dimer-tetramer equilibrium in solution. At low salt concentrations, Nup58/45 forms a stable tetrameric assembly, which suggests that the association is governed by electrostatic interactions (fig. S1).

From the purified Nup62 core complex, only the Nup58/45 core domain, composed of residues 327 to 415, crystallized, whereas Nup62, Nup54, and excess Nup58/45 remained intact in the drop solution (fig. S2). Two independent crystallization conditions yielded two Nup58/45 crystal forms, one belonging to the tetragonal space group  $P4_322$  and the other to the orthorhombic space group  $C222_1$ . The structures of both crystal forms were solved by single-wavelength anomalous dispersion (SAD), using osmium-derivatized crystals. The final model was refined to a 2.85 Å resolution with an  $R_{\text{work}}$  of 25.0% and an  $R_{\text{free}}$  of 28.8% and contains residues 327 to 411. No electron density was observed for the final four residues that are presumed to be disordered and therefore have been omitted from the final model (table S1).

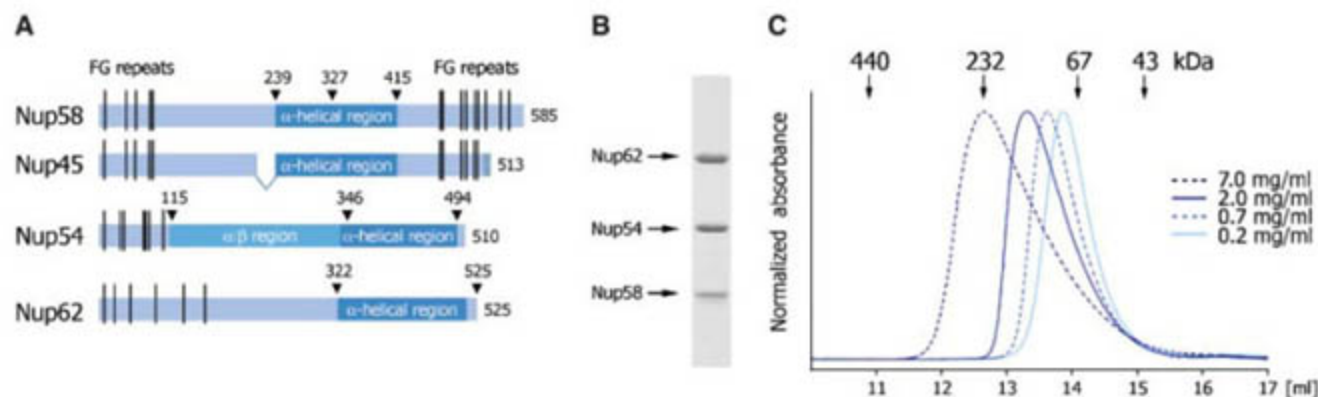
Nup58/45 tetramers in the two independent crystal forms exhibit entirely different crystal packing arrangements. The asymmetric units of the tetragonal and orthorhombic crystals contain 4 and 18 Nup58/45 protomers, respectively. In the packing of both crystals, the Nup58/45 tetramers result from the dimerization of identical dimers. In each of the two crystal forms, the tetrameric Nup58/45 assemblies are topologically identical, but display distinct structural differences. As the overall findings are similar, we will focus our discussion on the structural information obtained from the tetragonal crystal form.

The Nup58/45 protomer folds into an antiparallel hairpin structure, in which two  $\alpha$  helices (the N and the C helix) are connected by a short loop (Fig. 2A). The C helix protrudes from the hairpin structure and exposes three terminal helical turns.

The four protomers in the asymmetric unit of the tetragonal crystals are similar, and the topologically equivalent C $\alpha$  carbons superimpose with a root-mean-square deviation of  $\sim$ 0.4 Å. Furthermore, the protomers dimerize in an antiparallel arrangement, in which the N and C helices of one protomer pack against the N and C helices of the second protomer, forming a four-helix bundle with an interprotomer angle of  $\sim$ 156° (Fig. 2A). The two protomers in the dimer are primarily held together by numerous van der Waals contacts (fig. S3), burying  $\sim$ 2,550 Å<sup>2</sup> of surface area. The comparison of the average-temperature B-factors of the entire model ( $\sim$ 43 Å<sup>2</sup>) with the buried dimerization interface residues ( $\sim$ 34 Å<sup>2</sup>) suggests a rigid and well-defined dimer interface. The overall dimensions of the dimer are about 82 by 24 by 21 Å. Except for surface residues, the dimer is symmetric with a pseudo-two-fold axis running through the dimerization interface.

The two identified tetrameric assemblies in both crystal forms consist of two dimers that interact with each other in a “head-to-head” orientation with their N helices. Therefore, the resulting tetramerization interface is composed exclusively by the four N helices that form two antiparallel, intertwined pairs (Fig. 2B). The two tetramers (conformer 1 and 2) of the tetragonal crystal form have two-fold rotational symmetry, and the two-fold symmetry axis of each tetramer coincides with a crystallographic two-fold axis. However, although the crystallographic two-fold axis runs perpendicular to the long axis of the tetramerization interface in one tetramer, it runs parallel to the long axis in the other (Fig. 2B). The crystallographic consequence is that two of the four protomers in each tetramer are identical. The two conformers differ by an  $\sim$ 6 Å lateral displacement of their dimer subunits along the long axis of the tetramerization interface (Fig. 2C). We identified two similar, structurally distinct tetrameric assemblies in the orthorhombic crystal form (conformer 3 and 4), which exhibits an entirely different crystal packing arrangement (fig. S4). The conformation of these tetramers does not appear to be dominated by the crystal packing, as the crystal contains seven structurally independent tetrameric assemblies that give rise to two conformations. All seven tetramers contain a two-fold

**Fig. 1.** Organization and dynamic behavior of the Nup62 complex. (A) Domain structures of Nup58, Nup45, Nup54, and Nup62. The  $\alpha$ -helical regions (dark blue), unstructured regions (light blue), FG repeats (black lines), and the numbering of the Nup62 complex fragments are indicated. (B) Coomassie-stained SDS-polyacrylamide gel showing results of electrophoresis of the purified Nup62 core complex. (C) Gel filtration profiles of the minimal Nup62 complex at the indicated protein concentrations. The elution positions for molecular mass standards are shown. All profiles were obtained in a buffer containing 150 mM NaCl.





axis, which, as do the tetramers in the tetragonal crystal form, run either parallel (three tetramers, conformer 3) or perpendicular (four tetramers, conformer 4) to the long axis of the dimer-dimer interface. However, in contrast to the tetragonal crystal form, only one of the seven tetrameric assemblies is generated by a crystallographic two-fold axis (conformer 3). Thus, the observed tetramerization plasticity is likely an important functional feature of the oligomerization of Nup58/45. Furthermore, the dimer-tetramer dynamics observed in solution likely result from the reversible association of Nup58/45 dimers.

In contrast to the dimerization interface, which is almost entirely hydrophobic, the interactions

between the two dimers are solely electrostatic, which explains the salt concentration-dependent, dynamic behavior of Nup58/45 in solution. The tetramerization interface is formed by an extensive side-chain hydrogen bond network that ties the N helices of the four protomers together (Fig. 3). In this tetramerization interface, most of the interactions occur within each pair of aligned, antiparallel N helices, involving primarily the side chains of six residues (Arg<sup>333</sup>, Gln<sup>344</sup>, Arg<sup>347</sup>, Gln<sup>348</sup>, Glu<sup>351</sup>, and Asn<sup>355</sup>) of each protomer. Together, these residues form a continuous electrostatic surface, in which alternating positively and negatively charged side chains are distributed in the center of the interface. The majority of the interactions are

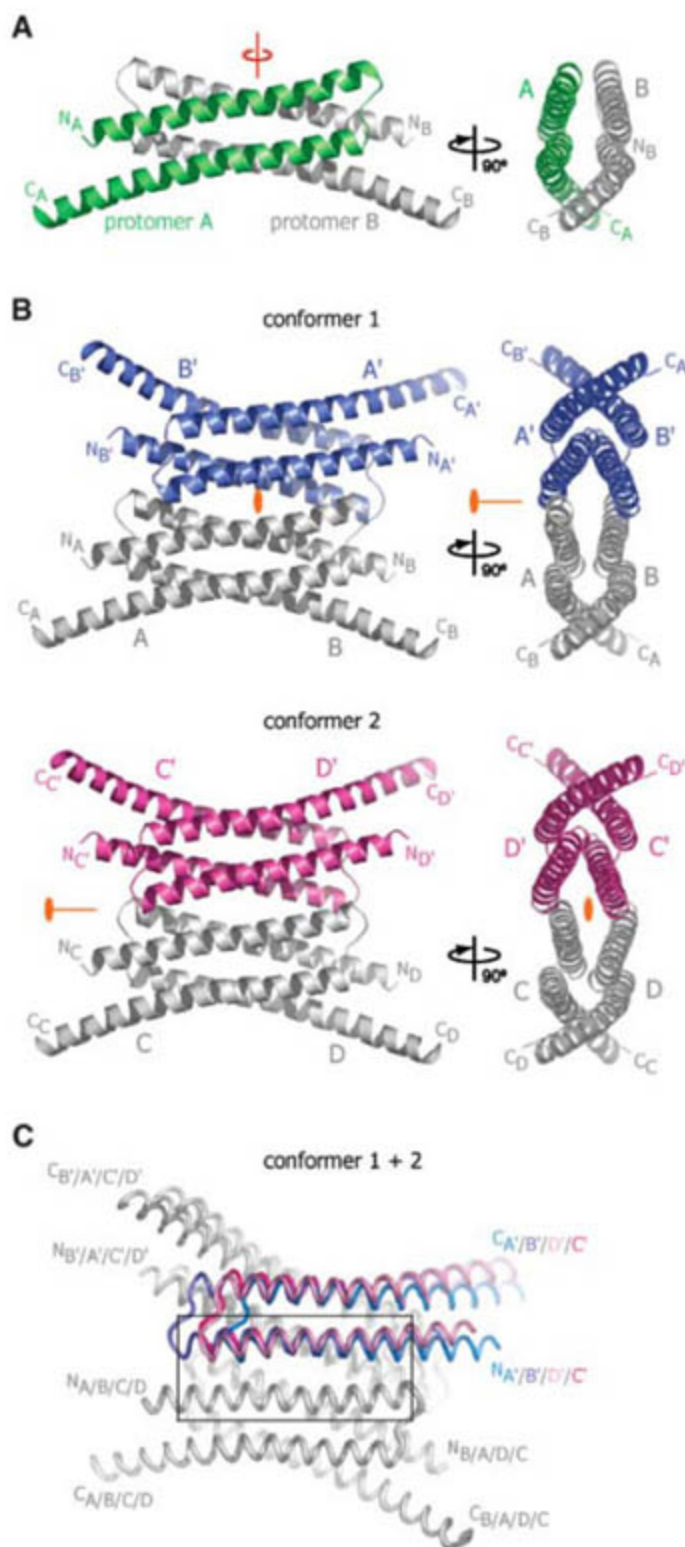
mediated by direct intermolecular contacts, although some residues make hydrogen bonds through water molecules trapped at the protein-protein interface. The tetragonal crystals contain two tetrameric Nup58/45 conformers that together contain four unique pairs of N helices. By superposition of all four pairs of N helices, we can discern four different configuration states (states I to IV) that exhibit a maximum lateral displacement of ~11 Å (Figs. 2C and 3). Furthermore, the superposition reveals that the lateral displacement between the two asymmetric tetrameric Nup58/45 conformers results from alternative hydrogen-bond networks, in which each side chain of the same set of interface residues has the propensity to switch interaction partners. For example, the side chain of Asn<sup>355</sup> engages four different residues in the two tetramers and forms hydrogen bonds with Gln<sup>344</sup>, Arg<sup>347</sup>, Gln<sup>348</sup>, or Glu<sup>351</sup> (Fig. 3). Overall, the Nup58/45 core domain is highly conserved in vertebrates (figs. S5 and S6). The residues of the Nup58/45 that are crucially involved in the formation of the dimer-dimer interface are invariant across vertebrates, underlining the significance of the Nup58/45 homo-tetramer.

The identification of multiple interaction states in which rigid Nup58/45 dimers are sequentially shifted along the dimer-dimer interface for a distance of ~11 Å suggests an intermolecular sliding mechanism. In general, sliding requires a series of energetically equivalent states along a sliding pathway with low transition energy barriers (24). Our sliding hypothesis is strengthened by the finding that the Nup58/45 core domain forms a salt concentration-dependent, dynamic dimer-tetramer equilibrium in solution; this implies that Nup58/45 dimers loosely associate and are indeed capable of freely rearranging into distinct tetrameric conformations. Each of the four states portrays a snapshot of the structural alterations that occur when two Nup58/45 dimers slide against each other on an ~11 Å sliding pathway (Figs. 2C and 3, and movies S1 to S3).

The rearrangement of the dimer-dimer interaction surface that results in the formation of alternative hydrogen-bond networks is enabled by an adaptable electrostatic surface with two major structural features: (i) The interaction surface is constructed by a group of residues that are arranged in a checkerboard-like distribution and that are capable of switching interaction partners by acting alternatively as either hydrogen-bond donors or acceptors, or as both. For example, Asn<sup>355</sup> alternates its roles in electrostatic interactions with Gln<sup>344</sup>, Arg<sup>347</sup>, Gln<sup>348</sup>, and Glu<sup>351</sup>; (ii) the plasticity of the interaction surface is supported by the relatively high flexibility of long side chains. In contrast to short side chains, long side chains are capable of sampling a substantially larger volume for interaction partners, as illustrated by the alternate conformations of the side chains of Arg<sup>333</sup> and Gln<sup>344</sup> in the different tetrameric assemblies.

The central channel of the NPC has the ability to alter its diameter (2, 13, 14, 16). The mutual arrangement of subunits within a single Nup58/45

**Fig. 2.** Structures of tetrameric Nup58/45 assemblies from the tetragonal crystal form. **(A)** Ribbon representation of a Nup58/45 dimer, showing protomer A in green and protomer B in gray; (right) a 90° rotated view. A pseudo-two-fold axis (red) is indicated. **(B)** Ribbon representations of the two tetrameric conformers, indicating the location of the crystallographic two-fold axes (orange), which run differently through the two tetramers. (Right) A 90° rotated view. The different coloring of dimers (blue, conformer 1; purple, conformer 2) illustrates the alternative tetrameric configurations of the two conformers. Symmetry-related protomers are indicated. Conformers 1 and 2 are constructed by the protomers A and B, C and D, and their symmetry-related protomers A' and B' and C' and D', respectively. **(C)** Superposition of the two tetrameric Nup58/45 conformers. The unique protomers of the two tetrameric assemblies are superimposed onto protomer A of conformer 1 to highlight the lateral shift between the different conformers. For clarity, only one protomer of each superposition is colored. The N and C termini are labeled according to (B). The inset is expanded in Fig. 3.





tetramer can be altered by a sliding distance of at least ~11 Å. Nup58 and Nup45 are the most abundant constituents of the NPC (4). We propose that circumferential sliding of Nup58/45 in the channel perimeter results in an adjustable diameter in response to transport activity. In such a potentially circular, eight-fold symmetric arrangement of tetrameric Nup58/45 modules in which each can expand by ~11 Å, the diameter of the channel could increase by ~30 Å (Fig. 4, A and B).

In the assembled NPC, Nup58 and Nup45 are intimately associated with Nup54 and Nup62

(17, 18, 25, 26). Although the atomic structures for Nup54 and Nup62 have not been determined, they share a similar domain organization and contain conserved, amphipathic  $\alpha$ -helical regions that may also permit sliding (figs. S7 to S9). A multiple beltlike arrangement of such "sliding modules" in the channel perimeter along a nucleocytoplasmic axis may facilitate localized changes in channel diameter as cargo passes across (Fig. 4C). The FG repeats are flanking the  $\alpha$ -helical regions of the channel nups and function as a restrictive barrier and transport facilitator. It is conceivable that

binding of transport factors and substrate to FG repeats is coupled to sliding of the amphipathic helices in the perimeter of the transport channel.

The sliding of such  $\alpha$ -helical regions may extend to other nucleoporins, because the export of preribosomal subunits has been shown to depend on the yeast homologs of Nup58 and Nup62 (27), as well as the coiled-coil domains of Nup214 and Nup88 (28). Our hypothesis of large-scale sliding facilitated by  $\alpha$ -helical surfaces to adjust the diameter of a transport channel for the passage of cargo is to our knowledge not found elsewhere and may be limited to macromolecular transport across the NPC.

**Fig. 3.** Molecular details of the intermolecular sliding of two Nup58/45 dimers. The direction and the approximate sliding distance are indicated by black arrows. States I and IV are derived from conformer 1; states II and III are derived from conformer 2. The helices are colored and numbered according to Fig. 2, and critical interface residues are labeled and individually colored in all four states according to state I (top). For clarity, only two of the N-helix pairs that generate the tetramerization interface are shown. The electrostatic interactions between two sliding N helices are represented by red dashed lines, and water molecules are visualized as blue spheres.

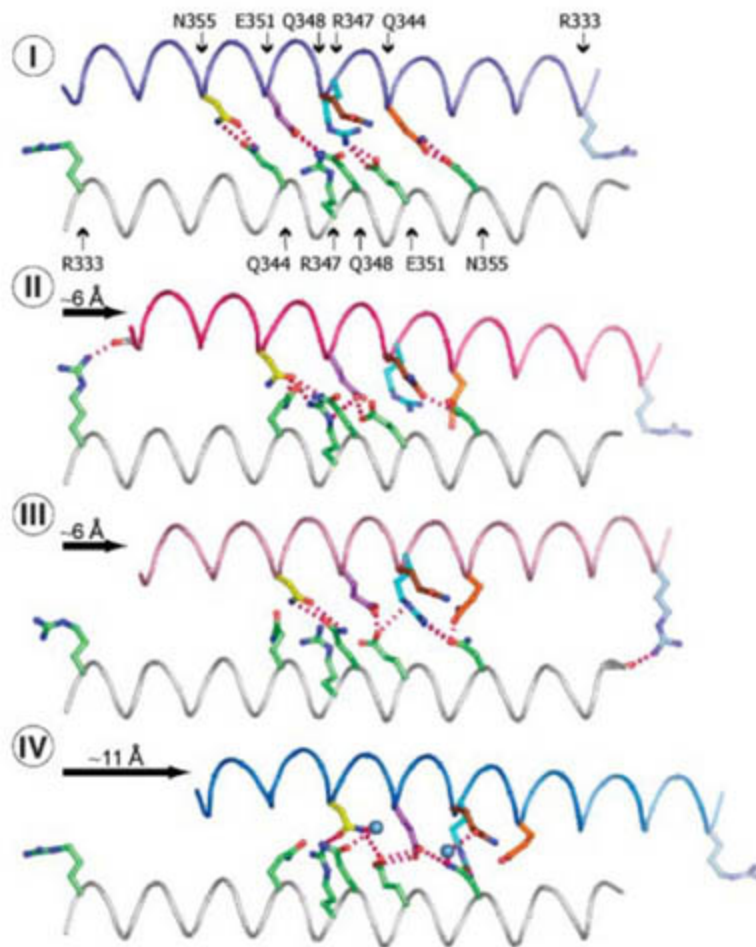
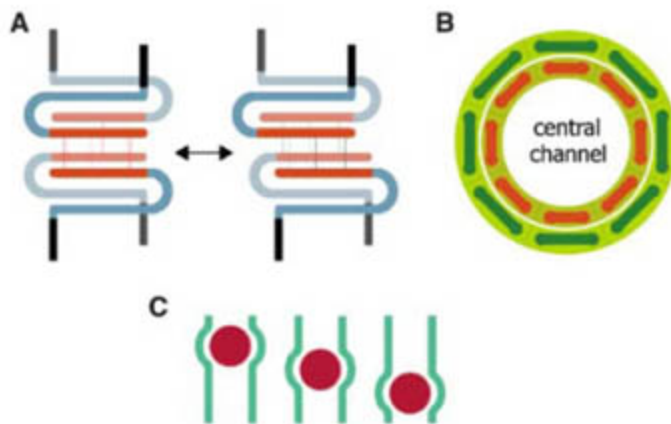


**Fig. 4.** Model of pore dilation by intermolecular sliding of Nup58/45 tetramers. (A) Schematic representation of the Nup58/45 sliding module. The four N helices that generate the tetramerization interface (orange), the C helices (light blue), and the C-terminal FG repeats (black) are indicated. The sliding of the Nup58/45 dimer surfaces formed by the N helices is facilitated by an alternative hydrogen bond network (red and green thin lines). Because the C helices with the attached FG repeats are likely to project to the inside of the central channel, the sliding N helices would face in the opposite direction. (B) Schematic representation of the central channel shown along the nucleocytoplasmic axis. Eight Nup58/45 tetrameric assemblies are circularly arranged to form a ring (red bars). The sliding of two Nup58/45 dimers against each other results in an overall extension of the Nup58/45 tetramer (green bars) that, in turn, causes the dilation of the central channel of the NPC. (C) Localized changes in channel diameter by  $\alpha$ -helical sliding in response to transport of cargo (red spheres) across the central channel (green).



**References and Notes**

1. D. Stoffler *et al.*, *J. Mol. Biol.* **328**, 119 (2003).
2. M. Beck *et al.*, *Science* **306**, 1387 (2004).
3. R. Reichelt *et al.*, *J. Cell Biol.* **110**, 883 (1990).
4. J. M. Cronshaw, A. N. Krutchinsky, W. Zhang, B. T. Chait, M. J. Matunis, *J. Cell Biol.* **158**, 915 (2002).
5. M. P. Rout *et al.*, *J. Cell Biol.* **148**, 635 (2000).
6. D. Devos *et al.*, *Proc. Natl. Acad. Sci. U.S.A.* **103**, 2172 (2006).
7. I. Ben-Efraim, L. Gerace, *J. Cell Biol.* **152**, 411 (2001).
8. K. Ribbeck, D. Gorlich, *EMBO J.* **20**, 1320 (2001).
9. R. Y. H. Lim *et al.*, *Proc. Natl. Acad. Sci. U.S.A.* **103**, 9512 (2006).
10. R. Bayliss, T. Littlewood, M. Stewart, *Cell* **102**, 99 (2000).
11. S. Fribourg, I. C. Braun, E. Izaurralde, E. Conti, *Mol. Cell* **8**, 645 (2001).
12. T. A. Isgro, K. Schulten, *Structure* **13**, 1869 (2005).
13. C. W. Akey, *Biophys. J.* **58**, 341 (1990).
14. C. W. Akey, D. S. Goldfarb, *J. Cell Biol.* **109**, 971 (1989).
15. E. Kiseleva, M. W. Goldberg, B. Daneholt, T. D. Allen, *J. Mol. Biol.* **260**, 304 (1996).
16. E. Kiseleva, M. W. Goldberg, T. D. Allen, C. W. Akey, *J. Cell Sci.* **111**, 223 (1998).
17. T. Guan *et al.*, *Mol. Biol. Cell* **6**, 1591 (1995).
18. T. Hu, T. Guan, L. Gerace, *J. Cell Biol.* **134**, 589 (1996).
19. T. Hu, L. Gerace, *Gene* **221**, 245 (1998).
20. E. C. Hurt, *EMBO J.* **7**, 4323 (1988).
21. S. R. Wente, M. P. Rout, G. Blobel, *J. Cell Biol.* **119**, 705 (1992).
22. P. Grandi, N. Schlaich, H. Tekotte, E. C. Hurt, *EMBO J.* **14**, 76 (1995).
23. L. A. Strawn, T. Shen, N. Shulga, D. S. Goldfarb, S. Wente, *Nat. Cell Biol.* **6**, 197 (2004).
24. M. Slutsky, L. A. Mirny, *Biophys. J.* **87**, 4021 (2004).
25. D. R. Finlay, E. Meier, P. Bradley, J. Horecka, D. J. Forbes, *J. Cell Biol.* **114**, 169 (1991).
26. C. Macaulay, E. Meier, D. J. Forbes, *J. Biol. Chem.* **270**, 254 (1995).
27. E. Hurt *et al.*, *J. Cell Biol.* **144**, 389 (1999).
28. R. Bernad, D. Engelsma, H. Sanderson, H. Pickersgill, M. Fornerod, *J. Biol. Chem.* **281**, 19378 (2006).
29. We thank Š. Melčáková, M. Müller, and T. Schwartz for help at the initial stages of the project; L. Gerace for the gift of cDNAs; B. Manjasetty (National Synchrotron Light Source) and C. Ralston (Advanced Light Source) for their excellent scientific support and help with x-ray measurements; T. Huber for stimulating discussions; E. Coutavas, M. King, A. Patke, and S. Solmaz for critical reading of the manuscript; and S. Etherton for help with editing of the manuscript. A.H. was supported by a grant from the Leukemia and Lymphoma Society. G.B. is an investigator of the Howard Hughes Medical Institute. The coordinates and structure factors have been deposited in the Protein Data Bank (accession code 2O5Z).

**Supporting Online Material**

www.sciencemag.org/cgi/content/full/315/5819/1729/DC1  
 Materials and Methods  
 Figs. S1 to S9  
 Table S1  
 References  
 Movies S1 to S3

29 September 2006; accepted 16 February 2007  
 10.1126/science.1135730



### Magnetic Molecule Isolation System

The MultiMACS Separator is a magnetic molecule isolation instrument for manual or automated use. Up to 96 samples such as mRNA, protein, virus particles, or biomolecule complexes can be extracted and purified in parallel via gentle, column-based procedures. This compact instrument can be integrated into robotic systems or operated manually on the bench, and centrifugation and vacuum steps are not needed. The isolation procedures rely on the small, paramagnetic MACS MicroBeads coupled to oligo (dT), protein A, protein G, streptavidin, or antibody molecules. Even small amounts of target molecules are captured.

**Miltenyi Biotec** For information +49 2204-8306-0 [www.miltenyibiotec.com](http://www.miltenyibiotec.com)



### Genotoxicity Screening Assay

GreenScreen HC is a novel human cell-based genotoxicity screening assay. Developed in a simple microplate format requiring less than 1 mg of compound, the assay is easily automated using standard laboratory equipment. According to the manufacturer, the GreenScreen HC's combination of high specificity and sensitivity make it the first in vitro mammalian cell assay suitable for early candidate screening. The test is designed to avoid the high number of positive results that can lead to time-consuming and expensive animal studies at the preclinical stage.

**Gentronix** For information +44 161 606 7268 [www.gentronix.co.uk](http://www.gentronix.co.uk)

### Real-Time PCR System

The StepOne Real-Time PCR System provides an easy and cost-effective way to conduct real-time polymerase chain reaction (PCR) experiments in a variety of applications that include gene expression, viral load, and genotyping experiments. Beginning users can benefit from the intuitive software wizards that guide them through set up, operation, and analysis. Experienced users seeking a personal real-time PCR system can customize experiment design parameters such as thermocycling protocols and nucleic acid template types. The low-throughput system features a space-saving small footprint.

**Applied Biosystems** For information 800-327-30022 [www.appliedbiosystems.com](http://www.appliedbiosystems.com)

### Faster RT-PCR

FastLane Kits streamline real-time reverse transcription-polymerase chain reaction (RT-PCR) analysis of cultured cells. By eliminating the need for RNA purification, the kits allow users to carry out real-time RT-PCR directly from cell lysates. The kits are suitable for experiments requiring rapid, high-throughput gene expres-

sion analysis, such as validation of small interfering RNA-mediated gene knockdown. The kits take only 12 minutes to prepare cell lysate, which can be used directly in reverse transcription or in real-time, one-step RT-PCR. To ensure reliable gene expression analysis in subsequent real-time PCR, RNA is immediately stabilized upon cell lysis and genomic DNA is effectively eliminated using a novel buffer.

**Qiagen** For information +49 (0) 21033-16410 [www.qiagen.com](http://www.qiagen.com)

### Homogenizer

The Dispomix instrument for sample homogenization and dispersion combines sterility with safety and ease of use. The closed, disposable Dispomix Tubes protect the sample and the environment from the moment of sampling to the final product transfer without the need for further sample manipulation. A septum ensures clean liquid transfers prior to and after the processing on the Dispomix Drive. The tube effectively avoids cross-contamination, aerosols, or contact by personnel with potentially infectious or toxic material.

**Xiril** For information +41 55 254 7777 [www.xiril.com](http://www.xiril.com)

### Orange Fluorescent Dye

A novel orange fluorescent dye can be used as a nuclear stain with living cells or as a cell location dye to define cell perimeter in a variety of cell-based assays. Water-soluble and membrane-permeable, CyTRAK Orange is suitable for live-cell imaging applications such as nucleus/cytoplasmic and cytoplasm/cytoplasmic membrane translocations, nucleus/cytoplasm translocations, and cell/cell boundary interactions as well as cell-based high-content screening and high-throughput screening, fixed-cell, and fluorescence in situ hybridization assays. This versatile fluorescent dye is

compatible with existing protocols and usable across a wide range of imaging platforms. It can be used in live cells in combination with common fluorophores such as green fluorescent protein fusions, fluorescein isothiocyanate (FITC) labeled antibodies, and far-red dyes. It permits the rapid staining of the nuclei of live or fixed cells, fluoresces at 615 nm, and is stable both photochemically and biologically. No cell lysing, washing, or ribonuclease is needed for use.

**Axxora** For information 800-900-0065 [www.axxora.com](http://www.axxora.com)

### Modular Detection Platform

The Paradigm Detection Platform is a modular system that allows easy configuration by the user. It features a selection of cartridges that can be interchanged in less than five minutes to meet different assay needs. Designed for labs with multiple users and applications, the high-throughput detector can read in formats from 6 to 1536 wells. Eight different cartridges will be available, based on detection modes including fluorescence polarization, time-resolved fluorescence, dual-fluorescence (including fluorescence resonance energy transfer), and luminescence. A monochromator-based absorbance cartridge will also be offered. The system software comes with a portfolio of generic protocol templates for the most common detection measurements. Assay protocols for third-party chemistry kits are also included.

**Beckman Coulter** For information 714-993-8955 [www.beckmancoulter.com](http://www.beckmancoulter.com)

Newly offered instrumentation, apparatus, and laboratory materials of interest to researchers in all disciplines in academic, industrial, and government organizations are featured in this space. Emphasis is given to purpose, chief characteristics, and availability of products and materials. Endorsement by *Science* or AAAS of any products or materials mentioned is not implied. Additional information may be obtained from the manufacturer or supplier.



## Classified Advertising



From life on Mars  
to life sciences

For full advertising details, go to [www.sciencecareers.org](http://www.sciencecareers.org) and click on **For Advertisers**, or call one of our representatives.

## United States &amp; Canada

E-mail: [advertise@sciencecareers.org](mailto:advertise@sciencecareers.org)  
Fax: 202-289-6742

**IAN KING** Sales Manager/Industry  
Phone: 202-326-6528

**DARYL ANDERSON** West/Midwest/Canada  
Phone: 202-326-6543

**ALLISON MILLAR** Northeast/Southeast  
Phone: 202-326-6572

## Europe &amp; International

E-mail: [ads@science-int.co.uk](mailto:ads@science-int.co.uk)  
Fax: +44 (0) 1223 326532

**TRACY HOLMES** Sales Manager  
Phone: +44 (0) 1223 326525

**CHRISTINA HARRISON**  
Phone: +44 (0) 1223 326510

**SVITLANA BARNES**  
Phone: +44 (0) 1223 326527

**LOUISE MOORE**  
Phone: +44 (0) 1223 326528

## Japan

**JASON HANNAFORD**  
Phone: +81 (0) 52-757-5360  
E-mail: [jhannaford@sciencemag.jp](mailto:jhannaford@sciencemag.jp)  
Fax: +81 (0) 52-757-5361

**To subscribe to Science:**  
In U.S./Canada call 202-326-6417 or 1-800-731-4939  
In the rest of the world call +44 (0) 1223-326-515

Science makes every effort to screen its ads for offensive and/or discriminatory language in accordance with U.S. and non-U.S. law. Since we are an international journal, you may see ads from non-U.S. countries that request applications from specific demographic groups. Since U.S. law does not apply to other countries we try to accommodate recruiting practices of other countries. However, we encourage our readers to alert us to any ads that they feel are discriminatory or offensive.

ScienceCareers.org  
We know science

## POSITIONS OPEN

Skidmore College seeks an **ASSOCIATE DIRECTOR** for its Microscopy Imaging Center (SMIC). The successful candidate will be expected to help run our microscopy facilities and work with faculty and students in microscopy-based teaching and research activities. The ongoing job duties will consist of maintaining the microscopes, image capture systems, preparatory equipment, and laboratories of SMIC. The Associate Director will help prepare and process materials for microscopy, train individuals on different microscopy systems, and maintain our image archives and website. The Associate Director will also participate in teaching and grantwriting opportunities as time permits. SMIC is an integrated unit with fluorescence, confocal laser scanning, scanning electron, EDS and transmission electron microscopy (TEM) facilities.

Candidates must have a Master's or Ph.D. in the natural sciences, preferably biology or micropaleontology, and significant experience in microscopy and microscopy-based preparation protocols. TEM and ultramicrotomy skills are highly desirable.

Please send curriculum vitae, three letters of recommendation, and a portfolio or publications demonstrating proficiency in light and electron microscopy. Application review will begin on April 15, 2007, and will continue until the position is filled.

Please send applications to: **Dr. David Domozych, Department of Biology, Skidmore College, 815 North Broadway, Saratoga Springs, NY 12866.**

Please note: This position is subject to May 2007 budget approval.

*Skidmore College is committed to being an inclusive campus community and, as an Equal Opportunity Employer, does not discriminate in its hiring or employment practices on the basis of gender, race or ethnicity, color, national origin, religion, age, disability, family or marital status, or sexual orientation.*

**FACULTY POSITION in NEURAL and BEHAVIORAL SCIENCES.** The Pennsylvania State University, College of Medicine, Department of Neural and Behavioral Sciences, in conjunction with the Program on Education in Human Structure, in Hershey, Pennsylvania, invites applications for a tenure-eligible faculty position at the **ASSISTANT PROFESSOR or ASSOCIATE PROFESSOR** level. Candidates must hold a Ph.D., M.D., or equivalent degree. Candidates should have experience in teaching gross anatomy and will play a major role in this team-taught course. The successful candidate will be expected to establish an active research program in neuroscience. The Department of Neural and Behavioral Sciences provides excellent facilities and opportunities for collaborative research and participation in graduate training programs. Applicants should send curriculum vitae, statement of research interests and goals, and contact information for three references to: **Search Committee, Department of Neural and Behavioral Sciences, H109, Penn State College of Medicine, P.O. Box 850, 500 University Drive, Hershey, PA 17033.** Closing date for applications: May 15, 2007. For your health, Hershey Medical Center is a smokefree campus. *Penn State is committed to Affirmative Action, Equal Opportunity and the diversity of its workforce.*

## ANATOMY/PHYSIOLOGY INSTRUCTOR

Santa Monica College is accepting applications for a full-time, tenure-track Anatomy/Physiology Instructor for fall 2007. Will teach lecture/laboratory courses in human anatomy and human physiology. Master's in any biological science, or Bachelor's in any biological science and Master's in biochemistry, biophysics, or marine science, or the equivalent. A strong background in human physiology is preferred. Salary is \$43,798 to \$103,536. Deadline to apply: April 17, 2007. For a district application and complete job description, please call telephone: 310-434-4336, or write to: **Santa Monica College, Human Resources, 1900 Pico Boulevard, Santa Monica, CA 90405,** or visit the website: <http://www.smc.edu>. *Equal Opportunity Employer.*

## POSITIONS OPEN

ASSISTANT/ASSOCIATE PROFESSOR of  
MICROBIOLOGY

Oklahoma State University Center for Health Sciences, College of Osteopathic Medicine, is seeking to fill a full-time, tenure-track faculty position in the Department of Biochemistry and Microbiology. This position requires a Ph.D. degree in microbiology, relevant postdoctoral experience, and a demonstrated potential for excellence in both medical mycology teaching and research. Interested candidates must apply online at website: <https://jobs.okstate.edu>, job number 02870. *Affirmative Action/Equal Opportunity Employer.*

ASSISTANT PROFESSOR  
Microbiology and Cell Science  
DIRECTORElectron Microscopy and Bioimaging Laboratory  
University of Florida

The Microbiology and Cell Science Department and the Interdisciplinary Center for Biotechnology Research (ICBR) at the University of Florida invite applications for an Assistant Professor tenure-track position to develop an externally funded research program in bioimaging and direct ICBR microscopy core facility.

Technical support staff will be provided to perform the daily service tasks of this ICBR research facility. As Director, the incumbent will be charged with setting the vision and acquiring the resources necessary to make this ICBR facility among the best in the nation. Candidates with interests in applying modern bioimaging technology, including electron microscopy, to important problems in cellular and/or molecular biology are especially encouraged to apply.

Applicants must have a Ph.D., postdoctoral experience, and a strong publication record. The successful candidate is expected to participate in our undergraduate and graduate programs. A very competitive startup package and salary are available to the successful candidate. Details of the Department and ICBR may be found at websites: <http://microcell.ufl.edu> and <http://www.biotech.ufl.edu>. Submit applications as a single PDF file containing a cover letter, curriculum vitae, and summary of research interests to **Dr. Peter Kima (e-mail: [pkima@ufl.edu](mailto:pkima@ufl.edu)).** Three letters of reference should also be sent directly to e-mail: [pkima@ufl.edu](mailto:pkima@ufl.edu). Review of applications will begin on April 2, 2007. *The University of Florida is an Equal Opportunity Employer.*

FACULTY POSITION  
University of Wisconsin, Madison  
Veterinary Pharmacology

The Department of Comparative Biosciences, School of Veterinary Medicine invites applications for a tenure-track faculty position (**ASSISTANT or ASSOCIATE PROFESSOR**). Qualifications include Ph.D. or equivalent, postdoctoral experience, commitment to excellent teaching, and ability to develop an extramurally funded research program. Preference will be given to research areas complementing existing departmental strengths. Teaching responsibilities include participation in veterinary pharmacology instruction. To apply, send curriculum vitae, brief statements of research interests and teaching philosophies, and three letters of reference to: **Gordon S. Mitchell, Chair, Department of Comparative Biosciences, University of Wisconsin, 2015 Linden Drive, Madison, WI 53706.** Apply by April 30, 2007. For additional information, see website: <http://www.vetmed.wisc.edu/jobs.html>. *Equal Opportunity/Affirmative Action Employer.*





**UPCOMING JOB OPPORTUNITIES**  
**Department of Health and Human Services**  
**National Institutes of Health (NIH)**  
**National Institute of Dental and Craniofacial Research (NIDCR)**

The Office of the Scientific Director (OSD), Division of Intramural Research (DIR), National Institute of Dental and Craniofacial Research (NIDCR) seeks a Deputy to the Scientific Director (Senior Investigator eligible or Senior Scientist, Cat.1). The mission of the DIR is to improve oral, dental and craniofacial health through research, research training, and the translation of discoveries to the public domain. The Division accomplishes this mission by: 1) performing distinctive basic and clinical research that emphasizes high quality and relevance to health; 2) training the next generation of researchers in its laboratories and clinic, and 3) translating the results of its research through publications and technology transfer.

The incumbent will serve as the Deputy Scientific Director for NIDCR with responsibility for management of a large scientific program and full delegation of authority to act for the Scientific Director, DIR, in matters related to the overall operation of the Institute's intramural research program. Specific responsibilities include aspects of administration that support and facilitate the DIR scientific mission. These may include, for example, coordinating reporting activities, assisting in budget preparation, preparation of the institute's Emergency Response Plan, overseeing renovations, serving as a liaison to the Executive Secretary to the Board of Scientific Counselors in preparation for reviews, reviewing and approving routine administrative actions and, when necessary, substituting for the Scientific Director in representing the NIDCR/DIR. The incumbent may be supported to carry out a focused independent research program, with associated effort being consistent with the duties of the Deputy Scientific Director. If the area of the individual's research expertise is appropriate, then (s)he may be involved in assisting in the planning and evaluation of the Division's research programs.

Applicants must have a DDS/DMD/MD/or Ph.D. degree and documented experience in leading an independent research program, as well as an interest and willingness to support the basic and clinical research programs of the NIDCR/DIR. In addition, they should have knowledge of all policies and procedures of the NIH intramural program. Applications from minorities, women and persons with disabilities are encouraged.

Applicants should submit a current CV, Bibliography and the names and contact information for three referees to: **Pamela McInnes, DDS, MSc.(Dent.), Search Committee Chairman, Director, CIBID, NIDCR, Bldg. 45, Room 4AN-12B, Bethesda, MD 20892-6402. Tel: 301-594-2419 Fax: 301-480-8319, Email: pmcinn@nider.nih.gov.** Applications will be accepted until **May 4, 2007**. Salary commensurate with qualifications and experience.

More detailed information about NIDCR can be obtained on our Home Page. Visit us at:

<http://www.nider.nih.gov/Research/Intramural/>



**Signal Transduction & Molecular Genetics**  
**in Tumorigenesis**

Postdoctoral Fellowships are available in the Division of Intramural Research, NIDDK, NIH. Members of the Metabolic Diseases Branch of NIDDK helped discover two genes causing hereditary endocrine cancers (MEN1 and HRPT2). Efforts are directed at the function of menin, the encoded protein from the multiple endocrine neoplasia type 1 (MEN1) tumor suppressor gene. Beginning with protein-protein interaction methods and later using models, such as from mouse-breeding, several menin partners have been identified. This lab also collaborates extensively with other labs on the NIH campus to study endocrine tumors. The positions involve creativity and laboratory expertise with cutting-edge methods. Applications are invited from individuals of the highest caliber who have obtained a Ph.D. or M.D. degree within the last 5 years. Salary and benefits will be commensurate with the experience of the applicant. Interested candidates should send their curriculum vitae, list of publications, a letter stating their interests and the names of three references to the appropriate individual by e-mail or by regular mail (**Stephen Marx MD, Bldg. 10 Rm. 9C101, NIDDK/NIH, Bethesda, MD 20892; Marx@mail.NIH.gov**).



**Deputy Director**  
**Fogarty International Center (FIC)**

The NIH is seeking exceptional candidates for the position of Deputy Director, Fogarty International Center (FIC) to advance health through international scientific cooperation and to promote and support scientific research and training internationally to reduce disparities in global health. This position offers a unique opportunity for the right individual to assist the Director, FIC in providing strong and visionary leadership to an organization dedicated to international health and global collaboration. This position serves as Deputy to the Director, FIC in coordination of all activities related to the mission and functions of the Center, in the development and execution of plans and policies of the FIC and in the allocation of resources. The Deputy Director provides expert advice and counsel to the Director on the development of and opportunities for international research and research capacity building; on the development and coordination of international agreements in which the NIH participates; and on the development and dissemination of information, nationally and internationally, on the Center's international research and training initiatives. Applicants may browse the FIC Home Page at <http://www.fic.nih.gov>. Applicants must possess an M.D., Ph.D., or equivalent degree and be an experienced administrator with a broad international programmatic or scientific background; able to interact with full authority; have the demonstrated capability to plan and direct programs of international importance; and have the ability to communicate with and obtain cooperation of the public, private and international organizations and individuals from the international sector. Salary is commensurate with his/her qualifications and experience. Full Federal benefits including leave, health and life insurance, long-term care insurance, retirement, and savings plan (401k equivalent) will be provided. A detailed vacancy announcement that includes application procedures is available at: <http://www.jobs.nih.gov> (under vacancy announcement FIC-07-174209). Questions may be addressed to Ms. Yolette Lee, 301-594-2792 e-mail: [leeyol@mail.nih.gov](mailto:leeyol@mail.nih.gov). CV and bibliography, including a statement addressing the qualifications, must be received by **April 30, 2007**.



## James Graham Brown Cancer Center Tumor Immunology Faculty Position

A tenure-track faculty position at the rank of Assistant Professor has opened in a collaborative research group focused on cellular and molecular tumor immunology. The successful candidate will be provided with generous start-up funds, a competitive salary, a primary tenure-track academic appointment in the Department of Microbiology and Immunology within the School of Medicine, and ample research laboratory space in proximity to the extensive core facilities of the Brown Cancer Center. Successful candidates will have, or be expected to establish, a productive extramurally funded research program and will bring teaching and mentoring capability to the immunology Ph.D. graduate program. Preference will be given to candidates with current NCI funding and/or who are capable of establishing collaborative research interactions with several of the existing members of the Tumor Immunobiology Program. The rank of Associate Professor will be considered for individuals who have an established research program and significant extramural research funding. Additional information on the research programs may be found at <http://www.louisville.edu/medschool/immunology> and <http://browncancercenter.org/bcc2005/research/program.aspx>.

Applicants must have 2 or more years of postdoctoral research experience with clear evidence of productivity and fundability. The search will remain open until the position is filled. Applicants should send a c.v. containing an abstract of research interest to [bobstout@louisville.edu](mailto:bobstout@louisville.edu) and arrange for 4 letters of reference to be sent to:

**Robert D. Stout, Ph.D., Professor and Chairman**  
Department of Microbiology and Immunology  
School of Medicine  
University of Louisville, Health Sciences Center  
Louisville, KY 40292

*University of Louisville is an Equal Opportunity Employer.*

## UNIVERSITY OF BIRMINGHAM

### School of Biosciences

We invite applications from outstanding candidates for three academic positions, as follows:

**Chair in  
Molecular Cell Biology** Ref: H38137

**Readership in  
Molecular Ecology** Ref: H38138

**Readership in  
Proteomics/Genomics** Ref: H38139

Informal enquiries may be directed to the Head of School, Professor John Heath on tel: 0121 414 7533 or e-mail: [j.k.heath@bham.ac.uk](mailto:j.k.heath@bham.ac.uk)

We plan to hold interviews in late May/early June.

Further details and the procedure for applying can be obtained from Sally Johnson ☎ +44 (0)121 415 8116; fax: +44 (0)121 414 7043; email: [senior-appointments@bham.ac.uk](mailto:senior-appointments@bham.ac.uk); web: [www.hr.bham.ac.uk/jobs](http://www.hr.bham.ac.uk/jobs)

Closing date: 30 April 2007.

A University of Fairness and Diversity.  
Work-Life Balance Award Winner 2003 and 2004.



## MRC Laboratory for Molecular Cell Biology

### Group Leaders

We are seeking new Group Leaders with research interests in Molecular Cell Biology. The posts will be ideal for scientists with three to six years postdoctoral research experience wishing to establish independent research careers, but established Group Leaders will also be considered.

The MRC Laboratory for Molecular Cell Biology is located in modern research facilities on the main University College London (UCL) campus in central London. It currently houses the MRC Cell Biology Unit (eight laboratories), as well as groups funded by Cancer Research UK, The Royal Society and The Wellcome Trust through UCL. Work in these groups is focussed on understanding fundamental aspects of cell biology and their relation to human disease. The new Group Leaders will be selected to enhance or complement the current research areas. The LMCB has an interactive environment, excellent facilities, with particular expertise in imaging, an innovative four-year Graduate Programme and close links to the UCL scientific community. Further information on the Institute can be found at <http://www.ucl.ac.uk/LMCB/>. Informal enquiries can be directed to Professor Mark Marsh ([m.marsh@ucl.ac.uk](mailto:m.marsh@ucl.ac.uk)).

Successful applicants will be expected to win competitive personal fellowships from funding agencies such as The Wellcome Trust, Cancer Research UK or the MRC. Applicants should send a full Curriculum Vitae, a brief outline of research interests, and the names and addresses of four referees to:

**Professor Mark Marsh**  
MRC LMCB, UCL, Gower Street  
London WC1E 6BT, UK

Closing date: 1 May 2007

*UCL Taking Action for Equality*



## MFPL Max F. Perutz Laboratories

### Faculty Openings

The Max F. Perutz Laboratories (MFPL) are a joint venture of the University of Vienna and the Medical University of Vienna. MFPL was created to strengthen research and training at both Universities and to provide fertile grounds for new developments in the molecular life sciences (for more information please visit us online at [www.mfpl.ac.at](http://www.mfpl.ac.at)).

### Junior Group Leader Positions (Molecular and Cell Biology)

We invite outstanding scientists in the field of Molecular and Cell Biology, covering all research areas that seek to understand cellular functions at the molecular level.

Group leader positions are offered initially for five years and include internationally competitive salaries and a generous start-up package.

Applications should include a CV, a brief summary of past research and future plans, up to three representative papers, and the contact addresses of three referees. Please email your application to [positions@mfpl.ac.at](mailto:positions@mfpl.ac.at), c/o Graham Warren. Closing date for applications is May 1, 2007.

MFPL wants to increase its share of female researchers and we explicitly encourage women to apply for these group leader positions.



universität  
wien



MEDIZINISCHE  
UNIVERSITÄT  
WIEN





**Forschungszentrum Karlsruhe**  
in der Helmholtz-Gemeinschaft

&



**Universität Karlsruhe (TH)**  
Research University · founded 1825

The **Karlsruhe Institute of Technology (KIT)** invites applications for the joint positions of

### Director

of the Institute for Biological Interfaces at the Forschungszentrum Karlsruhe

and

### Professor (W3) of Molecular Biology (Nanobiology)

at the University of Karlsruhe (Technical University).

Applicants are expected to have a strong scientific research profile in the field of nanobiology, for example in the areas of molecular or cellular interactions at nanostructured surfaces, or the nanostructuring of biological multifunctional materials. The successful candidate will head the Institute of Biological Interfaces (IBG) at the Forschungszentrum Karlsruhe. The research activities of the IBG form a major part of the Forschungszentrum's Nanobiology Program. The IBG, the Institute of Toxicology and Genetics and the Nano and Microsystems Program of the Forschungszentrum work tightly together with the CFN (Center for Functional Nanostructures) excellence cluster of the University of Karlsruhe to promote the close cooperation of groups working in the fields of biology, chemistry, physics, material science and electrical engineering. These research activities from the Forschungszentrum and the University of Karlsruhe will be integrated into the Center for Nanoscience of the Karlsruhe Institute of Technology (KIT).

The successful candidate is expected to take part in the teaching of molecular biology at the Faculty of Chemistry and Biological Sciences of the University of Karlsruhe. Habilitation or equivalent scientific experience is expected.

We are an equal opportunity employer, but as we wish to increase the proportion of females in higher management we especially encourage qualified women to apply for this position. In the case that applicants are equivalently qualified, handicapped candidates will be selected preferentially.

Applications including information about the candidate's previous research and lecturing experience as well as reprints of five major publications should be addressed to **Professor Dr. Reinhard Maschuw, Chairman of the Executive Board of Forschungszentrum Karlsruhe (acting head), Postfach 3640, 76021 Karlsruhe, Germany by May 04, 2007.**

Internet: [www.fzk.de](http://www.fzk.de)

Ruhr-University Bochum

Germany's Excellence Initiative



**Research School**

## 1. International Call for Research School Fellowships

- | Research School scholarships are offered as employment contracts for
- | Net salary after taxes approx. 1.100 € per month (E13/2 TVL)
- | Net salary for engineers after taxes approx. 1.800 € per month (E13 TVL)
- | In addition 1.000 € p.a lump sum for consumables and travel
- | PhD fellowship for three years

**Deadline for application is April 30, 2007.**

Details on the research fields and admission procedure can be obtained at [www.rub.de/research-school/application.html](http://www.rub.de/research-school/application.html)

### Thematic Priorities

#### Natural Sciences and Engineering

##### Interfacial Systems Chemistry

chemical complexity at interfaces | heterogeneous catalysis | systems chemistry and the origin of life | high-resolution analytics and imaging | theoretical chemistry and simulation

##### Plasma Science

fundamental plasma phenomena in laboratory and space | diagnostics, modelling and simulation of plasmas | novel sources and processes for plasma technology | plasma applications from nanoelectronics to medicine

##### Materials Science and Engineering

processing and analysis of novel nanoelectronic devices | quantum ballistic transport, magnetotransport, spintronics | band gap engineering | structure and microstructure diagnostics | multi-scale modelling and simulation of materials

##### Sustainable Infrastructure Engineering

geothermal exploitation | tunnel design and construction | modelling and simulation | underground freight transportation | multi-level energy supply

##### Security in Information and Communication Systems

cryptography, efficient algorithms | secure operating systems, embedded security, network security | public key algorithms | legal and economical aspects of IT security

##### Advanced Computational Sciences and Engineering (ACSE)

scale-traversing modelling and simulation | high performance computing | autonomic computing | advanced computational engineering | embedded computing

#### Life Sciences

##### Macromolecular Networks

signal and regulatory pathways | biotechnology | protein structure and networks

##### Neuronal and Cognitive Networks

computational neuroscience | perception, cognition and memory | development and plasticity of nervous system

#### Humanities and Social Sciences

##### Biomedical Ethics and Public Health

culture, religion and illness | intercultural bio-ethics, end of life issues in chinese bioethics | neuroethics, clinical ethics

##### Organisation and Transformation of Semantic Spaces

continuities and discontinuities in the historiography 20th century, Germany in an international perspective

##### Religion and Secularisation

religion and civil society, religious pluralism, empirical social research (esp. quantitative methods), sociology of religion

##### Human Security in the Process of Globalisation

effects of globalisation on growth and distribution in developing countries (quantitative approaches)

The coordination is handled by the Central Coordination Office (CCO) of the Research School. Further details regarding the announcement can be obtained at [www.rub.de/stellenboerse.html](http://www.rub.de/stellenboerse.html)



## Physiology and Biophysics Faculty

Stony Brook University's Department of Physiology and Biophysics, School of Medicine, invites applications for two tenure-track positions at the assistant or associate professor level. The Department of Physiology and Biophysics maintains facilities for faculty that include a confocal microscopy core (FCS, molecular tweezer, and TIRF) and a biochemical core. In addition the Institute for Molecular Cardiology is housed with the Department of Physiology and Biophysics with translational research interests that include cardiovascular physiology and stem cell biology. The Medical School also provides a variety of services including fluorescence associated cell sorting (FACS), DNA sequencing facilities, proteomics, and gene chip analysis.

First position will have primary appointment in Physiology and Biophysics. We are interested in outstanding clinician scientists with interests in human genetics, pediatric cardiology, cardiac electrophysiology, signal transduction, or systems physiology research but will consider any qualified candidate. The successful candidate will be expected to maintain an externally funded research program and participate in medical education with limited clinical responsibility.

**Required:** M.D., M.D./Ph.D., or equivalent, board certification. Clinical responsibility will be limited to 20% in a clinical department appropriate to the candidate's clinical expertise.

Second position will have an appointment in Physiology and Biophysics with primary responsibility within the Institute of Molecular Cardiology.

**Required:** Ph.D. or equivalent. Areas of interest include stem cell biology, proteomics, signal transduction, heart failure, and cardiac regeneration. Successful candidates will be expected to conduct a vigorous independent research program and interact productively with ongoing research programs in stem cell biology and cardiac regeneration. Candidates with active funding and a background in proteomics, biochemistry, and cell biology are encouraged to apply.

**Please send cover letter and C.V. to:** Search Committee, Department of Physiology and Biophysics, Health Sciences Center, Basic Science Tower T6-Room 140, Stony Brook University/SUNY Stony Brook, NY 11794-8661

Equal Opportunity/Affirmative Action Employer.  
Visit [www.stonybrook.edu/cjo](http://www.stonybrook.edu/cjo) to apply online and for employment information.



## THE ROYAL SOCIETY

### Support for collaboration between UK and India

For many years, the Royal Society has supported collaboration with India through short visits, networks, joint projects and the Incoming International Fellowships scheme. More information on these ongoing activities can be found on our website: [www.royalsoc.ac.uk/funding](http://www.royalsoc.ac.uk/funding).

In order to further strengthen scientific links, the Royal Society has recently entered into an agreement with the Indian Council for Scientific and Industrial Research (CSIR) to support a number of UK-India joint projects and fellowships:

- **Joint Projects** support collaborative research between UK and Indian scientists. Funding is available to cover the mobility costs of UK researchers and Indian researchers based in CSIR institutes to engage on a project spanning two years.

**Deadline: 13 June and 13 December 2007**

- **CSIR India-Royal Society, UK Industrial Research Fellowships** aim to foster science and technology links between the UK and India, and in particular to enhance knowledge transfer in science and technology between CSIR laboratories and UK industry and/or academia.

- Indian scientists holding a permanent position at a CSIR institute can spend between 6-12 months working either in UK industry, a UK research institute or higher education institute.
- UK scientists based in industry, a UK research institute or higher education institute can spend between 6-12 months at a CSIR laboratory in India.

**Deadline: 3 May 2007**

For more information on these Joint Projects and Fellowships, please visit the Royal Society website: [www.royalsoc.ac.uk/CSIR](http://www.royalsoc.ac.uk/CSIR), or email [international@royalsoc.ac.uk](mailto:international@royalsoc.ac.uk)

### Positions Available Division of Experimental Medicine Immunology of Chronic Infectious Diseases

The Department of Medicine of the University of California San Francisco is establishing a Division of Experimental Medicine with its laboratory space based at San Francisco General Hospital, not far from the new Mission Bay campus. The Division welcomes applications from physician scientists and PhD scientists engaged in hypothesis-driven, patient- or disease-oriented research on the immunology of chronic infectious diseases in humans. Appointments will be made at the Assistant to Full Professor level in the In-Residence series, depending upon qualifications. Successful candidates will also become members of the UCSF Graduate Program in Biomedical Sciences. Particular attention will be devoted to those who could assume the role of Associate Director, with responsibilities to help the Director form the program, providing leadership and mentorship to the staff. Experience in management of large teams required. Favorable attention will also be devoted to those applicants who could serve as a faculty advisor and supervisor of the following core lab functions: Flow Cytometry Core P containing a high-speed multiparameter cell sorter and several multiparameter flow cytometers. Animal Model Core P providing animal models of chronic infectious diseases on site and collaborating with other animal model cores elsewhere. Core Immunology Lab P focused on the analysis of immune phenotype and function in humans.

Applicants must have a MD and/or a PHD and demonstrated potential to lead an independent research program. Nationally competitive start-up packages are available. If interested, please send CV and three letters of reference to: **J.M.(Mike) McCune, MD, PhD, Chief, Division of Experimental Medicine, Department of Medicine, University of California at San Francisco, Chair, Translational Research Search Committee, Bldg 3, Rm 602, San Francisco General Hospital, 1001 Potrero Ave., San Francisco, CA 94110; [mmccune@gladstone.ucsf.edu](mailto:mmccune@gladstone.ucsf.edu).**

*UCSF seeks candidates whose experience, teaching, research, or community service has prepared them to contribute to our commitment to diversity and excellence. The University is an Equal Opportunity/Affirmative Action Employer. All qualified applicants are encouraged to apply, including minorities and women.*

### NATURE PUBLISHING GROUP SEEKS MARKETING MANAGER

Nature Publishing Group, publishers of Nature, the world-renowned weekly journal of science, and a family of related scientific journals, seeks a Marketing Manager to drive the sales and promotion of the Nature family of journals in Japan and throughout the Asia-Pacific region. The Marketing Manager will be based at NPG Nature Asia-Pacific in Tokyo, the headquarters for Nature's Asia-Pacific operations.

The Marketing Manager will occupy a senior position managing a comprehensive marketing program to promote NPG journals, and in particular, the series of physical science titles (Nature Photonics, Nature Nanotechnology, Nature Physics and Nature Materials) published under the Nature brand. NPG has been aggressive in adding new titles to its list in recent years, with the latest journal (Nature Geoscience) scheduled for publication beginning in January 2008. This is a challenging position, requiring the opening of new markets to a quality product.

Applicants should have an interest in science and strong skills in traditional marketing methods, including direct mail, as well as web based marketing tools. Prior experience in a Marketing position, preferably in a science-related industry, is preferred. As your key region will be Japan, fluency in either English or Japanese, with business-level ability in the other, will be essential. Korean or Chinese language ability would also be desirable, but are not essential. The candidate should be proactive, willing and able to learn quickly, and comfortable working in a multi-cultural environment.

The Marketing Manager should be highly motivated and results orientated, and be a team player in the Asia-Pacific marketing team. They shall report to the Senior Marketing Manager and shall be able to call upon the resources of the NPG Nature Asia-Pacific office, which currently has more than 40 full-time staff.

A performance-based bonus scheme is also offered. The successful applicant will be qualified to receive reimbursement for relocation expense. Applications, including a CV and salary history, as well as a statement outlining your suitability for the position, should be sent by e-mail, fax or post to

**Peter Yoshihara, Senior Marketing Manager, NPG Nature Asia-Pacific, Chiyoda Building 5F, 2-37 Ichigayatamachi, Shinjuku-ku, Tokyo 162-0843 Fax: +81-3-3267-8746. [p.yoshihara@natureasia.com](mailto:p.yoshihara@natureasia.com)**



# Life Sciences Careers @NUS

The National University of Singapore (NUS) is one of the premier research universities in the Asia-Pacific. The Office of Life Sciences (OLS) at NUS is actively seeking outstanding individuals to join the University for academic and research appointments. OLS coordinates, integrates and synergizes the various life sciences programmes at NUS and its affiliated research institutes. We have openings for tenure-track positions in Assistant/Associate/Full Professorships.

Diseases	Platform Technologies
Cancer	Bioinformatics / Computational Biology
Ageing/Neurobiology	Structural Biology / Functional Genomics
Cardiovascular biology / Angiogenesis	Bioengineering / Tissue Engineering
Hepatology	Immunology
Infectious diseases	Medicinal Chemistry / Toxicology / Clinical trials

NUS offers competitive salary package, conducive research environment and attractive start up funds comparable to most North American universities. Successful applicants will be appointed as faculty in related academic departments.

Singapore is a vibrant garden city with year round tropical climate and rich multicultural heritage. Many top international scientists have made Singapore their home taking advantage of the excellent facilities and strong funding support for R&D.



For further information, please contact

Director, Office of Life Sciences  
National University of Singapore  
Singapore

Website <http://www.ols.nus.edu.sg>  
Email: [olshead@nus.edu.sg](mailto:olshead@nus.edu.sg)



## Department of Biological Sciences Faculty of Science

### Faculty Search

The Department of Biological Sciences, National University of Singapore (NUS) invites applications for tenure-track faculty positions at Assistant Professorship and Associate Professorship levels.

Established in 1905, NUS has evolved into a quality teaching and research-intensive institution, which is internationally acknowledged as one of the finest universities in the Asia-Pacific. We are the largest life sciences department in NUS and have established state-of-the-art research facilities for structural biology, functional genomics, developmental biology and biodiversity. Faculty members can expect competitive salary levels and generous research support and start-up packages as at the top universities in USA and Europe.

Preference will be given to applicants who specialize in the following areas:

1. Structural biology and functional genomics, including cryoelectron microscopy and mass spectrometry
2. Chemical biology
3. Computational biology and systems biology
4. Environmental toxicology
5. Neurobiology and stem cells biology
6. Host-pathogen interaction

Outstanding individuals with postdoctoral experience and strong commitment to research and teaching are encouraged to send an application (form downloadable from [www.dbs.nus.edu.sg](http://www.dbs.nus.edu.sg)), along with curriculum vitae, a brief research plan and names of three external referees to:

Head, Department of Biological Sciences  
National University of Singapore  
14 Science Drive 4  
Singapore 117543  
Republic of Singapore  
Fax: (65) 67795671  
Email: [dbshead@nus.edu.sg](mailto:dbshead@nus.edu.sg)



## FACULTY POSITION Cellular Electrophysiology

### Department of Cell Biology and Molecular Medicine

The University of Medicine and Dentistry of New Jersey - New Jersey Medical School - Department of Cell Biology and Molecular Medicine and the Cardiovascular Research Institute, is seeking applicants for a tenure or non-tenure track faculty position with emphasis on myocardial and/or vascular electrophysiology. Applicants should have a Ph.D., M.D., or DVM and have demonstrated excellence in basic science research.

Strong core facilities in pathology, physiology and experimental surgery are available to support the cellular/molecular sciences.

CV's including names of at least three references, and a description of research interests should be sent to: **Stephen F. Vatner, M.D., Chair, Department of Cell Biology and Molecular Medicine, Cardiovascular Research Institute, UMDNJ-New Jersey Medical School, 185 S. Orange Avenue, MSB G609, PO Box 1709, Newark, NJ 07101-1709. E-mail: [vatnersf@umdnj.edu](mailto:vatnersf@umdnj.edu).** UMDNJ is an AA/EEO Employer, M/F/D/V and is a member of the University Health Systems of New Jersey. For more information, visit [www.umdnj.edu/hrweb](http://www.umdnj.edu/hrweb).



**NEW JERSEY  
MEDICAL SCHOOL**  
University of Medicine & Dentistry of New Jersey



## Dean LSUHSC School of Medicine

The Louisiana State University Health Sciences Center School of Medicine in New Orleans invites applications and nominations for the position of Dean of the School of Medicine. The successful candidate will be responsible for all facets of activity in the school, including undergraduate medical education, resident and fellow program accreditation, continuing medical education, faculty recruitment and retention, clinical practice development in public and private venues, and nurturing and development of basic science, clinical science and translational research programs. The successful candidate will also be responsible for the finances of the School of Medicine. The successful candidate will work with the Chancellor's Office and Dean's Office administrations, provide oversight and leadership to the faculty group practice (LSU HealthCare Network), and interface with various hospital entities and their administrations. The successful candidate must be capable of representing the School of Medicine to various diverse agencies and constituencies. The successful candidate will have a MD, PhD or MD/PhD and will also be board-certified in his or her specialty and eligible for or licensed to practice in Louisiana, if relevant. He or she must demonstrate leadership ability, a proven commitment to education and clinical service, and the ability to provide vision for the school that builds on its historic strengths. Achievements in teaching, multi-disciplinary collaborative research, mentorship, and administration that promote an inclusive environment are essential. The successful candidate must be qualified to be appointed at the professorial rank in accordance with School of Medicine and LSU System criteria; the compensation package will be competitive.

Candidates should provide a Curriculum Vitae including a full list of administrative accomplishments and scientific publications, and a brief statement of educational, research, service, and administrative interests, skills and strengths. These materials should be forwarded electronically or by conventional mail to: **Kurt Varner, PhD, Professor and Interim Head, Department of Pharmacology, LSUHSC School of Medicine, 1900 Perdido St., New Orleans, LA 70112; [kvarne@lsuhsc.edu](mailto:kvarne@lsuhsc.edu).**

Review of applications will commence immediately and will continue until the position is filled.

*LSUHSC is an Equal Opportunity/Affirmative Action Employer.*



Does your next career step  
need direction?



*For a career in science,  
I turn to Science*

*I have a great new research idea.  
Where can I find more grant options?*



# ScienceCa

## *We know science*

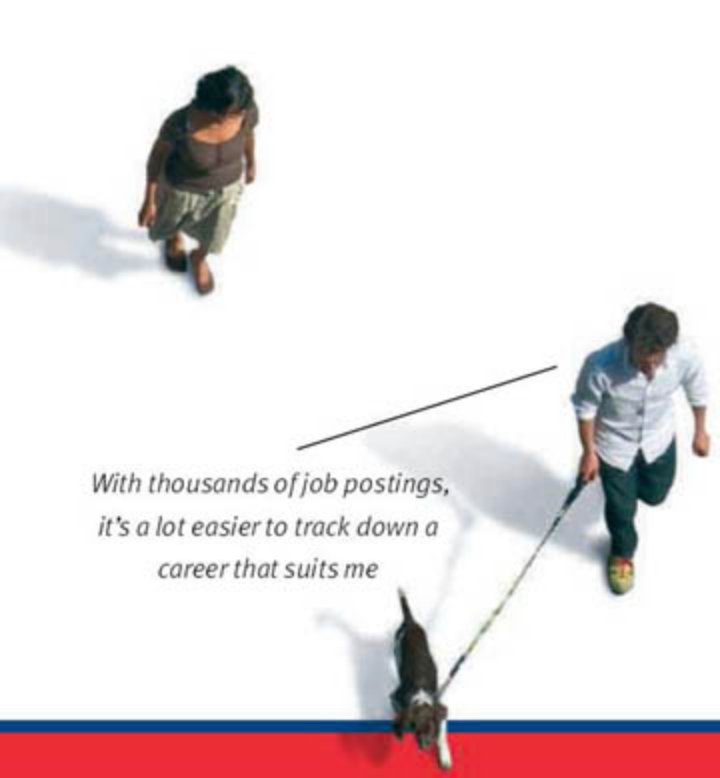


*You know, ScienceCareers.org  
is part of the non-profit AAAS*




*That means they're putting  
something back into science*





With thousands of job postings,  
it's a lot easier to track down a  
career that suits me




Now what?

I got the offer I've been  
dreaming of.

# careers.org



AAAS



I want a career,  
not just a job

There's only one place to go for career advice if you value the expertise of *Science* and the long experience of AAAS in supporting career advancement - ScienceCareers.org. The pages of *Science* and our website ScienceCareers.org offer:

- Thousands of job postings
- Career advice articles and tools
- Funding information
- Networking opportunities

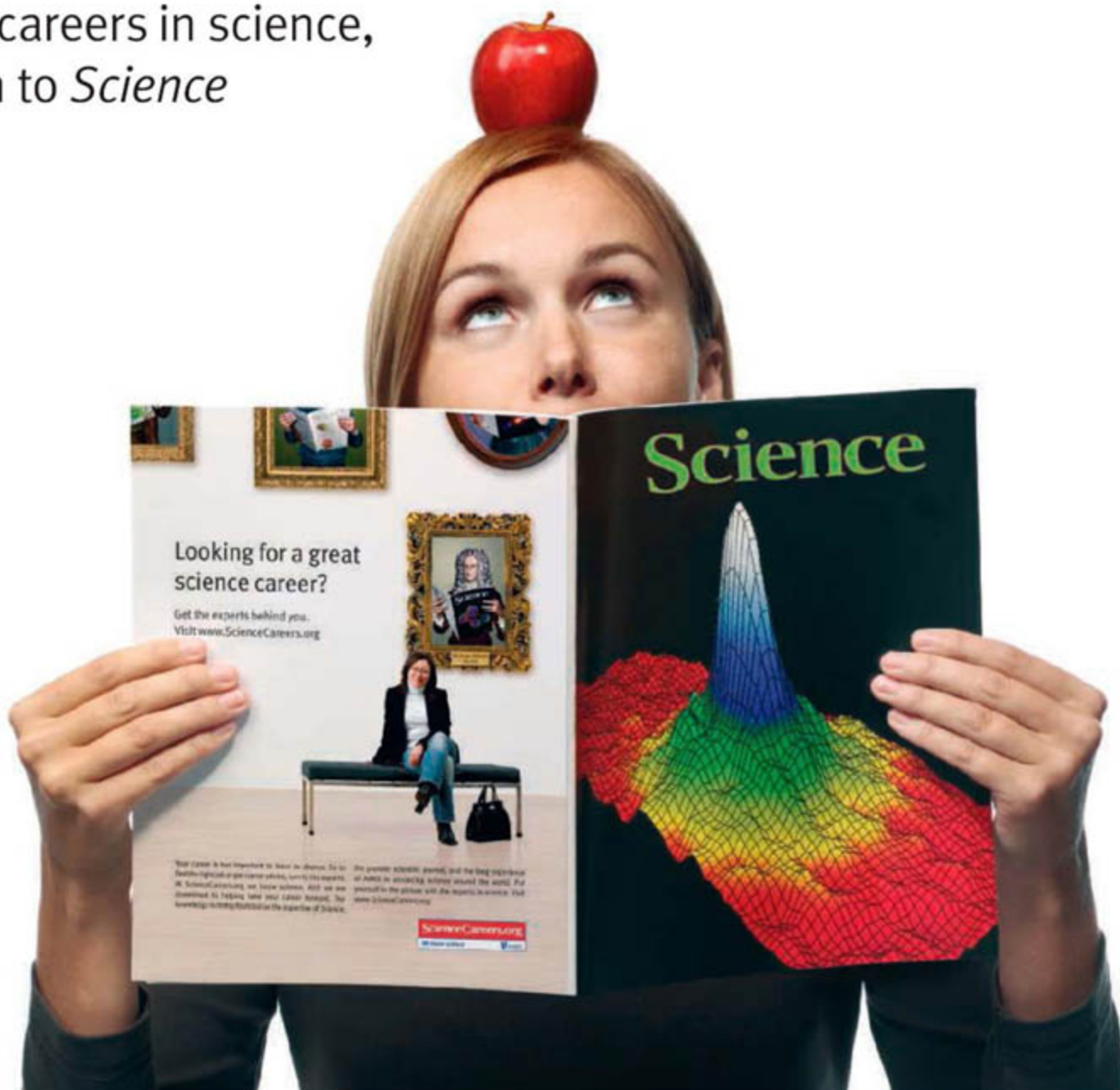
[www.sciencecareers.org](http://www.sciencecareers.org)





# From physics to nutrition

For careers in science,  
turn to *Science*



If you want your career to bear fruit, don't leave it to chance. At ScienceCareers.org we know science. We are committed to helping you find the right job, and to delivering the useful advice you need. Our knowledge is

firmly founded on the expertise of *Science*, the premier scientific journal, and the long experience of AAAS in advancing science around the world. ScienceCareers.org is the natural selection. [www.sciencecareers.org](http://www.sciencecareers.org)

Features include:

- Thousands of job postings
- Career tools from Next Wave
- Grant information
- Resume/CV Database
- Career Forum

**ScienceCareers.org**

We know science





# AAAS & NPA



## Here's your link to career advancement

AAAS is at the forefront of advancing early-career researchers — offering job search, grants and fellowships, skill-building workshops, and strategic advice through ScienceCareers.org and our Center for Careers in Science & Technology.

NPA, the National Postdoctoral Association, is providing a national voice and seeking positive change for postdocs—partnering with AAAS in career fairs, seminars, and other events. In fact, AAAS was instrumental in helping the NPA get started and develop into a growing organization and a vital link to postdoc success.

If you're a postdoc or grad student, go to the AAAS-NPA link to find out how to spell career success.

**[AAAS.org/NPA](http://AAAS.org/NPA)**





## Looking for Career Advice?

Then don't forget to read the *Science Careers* Features for fresh perspectives from leading science writers.

### UPCOMING FEATURES:

April 6— Careers in Cancer Research

April 20 — Postdoctoral Careers: Transferable Skills

April 27 — Biotech and Pharma

Also available online at:

[www.sciencecareers.org/businessfeatures](http://www.sciencecareers.org/businessfeatures)

**ScienceCareers.org**

We know science

AAAS

### HARVARD UNIVERSITY Assistant/Associate Professors Department of Genetics and Complex Diseases

The Department of Genetics and Complex Diseases (GCD) at the Harvard School of Public Health (HSPH) invites applications for tenure-track positions at the level of assistant professor. Exceptional associate professor candidates will also be considered. GCD is a major new initiative in the basic sciences in the HSPH Division of Biological Sciences. Through integrative programs in biology and genetics, the GCD group seeks to generate basic research insights related to complex human diseases. Current areas of research include nutrient sensing, protein translation and degradation, nuclear hormone receptor signaling, secretion and vesicular transport, oxidative and genotoxic stress response, DNA repair of oxidative damage, tumor metabolism, and regulation of carbohydrate, lipid, and energy homeostasis. Successful applicants will hold a PhD and/or MD degree and will have a record of outstanding productivity in an area that complements the existing research and training goals of the department. The candidate should possess the ability to work collaboratively with other scientists and the scholarly qualities required to mentor doctoral students in the graduate program in the Division of Biological Sciences. Generous start-up packages and state-of-the-art research facilities will be available. GCD has particular interest in recruiting individuals with research interests in the following areas:

- Aging in model organisms, including mice
- Organelle biology and dysfunction, particularly mitochondria or endoplasmic reticulum
- Control of protein synthesis, folding, and degradation
- Mechanisms of signal processing and integration, especially in the context of energy and nutrient sensing, fluxes and homeostasis
- Tumor metabolism
- Inflammatory and stress responses with emphasis on chronic metabolic or degenerative diseases
- Integrated physiology and genetics of complex diseases using cellular or mouse models; for example, neurological degeneration with metabolic dysfunction as an underlying feature

Please send a letter of application, including a statement of current and future research interests, curriculum vitae, sample publications, and the names of three references to the following address. Applicants should ask their three references to write independently to this address:

**Chair, GCD Search, c/o Julie Gound**  
Department of Genetics & Complex Diseases  
655 Huntington Avenue, Building II, 107  
Boston, MA 02115

*The Harvard School of Public Health is committed to increasing the representation of women and minorities in its faculty, and encourages applications from such candidates.*

### NEUROSCIENTIST

The **American University of the Caribbean (AUC), School of Medicine**, an internationally accredited institution with over 3,500 physician graduates, seeks a Neuroscientist with a Ph.D. degree in either Neuroscience, Neuroanatomy, or Neurophysiology, or an M.D. degree with teaching experience in neuroscience. All applicants should have teaching experience in LCME-accredited medical schools. Candidates with teaching awards from medical students will be given preference. We are particularly interested in candidates who have the ability to integrate neuroscience with other basic-clinical sciences.

The AUC faculty, largely drawn from the U.S., is strongly committed to the highest quality of medical education. Our student body is quite culturally diverse; the majority are U.S. citizens. AUC is located in St. Maarten, a popular tourist destination, easily reached by nonstop flights from major U.S. east-coast cities. Medical students complete their pre-clinical training in St. Maarten, and their clinical rotations in the U.S., UK, or Ireland.

Review of applicants will begin immediately and continue until the position has been filled. Interested candidates should electronically submit a curriculum vita with a brief summary of teaching interests, and contact information for three references to Dr. Susan DeMesquita, Chair Neuroscience Search Committee at [sdemesquita@aucmed.edu](mailto:sdemesquita@aucmed.edu).

Visit our website [www.aucmed.edu](http://www.aucmed.edu) to learn more about medical education and opportunities at AUC.



American University of the Caribbean  
School of Medicine

[www.aucmed.edu](http://www.aucmed.edu)



Q What's the quickest link to advances in the world of science?

AAAS

AAAS Advances—the free monthly e-newsletter exclusively for AAAS members.

Each month, AAAS members keep up with the speed of science via a quick click on the newsletter Advances.

Look for the next issue of Advances delivered to your inbox mid month. Look up archived issues at [aaas.org/advances](http://aaas.org/advances).

**Features include:**

- A special message to members from Alan Leshner, AAAS CEO
- Timely news on U.S. and international AAAS initiatives
- Just-released reports and publications
- Future workshops and meetings
- Career-advancing information
- AAAS members-only benefits

All for AAAS members only.

[aaas.org/advances](http://aaas.org/advances)



## Advances

Advances – The Monthly Newsletter for AAAS Members

Message to Members: [R&D Funding Trends](#)  
 AAAS in Action: [News to Note](#)  
 AAAS at Work: [Programs at the Forefront](#)  
 AAAS Science Careers: [Events, Tools, Advice](#)  
 AAAS Announcements: [Items of Interest](#)  
 Read On, Online: [Science Sites](#)

### Message to Members R&D FUNDING TRENDS

Dear AAAS Member,  
 As a continuing service to scientists, engineers, and others, AAAS provides timely, comprehensive, and in-depth analyses of R&D funding in the U.S. federal budget. A new AAAS analysis of the proposed Fiscal Year 2007 budget shows that R&D funding for most nondefense areas is projected to decline significantly over the next five years, while a few will in fact increase. Funding for the physical sciences, NSF, the Department of Energy, and the National Science Foundation and Technology will increase, as will weapons and space exploration. At the same time, the National Institutes of Health budget is slated to continue a decline over the next five years. For continuously updated coverage of the U.S. Congress and Executive Branch, go to [aaas.org](http://aaas.org). A book-length report on R&D in the FY 2007 budget was released at the AAAS Forum on S&T Policy and Innovation. AAAS continues to speak out, both directly and indirectly, in public forums, urging sound science policy and investment in critical areas such as the physical sciences, health, and energy resources, which is necessary to support innovation to benefit global society. We thank you for supporting these critical actions.

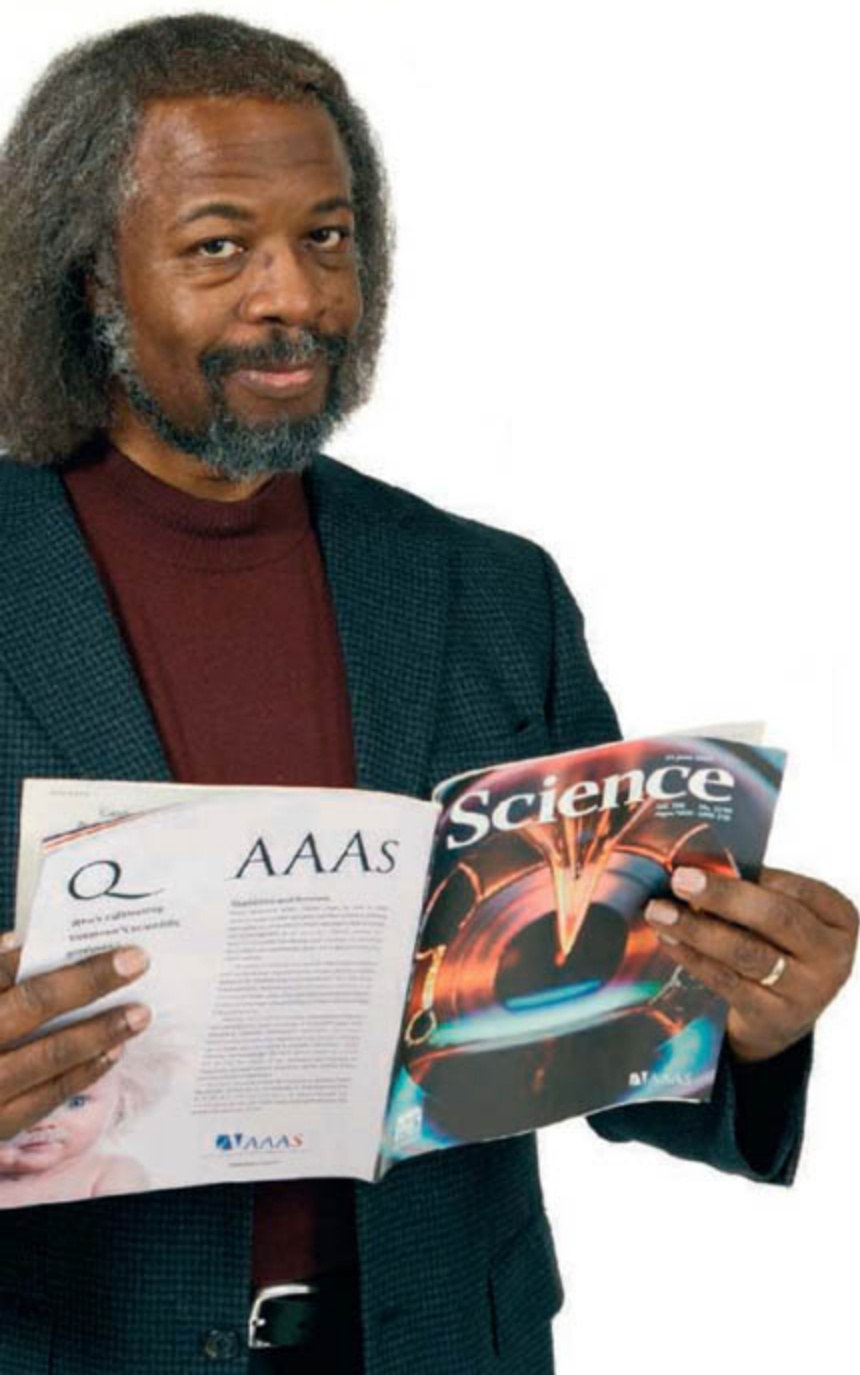
Sincerely,  
 Alan I. Leshner, CEO, AAAS

P.S. Symposium proposals are due 8 March 2007. AAAS Meeting, "Science and Technology for the Future," February in San Francisco.



# Q

Who's helping bring  
the gift of science  
to everyone?



# AAAS

“ As a child I got very interested in space travel. When I was six my father gave me some books on rockets and stars. And my universe suddenly exploded in size because I realized those lights in the sky I was looking at were actually places.



I wanted to go there. And I discovered that science and technology was a gift that made this possible. The thrill of most Christmas presents can quickly wear off. But I've found that physics is a gift that is ALWAYS exciting.

I've been a member of AAAS for a number of years. I think it's important to join because AAAS represents scientists in government, to the corporate sector, and to the public. This is very vital because so much of today's science is not widely understood.

I also appreciate getting *Science* because of the breadth of topics it covers. It gives me a great grounding for many activities in my professional life, such as advising government agencies and private corporations. ”

Jim Gates is a theoretical physicist and professor at the University of Maryland. He's also a member of AAAS.

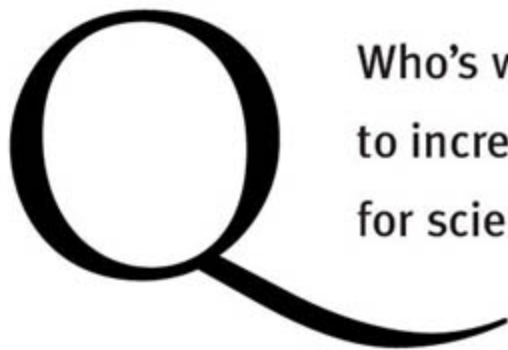
See video clips of this story and others at [www.aaas.org/stories](http://www.aaas.org/stories)

S. James Gates Jr., Ph.D.  
Theoretical physicist  
and AAAS member

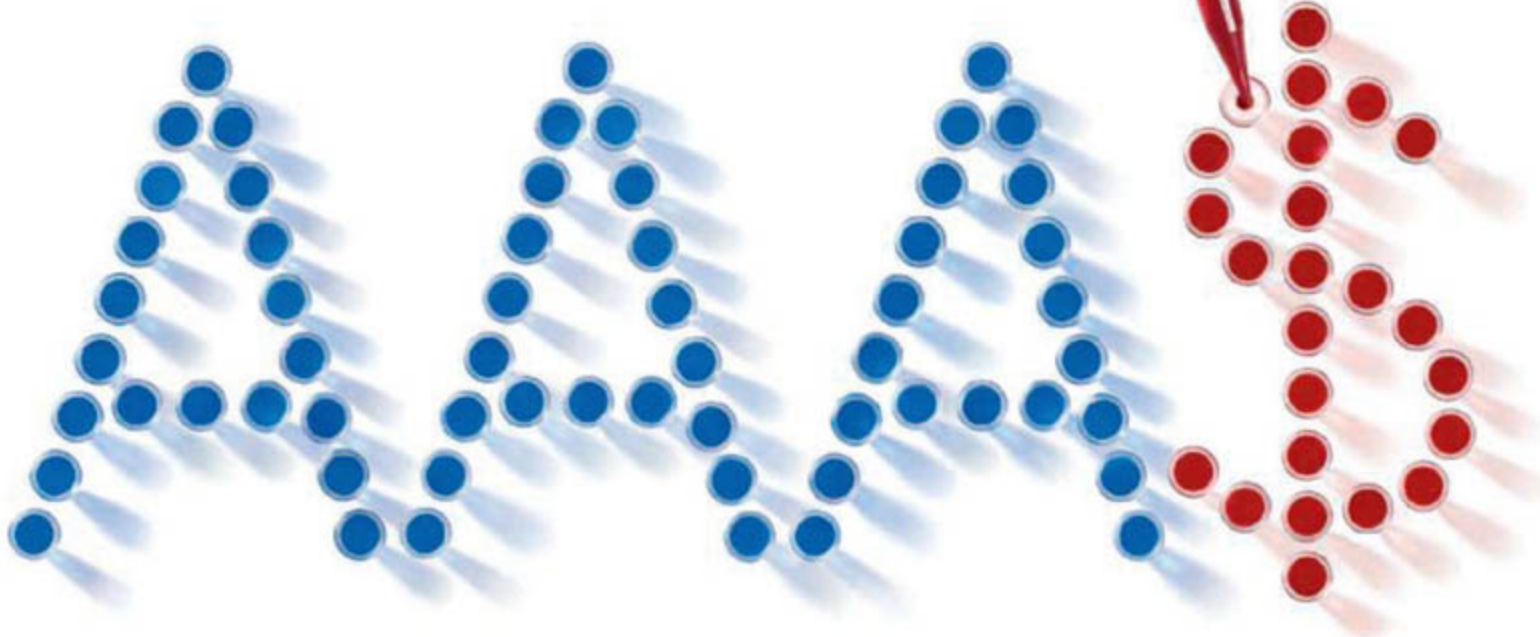


ADVANCING SCIENCE. SERVING SOCIETY.





## Who's working to increase support for science?



Top quality research depends on comprehensive support. AAAS is present at every stage of the process – from advising on funding policy initiatives to tracking the US Federal R&D budgeting process. As the experts, we brief Congressional staffers and representatives from

governments around the world. And only AAAS Funding Updates – sent out monthly – provide continual coverage of R&D appropriations. By actively working to increase support for research, AAAS advances science. To see how, go to [www.aaas.org/support](http://www.aaas.org/support)



ADVANCING SCIENCE, SERVING SOCIETY



POSITIONS OPEN

**RUSH UNIVERSITY  
MEDICAL CENTER**  
RADIATION ONCOLOGY INVESTIGATOR  
Chicago

Rush University Medical Center is seeking a mid to senior-level, funded, laboratory-based Oncology Investigator/Faculty Member for the Department of Radiation Oncology. The successful candidate will be expected to collaborate with other oncology investigators and clinicians, and to pursue translational issues appropriate to radiation oncology. Opportunity includes academic faculty position with tenure; joint appointment with appropriate basic science department; participation in Radiation Therapy Oncology Group translational studies; collegial environment with seven senior faculty members; and competitive salary and benefits. Ideal candidate will possess either a Ph.D. degree or M.D./Ph.D. degrees and will have a demonstrated track record of success in translational, oncological investigations. Program building is an essential component of this position.

Please contact: **Ross Abrams, M.D., Chairman and Hendrickson Professor, Department of Radiation Oncology, Rush University Medical Center, 500 S. Paulina, 013 Atrium Building, Chicago, IL 60612-3833. Telephone: 312-942-5771 or 312-942-5751. E-mail: ross\_a\_abrams@rush.edu.**

**DIRECTOR**

**University of California, Santa Barbara  
National Center for Ecological Analysis  
and Synthesis**

Applications and nominations are invited for the position of Director of the National Center for Ecological Analysis and Synthesis, a research center at the University of California, Santa Barbara (UCSB). The Center is supported by the National Science Foundation, matching funds from the University of California and the Santa Barbara campus, and private entities.

The Center promotes collaborative research on fundamental questions in ecology and many adjacent disciplines by supporting visiting scientists in Working Groups (about 500 scientists a year) and resident sabbatical (six a year) and postdoctoral associates (about 18 a year). The Center also has a large research and applications project in informatics and a Conservation and Resource Management Program.

For more information, please visit [website: http://www.nceas.ucsb.edu](http://www.nceas.ucsb.edu).

Applications and nominations should be submitted electronically to **e-mail: nceas\_search@msi.ucsb.edu** and will be accepted until April 16, 2007, or until the position is filled. Applications should include a letter of interest, curriculum vitae, and names of three people who have agreed to provide letters of recommendation. The letter of interest should include a vision statement for the Center and the applicant's career goals. For information about the search, contact: **Steve Gaines, Search Committee Chair, e-mail: gaines@msi.ucsb.edu; telephone: 805-893-3764.**

The Center is especially interested in candidates who can contribute to the diversity and excellence of the academic community through research, teaching, and service.

*UCSB is an Equal Opportunity/Affirmative Action Employer.*

**RESEARCH ASSOCIATE** with experience in protein purification. Send resume to: **M.K. Jain, Case Western Reserve University, School of Medicine, 2103 Cornell Road, Cleveland, OH 44106.** Must reference job code FF2007. *Equal Opportunity Employer.*

**RESEARCH ASSOCIATE** with experience in pathology. Send resume to: **V. Pompili, Case Western Reserve University, Department of Cardiology, 2103 Cornell Road, Cleveland, OH 44106.** Must reference job code FF1007. *Equal Opportunity Employer.*

POSITIONS OPEN

**FACULTY POSITION in QUANTITATIVE  
ECOLOGY**

**Texas A&M University  
Department of Wildlife and Fisheries Sciences**

The Department of Wildlife and Fisheries Sciences at Texas A&M University seeks an outstanding individual to join the faculty as an **ASSISTANT PROFESSOR** in quantitative ecology. This position is a 12-month, tenure-track appointment. This new position is charged with building a successful teaching and research program focused on quantitative approaches to ecology, conservation, and management of wildlife and fishery resources. Appropriate areas of research specialization include investigation of population abundance/dynamics and species interactions, statistical and numerical modeling of ecological processes in space and time, and bioinformatics.

Candidates must have a Ph.D. in an appropriate field and a record of research accomplishment as evidenced by authorship of peer-reviewed publications. A record reflecting acquisition of extramural research funding and experience in university-level teaching also is desirable.

Additional information on this position, the Department, Texas A&M University, and the Interdisciplinary Research Group in Ecology and Evolutionary Biology can be found at [website: http://www.wfsc.tamu.edu](http://www.wfsc.tamu.edu) and [website: http://eeb.tamu.edu](http://eeb.tamu.edu).

To apply, submit electronic curriculum vitae, and statements of teaching and research interests, plus contact information for three references to: **Dr. Daniel Roelke, Search Committee Chair, e-mail: droelke@tamu.edu.** Preference will be given to applications received by May 25, 2007. Applications received after this date are not guaranteed a review by the Search Committee. The position will remain open until a suitable candidate is identified.

*Texas A&M University is an Equal Opportunity Employer that seeks diversity in its workforce, student body, and program participation. Those requiring assistance in the application process should contact the Search Committee Chair.*

**FACULTY POSITION in NEUROGENETICS**

The Department of Physiology at the Medical College of Wisconsin (MCW) invites applications for a tenure-track faculty position at the **ASSISTANT or ASSOCIATE** level with research interests in studying genetic channelopathies of the central and peripheral nervous system underlying disease states. Favored candidates will complement the Department's strengths in understanding physiologic mechanisms of rhythm generation in respiratory control and epilepsy, cardiovascular and renal physiology. The Department faculty are closely tied to, affiliated with, and proximate to the MCW Human and Molecular Genetic Center (housing the National Heart, Lung, and Blood Institute Program of Genomic Applications), the Cardiovascular Center (housing the National Institute of Neurological Disorders and Stroke - Program Project Grant in stroke), the Biotechnology and Bioengineering Center (housing the NHLBI Center of Proteomics), and the Center of Kidney Research. We also have a close collaboration to investigate human epilepsy with pediatric and adult departments of neurology. Thus, superb opportunities exist to collaborate. We additionally have an outstanding graduate program in physiological genomics and systems biology and support of this program through teaching graduate and medical students is expected. The candidate must hold a Ph.D. and/or M.D. degree. Applicants should send their curriculum vitae, statement of interest, and three letters of recommendation to: **Allen W. Cowley, Jr., Ph.D., Chairman, Department of Physiology, e-mail: cowley@mcw.edu, website: http://www.phys.mcw.edu/index.htm.** *Equal Opportunity Employer. Persons with Disabilities/Minorities/Females/Veterans.*

**RESEARCH ASSOCIATE** with experience in medical mycology. Send resume to: **M. Christ, Case Western Reserve University, School of Medicine, 11100 Euclid Avenue, LKS 5028, Cleveland, OH 44106.** Must reference job code FF3007. *Equal Opportunity Employer.*

POSITIONS OPEN



**ASSISTANT PROFESSOR of FORENSIC  
SCIENCE**

Oklahoma State University Center for Health Sciences, College of Osteopathic Medicine, is seeking to fill a full-time, tenure-track faculty position in the Department of Forensic Sciences. The Assistant Professor of Forensic Science will teach, conduct relevant research, and mentor graduate students enrolled in the Graduate Program in Forensic Sciences. It is expected that the incumbent will be knowledgeable both in their individual subspecialty of forensic science, but also with the field as a whole so that students who graduate from the program will be well-trained and able to easily join the workforce as a competent forensic scientist. Doctorate degree required (Ph.D.). Must have experience in the practice of forensic science with potential to become an effective teacher and researcher, or, experience teaching forensic science and close ties to practitioners in their discipline of forensic science. Experience working in a forensic setting is highly desirable, especially one associated with law enforcement. Intellectual curiosity and a dedication to graduate instruction are musts. Interested candidates must apply online at [website: https://jobs.okstate.edu](https://jobs.okstate.edu), job number 02880. *Affirmative Action/Equal Opportunity Employer.*

**ASSOCIATE CHIEF of STAFF for RESEARCH AND DEVELOPMENT, Saint Louis Veterans Affairs Medical Center.** Full-time, Board-certified, health care specialty Physician responsible for overall coordination and evaluation of research activities. Participates with Director and Chief of Staff in managing health care programs, particularly those areas where integration of R&D programs can have a beneficial effect on patient care. Provides advice and guidance in administration and technical matters to investigators, and aids in recruitment, appointment, and employment of R&D personnel. Arranges for review of publications, scientific exhibits, and public information releases of R&D activities. Provides financial management: preparing estimates of budgetary requirements and administering R&D funds. Contact: **Alice Taylor, Human Resources, telephone: 314-894-6620.** *Equal Opportunity Employer.*

**POSTDOCTORAL POSITION  
Harvard Medical School**

Positions available to study DNA damage and transcriptional mechanisms involved in aging and neurodegenerative diseases. Projects focus on genomics, DNA damage, and the biology of genes involved in aging, Alzheimer's, and Parkinson's disease. For reference, see: *Nature* 429:883, 2004; *J. Biol. Chem.* 280:36895, 2005; *Hum. Mol. Genet.* 14:1231, 2005; *Neuron* 33:677, 2002. Experience in molecular biology, genomics, or transcription is desirable. Send curriculum vitae, a brief description of research experience, and names of three references to: **Dr. Bruce Yankner (e-mail: bruce.yankner@childrens.harvard.edu).**

**ASSOCIATE CHIEF of STAFF for EDUCATION, Saint Louis Veterans Affairs Medical Center.** Full-time, Board-certified, health care specialty Physician responsible for overall coordination and evaluation of education activities; directly responsible to the Chief of Staff. Identifies training needs and opportunities; coordinates submission of educational proposals and requests; and manages facility educational resources. Member of the Hospital Education Committee and serves as Regional Medical Education Center liaison. Field representative of and advisor to the Associate Chief Medical Director for Academic Affairs. Contact: **Alice Taylor, Human Resources, telephone: 314-894-6620.** *Equal Opportunity Employer.*



# IBD in Developing Countries Grants Available



We are interested in receiving innovative research proposals designed to elucidate the factors that may explain the low incidence of IBD in developing areas of the globe. Proposals should be exploratory in nature and designed as pilot projects aiming to explore new ideas. The research should shed light on the factors that determine low versus high areas of prevalence of the disease. The research should ultimately be helpful in uncovering the etiology of IBD and the factors that enhance or prevent the genesis of the disease.

- Letters of Interest from qualified nonprofit institutions are accepted year-round.
- Visit [www.broadmedical.org](http://www.broadmedical.org) for application guidelines.
- Contact us at [info@broadmedical.org](mailto:info@broadmedical.org) for more information.

**b m r p** broad medical research program  
The Broad Foundation



Dave Jensen  
Industry  
Recruiter

## Science Careers Forum

- How can you write a resume that stands out in a crowd?
- What do you need to transition from academia to industry?
- Should you do a postdoc in academia or in industry?

Let a trusted resource like ScienceCareers.org help you answer these questions. ScienceCareers.org has partnered with moderator Dave Jensen and four well-respected advisers who, along with your peers, will field career related questions.

Visit [ScienceCareers.org](http://ScienceCareers.org) and start an online dialogue.



Bring your career concerns to the table. Dialogue online with professional career counselors and your peers.

**ScienceCareers.org**

We know science





## POSITIONS OPEN



**POSTDOCTORAL RESEARCHER in  
QUANTITATIVE ECOLOGY**  
National Center for Ecological Analysis  
and Synthesis (NCEAS)  
University of California Santa Barbara

National Center for Ecological Analysis and Synthesis (NCEAS) seeks a Postdoctoral Scientist to develop quantitative analyses and models regarding ecological thresholds of potential concern that inform the management of key conservation issues within the Kruger National Park ecosystem in South Africa. Analyses and models will be implemented using an established data management framework, the Kepler scientific workflow system. The candidate will have a commitment to testing and extending Kepler by working closely with other scientists and technologists that are developing the Kepler framework. Principal research skills must include statistical data analysis and quantitative modeling techniques, and a background in some ecological or environmental science field. The candidate will collaborate with scientists from Kruger National Park, South Africa, on the quantitative management of savannah ecosystems. The conservation issues will span a suite of indicators from multiple taxonomic groups and both biotic and abiotic ecosystem components. The position will include outreach with Kruger scientists regarding the use and interpretation of the models and analyses that are produced. Further details, including application instructions are available on the NCEAS website: <http://www.nceas.ucsb.edu/> **opportunity**. Consideration of applications begins immediately and will continue until filled.

**FACULTY POSITION in MOLECULAR/  
CELLULAR MICROBIOLOGY,  
INFECTIOUS DISEASE IMMUNOLOGY**  
Department of Biomedical Sciences,  
University of Maryland, Baltimore (UMB)

A full-time tenure-track faculty position at the ASSISTANT or ASSOCIATE PROFESSOR level is currently available. We are interested in outstanding individuals who will establish independent research in molecular or cellular microbiology, or infectious disease immunology, with a focus on molecular mechanisms of pathogenesis, the cell biology of infection, or molecular/cellular mechanisms of the host response to infection. The successful applicant will join an internationally recognized community of researchers with related interests in infection and immunity across several departments in the Dental and Medical Schools. As the Department has recently acquired two new FEI electron microscopes, qualified researchers with expertise and/or interest in exploiting or developing leading edge methodologies involving cryo electron microscopy or electron tomography are particularly encouraged to apply.

For more information on research in molecular/cellular microbiology at University of Maryland, Baltimore, please visit websites: <http://bms.dental.umaryland.edu/>, <http://medschool.umaryland.edu/Microbiology/>, and <http://medschool.umaryland.edu/CVD/>.

Minimum qualifications: Ph.D. in microbiology and immunology, cell biology, or related discipline. The position will remain open until it is filled with a qualified candidate. To apply, please submit curriculum vitae, summary of research and teaching interests, and the names and addresses of three references to: Patrik Bavoil, Chair, Biomedical Science Search Committee, Room 9205, Department of Biomedical Sciences, University of Maryland Baltimore, Dental School, 650 West Baltimore Street, Baltimore, MD 21201. *We especially encourage women and minorities to apply. The University of Maryland is an Affirmative Action/Equal Employment Opportunity/ADA Employer.*

## POSITIONS OPEN

**DIRECTOR, ELECTRON MAGNETIC  
RESONANCE PROGRAM**

The National High Magnetic Field Laboratory (NHMFL) in Tallahassee, Florida, is seeking a senior researcher in electron resonance to lead the existing Electron Magnetic Resonance Program. The Program currently comprises four faculty-level in-house scientists who develop high field instrumentation, assist the external users, and develop their own research interests. In addition to the in-house research and outside collaborations, there is strong interaction with the electron paramagnetic resonance laboratories at Florida State University (FSU) and the University of Florida (UF) in the areas of structural biology, chemistry, physics, material science, and computation. The EMR Program features unique high-frequency spectrometers (up to 800 GHz) and access to uniquely high magnetic fields (up to 45 T). Research focus includes nano-scale magnets, metalloproteins, and instrument and technology development for high-frequency, time-domain EMR. Other opportunities include the use of a unique THz-infrared light source currently under design for installation at the NHMFL in the five to ten-year timeframe.

Minimum qualifications include a Ph.D. in physics, chemistry, biology, or related. The successful candidate has a track record of outstanding scientific scholarship, and is expected to define and develop a multidisciplinary long-term vision for the Program. Senior scientists with a strong international reputation and strong publication and grantsmanship records are encouraged to apply. Particular research interests in one or more of the following areas is preferred but not required: molecular magnets and other nano-scale magnetic material and/or metalloprotein structure and function. The appointment will be either at the SCHOLAR SCIENTIST level (nontenure track) in the NHMFL or a PROFESSORIAL position in an appropriate academic department at FSU.

To apply, please send your curriculum vitae and cover letter describing your experience, along with names and contact information of three references to: Prof. Peter Fajer, Chair, Electron Magnetic Resonance Director Search Committee, National High Magnetic Field Laboratory, Florida State University, 1800 E. Paul Dirac Drive, Tallahassee, FL 32310-2740, telephone: 850-645-1337, fax: 850-644-1366, or e-mail: [fajer@magnet.fsu.edu](mailto:fajer@magnet.fsu.edu). The selection will start on April 15, 2007, and will continue until position is filled. *An Equal Opportunity/Access/Affirmative Action Employer.*

## NEUROSCIENCE

Oberlin College invites applications for a one-to-two year, noncontinuing position beginning July 1, 2007. Each year incumbent will teach two sections introductory neuroscience laboratory and either two upper-level lecture courses with one accompanying laboratory, or one introductory course/seminar and one upper-level course with laboratory. Position open to all applicants, but candidates with expertise in developmental and cellular neuroscience are encouraged to apply. Ph.D. required (in hand or expected by July 1, 2007).

Submit applications including curriculum vitae, three letters of recommendation, and transcripts by April 15, 2007, to: Lynne Bianchi, Neuroscience Department, Oberlin College, Oberlin, OH 44074. Applications may be reviewed until position filled. *Affirmative Action/Equal Opportunity Employer.*

Full-time MICROBIOLOGIST for Atlanta, Georgia, location. Responsible for developing techniques and providing assistance to various countries in the areas of molecular diagnosis (i.e., HIV viral low antiretroviral resistance testing, immunophenotyping (i.e., CD4-testing). Implement laboratory activities overseas using flow cytometry. Must have a Ph.D. degree in microbiology, or a related field. Foreign degree equivalent accepted. Must have one year of experience in the job offered or position with same duties. Send resumes to: Kari Knowles, ATA Services, Incorporated, Reference 888, 165 S. Union Boulevard, Suite 350, Lakewood, CO 80228.

## POSITIONS OPEN



Two POSTDOCTORAL POSITIONS are available in the Center for Cardiovascular Sciences at Albany Medical College. The successful candidates will have a Ph.D. degree and proven research ability as demonstrated by publications in peer-reviewed journals and letters of recommendation. They will also possess a strong knowledge base in biochemistry, cell biology, signal transduction, molecular biology and physiology.

The laboratory of Dr. Mohamed Trebak is accepting applications for a Postdoctoral position that is available immediately. Topics of research focus on endothelial cell signaling, specifically, the role of transient receptor potential (TRP) ion channels-mediated calcium entry and reactive oxygen species in endothelial cell proliferation and angiogenesis. This laboratory uses a wide range of technologies including patch clamp electrophysiology, calcium imaging, molecular and cellular biology, and biochemical techniques. Special attention will be given to candidates with expertise, or the desire to obtain training, in the field of calcium imaging and patch clamp electrophysiology.

Interested individuals should send a cover letter and curriculum vitae and provide contact information of three references, preferably by e-mail to Dr. Mohamed Trebak at e-mail: [trebakm@mail.amc.edu](mailto:trebakm@mail.amc.edu).

The laboratory of Dr. Peter Vincent is accepting applications for a Postdoctoral position that is available immediately. The research focus of the laboratory is centered on the role of endothelial cell adherens junctions in the regulation of endothelial functions including maintenance the endothelial barrier and angiogenesis. The laboratory uses a variety of cell and molecular techniques as well as in vitro functional assays. Special attention will be given to candidates with expertise, or the desire to learn, morphological techniques including fluorescence recovery after photobleaching and fluorescence loss in photobleaching.

Interested candidates should send a letter of interest, curriculum vitae, and three letters of reference to Dr. Peter Vincent at e-mail: [vincenp@mail.amc.edu](mailto:vincenp@mail.amc.edu).

## PHYSICIST

Lawrence Berkeley National Laboratory has a unique opportunity for a Physicist to help quantify myocardial function using single photon computed tomography. Must have experience with finite element techniques, reconstruction software, and biomedical imaging data. Job includes research in discovery of new scintillation materials. Ph.D. or equivalent experience is highly preferred. Apply at website: <http://jobs.lbl.gov>. Choose search, then enter job 20369 in keyword field. *Affirmative Action/Equal Employment Opportunity.*

## MARKETPLACE

Widely Recognized Original & Guaranteed	<b>KlenTaq1</b>	8¢/u Truncated Taq DNA Polymerase Withstand 99°C
US Pat #5,436,149 Call: <b>Ab Peptides</b>		e-mail: <a href="mailto:abpeps@msn.com">abpeps@msn.com</a> 1-800-383-3362
Fax: 314-968-8988		<a href="http://www.abpeps.com">www.abpeps.com</a>

## Oligo Synthesis Columns

↳ Columns For All Synthesizers

↳ Standard and Specialty CPGs

↳ Bulk Column Pricing Available

**BIOSEARCH**  
TECHNOLOGIES  
*Chemistry for Genomics and Proteomics™*

+1.800.GENOME.1  
[www.bticolumns.com](http://www.bticolumns.com)



**Greater Speed. Greater Sensitivity. Greater Confocal Imaging.**



## Nikon Breakthrough Confocal Microscope Systems

Live Cell Confocal imaging just took a quantum leap.

At Nikon, innovation runs through everything we do. Case in point: our groundbreaking family of Digital Eclipse Confocal Microscopes, three systems that add speed, resolution and sensitivity to any research application.

### LiveScan SFC Confocal System

LiveScan utilizes proprietary Swept Field Confocal technology, which combines the advantages of spinning disk confocal imaging with the visual precision of high resolution conventional live cell microscopes. It's the first system to offer the user the choice of selecting multiple pinholes or multiple slit scanning positions, resulting in faster imaging while matched to the objective confocal capabilities.

### C1si Spectral Imaging System

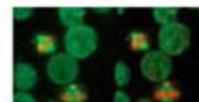
The C1si marries conventional fluorescence imaging with spectroscopy, creating a system that enables acquisition of spectral data faster and more accurately than ever before. With its one-shot acquisition ability, exclusive Diffraction Efficiency Enhancement system, and new FRAP and FRET macros, the C1si eliminates the need for cumbersome custom filter sets and provides an efficient, nondestructive and cost effective solution for acquiring optimum wavelength coverage at high spectral resolution.

### C1Plus Modular Confocal System

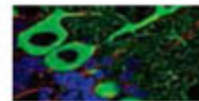
With its ultra-compact modular design, the C1 Plus features high performance scan head optics technology to generate faster image acquisition times and deliver true laser point scanning, 4-channel confocal imaging along with improved resolution, contrast, and fluorescence.

Learn more about Nikon Digital Eclipse Confocal Microscopes at [www.nikonconfocal.com](http://www.nikonconfocal.com) or call 1-800-52-NIKON.

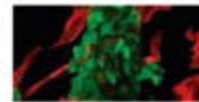
LiveScan SFC offers greater aperture choices, 3 pinhole radius sizes or 4 separate slit sizes are available providing more flexibility, greater resolution choices and faster acquisition times.



C1si features simultaneous 32 channel spectral image acquisition over a range of 320nm at 10nm spectral resolution or over smaller ranges of 5nm or 2.5nm.



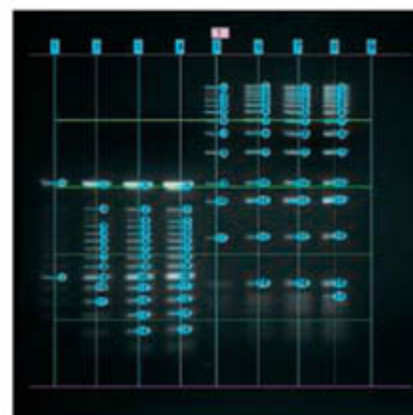
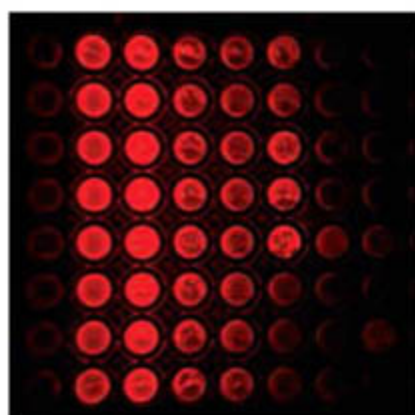
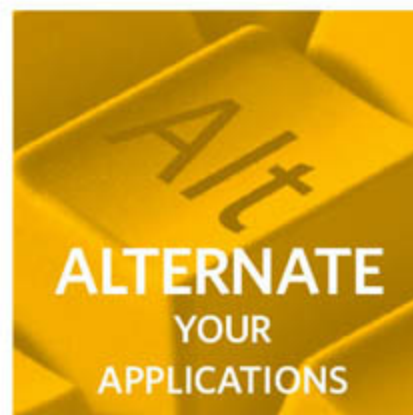
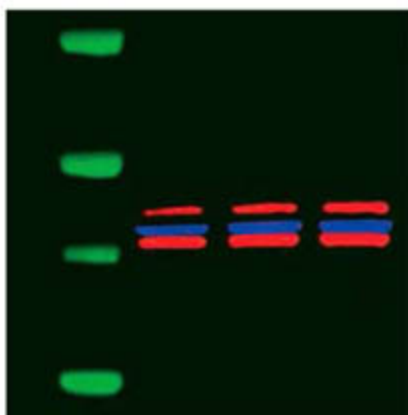
C1 Plus combines a modular design with high performance scan head optics, advanced scanning capabilities and 4-channel simultaneous detection abilities.



The Eyes of Science



# THE KEYS TO HIGH PERFORMANCE



Introducing the KODAK Image Station 4000MM Pro: the newest addition to the industry standard Image Station line brings precision automation and ease of use to an entirely new level. The IS4000MM Pro features a new automated high-performance 10X zoom lens and computer-controlled 10 excitation and 4 emission filter systems, providing reproducible and quantitative imaging of chemiluminescent, fluorescent, and chromogenic labels in gels, blots, plates and more. With 4-million pixel resolution, >4 OD dynamic range and optional x-ray and radioisotopic imaging capabilities, the KODAK Image Station 4000MM Pro provides the optimal combination of precision, performance and versatility.



[www.kodak.com/go/imagestation5](http://www.kodak.com/go/imagestation5)  
Call toll free:  
U.S. 1-877-747-4357, exp. code 7  
International +1-203-786-5657

**Kodak**  
Molecular Imaging Systems